T.C.
SAKARYA ÜNİVERSİTESİ
FEN BİLİMLERİ ENSTİTÜSÜ

PİRİDİN TÜREVİ İÇEREN BAZI GEÇİŞ METAL KOMPLEKSLERİNİN SENTEZİ, ELEKTRONİK YAPI HESAPLAMALARI VE α-GLUKOZİDAZ İNHİBİSYONLARI

DOKTORA TEZİ

Özgen ÖZGE

Fizik Anabilim Dalı

TEMMUZ 2025

T.C.
SAKARYA ÜNİVERSİTESİ
FEN BİLİMLERİ ENSTİTÜSÜ

PİRİDİN TÜREVİ İÇEREN BAZI GEÇİŞ METAL KOMPLEKSLERİNİN SENTEZİ, ELEKTRONİK YAPI HESAPLAMALARI VE α-GLUKOZİDAZ İNHİBİSYONLARI

DOKTORA TEZİ

Özgen ÖZGE

Fizik Anabilim Dalı

Tez Danışmanı: Prof. Dr. Davut AVCI

TEMMUZ 2025

Özgen Özge tarafından hazırlanan "Piridin Türevi İçeren Bazı Geçiş Metal Komplekslerinin Sentezi, Elektronik Yapı Hesaplamaları ve α-Glukozidaz İnhibisyonları" adlı tez çalışması 14.07.2025 tarihinde aşağıdaki jüri tarafından oy birliği ile Sakarya Üniversitesi Fen Bilimleri Enstitüsü Fizik Anabilim Dalı'nda Doktora tezi olarak kabul edilmiştir.

Tez Jürisi

Jüri Başkanı :	**Prof. Dr. Yusuf ATALAY** Sakarya Üniversitesi	.....
Jüri Üyesi :	**Prof. Dr. Davut AVCI (Danışman)** Sakarya Üniversitesi	.....
Jüri Üyesi :	**Prof. Dr. Fatih SÖNMEZ** Sakarya Uygulamalı Bilimler Üniversitesi	.....
Jüri Üyesi :	**Prof. Dr. Adil BAŞOĞLU** Sakarya Üniversitesi	.....
Jüri Üyesi :	**Prof. Dr. Betül USTA** Sakarya Uygulamalı Bilimler Üniversitesi	.....

ETİK İLKE VE KURALLARA UYGUNLUK BEYANNAMESİ

Sakarya Üniversitesi Fen Bilimleri Enstitüsü Lisansüstü Eğitim-Öğretim Yönetmeliğine ve Yükseköğretim Kurumları Bilimsel Araştırma ve Yayın Etiği Yönergesine uygun olarak hazırlamış olduğum "Piridin Türevi İçeren Bazı Geçiş Metal Komplekslerinin Sentezi, Elektronik Yapı Hesaplamaları ve α-Glukozidaz İnhibisyonları" başlıklı tezin bana ait, özgün bir çalışma olduğunu; çalışmamın tüm aşamalarında yukarıda belirtilen yönetmelik ve yönergeye uygun davrandığımı, tezin içerdiği yenilik ve sonuçları başka bir yerden almadığımı, tezde kullandığım eserleri usulüne göre kaynak olarak gösterdiğimi, bu tezi başka bir bilim kuruluna akademik amaç ve unvan almak amacıyla vermediğimi ve 20.04.2016 tarihli Resmi Gazete'de yayımlanan Lisansüstü Eğitim ve Öğretim Yönetmeliğinin 9/2 ve 22/2 maddeleri gereğince Sakarya Üniversitesi'nin abonesi olduğu intihal yazılım programı kullanılarak Enstitü tarafından belirlenmiş ölçütlere uygun rapor alındığını, çalışmamla ilgili yaptığım bu beyana aykırı bir durumun ortaya çıkması halinde doğabilecek her türlü hukuki sorumluluğu kabul ettiğimi beyan ederim.

14/07/2025

Özgen ÖZGE

TEŞEKKÜR

Doktora eğitimim sürecinde kıymetli bilgi ve birikimlerinden faydalandığım, kullandığı her kelimenin hayatıma kattığı önemini asla unutmayacağım, araştırmanın tüm aşamalarında yardımlarını esirgemeyen, kendisine ne zaman danışsam bana kıymetli zamanını ayırıp sabırla ve büyük bir ilgiyle bana faydalı olabilmek için elinden gelenden fazlasını sunan, her sorun yaşadığımda yanına çekinmeden gidebildiğim, zamanını ve samimiyetini benden esirgemeyen ve mesleki hayatımda da bana verdiği değerli bilgilerinden yararlanacağım değerli danışman hocam Prof. Dr. Davut AVCI' ya teşekkürlerimi sunarım.

Laboratuvar çalışmalarında bilgilerini, değerli tecrübelerini ve yardımlarını esirgemeyen sayın hocalarım Prof. Dr. Davut AVCI ve Prof. Dr. Fatih SÖNMEZ, ayrıca bilgi ve deneyimlerini aktaran ve çalışmalarımız boyunca destek olan sayın hocalarım Prof. Dr. Ömer TAMER, Prof. Dr. Adil BAŞOĞLU ve Prof. Dr. Yusuf ATALAY'a teşekkür ederim.

Kristal yapı tanımlama analizleri için Ondokuz Mayıs Üniversitesi Fen Edebiyat Fakültesi öğretim üyesi Prof. Dr. Necmi DEGE'ye ve enzim aktivite çalışmalarına katkılarından dolayı Bezmialem Vakıf Üniversitesi Eczacılık Fakültesinden Doç. Dr. Belma ZENGİN KURT'a teşekkürü bir borç bilirim.

Doktora eğitimim boyunca maddi ve manevi desteğini hiçbir zaman esirgemeyen sevgili aileme sonsuz teşekkürlerimi sunarım. Ayrıca bu çalışmanın maddi açıdan desteklenmesine olanak sağlayan YÖK 100/2000 Doktora Programı nezdinde YÖK kurumuna ve Sakarya Üniversitesi Bilimsel Araştırma Projeleri Koordinatörlüğü'ne teşekkür ederim.

Özgen ÖZGE

İÇİNDEKİLER

Sayfa

KISALTMALAR

DFT	: Yoğunluk fonksiyon teorisi
DNA	: Deoksiriboz nükleik asit
HOMO	: En yüksek enerjili dolu moleküler orbital
IC_{50}	: Yarı maksimal inhibitör konsantrasyonu
ILCT	: Ligant içi yük transferi
LLCT	: Ligant-ligant yük transferi
LUMO	: En düşük enerjili boş moleküler orbital
MEP	: Moleküler elektrostatik potansiyel
MLCT	: Metal-ligant yük transferi
NBO	: Doğal bağ orbitali
NIDDM	: Noninsülin bağımlı tip 2 diyabet
NLO	: Non-lineer optik
OAD	: Oral anti-diyabetik ilaçlar
T2DM	: Tip 2 diyabet
TD-DFT	: Zamana bağımlı yoğunluk fonksiyon teorisi
XRD	: X-Işını Kırınım yöntemi

SİMGELER

χ	: Elektronegatiflik
η	: Kimyasal sertlik
$\Delta\alpha$	: Statik anizotropik kutuplanabilirlik
D	: Elektriksel yer değiştirme
E	: Dış elektrik alanı
$\mathbf{E^2}$	: Stabilasyon enerjisi
n	: Kırılma indisi
P	: Kutuplanma
$\mathbf{P^{(1)}}$	: Doğrusal polarizasyon parametresi
$\mathbf{P^{(2)}}$	: İkinci dereceden polarizasyon parametresi
$\mathbf{P^{(3)}}$	: Üçüncü dereceden polarizasyon parametresi
S	: Kimyasal yumuşaklık
α	: Statik izotropik kutuplanabilirlik
β	: 1. mertebeden statik yüksek kutuplanabilirlik
γ	: 2. mertebeden statik yüksek kutuplanabilirlik
ε_0	: Boşluğun elektriksel geçirgenliği
ε_r	: Ortamın bağıl elektriksel geçirgenliği
μ	: Dipol moment
φ	: Nükleofilik indeks
χ	: Elektronegatiflik
$\chi^{(1)}$	: Doğrusal optik duyarlılık
$\chi^{(2)}$	: İkinci dereceden doğrusal olmayan optik duyarlılık
$\chi^{(3)}$	: Üçüncü dereceden doğrusal olmayan optik duyarlılık
χ_e	: Elektriksel duyarlılık
ω	: Elektrofilik indeks

ŞEKİL LİSTESİ

Sayfa

PİRİDİN TÜREVİ İÇEREN BAZI GEÇİŞ METAL KOMPLEKSLERİNİN SENTEZİ, ELEKTRONİK YAPI HESAPLAMALARI VE α-GLUKOZİDAZ İNHİBİSYONLARI

ÖZET

Koordinasyon kompleksleri, koordinasyon merkezi olarak adlandırılan merkezi bir metalik atom veya iyondan ve bunu çevreleyen ligantlardan oluşan kimyasal bir bileşiktir. Bir ligantın içindeki, merkezi metal iyonu ya da atomuna bağlı atoma donör atom denir. Tipik bir komplekste, bir metal iyonu aynı veya farklı olabilen birkaç donör atomuna bağlıdır. Çok dişli bir ligant, ligantın atomlarından birkaçı vasıtasıyla merkezi atoma bağlanan bir iyon veya moleküldür. Metal kompleksleri tarım, eczacılık ve endüstriyel kimyada önemli bir rol oynar.

C_6H_5NO kimyasal formülüne sahip organik bir bileşik olan 2-piridin karboksaldehit, koordinasyon kimyası ve farmasötiklerde ilgi çeken bileşiklerden biridir. Piridin aldehitleri tipik olarak hidroksimetil veya metilpiridinlerin oksidasyonuyla hazırlanırlar. Schiff bazlarının tıbbi açıdan önemli olduğu ve tıbbi bileşiklerin tasarımı için kullanıldığı bilinmektedir. Koordinasyon kimyasında önemli bir rol oynayan Schiff bazları yaygın olarak kullanılmaktadır. İmin grubu Schiff bazlarında, geniş biyolojik aktiviteye sahip bu moleküllerin üretilmesinde belirgin bir işlev sağlar. Geniş endüstriyel uygulamalarına ek olarak antifungal, antiinflamatuar, antipiretik, antiviral antiproliferatif ve antibakteriyel özellikler gibi çok çeşitli fizyolojik aktiviteler sergilerler.

α-glukozidaz, polisakkarit ve disakkaritleri bağırsaktan emilim için glikoza hidrolize eden bir enzimdir. Bu enzimin inhibisyonu, bir öğünden sonra karbonhidrat emilimini geciktirir ve yemek sonrası glikoz seviyelerini düşürür. Vogliboz, akarboz ve miglitol mevcut kullanılan α-glukozidaz inhibitörleridir. Akarboz, ince bağırsakta görev yapan α-glukozidaz enzimini geçici ve seçici bir biçimde engelleyerek etkisini gösterir. Bu etki, karbonhidratların parçalanmasını yavaşlatarak glikozun kana karışma süresini uzatır ve emilim hızını düşürür. Böylece kan şekeri seviyelerinde ani yükselmeler önlenebilir. Bu özelliği sayesinde, akarboz diyabetin klinik belirtilerinin ortaya çıkmasını geciktirme potansiyeline sahiptir. Bu tür inhibitörler, sıklıkla diğer kan şekeri düzenleyici ilaçlarla birlikte tedavi protokollerinde yer almaktadır.

Elektronik Schrödinger denkleminin çözümlerinden elde edilen enerji değerleri ve dalga fonksiyonları, incelenen sistemlerin tam olarak tanımlanması için tek başına yeterli değildir. Bu nedenle, atomik ve moleküler düzeyde daha kapsamlı nicel verilerin hesaplanması gerekmektedir. Özellikle, moleküllerin temel hal geometrisinin optimize edilmesi, titreşim modlarının belirlenmesi, dipol momentlerin hesaplanması, doğrusal ve yüksek dereceli doğrusal olmayan kutuplanabilirlik gibi özelliklerin değerlendirilmesi önem taşır. Ayrıca, uyarılmış durumlara ait elektronik geçişlerin anlaşılabilmesi için absorpsiyon dalga boyları, osilatör şiddetleri ve geçiş dipol momentleri gibi parametrelerin hesaplanması gereklidir. Bu tür hesaplamalar, deneysel bulgularla kuramsal verilerin birbirleriyle uyumu açısından kritik bir öneme sahiptir. Teorik yöntemler, bir maddenin sentezlenmesinden önce yapı-özellik

ilişkilerinin değerlendirilmesine olanak tanıması ve deneysel ölçümlerin uygulanabilirliği hakkında öngörü sağlaması bakımından oldukça değerlidir. Ancak çeşitli hesaplama yaklaşımlarının başarısı, deneysel verilerle uyumlu olması bakımından değerlendirilebilir.

Bu tez kapsamında, *N*-(piridin-2-ilmetilen)metanamin (L_1)'nin izotiyosiyanat ile $[Mn(L_1)_2(NCS)_2]$ (**1**), $[Co(L_1)_2(NCS)_2]$ (**2**), $[Ni(L_1)_2(NCS)_2]$ (**3**), $[Cd(L_1)_2(NCS)_2]$ (**4**), $[Zn(L_1)_2(NCS)_2]$ (**5**) , $[Cu(L_1)_2(NCS)_2]$ (**6**), $[Ag(L_1)(NCS)_2]$ (**7**), $[Hg(L_1)_2(NCS)Cl]$ (**8**) ve azid ile $[Mn(L_1)_2(N_3)_2]$ (**9**), $[Ni(L_1)_2(N_3)]$ (**10**), $[Co_2(L_1)_2(N_3)_2]\cdot 2H_2O$ (**11**), $[Cu_2(L_1)_2(N_3)_3]$ (**12**), $[Hg(L_1)_2(N_3)\cdot H_2O]$ (**13**), $[Cd(L_1)_2(N_3)]$ (**14**), $[Ag(L_1)(N_3)_2\cdot 2H_2O]$ (**15**), $[Zn_2(L_1)_2(N_3)_2Cl_2\cdot 4H_2O]$ (**16**) kompleksleri sentezlenmiştir. Sentezlenen komplekslerden $[Mn(L_1)_2(NCS)_2]$, (**1**), $[Co(L_1)_2(NCS)_2]$ (**2**), ve $[Cd(L_1)_2(NCS)_2]$, (**4**) tek kristal yapıda elde edilerek yapıları X–ışını kırınım yöntemi (XRD) kullanılarak aydınlatılmıştır. Diğer izotiyosiyanat içeren $[Ni(L_1)_2(NCS)_2]$, (**3**), $[Zn(L_1)_2(NCS)_2]$, (**5**), $[Cu\ (L_1)_2(NCS)_2]$, (**6**), $[Ag(L_1)(NCS)_2]$, (**7**), $[Hg(L_1)_2(NCS)Cl]$ (**8**) ve sodyum azid içeren $[Mn(L_1)_2(N_3)_2]$, (**9**), $[Ni(L_1)_2(N_3)]$, (**10**), $[Co_2(L1)_2(N_3)_2]$ $\cdot 2H_2O$, (**11**), $[Cu_2(L_1)_2(N_3)_3]$, (**12**), $[Hg(L_1)_2(N_3)\cdot H_2O]$, (**13**), $[Cd(L_1)_2(N_3)]$, (**14**), $[Ag(L_1)(N_3)_2\cdot 2H_2O]$, (**15**), $[Zn_2(L_1)_2(N_3)_2Cl_2\cdot 4H_2O]$, (**16**) kompleksleri toz ürün olarak elde edilerek yapıları kütle spektroskopisi yöntemi kullanılarak aydınlatılmıştır. Yapısal özellikleri belirlendikten sonra FT–IR spektrumları titreşim frekanslarını incelemek için UV–Vis spektrumları ise elektronik geçişleri incelelemek için kaydedilmiştir. Deneysel yöntemlerle detaylı analizi yapılan komplekslerin taban durumundaki yapısal ve titreşim özelliklerinin teorik analizi hibrit yoğunluk fonksiyonu teorisi (DFT) metodu kullanılarak yapılmıştır. Bunun yanı sıra, elektronik spektrumlar zamana bağlı DFT (TD–DFT) yöntemi ile sağlanmıştır. Hesaplanmış sonuçlar ve deneysel sonuçların birbirleriyle uyumu karşılaştırılmalı olarak verilmiştir. Sentezlenen komplekslerinin elektrik dipol momenti, kutuplanabilirlik, 1. ve 2. mertebeden lineer olmayan optik parametreler teorik olarak incelenerek, π-elektronlarının delokalize etkisi, substitute ve yük transferi gibi faktörlerin bu NLO özellikleri ile ilişkisi araştırılmıştır. Kompleks yapılar için sınır orbitallerdeki HOMO (en yüksek enerjili dolu moleküler orbital) ve LUMO (en düşük enerjili boş moleküler orbital) enerjileri hesaplanarak kaydedilmiştir. Bu enerjiler kullanılarak, HOMO–LUMO enerji aralığı, elektronegatiflik, kimyasal yumuşaklık ve kimyasal sertlik gibi moleküler reaktivite parametreleri elde edilmiştir. Bunlara ek olarak SWizard ve Chemissian programaları kullanılarak moleküler orbitallerden elektronik geçişlere gelen katkılar belirlenmiştir. Doğal bağ orbitali (NBO) analizi ile molekül içi ve moleküller arası bağların yanı sıra yük aktarımı ve konjugasyonla ilişkili etkileşimleri detaylı biçimde ortaya çıkarılmıştır. Ayrıca, azot, oksijen ve metal merkezleri üzerinde bulunan eşleşmemiş elektronlar arasındaki etkileşim enerjileri de net biçimde belirlenmiştir. Moleküler elektrostatik potansiyel (MEP) yüzeyler DFT metodu vasıtasıyla oluşturulmuştur. Bu komplekslerin α-glukozidaz inhibisyon etkileri incelenmiştir. Ayrıca inhibisyon mekanizmaları ve yapı aktivite ilişkilerini belirlemek amacıyla moleküler yerleştirme çalışmaları yapılmıştır.

Kompleksler **1–3** için UV–Vis bölgesinde metanol ortamında elde edilen deneysel üçüncü derece doğrusal olmayan optik (NLO) duyarlılık ($\chi^{(3)}$) sonuçları; sırasıyla 4,68, 4,21 ve 5,25 eV foton enerjilerinde maksimum zirvelerde yaklaşık olarak aynı değerde bulunmuştur ($\chi^{(3)} = 51{,}65\times10^{-13}$, $51{,}42\times10^{-13}$ ve $51{,}42\times10^{-13}$ esu). Bu çalışmada teorik ve deneysel olarak elde edilen üçüncü derece NLO parametreleri, kompleks **1**'in optoelektronik cihazların geliştirilmesinde kullanılabileceğini göstermektedir. Kompleksler **4-8**'de, α-glukozidaza karşı IC_{50} değeri 5,618 μM olan kompleks **6**'nın,

β ve γ parametreleri dikkate alındığında umut verici bir NLO (nonlineer optik) materyal adayı olarak değerlendirilebileceği öngörülmüştür. Bu çalışmada, L_1 ve NCS ligantlarının metal kompleksleri bağlamında*; in vitro*/doking ve NLO sonuçları dikkate alındığında, kompleks **8**'in (IC_{50}=0,2376 μM) tip 2 diyabet (T2DM) için alternatif bir ilaç adayı, kompleks **6**'nın ise NLO materyal adayına sahip yapılar olduğu belirtilebilir. Kompleks **9** için en yüksek <γ(0;0,0,0)> değeri, CAM-B3LYP düzeyine göre $2216{,}40\times10^{-36}$ esu olarak elde edilmiş olup, bu değer pNA'ya (15×10^{-36} esu) göre 147,76 kat, üreye ($7x10^{-36}$ esu) göre ise 316,63 kat daha büyüktür. β ve γ sonuçları, sırasıyla kompleks **10** ve **9**'un mikroskobik ikinci ve üçüncü dereceden NLO özellikler açısından oldukça etkili olduğunu göstermektedir. Bu sonuçların $\chi^{(2)}$ ve $\chi^{(3)}$ parametrelerinin sonuçlarıyla da desteklendiği görülmektedir. Lineer azid anyonunun, kompleks **10**'un geometrisi, γ işareti ve büyüklüğü üzerinde bir etkisi olduğu gözlemlenmiştir. Kompleksler **12–16** için IC_{50} değerleri 0,2802 ± 0.62 ile 420,88 ± 1.42 μM aralığında elde edilmiştir. Kompleks **13**, en yüksek α-glukozidaz inhibitör aktivitesini gösterirken, kompleks **14** en düşük inhibitör aktiviteye sahiptir. Ayrıca, kompleks **12** (1,562±0,83 μM) ve kompleks **15** (1,274± 0,32 μM)'de etkili IC_{50} değerlerine sahiptir. Bu sonuçlar, reseptör-ligant etkileşimlerini ortaya koyan doking çalışmaları ile desteklenmiştir. Ek olarak, toplam 50 ns'lik moleküler dinamik (MD) simülasyonları ile yapılan çalışmalarda, bileşiklerin MD simülasyonu boyunca kararlı olduğu gösterilmiştir. Kompleks **15** ve kompleks **12**, α-glukozidaza karşı anlamlı IC_{50} değerleri gösterirken, aynı zamanda β ve γ sonuçları, sırasıyla bu komplekslerin mikroskobik ikinci ve üçüncü dereceden NLO özellikler açısından oldukça etkili olduğunu göstermektedir. Sonuç olarak, Schiff baz–azid metal kompleksleri arasında, kompleks **13**'ün tip-2 diyabet için alternatif bir anti-diyabetik inhibitör olabileceği, kompleks **12** ve kompleks **15**'in ise NLO materyal adayları olarak önerilebileceği düşünülmektedir. Moleküler doking ve *in vitro* sonuçlarına göre, yapı–aktivite ilişkileri dikkate alındığında Cu, Ag ve Hg atomlarını içeren metal komplekslerin α-glukozidaza karşı iyi inhibitör özellik sergilediği sonucuna varılmıştır.

SYNTHESIS, ELECTRONIC STRUCTURE CALCULATIONS, AND α-GLUCOSIDASE INHIBITIONS OF SOME TRANSITION METAL COMPLEXES CONTAINING PYRIDINE DERIVATIVES

SUMMARY

Coordination complexes are chemical compounds composed of a central metallic atom or ion, known as the coordination center, and surrounding ligands. Within a ligand, the atom that directly bonds to the central metal ion or atom is referred to as the donor atom. In a typical coordination complex, the metal ion is coordinated to multiple donor atoms, which may be identical or different in nature. A polydentate ligand is an ion or molecule that attaches to the central atom through several of its own atoms. Metal complexes play a crucial role in various fields, including agriculture, pharmaceuticals, and industrial chemistry.

2-Pyridinecarboxaldehyde (chemical formula: C_6H_5NO) is an organic compound of interest in coordination chemistry and pharmaceuticals. Pyridine aldehydes are typically synthesized through the oxidation of hydroxymethyl- or methylpyridines. Schiff bases are known to be medically significant and are widely employed in the design of pharmaceutical compounds. In coordination chemistry, Schiff bases play an important role and are commonly utilized. The imine group plays a prominent role in the formation of Schiff bases, which are known for their broad spectrum of biological activities. In addition to their extensive industrial applications, these compounds exhibit a wide range of physiological effects, including anti-inflammatory, antibacterial, antiproliferative, antifungal, antipyretic, and antiviral properties.

α-Glucosidase is an enzyme that hydrolyzes polysaccharides and disaccharides into glucose for intestinal absorption. Inhibition of this enzyme postpones carbohydrate absorption after a meal and lowers postprandial glucose levels. Voglibose, acarbose, and miglitol are currently used as α-glucosidase inhibitors. Acarbose inhibits α-glucosidase in the intestine, competitively. That reduces the rate of glucose absorption through postponed carbohydrate digestion and prolonged digestion time. Therefore, these inhibitors are used in combination with other anti-diabetic agents.

In theoretical calculations, the energies and wave functions obtained from the solutions of the electronic Schrödinger equation are not sufficient on their own for characterizing the materials under investigation. In such cases, it becomes necessary to compute additional quantities that provide a more comprehensive characterization of atomic and molecular systems. In particular, determining parameters such as ground-state molecular geometry optimization, vibrational frequencies, dipole moment, linear polarizability, and higher-order nonlinear polarizability, as well as electronic absorption wavelengths, oscillator strengths, and transition dipole moments for excited-state electronic transitions, is crucial for establishing connections with experimental results and assessing the agreement between theoretical and experimental data. Theoretical calculations hold particular significance as they allow for the investigation of structure–property relationships prior to detailed synthesis and experimental characterization, and they also provide insight into whether

measurements are feasible. However, the reliability of various computational approaches can only be evaluated based on their consistency with experimental data.In this thesis, the complexes of N-(pyridin-2-ylmethylene)methanamine (L_1) with isothiocyanate {[$Mn(L_1)_2(NCS)_2$] (**1**), [$Co(L_1)_2(NCS)_2$] (**2**), [$Ni(L_1)_2(NCS)_2$] (**3**), [$Cd(L_1)_2(NCS)_2$] (**4**), [$Zn(L_1)_2(NCS)_2$] (**5**), [$Cu(L_1)_2(NCS)_2$] (**6**), [$Ag(L_1)(NCS)_2$] (**7**), [$Hg(L_1)_2(NCS)Cl$] (**8**)} and with azide {[$Mn(L_1)_2(N_3)_2$] (**9**), [$Ni(L_1)_2(N_3)$] (**10**), [$Co_2(L_1)_2(N_3)_2]\cdot 2H_2O$ (**11**), [$Cu_2(L_1)_2(N_3)_3$] (**12**), [$Hg(L_1)_2(N_3)\cdot H_2O$] (**13**), [$Cd(L_1)_2(N_3)$] (**14**), [$Ag(L_1)(N_3)_2\cdot 2H_2O$] (**15**), [$Zn_2(L_1)_2(N_3)_2Cl_2.4H_2O$] (**16**)} were synthesized. Among the synthesized complexes, [$Mn(L_1)_2(NCS)_2$] (**1**), [$Co(L_1)_2(NCS)_2$] (**2**), and [$Cd(L_1)_2(NCS)_2$] (**4**) were obtained as single crystals and their structures were elucidated using X-ray diffraction (XRD) analysis. The remaining complexes {[$Ni(L_1)_2(NCS)_2$] (**3**), [$Zn(L_1)_2(NCS)_2$] (**5**), [$Cu(L_1)_2(NCS)_2$] (**6**), [$Ag(L_1)(NCS)_2$] (**7**), [$Hg(L_1)_2(NCS)Cl$] (**8**)}, and the azide-containing {[$Mn(L_1)_2(N_3)_2$] (**9**), [$Ni(L_1)_2(N_3)$] (**10**), [$Co_2(L_1)_2(N_3)_2]\cdot 2H_2O$ (**11**), [$Cu_2(L_1)_2(N_3)_3$] (**12**), [$Hg(L_1)_2(N_3).H_2O$] (**13**), [$Cd(L_1)_2(N_3)$] (**14**), [$Ag(L_1)(N_3)_2\cdot 2H_2O$] (**15**), [$Zn_2(L_1)_2(N_3)_2Cl_2\cdot 4H_2O$] (**16**)} were obtained as powder products and characterized using mass spectromery. Following structural determination, FT–IR spectra were recorded to investigate their vibrational properties, and UV–Vis spectra were obtained to study electronic transitions and charge transfer interactions. The synthesized complexes were subjected to a comprehensive theoretical investigation at their optimized ground-state geometries using hybrid density functional theory (DFT), with their electronic absorption characteristics modeled through time-dependent DFT (TD-DFT). The comparison between computed and experimental data revealed a high degree of consistency. Essential electronic and optical features including dipole moment, polarizability, and both first- and second-order nonlinear optical (NLO) responses were explored in relation to structural parameters such as π-conjugation, electron delocalization, and substituent-driven charge redistribution. To evaluate electronic behavior, the energies of frontier orbitals (HOMO and LUMO) were computed, enabling the derivation of molecular reactivity descriptors like energy gap, chemical hardness and softness, and electronegativity. The roles of specific molecular orbitals in electronic transitions were elucidated with the aid of SWizard and chemissian softwares. In addition, Natural Bond Orbital (NBO) analysis was employed to unravel intra- and intermolecular interactions, revealing insights into bonding characteristics, charge delocalization, and interactions involving lone electron pairs on electronegative atoms and metal centers. Electrostatic potential surfaces, obtained through DFT calculations, provided further information on reactive regions within the molecular frameworks. Lastly, the α-glucosidase inhibition profiles of the complexes were evaluated, and molecular docking simulations were performed to clarify the binding mechanisms and structure–activity correlations underlying their biological function.

For complexes **1–3**, the experimentally obtained third-order nonlinear optical (NLO) susceptibilities ($\chi^{(3)}$) in the UV–Vis region in methanol exhibited maximum peaks at photon energies of 4.68, 4.21, and 5.25 eV, respectively, with approximately equal $\chi^{(3)}$ values ($\chi^{(3)} = 51.65 \times 10^{-13}$, 51.42×10^{-13}, and 51.42×10^{-13} esu). In this study, both the theoretical and experimental third-order NLO parameters indicate that complex **1** may be a promising candidate for the development of optoelectronic devices. Among complexes **4–8**, complex **6**, which exhibited an IC_{50} value of 5.618 μM against α-glucosidase, can be considered a promising NLO material candidate based on its calculated β and γ parameters. Considering both the in vitro/docking and NLO results in the context of metal complexes with L_1 and NCS ligands, it can be suggested that

complex **8** (IC_{50} = 0.2376 μM) represents a potential alternative drug candidate for type 2 diabetes mellitus (T2DM), while complex **6** appears to be a structurally viable NLO material candidate. For complex 9, the highest $\langle\gamma(0;0,0,0)\rangle$ value was obtained as 2216.40×10^{-36} esu at the CAM-B3LYP level, which is 147.76 times greater than that of p-nitroaniline (pNA, 15×10^{-36} esu) and 316.63 times greater than that of urea (7×10^{-36} esu). The β and γ results indicate that complexes **10** and **9** exhibit significant microscopic second- and third-order NLO properties, respectively. These findings are further supported by the $\chi^{(2)}$ and $\chi^{(3)}$ parameters. It was observed that the linear azide anion has an influence on the geometry, sign, and magnitude of γ in complex **10**. For complexes **12–16**, IC_{50} values ranged from 0.2802±0.62 to 420.88±1.42 μM. Among them, complex **13** showed the highest α-glucosidase inhibitory activity, while complex **14** exhibited the lowest. In addition, complex **12** (1.562±0.83 μM) and complex **15** (1.274±0.32 μM) also showed effective IC_{50} values. These results are supported by docking studies that reveal receptor–ligand interactions.

Furthermore, molecular dynamics (MD) simulations conducted over 50 ns demonstrated that the compounds remained stable throughout the simulation period. Complexes **15** and **12** not only showed notable IC_{50} values against α-glucosidase, but their β and γ results also confirmed their significant microscopic second- and third-order NLO characteristics, respectively.

In conclusion, among the Schiff base–azide metal complexes studied, complex **13** may be proposed as a potential alternative anti-diabetic inhibitor for type 2 diabetes, while complexes **12** and **15** are promising candidates for NLO materials. Based on the results of molecular docking and in vitro studies, and considering structure–activity relationships, it can be concluded that metal complexes containing Cu, Ag, and Hg exhibit notable inhibitory properties against α-glucosidase.

1. GİRİŞ

Koordinasyon kompleksleri, merkezinde genellikle bir geçiş metali iyonu bulunan ve bu merkeze çeşitli ligantların bağlandığı kimyasal türlerdir. Ligantlar, merkez atom veya iyonla koordine kovalent bağlar oluşturarak kompleks yapının oluşmasını sağlar. Bu kompleksler, biyolojik sistemlerden katalizöre, ilaç tasarımından malzeme bilimine kadar çok geniş bir uygulama alanına sahiptir. Koordinasyon kimyası, bileşiklerin yapısal çeşitliliği, bağlanma geometrileri ve reaktivite profilleri nedeniyle oldukça zengin ve karmaşık bir çalışma alanı sunar. Bu çeşitlilik, kimi zaman koordinasyon komplekslerinin yapısal ve elektronik özelliklerinin anlaşılmasını zorlaştırsa da aynı zamanda onların fonksiyonel özelliklerini belirleyen temel unsurları oluşturur. Bu nedenle, koordinasyon komplekslerinin sentezi, karakterizasyonu ve teorik olarak incelenmesi, modern kimya ve fizik araştırmalarının önemli bir parçası haline gelmiştir. Bir ligantın içindeki, merkezi metal atomuna (veya iyonuna) bağlı atoma donör atom denir. Karakteristik bir komplekste, bir metal iyonu aynı ya da farklı birkaç donör atomuna bağlıdır. Çok dişli bir ligant, ligantın atomlarından birkaçı vasıtasıyla merkezi atoma bağlanmış bir molekül ya da iyon olarak tanımlanır. Merkezi atomla 2, 3, 4 ,5 veya hatta 6 bağ yapabilen ligantlar yaygındır. Bu tür kompleksler şelat kompleksleri olarak adlandırılır. Bu tip komplekslerin meydana gelişine koordinasyon denmektedir. Merkezde yer alan atom ya da iyon, etrafındaki bütün ligantlar ile birlikte koordinasyon küresi olarak adlandırılan yapısal birimi oluşturur. Koordinasyon küresi, kompleksin geometrisini ve kimyasal özelliklerini belirleyen temel bileşendir. Bu yapı, ligantların sayısı, türü ve bağlanma biçimine bağlı olarak farklı geometriler (oktahedral, tetrahedral, kare düzlem vb.) sergileyebilir. Dolayısıyla, koordinasyon küresinin doğru anlaşılması, kompleks bileşiklerin fonksiyonel özelliklerinin tayininde kritik öneme sahiptir. Koordinasyon, ligantlar ve merkezi atom arasındaki koordinat kovalent bağlarını ifade eder. Başlangıçta "kompleks" terimi, moleküller, atomlar veya iyonlar arasında zayıf kimyasal bağlarla oluşan ve tersine çevrilebilir nitelikteki birleşmeleri tanımlamak için kullanılmıştır. Ancak bu kavram, koordinasyon kimyasına uyarlanmasıyla birlikte daha geniş ve derin bir anlam kazanmıştır. Günümüzde bazı metal kompleksleri neredeyse geri

dönüşü olmayan biçimde oluşmakta ve bu tür yapılar, çoğunlukla oldukça kuvvetli koordinatif bağlarla stabilize edilmektedir (Lawrence, 2010; IUPAC., 1997; Greenwood ve Earnshaw, 1997; Bochmann ve ark., 1999; Miessler ve Tarr, 1999).

Metal kompleksleri tarım, eczacılık ve endüstriyel kimyada önemli bir rol oynar. Schiff bazlarının tıbbi açıdan önemli olduğu ve tıbbi bileşiklerin tasarımı için kullanıldığı bilinmektedir. Hugo Schiff ilk olarak yaklaşık 160 yıl önce Schiff bazını karakterize etti (Ambike ve ark., 2007), o zamandan beri kendi adıyla, "Schiff" olarak bilinmektedir. Schiff baz ligantları koordinasyon kimyasında önemli rol oynayan ve yaygın olarak kullanılan organik bileşiklerdir (da Silva ve ark., 2011). Boyalar ve pigmentler, katalizörler, organik sentez ara maddeleri ve polimer stabilizatörleri olarak kullanılırlar (Zhang ve ark., 2018; Vitago ve Tamburini, 2014). İmin grubu Schiff bazlarında, geniş biyolojik aktiviteye sahip bu moleküllerin üretilmesinde belirgin bir işlev sağlar (Abu-dief ve Mohammed, 2015). Geniş endüstriyel uygulamalarına ek olarak antifungal, antiproliferatif, antibakteriyel, antiinflamatuar, antiviral ve antipiretik özellikler gibi çok çeşitli fizyolojik aktiviteler sergilerler (Kaur ve ark., 2021; Plesh ve ark., 1998). Sentezlerinin ve metal kompleksleşmelerinin basitliği nedeniyle, bilim camiasının büyük ilgisini çekmişlerdir.

C_6H_5NO kimyasal formülüne sahip organik bir bileşik olan 2-piridin karboksaldehit, üç izomerik piridinaldehitten biridir. Diğer izomerler 3-piridin karboksaldehit ve piridin 4-karboksaldehittir. 2-piridin karboksaldehit, belirgin bir kokuya sahip renksiz yağlı bir sıvıdır. Koordinasyon kimyası ve farmasötiklerde ilgi çeken diğer bileşiklerin öncüsü olarak hizmet eder. Piridin aldehitleri tipik olarak hidroksimetil veya metilpiridinlerin oksidasyonuyla hazırlanırlar (Shimizu ve ark., 2007)

α-glukozidaz, nişastaları ve disakkaritleri bağırsaktan emilim için glikoza hidrolize eden bir enzimdir. α-glukozidazın inhibisyonu, bir öğünden sonra karbonhidrat emilimini geciktirir ve yemek sonrası glikoz seviyelerini düşürür. Akarboz, miglitol ve vogliboz mevcut α-glukozidaz inhibitörleridir, ancak T2DM'ye ilerlemeye ilişkin veriler akarbozla sınırlıdır. Akarboz, α-glukozidaz enzimine karşı seçici bir inhibitör olarak görev yapar ve bu etkiyi bağırsaklarda, enzime geçici ve rekabetçi şekilde bağlanarak gösterir. Bu bağlanma, karbonhidratların sindirim sürecini yavaşlatır ve glikozun emilim hızını düşürerek kan şekerinde ani yükselmeleri engeller. Bu yönüyle akarboz, diyabetle ilişkili klinik belirtilerin ortaya çıkmasını engelleyici bir rol üstlenebilir. (Bischoff, 1995). Bu bağlamda, α-glukozidaz inhibitörleri, örneğin

akarboz genellikle diğer anti-diyabetik ajanlarla birlikte kombine tedavi yaklaşımlarında kullanılmaktadır. Yapılan çalışmalar, luteolin adlı bileşiğin de güçlü bir α-glukozidaz inhibitörü olduğunu ortaya koymuştur. Bu bileşik, 0,5 mg/mL'lik bir derişimde enzimin aktivitesini yaklaşık %36 oranında baskılayabilmektedir. (Kim ve ark., 2000). 2016 yılı itibarıyla söz konusu bileşik, sıçan ve fare modellerinin yanı sıra hücre kültürü sistemlerinde test edilmektedir. Ayrıca, flavonoid türevlerinin de α-glukozidaz enzimi üzerinde inhibe edici etki gösterdiği belirlenmiştir. (Zhen ve ark., 2017).

Teorik çalışmalarda, elektronik Schrödinger denkleminden elde edilen enerji değerleri ve dalga fonksiyonları, incelenen malzemelerin kapsamlı bir şekilde tanımlanması için tek başına yeterli değildir. Bu nedenle, atomik ve moleküler düzeyde daha fazla sayıda fiziksel parametrenin hesaplanması gerekmektedir. Özellikle, moleküllerin temel hal geometrilerinin optimize edilmesi, titreşimsel modların belirlenmesi, dipol momentin yanı sıra doğrusal ve doğrusal olmayan (yüksek mertebeli) kutuplanabilirlik gibi özelliklerin değerlendirilmesi büyük önem taşır. Ayrıca, uyarılmış durumlara ait elektronik geçişlerin anlaşılması için soğurma dalga boylarının, osilatör şiddetlerinin ve geçiş dipol momentlerinin hesaplanması, teorik verilerin deneysel bulgularla karşılaştırılabilirliğini sağlamak açısından gereklidir. Bu tür hesaplamalar, yalnızca deneysel sonuçlarla ilişki kurmakla kalmaz; aynı zamanda yapı-özellik ilişkilerinin sentez ve karakterizasyon sürecinden önce değerlendirilmesine de olanak tanır. Ancak bu yaklaşımların güvenilirliği, hesaplama sonuçlarının deneysel verilerle ne derece örtüştüğüyle doğrudan ilişkilidir. (Foresman ve Frisch, 1996). Yoğunluk Fonksiyonel Teorisi (DFT), moleküler sistemlerin temel hal özelliklerini incelemek amacıyla geliştirilen ve yarı-deneysel yaklaşımlar ile Hartree–Fock (HF) yöntemlerine bir alternatif olarak öne çıkan modern bir teorik çerçevedir. Bu kurama göre, sistemin temel hal elektronik enerjisi, yalnızca elektron yoğunluğunun uzaydaki dağılımı (ρ) ile belirlenebilir ve bu enerji $E(\rho)$ fonksiyonu ile tanımlanır. DFT'nin kuramsal temelleri ilk olarak 1964 yılında Hohenberg ve Kohn tarafından ortaya konmuş; böylece bir sistemin taban durum özelliklerinin yalnızca elektron yoğunluğu aracılığıyla belirlenebileceği gösterilmiştir (Mueller, 2001). Teorinin uygulanabilir bir forma kavuşması ise, Kohn ve Sham tarafından Hartree–Fock yaklaşımına benzer biçimde geliştirilen denklemler aracılığıyla mümkün olmuştur.

Bu tez kapsamında, 2-piridinkarbaldehitten yola çıkılarak elde edilen *N*-(piridin-2-ilmetilen)metanamin (L_1)'nin izotiyosiyanat ile 8 adet ve azit ile de 8 adet olmak üzere toplam 16 adet karışık ligatlı metal kompleksleri sentezlenmştir. Elde edilen komplekslerin yapıları X–ışını kırınım yöntemi (XRD) veya kütle spektroskopisi yöntemi kullanılarak aydınlatılmıştır.

Yapısal özellikleri belirlendikten sonra FT–IR spektrumları titreşim frekansları incelemek için yük transferi etkileşimleri ve elektronik geçişleri incelemek içinde UV–Vis spektrumları kullanılmıştır. Deneysel yöntemlerle detaylı analizi yapılan komplekslerin taban durumundaki yapısal ve titreşim özelliklerinin teorik analizi hibrit yoğunluk fonksiyonu teorisi (DFT) metodu kullanılarak yapılmıştır. Bunun yanı sıra, elektronik spektrumlar zamana bağlı DFT (TD–DFT) yöntemi ile sağlanmıştır. Hesaplanmış sonuçlar ve deneysel sonuçların birbirleriyle uyumu karşılaştırılmalı olarak verilmiştir. Sentezlenen komplekslerinin elektrik dipol momenti, kutuplanabilirlik, 1. ve 2. mertebeden lineer olmayan optik parametreler teorik olarak incelenerek, π-elektronlarının delokalize etkisi, substitute ve yük transferi gibi faktörlerin bu NLO özellikleri ile ilişkisi araştırılmıştır. Kompleks yapılar için sınır orbitallerdeki HOMO (en yüksek enerjili dolu moleküler orbital) ve LUMO (en düşük enerjili boş moleküler orbital) enerjileri hesaplanarak kaydedilmiştir. Bu enerjiler kullanılarak, HOMO–LUMO enerji aralığı, elektronegatiflik, kimyasal yumuşaklık ve kimyasal sertlik gibi moleküler reaktivite parametreleri elde edilmiştir. Bunlara ek olarak SWizard yazılımı yardımıyla moleküler orbitallerden elektronik geçişlere katkılar belirlenmiştir. Kompleks içinde, optimize yapılar üzerine doğal bağ orbitali (NBO) analizi yapılmıştır. Bu analiz, molekül içi ve moleküller arası bağların yanı sıra yük aktarımı ve konjugasyonla ilişkili etkileşimleri detaylı biçimde ortaya koymuştur. Ayrıca, azot, oksijen ve metal merkezleri üzerinde bulunan eşleşmemiş elektronlar arasındaki etkileşim enerjileri de net biçimde belirlenmiştir. Moleküler elektrostatik potansiyel (MEP) yüzeyler DFT metodu vasıtasıyla oluşturulmuştur. Bu komplekslerin α-glukozidaz inhibisyon etkileri incelenmiştir. Ayrıca inhibisyon mekanizmaları ve yapı aktivite ilişkilerini belirlemek amacıyla moleküler yerleştirme çalışmaları yapılmıştır.

2. LİTERATÜR ARAŞTIRMASI

Diyabet, Diyabet, kronik metabolik ve bulaşıcı olmayan bir hastalıktır, birden fazla etiyolojiye sahip dünyadaki ölüm nedenlerinde önde gelen beş hastalıktan biridir (Wild ve ark., 2004; Alam, 2012). Bu hastalık mutlak veya göreceli insülin eksikliği nedeniyle hiperglisemi ile karakterize edilen sosyoekonomik önemi olan bir klinik sendromdur (Aguwa, 2004; Balan ve ark., 2017). Diyabet, klinik olarak tip 1 ve tip 2 şeklinde iki ayrı gruba ayrılır. İlk olarak, tip 1 diyabetin ana nedeni β-hücrelerinin otoimmün yıkımıdır (Thomas ve Kay, 2000; Iwahashi ve ark., 1998). Bununla birlikte, tip 2 diyabet sınıfı, doğası gereği karmaşık olmasına rağmen bozulmuş insülin sekresyonu nedeniyle, insülin direnci, genetik ve çevresel faktörlerin bu tür diyabetle bağlantılı olduğu belirtilmektedir (Iwahashi ve ark., 1998; Kumari ve Jain, 2012; Tripath ve ark., 2014).

Diyabet hastalığını tedavi etmek için benimsenen stratejilerden biri bağırsakta karbonhidrat sindiriminin yavaşlatılması ve glikoz emiliminin geciktirilmesi ile ilişkili olarak α-amilaz karbonhidrat sindiren enzimler ve gastrointestinal sistemde α-glukozidaz gibi enzimlerin inhibisyonunu içerir (Rhabasa-Lhoret ve Chiasson, 2004).

α-Glukozidaz, glikoproteinlerin oligosakarit kısmını oluşturmak, polisakkaritleri ve glikokonjugatları metabolize etmek ve diğer temel biyolojik tanıma süreçleri için önemlidir. α-Glukozidaz, disakkaritleri ince bağırsakta monosakkaritlere dönüştüren bir enzimdir. Bu enzimi inhibe etmek sindirimi ve hem yemek sonrası hipergliseminin hem de aşırı insülin sekresyonu bastırılması sonucu karbonhidratların emilmesini geciktirir (Miyazaki ve ark., 2016). Yapılan çalışmalar α-glukozidaz aktivitesinin kontrolünün veya düzenlenmesinin metabolik bozuklukların neden olduğu hastalıkları, bağışıklık tepkileri, sinir hücrelerinin farklılaşması, tümör metastazları ve diyabet, kanser ve HIV gibi viral enfeksiyonları (Zhu ve ark., 2008; Naowaboot ve ark., 2009; Raju ve ark., 2010; Yao ve ark., 2010) önleyebildiğini göstermiştir (Bertozzi ve Kiessling, 2001; Horii ve ark., 1986; Floris ve ark., 2005; Fernandes ve ark., 1991; Ogawa ve ark., 2001). Bununla birlikte, iyi bilinen glukozidaz inhibitörlerinin çoğu şeker taklitleridir. Noninsülin bağımlı tip 2 diyabet (NIDDM,

T2DM) tedavisinde oral antidiyabetik ilaçlar (OAD)'ın etkisi α-glukozidaz aktivitesinin inhibisyonuna dayanmaktadır (Zheng ve Ma, 2015). α-Glukozidaz inhibitörleri oral antidiyabetik ilaç sınıfıdır. Yaygın olarak bilinen ve kullanılan dört tip α-glukozidaz inhibitörü (miglitol, vogliboz, genistein ve akarboz) Şekil 1'de verilmektedir (Miyazaki ve ark., 2016).

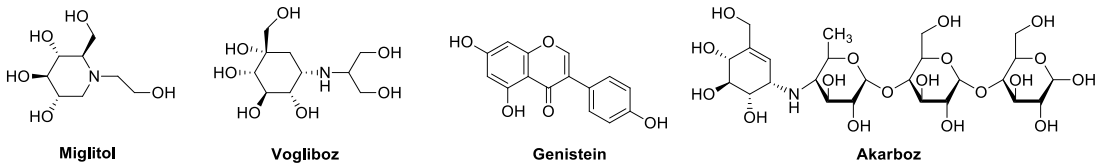

Şekil 2.1. Miglitol, vogliboz, akarboz ve genistein'in yapısı (Miyazaki ve ar., 2016)

Azometin (imin) grubu (-C=N-) önemli organik bileşik sınıflarından biridir ve bu bileşklerin biyolojik açıdan önemli olduğu ve tıbbi bileşiklerin tasarımı için kullanıldığı bilinmektedir (Khan ve ark., 2008; Iqbal ve ark., 2009). Bu grubu içeren moleküllerin antibakteriyel, antifungal, antimalaryal, anti-enflamatuar ve antipiretik gibi çeşitli farmakolojik aktivitelerinin yanı sıra boyalar, başlangıç materyalleri, organik sentez ara maddeleri, katalizörler ve polimer stabilizatörleri olarak kullanımları da bilinmektedir. Genel olarak bu moleküllerdeki ikame gruplarının değiştirilmesi bu özellikleri önemli şekilde etkileyebilmektedir. Ayrıca azometin grupları organometalik kimyada çok etkili ligantlar olarak bilinir. Çünkü metal iyonları ile şelatlar oluşturan imin grupları özellikle geçiş metal iyonlarıyla güçlü koordinasyon oluşturur (Ghosh ve ark., 2018; Xia ve ark., 2015; Sönmez ve ark., 2019). Bu nedenle, azometin grubu içeren koordinasyon bileşiklerinin sentezi potansiyel biyolojik aktiviteleri nedeniyle önemli derecede odak noktası olmuştur (da Silva ve ark., 1997; Al-Amiery, 2012).

Azometin grubu içeren ligant sistemlerinin antipatojenik aktiviteleri incelenmiş ve metal kompleksleri olarak uygulandığında bu bileşiklerin daha etkili olduğu bulunmuştur (Rodríguez-Argüelles ve ark., 2009). Benzer şekilde, bazı ilaçlar geçiş metalleri ile kompleks hale getirildiğinde daha fazla aktiviteye sahip olduğu belirlenmiştir (You ve ark., 2008). Bu nedenle, azometin grubu içeren metal komplekslerinin α-glukozidaz inhibisyonunu arttırabileceği düşünülmektedir.

2015 ve 2016 yıllarında Zheng ve Ma (Zheng ve Ma, 2015, 2016a) tarafından Şekil 2.2.'de gösterilen imin grubu içeren bazı Ag(I) kompleksleri sentezlenmiş ve α−glukozidaz enzim aktivitesine karşı IC_{50} değerleri 0,00431 μM ile 0,492 μM

arasında rapor edilmiştir. Bu çalışmada, Ag(I) iyonunun ve –NH grubunun inhibitör aktivite için çok önemli olduğu açık şekilde belirtilmiştir.

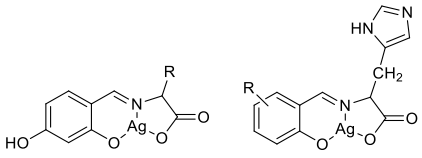

Şekil 2.2. İmin grubu içeren bazı Ag(I) komplekslerin yapısı (Zheng ve Ma, 2015, 2016a)

2017 yılında Balan ve arkadaşları (Balan ve ark., 2017) tarafından N_2O_2 içeren Zn kompleksinin *in vitro* α−amilaz ve α−glukozidaz inhibitör potansiyelinin değerlendirilmesi başlıklı çalışmada α−glukozidaz inhibisyonu için IC_{50} değeri 0,23 mM olarak bulunmuştur (Şekil 2.3.).

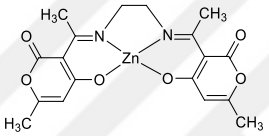

Şekil 2.3. N_2O_2 içeren Zn kompleksinin yapısı (Balan ve ark., 2017)

Şekil 2.4'te verilen bazı Co(II) ve etilendiamin komplekslerinin sentezi, spektral, elektrokimyasal analizi ve α−glukozidaz inhibisyonu çalışması, 2014 yılında Tripath ve arkadaşları (Tripath ve ark., 2014) tarafından yapılmıştır. Bu çalışmada elde edilen $[Co(en)_3]\cdot SO_4$ ve $[Co(en)_3]\cdot 2Cl$ kompleksleri için α−glukozidaz inhibisyon değerleri 927,89 µM ve 784,12 µM olarak rapor edilmiştir.

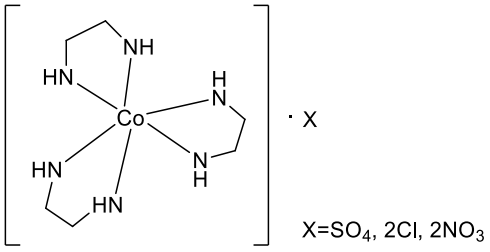

Şekil 2.4. $[Co(en)_3]\cdot SO_4$, $[Co(en)_3]\cdot 2Cl$ ve $[Co(en)_3]\cdot 2NO_3$ komplekslerinin yapısı (Tripath ve ark., 2014)

2017 yılında Philip ve arkadaşları (Philip ve ark., 2017) tarafından rapor edilen 6-metil-3-formil kromon türevi hidrazonların ve bunların metal(II) komplekslerinin tasarımı, sentezi, DNA bağlanması ve antidiyabetik aktivitesi çalışmasında, elde edilen metal(II) komplekslerinin yapısı Şekil 2.5.'te verilmiştir. Bu metal kompleksler

için α−glukozidaz enzimine karşı IC_{50} değerleri 0,1471 mM ile 0,2320 mM arasında elde edilmiştir. Bu sonuçlardan en iyi inhibe edici kompleks Cu(II) iyonu ile elde edilen yapı olduğu görülmektedir.

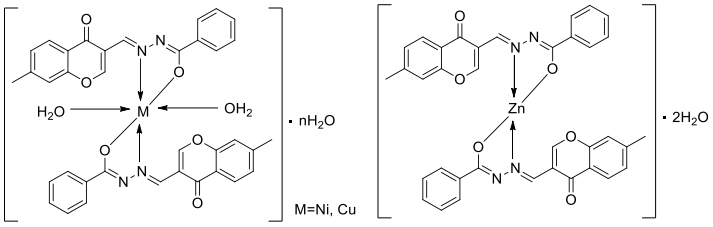

Şekil 2.5. 6-metil-3-formil kromon türevi hidrazonların metal(II) komplekslerinin yapısı (Philip ve ark., 2017)

İnsülin benzeri etkileri incelemek amacıyla, sıçan adipositlerinden FFA salınımının inhibisyonu literatürde yaygın bir deneysel yöntem olarak kullanılmaktadır (Yoshikawa ve ark., 2002). Piridin türevleri içeren bazı geçiş metali komplekslerinde, IC_{50} değerleri nikel, mangan, kobalt ve krom kompleksleri için tespit edilememiş; buna karşın diğer metallerle oluşturulan komplekslerde bu değerler 0,92 mM ile 0,22 mM aralığında hesaplanmıştır (Yoshikawa vd., 2002; Yasumatsu vd., 2007; Yoshikawa vd., 2009). Ayrıca, bu komplekslerin dışında, Wang ve arkadaşları tarafından 2004 yılında yapılan çalışmada Mg^{+2}, Mn^{+2}, Ca^{+2}, Ni^{+2}, V^{+5}, V^{+4}, Fe^{+2}, Zn^{+2}, Cu^{+2}, Hg^{+2}, Ag^{+} ve Pb^{+2} gibi çeşitli metal iyonlarının α–glukozidaz üzerine etkisi rapor edilmiştir (Wang ve ark., 2004). Bu raporda, en iyi inhibe eden 2,28 μM değerinde Cu^{+2} iyonu iken en az inhibe eden 217 μM değerinde Fe^{+2} iyonu olduğu belirtilmektedir. Ayrıca, Zn^{+2} ve V^{+4} iyonları için de 99,3 μM ve 44,8 μM değerleri verilmiştir. Bu bağlamda, seçilen bazı metallerin yer alacağı ve azot içeren heterosiklik yapılı (*N*-(piridin-2-ilmetilen)metan/etan-amin, 2,2'-bipiridil, 1,10-fenantrolin, gibi) farklı koordinasyon komplekslerde α–glukozidaz aktivitelerin ve sitotoksisite özelliklerinin incelenmesinin yanı sıra elektronik özelliklerinin deneysel ve kuramsal olarak araştırılması da yapı-aktivite ilişkilerinin ve inhibisyon mekanizmalarının ortaya çıkarılması açısından büyük önem taşımaktadır.

Avcı ve çalışma arkadaşları tarafından sentezlenen 6−metilpikolinik asit içeren karışık ligantlı farklı metal komplekslerin α−glukozidaz enzim aktivite çalışmaları sonucunda IC_{50} değerleri 0,161 μM ile >600 μM (Avcı ve ark., 2018, 2019a, 2019b, 2019c, 2020a, 2020b, 2021) arasında değişen değerler olarak bulunmuştur. Elde edilen bulgular, α-glukozidaz enzimi üzerinde en güçlü inhibitör etkinin Hg(II) metal tuzu ile oluşturulan

komplekslerde gözlendiğini, ayrıca Zn(II), Cr(III), Fe(II), Cd(II) ve Cu(II) komplekslerinin de enzimi mikromolar düzeyde inhibe edebildiğini ortaya koymuştur. Bazı kompleks yapılar ve IC_{50} değerleri Şekil 2.6.'da verilmiştir.

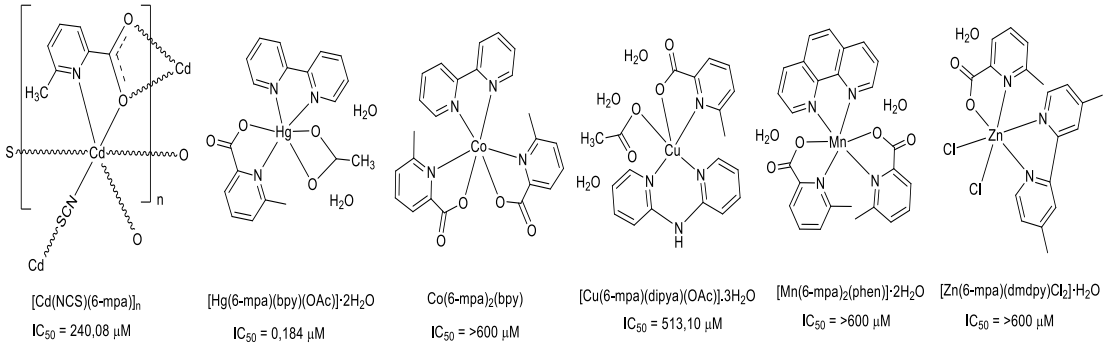

Şekil 2.6. 6−metilpikolinik asit içeren karışık ligantlı bazı metal komplekslerin yapısı ve IC_{50} değerleri (Avcı ve ark., 2018, 2019b, 2019c, 2020a, 2020b)

Şekil 2.6.'da verilen Hg kompleksinin enzim inhibisyonu için elde edilen IC_{50} değeri 0,184±0,015 μM iken MTT (3-(4,5-Dimetil-2-tiyazolil)-2,5-difenil-2H-tetrazolyum bromür) metodu ile yapılan sitotoksisite çalışmasındaki IC_{50} değeri 24,141±1,039 μM olarak bulunmuştur. Bu sonuca göre, inhibisyon konsantrasyonu sitotoksik etki gösterdiği konsantrasyondan 131,20 kat daha düşüktür ve bu değerler dikkate alındığında Hg kompleksinin sağlıklı hücre üzerindeki toksik etkisinin ihmal edilebilir seviyede olduğu söylenebilir (Avcı ve ark., 2019b). Bu nedenle, ağır metal olarak bilinen civa ve kadmiyumun kompleks yapı içerisinde canlı hücre üzerindeki toksik etkilerinin ihmal edilebilir seviyede olması α–glukozidaz inhibitörü olarak kullanımının uygun olacağı düşünülebilir.

Yukarıda verilen çalışmalarda gerek heteroatom içeren ligantların metal komplekslerinin gerekse de azometin grubu içeren komplekslerin α-glukozidaz enzimini inhibe ettiği görülmüştür. Bu doğrultuda, heteroatom içeren ligantlara ait metal komplekslerinin, biyolojik sistemlerde yer alan enzim-substrat kompleksleriyle yapısal, spektroskopik ve katalitik benzerlikler taşıdığı bilimsel çalışmalarla ortaya konmuştur (Constable ve Steel, 1989; Adams ve ark., 1990; Driessen ve ark., 1994; Gollapalli ve ark., 2019; Ghani, 2015). Malzeme ve tıbbi kimyadaki birçok uygulama nedeniyle, azot içeren heterosiklik yapılar (*N*-(piridin-2-ilmetilen)metan/etan-amin, 2,2'-bipiridil, 1,10-fenantrolin, gibi) farklı koordinasyon komplekslerinin sentezi ve dizaynı, kataliz, doğrusal olmayan optik, luminesans gibi fizikokimyasal özelliklerin araştırılması, biyolojik ve farmasötik aktivitelerin incelenmesi bakımından büyük

önem taşımaktadır (Demadis ve Katarachia, 2004; Monot ve ark., 2008; Umeda ve ark., 2010; Saito ve ark., 1972; Amani ve ark., 2007; Mobin ve ark., 2016; Tamer ve ark., 2018; Zhu Li-N ve ark., 2008; Yang ve ark., 2016; Barquín ve ark., 2010; Santos ve ark., 2018). Literatür ve önceki çalışmalardan elde edilen sonuçlar incelendiğinde Cu, Zn, Cd, Hg ve Ag gibi metalleri içeren komplekslerin α–glukozidaz inhibitör aktivitelerinin mikromolar seviyesinde olmasından dolayı tez çalışmasında bu metal tuzları seçilmiştir. Ayrıca metil, etil gibi alkil gruplarının indüktif olarak elektron desteği sağlamalarının hem kompleks oluşumunda hem de biyolojik aktiviteye katkı sağlayacağı düşünülmektedir. Ayrıca metal iyonları, heterosiklik yapılar ve azometin gruplarını içeren kompleks yapıların enzim aktif bölgesi ile etkileşerek inhibisyonu arttıracağı, ayrıca düşük sitotoksiteye sahip olacağı öngörülmektedir.

Bilim ve teknolojideki ilerlemeler açısından, kuantum kimyasal verilerin deneysel bulgularla ilişkilendirilmesi ve deneysel olarak doğrudan ölçülebilen niceliklerin kuramsal yöntemlerle hesaplanması ilgi çekmektedir. Son zamanlarda yapılan çalışmalar, kuramsal ve deneysel araştırmaların birlikte ele alındığını ve yoğunluk fonksiyonel teorisi (DFT) metotlarının yoğun bir şekilde kullanıldığını göstermektedir (Castet ve ark., 2013; Clays ve Coe, 2003; Kukovec ve ark., 2013; Altürk ve ark., 2016; Avcı ve ark., 2018). Buda yeni malzemelerin hem deneysel hem de kuramsal olarak incelenmesine olanak sağlanmaktadır. Ayrıca teorik yöntemlerin kullanılmasıyla elde edilecek bileşiklerin farklı moleküler özelliklerin (mikroskobik boyutta doğrusal olmayan optik gibi) incelenmesine imkan verecektir. Bu durum, deneysel çalışma yapmanın mümkün olmadığı durumlarda DFT yöntemleri kullanılarak ikinci ve üçüncü mertebeden NLO parametrelerinin kuramsal olarak incelenmesi, birinci ve ikinci mertebeden statik/dinamik yüksek kutuplanabilirlik (β ve γ) değerlerinin hesaplanmasıyla mümkün olmaktadır. Bununla birlikte, DFT ve TD-DFT yöntemleri kullanılarak temel ve uyarılmış hal özelliklerinin belirlenmesi, atom ve molekül fiziği, katıhal fiziğinin yanı sıra malzeme ve kimya gibi farklı bilim alanlarında da kullanılmaktadır.

3. SENTEZ, KRİSTAL YAPILAR VE DFT HESAPLAMALARI: İZOTİYOSİYANAT İÇEREN *N*-(PİRİDİN-2-İLMETİLEN)METANAMİN YENİ MN(II), CO(II) VE Nİ(II) KOMPLEKSLERİNİN UMUT VADEDEN OPTİK MALZEMELER OLARAK İNCELENMESİ

Bu bölüm Ek A'da verilen "Avcı, D., Özge, Ö., Başoğlu, A., Sönmez, F., Tamer, Ö., Dege, N., & Atalay, Y. (2023). Synthesis, crystal structures, and DFT calculations: novel Mn (II), Co (II) and Ni (II) complexes of *N*-(pyridin-2-ylmethylene) methanamine with isothiocyanate as promising optical materials. Optical and Quantum Electronics, 55, 408." künyeli makaleden oluşturulmuştur.

Bu çalışmada, sentezlenen komplekslerin optik özelliklerini incelemek amacıyla, elektronik özelliklerine dair yapılan deneysel ve teorik araştırmalar, yapı–özellik ilişkilerinin ortaya konulması açısından büyük önem taşımaktadır.

Optik parametreleri incelemek amacıyla, 2-piridin karboksaldehit ile metilaminin kondenzasyon reaksiyonu sonucu Schiff bazı olarak elde edilen *N*-(piridin-2-ilmetilen)metanamin (L_1) ve izotiyosiyanat içeren yeni metal kompleksleri {$[Mn(L_1)_2(NCS)_2]$ (**1**), $[Co(L_1)_2(NCS)_2]$ (**2**), $[Ni(L_1)_2(NCS)_2]$ (**3**)} sentezlenmiştir (Avcı ve ark., 2023). Kompleks **1**, **2** ve **3**'ün spektral özellikleri FT–IR ve UV–Vis spektroskopisi ile incelenmiş, yapısal karakterizasyonları ise XRD (kompleks **1** ve **2** için) ve LC-HRMS (kompleks **3** için) ile gerçekleştirilmiştir. Ayrıca, kompleksler **1** ve **2** için moleküller arası etkileşimleri tanımlamak amacıyla Hirshfeld yüzey analizi yapılmıştır. Kompleks **1–3'**ün optimum yapıları, spektral ve doğrusal olmayan optik parametreleri ile elektronik geçişlerdeki önemli katkıları belirlemek üzere DFT/TD-DFT yöntemleri kapsamında CAM-B3LYP ve ωB97XD/6–311+G(d,p)//LanL2DZ düzeylerinde teorik hesaplamalar gerçekleştirilmiştir. Orta IR bölgesinde kompleksler **1**–**3** için ortalama kırılma indisi/kutuplanabilirlik değerleri sırasıyla $1{,}63/5{,}87\times10^{-24}$ esu, $1{,}46/4{,}80\times10^{-24}$ esu ve $1{,}50/4{,}48\times10^{-24}$ esu olarak bulunmuştur. UV–Vis soğurma parametreleri dikkate alınarak, metanoldeki kompleks **1**–**3** için deneysel kırılma indisi, optik bant aralığı, kutuplanabilirlik, optik iletkenlik ve üçüncü dereceden doğrusal olmayan optik duyarlılık parametreleri incelenmiştir. 4,68, 4,21 ve 5,25 eV foton enerjilerinde maksimum üçüncü derece NLO duyarlılık değerleri sırasıyla $51{,}65 \times 10^{-13}$, $51{,}42\times10^{-13}$ ve $51{,}42\times10^{-13}$ esu olarak elde edilmiştir. Kısaca, sentezlenen

kompleksler için yapı–özellik ilişkisi bağlamında detaylı deneysel ve teorik spektral ve optik parametreler araştırılmıştır. Elde edilen NLO sonuçlar, kompleks **1**'in gelecekte veri depolama, telekomünikasyon, lazer teknolojisi vb. alanlarda NLO malzeme adayı olabileceğini göstermektedir.

4. İZOTİYOSİYANAT İÇEREN SCHİFF BAZI METAL KOMPLEKSLERİ ÜZERİNE SENTEZ, DFT HESAPLAMALARI, A-GLUKOZİDAZ İNHİBİTÖR AKTİVİTESİ VE YERLEŞTİRME ÇALIŞMALARI

Bu bölüm Ek B'de verilen "Özge, Ö., Avcı, D., Sönmez, F., Tamer, Ö., Dege, N., Başoğlu, A., Atalay, Y., & Zengin Kurt, B. (2023). Synthesis, DFT calculations, α-glucosidase inhibitor activity, and docking studies on Schiff base metal complexes containing isothiocyanate. Applied Organometallic Chemistry, 37(5), e7084." künyeli makaleden oluşturulmuştur.

Bu çalışma, mevcut bileşiklerden daha etkili α-glukozidaz inhibitörleri tasarlamak ve sentezlemek amacıyla gerçekleştirilmiştir. Bu bağlamda, sentezlenen komplekslerin α-glukozidaz aktivitelerinin incelenebilmesi için elektronik özelliklerine yönelik deneysel ve hesaplamalı araştırmalar, yapı-aktivite ilişkilerinin ve inhibisyon mekanizmalarının ortaya konulması açısından büyük önem taşımaktadır. Bu kapsamda, *N*-(piridin-2-ilmetilen)metanamin ve izotiyosiyanat içeren yeni bir metal kompleks serisi (**4–8**) sentezlenmiştir (Özge ve ark., 2023). Kristal yapısı XRD yöntemi ile tanımlanan Cd (II) kompleksi (**4**) haricinde, diğer komplekslerin (**5–8**) yapıları LC-HRMS ve FT–IR spektrumlarıyla karakterize edilmiştir. Kompleks **4–8**'in α-glukozidaz inhibitör aktiviteleri belirlenmiştir. Ayrıca, komplekslerin elektronik spektral davranışları deneysel ve teorik olarak detaylı şekilde incelenmiştir. Son olarak, ligantların hedef proteinle olan etkileşimlerini belirlemek ve *in vitro* α-glukozidaz aktivite sonuçlarını yorumlayabilmek amacıyla yerleştirme (docking) analizleri gerçekleştirilmiştir.

Diyabet, 21. yüzyılın en hızlı büyüyen küresel sağlık krizlerinden biridir. Diyabet tedavisinde kullanılan mevcut terapötik yaklaşımlardan biri, α-glukozidaz gibi karbonhidrat hidrolizleyen enzimlerin baskılanmasına dayanmaktadır. Bu bağlamda, α-glukozidaz inhibitörleri, diyabetin tedavisinde ve önlenmesinde önemli bir rol oynamaktadır. Bu nedenle, izotiyosiyanat içeren yeni Schiff bazı kompleksleri {$[Cd(L_1)_2(NCS)_2]$ (**4**), $[Zn(L_1)_2(NCS)_2]$ (**5**), $[Cu(L_1)_2(NCS)_2]$ (**6**), $[Ag(L_1)(NCS)_2]$ (**7**), $[Hg(L_1)_2(NCS)Cl]$ (**8**); L_1: *N*-(piridin-2-ilmetilen)metanamin} sentezlenmiş ve α-glukozidaz inhibitör potansiyelleri araştırılmıştır. Kompleksler **4–8**'in IC_{50} değerleri

0,2376 ± 0,82 ile 251,403 ± 2,54 μM arasında bulunmuştur. Bu kompleksler arasında, kompleks **8** en yüksek α-glukozidaz inhibitör özelliğine sahiptir. Ayrıca, komplekslerin optimum yapılarının, spektral özelliklerinin, lineer ve doğrusal olmayan optik (NLO) özelliklerinin elde edilebilmesi amacıyla CAM-B3LYP ve ωB97XD/6–311+G (d,p) // LanL2DZ düzeylerinde TD-DFT/DFT hesaplamaları yapılmıştır. Elde edilen teorik NLO sonuçlarına göre, kompleks **6** mikroskobik doğrusal olmayan optik özellikler açısından güçlü bir gösterge niteliğindedir.

5. YENİ SCHİFF BAZI-AZİD METAL KOMPLEKSLERİ: SENTEZ, SPEKTRAL, DOĞRUSAL OLMAYAN OPTİK VE DFT ÇALIŞMALARI

Bu bölüm Ek C'de verilen "Avcı, D., Özge, Ö., Sönmez, F., Başoğlu, A., Tamer, Ö., & Atalay, Y. (2024). Novel schiff base-azide metal complexes: Synthesis, spectral, nonlinear optics, and DFT studies. Materials Science in Semiconductor Processing, 179, 108523." künyeli makaleden oluşturulmuştur.

Kullanışlı NLO (doğrusal olmayan optik) materyaller geliştirmek ve üretmek amacıyla, *N*-(piridin-2-ilmetilen)metanamin (L_1) ve azido ($-N_3$) ligantlarını içeren yeni metal kompleksleri (**9–11**) sentezlenmiştir (Avcı ve ark., 2024a). Bu kompleks yapıların (**9–11**) karakterizasyonları, kütle spektrometrisi (LC-HRMS), toz XRD ve FT-IR spektrumları ile gerçekleştirilmiştir. Sentezlenen komplekslerin teorik mikroskobik NLO ve elektronik özellikleri deneysel ve DFT yöntemleri kullanılarak incelenmiş ve yapı-aktivite ilişkileri belirlenmiştir. Ayrıca, koordinasyon bileşiklerinin yapı-özellik ilişkileri DFT/ωB97XD ve DFT/CAM-B3LYP fonksiyonelleri kullanılarak kapsamlı bir şekilde araştırılmıştır.

Doğrusal olmayan optik (NLO) tabanlı teknolojilerin geliştirilmesi amacıyla, güncel araştırmalar koordinasyon malzemelerinin tasarımı ve sentezine odaklanmaktadır. Bu bağlamda, spektral ve teorik doğrusal optik (LO)/doğrusal olmayan optik (NLO) davranışları incelemek üzere azid içeren yeni metal kompleksleri {$[Mn(L_1)_2(N_3)_2]$, (**9**); $[Ni(L_1)_2(N_3)]$, (**10**); $[Co_2(L_1)_2(N_3)_2]\cdot 2H_2O$, (**11**); L_1: *N*-(piridin-2-ilmetilen)metanamin} sentezlenmiştir. Kompleks **9–11**'in titreşimsel ve elektronik spektral özellikleri FT–IR ve UV–Vis spektrumları ile incelenmiştir. Komplekslerin merkez metal iyonuna ve koordinasyon geometrilerine bağlı olarak mikroskobik statik doğrusal olmayan davranışları, CAM-B3LYP/ ve ωB97XD/6–311+G(d,p)//LanL2DZ düzeylerinde yoğunluk fonksiyonel teorisi (DFT) kullanılarak araştırılmıştır. Ayrıca, aynı düzeyde zaman-bağımlı yoğunluk fonksiyonel teorisi (TD-DFT/DFT) ile kompleks **9–11**'in titreşimsel ve elektronik özellikleri analiz edilmiştir. Bununla birlikte, kompleks **9–11** için doğrusal optik, ikinci ve üçüncü dereceden doğrusal olmayan optik duyarlılık olarak bilinen teorik $\chi^{(1)}$, $\chi^{(2)}$ ve $\chi^{(3)}$ parametreleri ile doğrusal, ikinci ve üçüncü dereceden polarizasyon parametreleri ($P^{(1)}$, $P^{(2)}$ ve $P^{(3)}$) incelenmiştir.

CAM-B3LYP düzeyinde elde edilen en yüksek <β(0; 0,0)> değeri, kompleks **10** için $262{,}55\times10^{-30}$ esu olarak bulunmuş olup, bu değer üre ile karşılaştırıldığında sırasıyla 820,5 ve 2019,6 kat daha büyüktür (üre için <β>: $0{,}32\times10^{-30}$ esu ve $0{,}130\times10^{-30}$ esu). <γ(0; 0,0,0)> sonuçları, CAM-B3LYP düzeyinde $2216{,}40\times10^{-36}$ esu ile kompleks **9**'un en yüksek değeri verdiğini göstermekte olup, bu değer pNA (15×10^{-36} esu) ve üre (7×10^{-36} esu) ile karşılaştırıldığında sırasıyla 47,76 ve 316,63 kat daha yüksektir. Kompleksler **10** ve **9** sırasıyla umut verici mikroskobik ikinci ve üçüncü dereceden NLO özellikler sergilemiştir. Bu bulgulardan, optoelektronik ve telekomünikasyon alanlarında uygulama potansiyeli olan NLO malzemelerine dair kayda değer bilgileri içerdiği sonucuna varılmıştır.

6. YENİ AZİD METAL KOMPLEKSLERİ ÜZERİNE İN VİTRO A-GLUKOZİDAZ, MOLEKÜLER YERLEŞTİRME VE YOĞUNLUK FONKSİYON TEORİSİ ÇALIŞMALARI

Bu bölüm Ek D'de verilen "Avcı, D., Özge, Ö., Sönmez, F., Tamer, Ö., Başoğlu, A., Atalay, Y., & Zengin Kurt, B. (2024). In vitro α-glucosidase, docking and density functional theory studies on novel azide metal complexes. Future Medicinal Chemistry, 16(11), 1109–1125." künyeli makaleden oluşturulmuştur.

Azometin ve azid grupları, koordinasyon kimyasının tıbbi uygulamalarında oldukça etkili ligantlar olarak kabul edilmektedir (Montazerozohori ve ark., 2015; Thamilarasan ve ark.,2015; Balan ve ark., 2017; Miyazaki ve ark., 2016) Bu ligantlar, tek dişli, iki dişli veya çok dişli komplekslerin oluşumuna katılabilecek yüksek derecede koordinasyon esnekliğine sahiptir. Ayrıca, potansiyel biyolojik aktivitelerde önemli roller üstlendikleri iyi bilinmektedir. Bu nedenle, hedef komplekslerin sentezinde bu ligantlar tercih edilmiştir. Bu çalışmada, daha güçlü α-glukozidaz inhibitörleri tasarlamak ve geliştirmek amacıyla, *N*-(piridin-2-ilmetilen)metanamin (L_1) ve azid (N_3^-) ligantlarını içeren beş yeni metal kompleksi (**12–16**) sentezlenmiştir (Avcı ve ark., 2024b). Bu komplekslerin yapıları ^1H ve ^{13}C NMR (Cu içeren kompleks **12** hariç), kütle (LC-HRMS) ve FTIR spektroskopi yöntemleri ile belirlenmiştir. Komplekslerin α-glukozidaz üzerindeki IC_{50} değerleri elde edilmiştir. Sentezlenen kompleksler üzerinde yapılan *in vitro* α-glukozidaz çalışmaları ve bunların elektronik özelliklerinin deneysel ve DFT yöntemleriyle incelenmesi, yapı–aktivite ilişkilerinin belirlenmesinde önemli rol oynamaktadır. Ayrıca, hedef protein ile ligantlar arasındaki etkileşimleri belirlemek ve aktivite sonuçlarını yorumlamak amacıyla moleküler kenetleme (doking) çalışmaları gerçekleştirilmiştir. Bunun yanı sıra, DFT/ωB97XD ve DFT/CAM-B3LYP fonksiyonellerinin özgün özellikleri ve yetenekleri, bu yöntemlerin metal komplekslerinin yapı–özellik ilişkileri bağlamında davranışlarını daha derinlemesine anlamada fayda sağlamasını mümkün kılmaktadır.

Bu çalışmada sentezlenen metal komplekslerinin (**12–16**) tip 2 diyabet tedavisinde α-glukozidaz inhibitörü olarak kullanılabilme potansiyelleri araştırılmıştır. Bu komplekslerin hedef proteinle etkileşimleri moleküler kenetleme (doking),

çalışmasıyla ve titreşimsel, elektronik ve doğrusal olmayan optik özellikleri yoğunluk fonksiyonel teorisi (DFT) çalışmalarıyla araştırılmıştır. Kompleksler arasında, Hg iyonu içeren kompleks **13** (IC_{50} = 0,2802 ± 0,62 μM), en yüksek α-glukozidaz inhibitör etkisini göstermiştir. Öte yandan, Cu ve Ag iyonları içeren komplekslerde de kayda değer sonuçlar elde edilmiştir. *In vitro* ve doking analiz sonuçlarına göre, kompleks **13** potansiyel bir alternatif anti-diyabetik inhibitör adayı olabilme potansiyeline sahiptir.

7. SONUÇ VE ÖNERİLER

Yüksek derecede koordinasyon esnekliğine sahip Schiff baz, izotiyosiyanat ve azid içeren koordinasyon bileşiklerin tıbbi ve doğrusal olmayan optik uygulamalarında etkili ligantlar olduğu bilinmektedir. Ayrıca, potansiyel biyolojik aktivitelerde önemli roller üstlendikleri dikkate alınarak, bu çalışma mevcut bileşiklerden daha etkili α-glukozidaz inhibitörleri tasarlamak ve sentezlemek amacıyla gerçekleştirilmiştir. Bu bağlamda, sentezlenen komplekslerin α-glukozidaz aktivitelerinin incelenebilmesi için elektronik özelliklerine yönelik deneysel ve hesaplamalı araştırmalar, yapı-aktivite ilişkilerinin ve inhibisyon mekanizmalarının ortaya konulması açısından büyük önem taşımaktadır. Ayrıca teorik yöntemlerin kullanılmasıyla elde edilen bileşiklerin farklı moleküler özelliklerinin (mikroskobik boyutta doğrusal olmayan optik gibi) incelenmesine olanak sağlanmaktadır. Bu durum, deneysel çalışma yapmanın mümkün olmadığı durumlarda DFT yöntemleri kullanılarak ikinci ve üçüncü mertebeden NLO parametrelerinin kuramsal olarak incelenmesi, birinci ve ikinci mertebeden statik yüksek kutuplanabilirlik (β ve γ) değerlerinin hesaplanmasıyla mümkün olmaktadır. Bununla birlikte, DFT ve TD-DFT yöntemleri kullanılarak temel ve uyarılmış hal özelliklerinin belirlenmesi, atom ve molekül fiziği, katıhal fiziğinin yanı sıra malzeme ve kimya bilimi gibi farklı alanlarda da kullanılmaktadır. Bu kapsamda, *N*-(piridin-2-ilmetilen)metanamin (L_1), izotiyosiyanat ve azid içeren yeni metal kompleksler serisi (**1–16**) sentezlenmiştir. Bu komplekslerden 3 tanesi {$[Mn(L_1)_2(NCS)_2]$, (**1**), $[Co(L_1)_2(NCS)_2]$, (**2**) ve $[Cd(L_1)_2(NCS)_2]$, (**4**)} tek kristal yapıda elde edilmiş olup XRD yöntemi ile yapıları tanımlanmıştır. Diğer 13 kompleksin (**3**,**5–16**) yapıları kütle (LC-HRMS) ve FT–IR spektrumlarıyla karakterize edilmiştir.

Kompleksler **1–3** için UV–Vis bölgesinde metanol ortamında elde edilen deneysel üçüncü derece doğrusal olmayan optik (NLO) duyarlılık ($\chi^{(3)}$) sonuçları; sırasıyla 4,68, 4,21 ve 5,25 eV foton enerjilerinde maksimum zirvelerde yaklaşık olarak aynı değerde bulunmuştur ($\chi^{(3)}$ = 51,65 × 10^{-13}, 51,42 × 10^{-13} ve 51,42 × 10^{-13} esu) (Ek A). Bu çalışmada Z-tarama (Z-scan) tekniği ile üçüncü derece NLO duyarlılığı, doğrusal olmayan kırılma indisi ve soğurma parametreleri ölçülememiş olsa da, teorik ve

deneysel olarak elde edilen üçüncü derece NLO parametreleri, kompleks **1**'in optoelektronik cihazların geliştirilmesinde kullanılabileceğini göstermektedir.

Kompleksler **4-8**'de, α-glukozidaza karşı IC_{50} değeri 5,618 μM olan kompleks **6**'nın, β ve γ parametreleri dikkate alındığında umut verici bir NLO (nonlineer optik) materyal adayı olarak değerlendirilebileceği öngörülmüştür. Bu çalışmada, L_1 ve NCS ligantlarının metal kompleksleri bağlamında*; in vitro*/doking ve NLO sonuçları dikkate alındığında, kompleks **8**'in (IC_{50}=0,2376 μM) tip 2 Diyabet (T2DM) için alternatif bir ilaç adayı, kompleks **6**'nın ise NLO materyal adayına sahip yapılar olduğu belirtilebilir.

CAM-B3LYP düzeyine göre, χ, η ve ω değerleri küçükten büyüğe şu sırayla elde edilmiştir: Kompleks **11** < kompleks **10** < kompleks **9**. En küçük değerler, köprülü bir yapıya sahip olan kompleks **11**'de elde edilmiştir. Polarizasyon eğilimindeki artış ise şu sırayla gözlemlenmiştir: Kompleks **10** < kompleks **9** < kompleks **11**. Kompleksler arasında, en yüksek <β(0; 0,0)> değeri kompleks **10**'da gözlenmiştir. CAM-B3LYP düzeyine göre bu değer ($262,55\times10^{-30}$ esu), üre sonuçlarına göre ($0,32\times10^{-30}$ esu ve $0,130\times10^{-30}$ esu) sırasıyla 820,5 ve 2019,6 kat, pNA sonucuna göre ise ($9,2\times10^{-30}$ esu) 28,5 kat daha büyüktür. Bu parametrenin yüksek olmasının, Ni iyonu içeren kompleks **10**'un simetri merkezi olmayan (non-centrosymmetric) yapısına bağlı olduğu düşünülebilir. Kompleks **9** için en yüksek <γ(0;0,0,0)> değeri, CAM-B3LYP düzeyine göre $2216,40\times10^{-36}$ esu olarak elde edilmiş olup, bu değer pNA'ya (15×10^{-36} esu) göre 147,76 kat, üreye (7×10^{-36} esu) göre ise 316,63 kat daha büyüktür. β ve γ sonuçları, sırasıyla kompleks **10** ve **9**'un mikroskobik ikinci ve üçüncü dereceden NLO özellikler açısından oldukça etkili olduğunu göstermektedir. Bu sonuçların $\chi^{(2)}$ ve $\chi^{(3)}$ parametrelerinin sonuçlarıyla da desteklendiği görülmektedir. Lineer azid anyonunun, kompleks **10**'un geometrisi, γ işareti ve büyüklüğü üzerinde dramatik bir etkisi olduğu gözlemlenmiştir.

Kompleksler **12–16** için IC_{50} değerleri 0,2802 ± 0.62 ile 420,88 ± 1.42 μM aralığında elde edilmiştir. Kompleks **13**, en yüksek α-glukozidaz inhibitör aktivitesini gösterirken, kompleks 14 en düşük inhibitör aktiviteye sahiptir. Ayrıca, kompleks **12** (1,562 ± 0,83 μM) ve kompleks **15** (1,274 ± 0,32 μM)'de anlamlı IC_{50} değerlerine sahiptir. Bu sonuçlar, reseptör-ligant etkileşimlerini ortaya koyan doking çalışmaları ile desteklenmiştir. Ek olarak, toplam 50 ns'lik moleküler dinamik (MD) simülasyonları ile yapılan çalışmalarda, bileşiklerin MD simülasyonu boyunca kararlı

olduğu gösterilmiştir. Kompleks **15** ve kompleks **12**, α-glukozidaza karşı anlamlı IC_{50} değerleri gösterirken, aynı zamanda β ve γ sonuçları, sırasıyla bu komplekslerin mikroskobik ikinci ve üçüncü dereceden NLO özellikler açısından oldukça etkili olduğunu göstermektedir. Sonuç olarak, Schiff baz–azid metal kompleksleri arasında, kompleks **13**'ün Tip-2 diyabet için alternatif bir anti-diyabetik inhibitör olabileceği, kompleks **12** ve kompleks **15**'in ise NLO materyal adayları olarak önerilebileceği düşünülmektedir.

Moleküler doking ve *in vitro* sonuçlarına göre, yapı–aktivite ilişkileri dikkate alındığında Cu, Ag ve Hg içeren metal komplekslerin α-glukozidaza karşı iyi inhibitör özellik sergilediği sonucuna varılmıştır. Yüksek inhibe özelliği gösteren bu komplekslerin ve daha fazlasının ileri araştırmalar ve *in vivo* çalışmaları için çok disiplinli yeni akademik iş birliğine katkı sağlayacağı düşünülmektedir.

Bu tez çalışması kapsamında 4 adet SCI kapsamında makale yayımlanarak çıktıları literatüre kazandırılarak bilim dünyası ile paylaşılmıştır.

KAYNAKLAR

Abu-dief, A. M., & Mohamed, I. M. A. (2015). A review on versatile applications of transition metal complexes incorporating Schiff bases. *Beni-Suef University Journal of Basic and Applied Sciences*, 4(2), 119–133. https://doi.org/10.1016/j.bjbas.2015.05.004

Adams, H., Bailey, N.A., Crane, J.D., Fenton, D.E., Latour, J.M., Williams, J.M. (1990). "Manganese(II) and iron(III) complexes of the tridentate ligands bis(benzimidazol-2-ylmethyl)-amine (L^1) and -methylamine (L^2). Crystal structures of $[MnL^1(CH_3CO_2)_2]$, $[FeL^2Cl_3]$, and $[Fe_2L^1{}_2(\mu\text{-}O)\{\mu\text{-}(CH_3)_3CCO_2\}_2][ClO_4]_2$" , *Journal of the Chemical Society, Dalton Transactions*, 5, 1727-1735. https://doi.org/10.1039/DT9900001727

Alam, E.A. (2012). "Initiation of Pharmaceutical Factories depending on more Application of Biotechnology on some Medicinal Plants Review Article (In Vitro Production of some Antioxidant, Analgesic, Antibacterial, Antidiabetic agents)", *Research Journal of Recent Sciences*, 1(ISC-2011), 398-404. E-ISSN : 2277 - 2502

Al-Amiery, A. A. (2012). "Synthesis and antioxidant, antimicrobial evaluation, DFT studies of novel metal complexes derivate from Schiff base", *Research on Chemical Intermediates*, 38(3), 745-759. https://doi.org/10.1007/s11164-011-0414-8

Altürk, S., Avcı, D., Tamer, Ö., Atalay, Y., Şahin, O. (2016). "A cobalt (II) complex with 6−methylpicolinate: Synthesis, characterization, second− and third−order nonlinear optical properties, and DFT calculations", *Journal of Physics and Chemistry of Solids*, 98, 71-80. https://doi.org/10.1016/j.jpcs.2016.06.008

Amani, V., Safari, N., Khavasi, H.R. (2007). "Synthesis, characterization and crystal structure determination of iron(III) hetero-ligand complexes containing 2,2'-bipyridine, 5,5'-dimethyl-2,2'-bipyridine and chloride, $[Fe(bipy)Cl_4][bipy{\cdot}H]$ and $[Fe(dmbipy)_2Cl_2][FeCl_4]$", *Polyhedron* 26, 4257-4262. https://doi.org/10.1016/j.poly.2007.05.050

Ambike, V., Adsule, S., Ahmed, F., Wang, Z., Afrasiabi, Z., Sinn, E., Sarkar, F., & Padhye, S. (2007). Copper conjugates of nimesulide Schiff bases targeting VEGF, COX and Bcl-2 in pancreatic cancer cells. *Journal of Inorganic Biochemistry*, 101(10), 1517–1524. https://doi.org/10.1016/j.jinorgbio.2007.06.028

Avcı, D., Altürk, S., Sönmez, F., Tamer, Ö., Başoğlu, A., Atalay, Y., Kurt, B.Z., Dege, N. (2018). "Three novel Cu(II), Cd(II) and Cr(III) complexes of 6−Methylpyridine−2−carboxylic acid with thiocyanate: Synthesis, crystal structures, DFT calculations, molecular docking and α-Glucosidase inhibition studies", *Tetrahedron*, 74, 7198-7208. https://doi.org/10.1016/j.tet.2018.10.054

Avcı, D., Altürk, S., Sönmez, F., Tamer, Ö., Başoğlu, A., Atalay, Y., Zengin Kurt, B., Dege, N. (2019). "A novel series of M(II) complexes of 6-methylpyridine-2-carboxylic acid with 4(5)-methylimidazole: Synthesis, crystal structures, α-glucosidase activity, density functional theory calculations and molecular docking", *Applied Organometallic Chemistry*, 33, e4935. https://doi.org/10.1002/aoc.6591

Avcı, D., Altürk, S., Sönmez, F., Tamer, Ö., Başoğlu, A., Atalay, Y., Zengin Kurt, B., Dege, N. (2019). "A novel series of mixed-ligand M(II) complexes containing 2,2′-bipyridyl as potent α-glucosidase inhibitor: synthesis, crystal structure, DFT calculations, and molecular docking", *JBIC Journal of Biological Inorganic Chemistry*, 24, 747–764. https://doi.org/10.1007/s00775-019-01688-9

Avcı, D., Altürk, S., Sönmez, F., Tamer, Ö., Başoğlu, A., Atalay, Y., Zengin Kurt, B., Dege, N. (2019). "Novel Cu(II), Co(II) and Zn(II) metal complexes with mixed-ligand: Synthesis, crystal structure, α-glucosidase inhibition, DFT calculations, and molecular docking. *Journal of Molecular Structure*, 1197, 645-655. https://doi.org/10.1016/j.molstruc.2019.07.039

Avcı, D., Altürk, S., Sönmez, F., Tamer, Ö., Başoğlu, A., Atalay, Y., Zengin Kurt, B., Dege, N. 2020a. "Synthesis, spectral properties, in vitro α-glucosidase inhibitory activity and quantum chemical calculations of novel mixed-ligand M(II) complexes containing 1,10-phenanthroline", *Applied Organometallic Chemistry*, 34, e5412. https://doi.org/10.1002/aoc.5412

Avcı, D., Altürk, S., Sönmez, F., Tamer, Ö., Başoğlu, A., Atalay, Y., Zengin Kurt, B. 2020). "Synthesis, DFT calculations and molecular docking study of mixed ligand metal complexes containing 4,40-dimethyl-2,20-bipyridyl as α-glucosidase inhibitors", *Journal of Molecular Structure*, 1205, 127665. https://doi.org/10.1016/j.molstruc.2019.127655

Avcı, D., Özge, Ö., Başoğlu, A., Sönmez, F., Tamer, Ö., Dege, N., & Atalay, Y. (2023). Synthesis, crystal structures, and DFT calculations: novel Mn(II), Co(II) and Ni(II) complexes of *N*-(pyridin-2-ylmethylene)methanamine with isothiocyanate as promising optical materials. *Optical and Quantum Electronics*, 55, 408. https://doi.org/10.1007/s11082-023-04668-1

Avcı, D., Özge, Ö., Sönmez, F., Başoğlu, A., Tamer, Ö., & Atalay, Y. (2024). Novel schiff base-azide metal complexes: Synthesis, spectral, nonlinear optics, and DFT studies. *Materials Science in Semiconductor Processing*, 179, 108523. https://doi.org/10.1016/j.mssp.2024.108523

Avcı, D., Özge, Ö., Sönmez, F., Tamer, Ö., Başoğlu, A., Atalay, Y., & Zengin Kurt, B. (2024). In vitro α-glucosidase, docking and density functional theory studies on novel azide metal complexes. *Future Medicinal Chemistry*, 16(11), 1109–1125. https://doi.org/10.1080/17568919.2024.2342650

Balan, K. Ratha, P., Prakash, G., Viswanathamurthi, P., Adisakwattana, S., Palvannan, T. (2017). "Evaluation of in vitro α -amylase and α -glucosidase inhibitory potential of N_2O_2 schiff base Zn complex", *Arabian Journal of Chemistry*, 10, 732–738. https://doi.org/10.1016/j.arabjc.2014.07.002

Bertozzi, C.R., Kiessling, L.L. (2001). "Chemical glycobiology", *Science*, 291, 2357-2364. https://www.science.org/doi/10.1126/science.1059820

Bischoff, H. (1995). The mechanism of alpha-glucosidase inhibition in the management of diabetes. *Clinical and Investigative Medicine*, 18(4), 303. https://pubmed.ncbi.nlm.nih.gov/8549017

Bochmann, M., Cotton, F. A., Wilkinson, G., & Murillo, C. A. (1999). Advanced inorganic chemistry (6th ed., p. 1355). *John Wiley & Sons*. ISBN: 978-0-471-19957-1

Castet, F., Rodriguez, V., Pozzo, J.-L., Ducasse, L., Plaquet, A., Champagne, B. (2013). "Design and Characterization of Molecular Nonlinear Optical Switches", *Accounts of Chemical Research*, 46(11), 2656-2665. https://pubs.acs.org/doi/10.1021/ar4000955

Clays, K., Coe, B. J. (2003). "Design strategies versus limiting theory for engineering large second-order nonlinear optical polarizabilities in charged organic molecules", *Chemistry of Materials*, 15(3), 642-648. https://doi.org/10.1021/cm0212111

Constable, E.C., Steel, P.J. (1989). "N,N'-Chelating biheteroaromatic ligands; a survey", *Coordination Chemistry Reviews*, 93(2), 205-223. https://doi.org/10.1016/0010-8545(89)80016-5

da Silva, C. M., da Silva, D. L., Modolo, L. V., Alves, R. B., Resende, M. A., Martins, C. V. B., & de Fátima, A. (2011). Schiff bases: A short review of their antimicrobial activities. *Journal of Advanced Research*, 2(1), 1–8. https://doi.org/10.1016/j.jare.2010.05.004

da Silva, M.A.V.R., da Silva, M.D.M.C.R, Monte, M.J.S., Gonçalves, J.M., Fernandes, É.M.R. (1997). "Energetics of metal–ligand binding in copper (II) and nickel (II) complexes of two Schiff bases", *Journal of the Chemical Society*, Dalton Transactions, 7, 1257-1262. https://doi.org/10.1039/A607745E

Demadis, K.D., Katarachia, S.D. (2004). "Metal-phosphonate chemistry: synthesis, crystal structure of calcium-amino tris-(methylene phosphonate) and inhibition of $CaCO_3$ crystal growth", Phosphorus, Sulfur, Silicon 179(3), 627-648. https://doi.org/10.1080/10426500490441514

Driessen, W., De Graaff, R., Parlevliet, F., Reedijk, J., De Vos, R. (1994). "Transition metal compounds of the tridentate pyrazole substituted amine ligand bis (2-(3,5-dimethyl-1-pyrazolyl) ethyl) ethylamine (ddae). X-ray structures of $[Co(ddae)(NO_3)_2]$,$[Cu(ddae)(NO_3)(H_2O)](NO_3)$ and $[Cu(ddae)(Cl)_2]C_2H_5OH$.", *Inorganica Chimica Acta*, 216, 43-49. https://doi.org/10.1016/0020-1693(93)03707-H

Fernandes, B., Sagman, U., Auger, N., Demetrio, M., Dennis, J.W. (1991). "β1–6 branched oligosaccharides as a marker of tumor progression in human breast and colon neoplasia", *Cancer Research*, 51(2), 718-723. https://pubmed.ncbi.nlm.nih.gov/1985789/

Floris, A.L., Peter, L.L., Reinier, P., Eloy, H.L., Guy, E.R., Chris, W. (2005). "α-Glucosidase inhibitors for patients with type 2 diabetes: results from a Cochrane systematic review and meta-analysis", *Diabetes Care*, 28, 154-163. https://doi.org/10.2337/diacare.28.1.154

Foresman, J. B., Frisch, Æ. (1996). Exploring chemistry with electronic structure methods (Second Edition), Pittsburgh, PA. ISBN 13: 9781935522034

Ghani, U. (2015). "Re-exploring promising a-glucosidase inhibitors for potential development into oral anti-diabetic drugs: finding needle in the haystack", *European Journal of Medicinal Chemistry*, 103, 133-162. https://doi.org/10.1016/j.ejmech.2015.08.043

Ghosh, S., Roy, N., Singh, T. S., & Chattopadhyay, N. (2018). "Photophysics of a coumarin based Schiff base in solvents of varying polarities*", Spectrochimica Acta Part A: Molecular and Biomolecular Spectroscopy*, 188, 252-257. https://doi.org/10.1016/j.saa.2017.07.006

Gollapalli, M., Taha, M., Javid, M.T., Almandil, N.B., Rahim, F., Wadood, A., Mosaddik, A., Ibrahim, M., Alqahtani, M.A., Bamarouf, Y.A. (2019). "Synthesis of benzothiazole derivatives as a potent α−glucosidase inhibitör", *Bioorganic Chemistry*, 85, 33-48. https://doi.org/10.1016/j.bioorg.2018.12.021

Greenwood, N. N., & Earnshaw, A. (1997). Chemistry of the elements (2nd ed.). *Butterworth-Heinemann*. https://www.sciencedirect.com/book/9780750633659/chemistry-of-the-elements

Horii, S., Fukase, H., Matsuo, T., Kameda, Y., Asano, N., Matsui, K. (1986). "Synthesis and. alpha.-D-glucosidase inhibitory activity of N-substituted valiolamine derivatives as potential oral antidiabetic agents", *Journal of Medicinal Chemistry*, 29(6), 1038-1046. https://doi.org/10.1021/jm00156a023

Iqbal, M.S., Khan, A.H., Loothar, B.A., Bukhari, I.H. (2009). "Effect of derivatization of sulfamethoxazole and trimethoprim with copper and zinc on their medicinal value", *Medicinal Chemistry Research*, 18(1), 31-42. https://doi.org/10.1007/s00044-008-9104-5

IUPAC. (1997). Compendium of chemical terminology (2nd ed.). (A. D. McNaught & A. Wilkinson, Eds.). *Blackwell Science*. https://goldbook.iupac.org/

Iwahashi, H., Itoh, N., Yamagata, K., Imagawa, A., Nakajima, H., Tomita, K., Moriwaki, M., Waguri, M., Yamamoto, K., Miyagawa, J., Namba, M., Hanafusa, T., Matsuzawa, Y. (1998). "Molecular mechanisms of pancreatic beta-cell destruction in autoimmune diabetes: potential targets for preventive therapy", *Cytokines, Cellular & Molecular Therapy*, 4(1), 45-51. https://pubmed.ncbi.nlm.nih.gov/9557216/

Kaur, M., Kumar, S., Younis, S. A., Yusuf, M., Lee, J. J., Weon, S., Kim, K., & Malik, A. K. (2021). Post-synthesis modification of metal-organic frameworks using Schiff base complexes for various catalytic applications. *Chemical Engineering Journal*, 423, 130230. https://doi.org/10.1016/j.cej.2021.130230

Khan, A., Sarkar, S., Sarkar, D. (2008). "Bactericidal activity of 2-nitroimidazole against activereplicating stage of Mycobacterium bovis BCG and M. tuberculosis with intracellular efficacy in THP-1 macrophage", *International Journal of Antimicrobial Agents*, 32(1), 40-45. https://doi.org/10.1016/j.ijantimicag.2008.02.022

Kim, J. S., Kwon, J. S., & Son, K. H. (2000). Inhibition of alpha-glucosidase and amylase by luteolin, a flavonoid. *Bioscience, Biotechnology, and Biochemistry*, 64(11), 2458–2461. https://doi.org/10.1271/bbb.64.2458

Kukovec, B. –M., Kodrin, I., Vojković, V., Popović, Z., 2013. "Synthesis, X−ray structural, IR spectroscopic, thermal and DFT studies of nickel(II) and copper(II) complexes with 3−methylpicolinic acid. UV–Vis spectrophotometric study of complexation in the solution", *Polyhedron*, 52, 1349–1361. https://doi.org/10.1016/j.poly.2012.06.006

Kumari, M. and Jain, S. 2012. "Tannins: An Antinutrient with Positive Effect to Manage Diabetes", *Research Journal of Recent Sciences*, 1(12), 70-73. https://www.isca.in/rjrs/archive/v1/i12/14.ISCA-RJRS-2012-113.php ISSN 2277-2502

Lawrance, G. A. (2010). Introduction to coordination chemistry. *Wiley*. https://www.wiley.com/en-us/Introduction+to+Coordination+Chemistry-p-9781118681404 ISBN: 978-1-118-68140-4

Miessler, G. L., & Tarr, D. A. (1999). Inorganic chemistry (3rd ed., p. 642). *Prentice Hall.* https://tech.chemistrydocs.com/Books/InOrganic/Inorganic-Chemistry-By-Gary-L.-Miessler-3rd-Edition.pdf

Miyazaki, R., Yasui, H., & Yoshikawa, Y. (2016). α-Glucosidase inhibition by new Schiff base complexes of Zn(II). *Open Journal of Inorganic Chemistry*, 6(4), 114–124. https://doi.org/10.4236/ojic.2016.62007.

Mobin, S.M., Saini, A.K., Mishra, V., Chaudhary, A. (2016). "A series of new heteroleptic Hg(II) complexes: synthesis, crystal structures and photophysical properties", *Polyhedron* 110, 131-141. https://doi.org/10.1016/j.poly.2016.02.037

Monot, J., Petit, M. Lane, S.M., Guisle, I., Léger, J., Tellier, C., Talham, D.R., Bujoli, B. (2008). "Towards zirconium phosphonate-based microarrays for probing DNA-protein interactions: critical influence of the location of the probe anchoring groups", *J. Am. Chem. Soc.* 130(19), 6243-6251. https://doi.org/10.1021/ja711427q

Montazerozohori, M., Mojahedi Jahromi, S., Masoudiasl, A., & et al. (2015). Nano structure zinc (II) Schiff base complexes of a N_3- tridentate ligand as new biological active agents: Spectral, thermal behaviors and crystal structure of zinc azide complex. Spectrochimica Acta Part A: Molecular and Biomolecular Spectroscopy, 138, 517–528. https://doi.org/10.1016/j.saa.2014.11.055

Mueller, M. (2001). Fundamentals of quantum chemistry: Molecular spectroscopy and modern electronic structure computations (1st ed.). *Kluwer Academic/Plenum Publishers.* https://doi.org/10.1007/b113924

Naowaboot, J., Pannangpetch, P., Kukongviriyapan, V., Kukongviriyapan, U., Nakmareong, S., Itharat, A. (2009). "Mulberry leaf extract restores arterial pressure in streptozotocin-induced chronic diabetic rats", *Nutrition Research*, 29(8), 602-608. https://doi.org/10.1016/j.nutres.2009.06.002

Ogawa, S., Maruyama, A., Odagiri, T., Yuasa, H., Hashimoto, H. (2001). "Synthesis and Biological Evaluation of α-L-Fucosidase Inhibitors: 5a-Carba-α-L-fucopyranosylamine and Related Compounds", *European Journal of Organic Chemistry*, 5, 967-974. https://doi.org/10.1002/1099-0690(200103)2001:5<967::AID-EJOC967>3.0.CO;2-J

Özge, Ö., Avcı, D., Sönmez, F., Tamer, Ö., Dege, N., Başoğlu, A., Atalay, Y., & Zengin Kurt, B. (2023). Synthesis, DFT calculations, α-glucosidase inhibitor activity, and docking studies on Schiff base metal complexes containing isothiocyanate. *Applied Organometallic Chemistry*, 37(5), e7084. https://doi.org/10.1002/aoc.7084

Philip, J.E., Shahid, M., Prathapachandra Kurup, M.R., Velayudhan, M.P. (2017). "Metal based biologically active compounds: Design, synthesis, DNA binding and antidiabetic activity of 6-methyl-3-formyl chromone derived hydrazones and their metal (II) complexes", *Journal of Photochemistry & Photobiology, B: Biology*, 175, 178–191. https://doi.org/10.1016/j.jphotobiol.2017.09.003

Plesch G., Kettmann, V., Sivy, J., Svajlenova, O., & Friebel, C. (1998). Coordination geometries and cooperative ordering effects in copper(II) complexes with tridentate Schiff base dianions—VI Structure and EPR spectra of (imidazole)(N-salicylidene-beta-alaninato)copper(II). *Polyhedron*, 17(4), 539–545. https://doi.org/10.1016/S0277-5387(97)00337-9

Raju, B.C., Ashok, A.K., Kumar, J.A., Ali, A.Z., Agawane, S.B., Saidachary, G., Madhusudana, K. (2010). "α-Glucosidase inhibitory antihyperglycemic activity of substituted chromenone derivatives", *Bioorganic & Medicinal Chemistry*, 18(1), 358-365. https://doi.org/10.1016/j.bmc.2009.10.047

Rhabasa-Lhoret, R., Chiasson, J.L. (2004). "Alpha-glucosidase inhibitors". In: Defronzo, R.A., Ferrannini, E., Keen, H., Zimmet, P. (Eds.), International Textbook of Diabetes Mellitus, 3rd Ed., vol. *John Wiley*, UK. https://doi.org/10.1002/0470862092.d0612

Rodríguez-Argüelles, M.C., Tourón-Touceda, P., Cao, R., García-Deibe, A.M., Pelagatti, P., Pelizzi, C., Zani, F. (2009). "Complexes of 2-acetyl-γ-butyrolactone and 2-furancarbaldehyde thiosemicarbazones: antibacterial and antifungal activity*", Journal of Inorganic Biochemistry*, 103(1), 35-42. https://doi.org/10.1016/j.jinorgbio.2008.08.015

Saito, B.Y., Takemoto, J., Hutchinson, B., Nakamoto, K. (1972). "Infrared studies of coordination compounds containing low-oxidation-state metals. I. Tris(2,2'-bipyridine) and tris(1,10-phenanthroline) complexes*", Inorganic Chemistry*, 11(9), 2003-2011. https://pubs.acs.org/doi/10.1021/ic50115a004

Shimizu, S., Watanabe, N., Kataoka, T., Shoji, T., Abe, N., Morishita, S., & Ichimura, H. (2007). Pyridine and pyridine derivatives. *In Ullmann's Encyclopedia of Industrial Chemistry. Wiley-VCH.* https://doi.org/10.1002/14356007.a22_399

Shisheva, A., Gefel, D., & Shechter, Y. (1992). Insulin-like effects of zinc ion in vitro and in vivo: Preferential effects on desensitized adipocytes and induction of normoglycemia in streptozocin-induced rats. *Diabetes*, 41(8), 982–988. https://doi.org/10.2337/diab.41.8.982

Sönmez, F., Güneşli, Z., Zengin Kurt, B., Gazioğlu, I., Avcı, D., Küçükislamoğlu, M. (2019). "Synthesis, antioxidant activity and SAR study of novel spiro-isatin-based Schiff bases", *Molecular Diversity*, 23, 829–844. https://doi.org/10.1007/s11030-018-09910-7

Tamer, Ö., Arabacı Tamer, S. Idil, Ö., Avcı, D., Vural, H., Atalay, Y. (2018). "Antimicrobial activities, DNA interactions, spectroscopic (FT-IR and UV-Vis) characterizations, and DFT calculations for pyridine-2-carboxylic acid and its derivates", *Journal of Molecular Structure*, 1152, 399-408. https://doi.org/10.1016/j.molstruc.2017.09.100

Thamilrasan, V., Jayamani, A., & Sengottuvelan, N. (2015). Synthesis, molecular structure, biological properties and molecular docking studies on Mn(II), Co(II) and Zn(II) complexes containing bipyridine–azide ligands. European Journal of Medicinal Chemistry, 89(7), 266–278. https://doi.org/10.1016/j.ejmech.2014.09.073

Thomas, H.E., Kay, T.W. (2000). "Beta cell destruction in the development of autoimmune diabetes in the non-obese diabetic (NOD) mouse*",* *Diabetes/Metabolism Research and Reviews*, 16(4), 251-261. https://doi.org/10.1002/1520-7560(200007/08)16:4<251::AID-DMRR126>3.0.CO;2-C

Tripath I.P., Kumar, M.M., Ruchita, T., Chinmayi, M., Arti, K., Laxmikant, S., Atul, D., Kumar, S.U., Bhihari, P.K. 2014. "Synthesis, Spectral, Electrochemical analysis and Screening for α-Glucosidase inhibition of some complexes of Cobalt (II) and Ethylenediamine", *Research Journal of Chemical Sciences*, 4(6), 13-17. https://doi.org/10.15373/2249555X/MAY2014/21

Umeda, J., Suzuki, M., Kato, M., Moriya, M., Sakamoto, W., Yogo, T. (2010). "Proton conductive inorganiceorganic hybrid membranes functionalized with phosphonic acid for polymer electrolyte fuel cell", *Journal of Power Sources*, 195(18), 5882-5888. https://doi.org/10.1016/j.jpowsour.2009.12.078

Vitago, P. A., & Tamburini, S. (2014). The challenge of cyclic and acyclic Schiff bases and related derivatives. *Coordination Chemistry Reviews*, 248(17–20), 1717–2128. https://doi.org/10.1016/j.cct.2003.09.003

Wang, Y., Ma, L., Li, Z., Du, Z., Liu, Z., Qin, J., Wang, X., Huang, Z., Gu, L., Chen, A.S. (2004). "Synergetic inhibition of metal ions and genistein on α-glucosidase", *FEBS Letters*, 576, 46-50. https://doi.org/10.1016/j.febslet.2004.08.059

Wild, S., Roglic, K., Green, A., Sicree, R. and King, H. (2004). "Global prevalence of diabetes, Estimation for the year 2000 and projections for 2030", *Diabetes Care*, 27, 1047–1053. https://doi.org/10.2337/diacare.27.5.1047

Xia, L., Xia, Yu-F., Huang, Li- R., Xiao, X., Lou, Hua-Y., Liu, Tang-J., Pan, Wei-D., Luo, H. (2015). "Benzaldehyde Schiff bases regulation to the metabolism, hemolysis, and virulence genes expression in vitro and their structure–microbicidal activity relationship", *European Journal of Medicinal Chemistry*, 97, 83-93. https://doi.org/10.1016/j.ejmech.2015.04.042

Yang, Li-J., Liu, Qing-L., Wang, Ming-X., Gu, Lian-S., Luo, Yang-H., Sun, Bai-W. (2016). "Complexation of different transition metals with 4,4'-dimethyl-2,2'-bipyridine: crystal structure, UV spectra and Hirshfeld surfaces", *Spectrochimica Acta Part A: Molecular and Biomolecular Spectroscopy,* 166, 1-7. https://doi.org/10.1016/j.saa.2016.04.048

Yao, Y., Sang, W., Zhou, M., Ren, G. (2010). "Antioxidant and α-glucosidase inhibitory activity of colored grains in China", *Journal of Agricultural and Food Chemistry*, 58(2), 770-774. https://doi.org/10.1021/jf903234c Yasumatsu, N., Yoshikawa, Y., Adachi, Y., Sakurai, H. (2007). "Antidiabetic copper (II)-picolinate: impact of the first transition metal in the metallopicolinate complexes", *Bioorganic & Medicinal Chemistry*, 15, 4917-4922. https://doi.org/10.1016/j.bmc.2007.04.062

Yoshikawa, Y., Hirata, R., Yasui, H., Sakurai, H. (2009). "Alpha-glucosidase inhibitory effect of anti-diabetic metal ions and their complexes", *Biochimie,* 91, 1339-1341. https://doi.org/10.1016/j.biochi.2009.06.005

You, Z.L., Shi, D.H., Xu, C., Zhang, Q., Zhu, H.L. (2008). "Schiff base transition metal complexes as novel inhibitors of xanthine oxidase*", European Journal of Medicinal Chemistry*, 43(4), 862-871. https://doi.org/10.1016/j.ejmech.2007.06.015

Zhang, J., Xu, L., & Wong, W. Y. (2018). Energy materials based on metal Schiff base complexes. *Coordination Chemistry Reviews*, 355, 180–198. https://doi.org/10.1016/j.ccr.2017.08.007

Zhen, J., Dai, Y., Villani, T., Giurleo, D., Simon, J. E., & Wu, Q. (2017). Synthesis of novel flavonoid alkaloids as α-glucosidase inhibitors. *Bioorganic & Medicinal Chemistry*, 25(20), 5355–5364. https://doi.org/10.1016/j.bmc.2017.07.055

Zheng, J., Ma, L. (2015). "Silver(I) complexes of 2,4-dihydroxybenzaldehyde–amino acid Schiff bases—Novel noncompetitive a-glucosidase inhibitors", *Bioorganic & Medicinal Chemistry Letters*, 25, 2156–2161. https://doi.org/10.1016/j.bmcl.2015.03.078

Zheng, J.-W., Ma, L. (2016). "Assessment of silver(I) complexes of salicylaldehyde derivatives—histidine Schiff base as novel α-glucosidase inhibitors", *Chinese Chemical Letters*, 27(2), 283-286. https://doi.org/10.1016/j.cclet.2015.11.015

Zhu, Li-N., Jin, Ya-W., Li, Xiao-Z., Wang, J., Kong, De-M., Mi, Huai-F, Liao, Dai-Z., Shen, Han-X. (2008). "Synthesis, structure and DNA cleavage activity of two 4,4'-dimethyl-2,2'-bipyridyl manganese(II) complexes", *Inorganica Chimica Acta*, 361(1), 29-35. https://doi.org/10.1016/j.ica.2007.06.032

Zhu, Y.P., Yin, L.J., Cheng, Y.Q., Yamaki, K., Mon, Y., Su, Y.C., Li, L.T. (2008). "Effects of sources of carbon and nitrogen on production of α-glucosidase inhibitor by a newly isolated strain of Bacillus subtilis B2", *Food Chemistry*, 109(4), 737-742. https://doi.org/10.1016/j.foodchem.2008.01.006

EKLER

EK A. Avcı, D., Özge, Ö., Başoğlu, A., Sönmez, F., Tamer, Ö., Dege, N., & Atalay, Y. (2023). Synthesis, crystal structures, and DFT calculations: novel Mn(II), Co(II) and Ni(II) complexes of N-(pyridin-2-ylmethylene)methanamine with isothiocyanate as promising optical materials. Optical and Quantum Electronics, 55, 408. https://doi.org/10.1007/s11082-023-04668-1

Optical and Quantum Electronics (2023) 55:408
https://doi.org/10.1007/s11082-023-04668-1

Synthesis, crystal structures, and DFT calculations: novel Mn(II), Co(II) and Ni(II) complexes of *N*-(pyridin-2-ylmethylene)methanamine with isothiocyanate as promising optical materials

Davut Avcı[1] · Özgen Özge[1,2] · Adil Başoğlu[1] · Fatih Sönmez[3] · Ömer Tamer[1] · Necmi Dege[4] · Yusuf Atalay[1]

Received: 5 December 2022 / Accepted: 7 February 2023

Abstract
To investigate the optical parameters, novel metal complexes of *N*-(pyridin-2-ylmethylene)methanamine (L_1), obtained as Schiff base by the condensation reaction of 2-pyridinecarboxaldehyde with methylamine, and isothiocyanate {$[Mn(L_1)_2(NCS)_2]$, (**1**), $[Co(L_1)_2(NCS)_2]$, (**2**), $[Ni(L_1)_2(NCS)_2]$, (**3**)} were synthesized. FT–IR and UV–Vis spectra were applied to examine the spectral features for complexes **1,2/3** characterized by XRD/LC-HRMS. Hirshfeld surface analysis was performed to describe intermolecular interactions for complexes **1** and **2**. Moreover, the CAM-B3LYP and ωB97XD/6–311 + G(d,p)//LanL2DZ levels of DFT/TD-DFT methods were used to survey optimal complex structures, spectral and nonlinear optical parameters, as well as remarkable contributions in the electronic transitions for synthesized complexes **1–3**. In the mid-IR region, the mean refractive index/polarizability parameters for **1–3** were found to be $1.63/5.87 \times 10^{-24}$ esu, $1.46/4.80 \times 10^{-24}$ esu, and $1.50/4.48 \times 10^{-24}$ esu, respectively. By considering the UV–Vis absorption parameters, the experimental refractive index, optical band gap, polarizability, optical conductivity, and third-order nonlinear optical susceptibility parameters for complexes **1–3** in methanol were examined. The maximum third-order NLO susceptibility values in the photon energies of 4.68, 4.21, and 5.25 eV were obtained at 51.65×10^{-13}, 51.42×10^{-13}, and 51.42×10^{-13} esu, respectively. In short, detailed experimental and corresponding theoretical spectral and optical parameters for the synthesized complexes were investigated in terms of structure–property. The NLO results display that complex **1** may be a candidate for NLO material using in data storage, telecommunications, laser technology, etc. sectors in the future.

Keywords Schiff base · Isothiocyanate · Metal complex · SC-XRD, UV–Vis absorption spectra · Hirshfeld surface analysis · Optical properties · Density functional theory

✉ Davut Avcı
davci@sakarya.edu.tr

Extended author information available on the last page of the article

Published online: 07 March 2023

1 Introduction

In recent years, the synthesis and design of new organic, metal–organic compounds in nonlinear optics owing to their implementations in the improvement of photonic devices such as optical switches, optical communication and limiting, etc. has been great attention (Derkowska-Zielinskaa et al. 2020; Uddin et al. 2022; Kanwal et al. 2022). Organic compounds in NLO materials are usually formed by connecting electron-donating and withdrawing groups via a π-electronic bridge with a major D-π-A delocalized system. The presence of *N* and *O* atoms in heteroaromatic rings, as electron donor parts in coordination systems, is important both for providing coordination flexibility with metal ions and for the construction of new second and third-order effective NLO materials. In these compounds, Schiff base complexes among NLO materials may be of interest (Lacroix et al. 1996; Lacroix 2001; Liu et al. 2006; Costes et al. 2005). It is known that compounds containing the azomethine or imine group (–C=N–), which is one of the important classes of organic compounds, have a biologically important place and are also used in the design of medicinal compounds (Uddin et al. 2022; Kanwal et al. 2022; Khan et al. 2008; Iqbal et al. 2009; Sönmez et al. 2019). These compounds exhibit diverse pharmacological properties such as anti-inflammatory, antimalarial, antibacterial, antifungal, and antipyretic, as well as starting materials, catalysts, intermediates, and polymer stabilizers (Abdalkarim et al. 2021; Petrus et al. 2013). In addition, azomethine groups are very effective ligands in organometallic chemistry due to their versatile coordination and coordination flexibility (Ghosh et al. 2018; Xia et al. 2015). Therefore, the synthesis of azomethine-containing coordination compounds has been a major focus due to their potential biological and optical activities (Lacroix et al. 1996; Lacroix 2001; Liu et al. 2006; Costes et al. 2005; Khan et al. 2008; Iqbal et al. 2009; Abdalkarim et al. 2021; Petrus et al. 2013; Ghosh et al. 2018; Xia et al. 2015; Sarkar et al. 2008; Silva et al. 1997; Al-Amiery 2012).

It is reported that heteroatom-based metal complexes are match to some enzyme–substrate structures in living organisms in terms of structural, spectroscopic and catalytic properties (Constable and Steel 1989; Driessen et al. 1994; Gollapalli et al. 2019; Ghani 2015). By considering recent advances in complex structures containing azomethine besides examining biological and pharmaceutical activities, the synthesis and design of different coordination complexes of nitrogen-containing heterocyclic structures/pseudohalides (such as *N*-(pyridin-2-ylmethylene)methanamine, 4,4′-dimethyl-2,2′-bipyridine, azide, isothiocyanate, thiocyanate, etc.), as well as physicochemical features (nonlinear optics, catalysis, luminescence etc.) have been broadly investigated (Avcı et al. 2018, 2019, 2020, 1205, 2021a; Saito et al. 1972; Mobin et al. 2006; Li-J. Yang, Qing-L. Liu, Ming-X. Wang, Lian-S. Gu, Yang-H. Luo, Bai-W. 2016; Barquín et al. 2010; Amirnasr et al. 2006; Habib et al. 2008; Li et al. 2003; Mukherjee et al. 2000; Richmond et al. 1988). Besides, the terminal and bridging modes come to the fore in the coordination of pseudohalides, NCS/SCN, and N_3, with metal ions (Li et al. 2003; Mukherjee et al. 2000; Richmond et al. 1988; Mehkoom et al. 2022a; Faizan et al. 2021). Regarding the results obtained in the literature, the complexes containing Mn, Fe, Co, Ni, and Cu metal ions, etc., (Lacroix et al. 1996; Costes et al. 2005; Avcı et al. 2018, 2019, 2020, 1205, 2021a) and organic compounds (Mehkoom et al. 2022a, 2021, 2022b; Faizan et al. 2021; Kamaal et al. 2021) play an effective role in the optical activity and especially third-order nonlinear optical surveys.

In this study, to examine optical properties of synthesized complexes, experimental and theoretical investigation of their electronic properties is of great importance in terms of revealing structure–property relationships. We synthesized novel metal complexes (**1–3**)

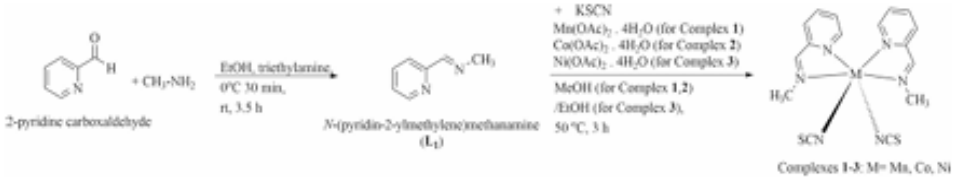

Scheme 1 Synthesis of complexes **1–3**

including *N*-(pyridin-2-ylmethylene)methanamine and isothiocyanate. The XRD spectroscopic technique were applied to characterize the crystal structures of compounds **1** and **2** (Mn(II) and Co(II) complexes) the LC-HRMS and FT-IR spectra were used to confirm the structure of compound **3** (Ni(II) complex). Optical properties of the characterized complexes were performed. The detailed experimental and theoretical examines of electronic spectral behavior of **1–3** were carried out.

2 Material and methods

2.1 Spectroscopy instruments

The Varian Infinity Plus NMR spectrometer was used to verify the structure of the synthesized L_1 ligand. The complexes **1,2** obtained as single crystals were described by using the data obtained from the STOE brand IPDS (II) Imaging Plate model diffraction device. FT−IR spectra for complexes **1–3** were recorded with Perkin Elmer UATR−TWO (Perkin Elmer Spectrum−two equipped with ATR) spectrophotometer in the range of 4000−400 cm^{-1}. The structure of the non-crystalline complex **3** was confirmed using the SHIMADZU LCMS-9030 model triple quadrupole liquid chromatograph mass spectrometer. The electronic absorption spectra for complexes **1–3** in the 900−200 nm range were examined by using the SHIMADZU UV−2600 UV−Vis spectrophotometer.

The detailed determinations of single crystal structures of compounds **1** and **2** are presented in supplementary material.

2.2 Materials and synthesis of the N-(pyridin-2-ylmethylene)methanamine (L_1) and complexes 1–3 {$[Mn(L_1)_2(NCS)_2]$, (1), $[Co(L_1)_2(NCS)_2]$, (2), $[Ni(L_1)_2(NCS)_2]$, (3)}

All chemical reagents (2-Pyridinecarboxaldehyde, methylamine solution purum (33% in absolute ethanol), potassium thiocyanate, metal(II) acetates) were purchased from Sigma-Aldrich and used without any specific re-handling. The synthesis methods of the *N*-(pyridin-2-ylmethylene)methanamine (L_1), obtained by the condensation reaction, and complexes **1–3** are given the following methods (see Scheme 1):

Synthesis of Schiff base, namely, the *N*-(pyridin-2-ylmethylene)methanamine (L_1): 0.1 mol of 2-pyridine carboxaldehyde was dissolved in 10 mL of ethanol (EtOH) and 2 drops of triethylamine were dropped on it. The solution was cooled by taking it into an ice bath, and 0.1 mol of methylamine (33% ethanol solution) was added to it and stirred in an ice bath for 30 min, and at room temperature for 3.5 h. The alcohol in the mixture was evaporated by the rotary evaporator and 100 mL of chloroform was added to the mixture. The solution was washed three times with 25 mL of water. The organic layer was dried

with anhydrous $MgSO_4$, filtered and evaporated by the rotary evaporator. The structure of the obtained *N*-(pyridin-2-ylmethylene)methanamine (L_1) compound was verified by ^1H and ^{13}C NMR spectra. ^1H NMR ($CDCl_3$, 300 MHz) δ/ppm: 8.40–8.43 (1H, dt, $J_1 = 0.9$ Hz, $J_2 = 5.0$ Hz), 8.17 (1H, d, $J = 1.4$ Hz), 7.72–7.75 (1H, dd, $J_1 = 0.9$ Hz, $J_2 = 7.9$ Hz), 7.48–7.54 (1H, td, $J_1 = 1.4$ Hz, $J_2 = 6.1$ Hz), 7.06–7.10 (1H, m), 3.34 (3H, d, $J = 1.8$ Hz). ^{13}C NMR ($CDCl_3$, 75 MHz) δ/ppm: 163.4, 154.4, 149.4, 136.7, 124.8, 121.1, 48.2.

Synthesis of the complexes **1** and **2**: Solution of 1 mmol metal salts ($Mn(CH_3COO)_2{\cdot}4H_2O$ for complex **1**, $Co(CH_3COO)_2{\cdot}4H_2O$ for complex **2**) in 10 mL methanol (MeOH), *N*-(pyridin-2-ylmethylene)methanamine (L_1) prepared in 10 mL MeOH (2 mmol) was added to the solution and stirred at 50 °C for about 15 min. Potassium thiocyanate (2 mmol) solution prepared in 10 mL MeOH was added onto the solution. It was stirred at 50 °C for 3 h, and then evaporated at room temperature. Complex products in crystalline form were obtained in about 7–10 days. The structures of these products were confirmed by XRD. The single crystals for the complexes was obtained with colorless (complexes **1**), red color (complex **2**) in prism-shaped.

Synthesis of the complex **3**: 1 mmol metal salt ($Ni(OCOCH_3)_2{\cdot}4H_2O$) was added to *N*-(pyridin-2-ylmethylene)methanamine (L_1) (2 mmol) solution prepared in EtOH (15 mL) and stirred at 50 °C for about 15 min. Potassium thiocyanate (2 mmol) solution prepared in EtOH (10 mL) was added to the solution. It was stirred at 50 °C for 3 h, then allowed to evaporate at room temperature. Complex product in powder form was obtained in about 7–10 days. This powder product was verified by mass spectroscopy. In this analysis, the flight tube temperature was arranged at 42 °C and elution was performed with 50% methanol and 50% water. An eluent flow rate of 0.5 mL/min was used and mass spectrometric data was collected over the mass range of 150–550, in positive or negative ion mode on a time-of-flight mass spectrometer. Calculated exact mass (m/z): 414.0231 ($C_{16}H_{16}N_6NiS_2$). Found: LC-HRMS (m/z): 415.0419 ($[M]^+$). Fig. S1 depicts the MS spectrum of complex **3**.

2.3 Theoretical procedure

The Gaussian 16, Revision C.01 (2016) and GaussView 6 (2016) programs were used to examine the structural, spectral, and linear/non-linear optical properties. In the synthesized complexes **1–3**, to survey the conjugative interactions, interaction among bonds, as well as the coordination geometry in the ground state, the vibrational frequencies and natural bond orbital (NBO) (Glendening et al. 1998) studies based on optimized complex structures were fulfilled at CAM-B3LYP (long range corrected version of B3LYP (Becke-3-parameter-Lee–Yang–Parr) using the Coulomb-attenuating method, CAM) (Yanai et al. 2004) and ωB97XD (the latest functional developed from Head-Gordon and coworkers, including long range corrections and empirical dispersion described by Chai and coworkers) (Chai and Head-Gordon 2008) methods with 6–311 + G(d,p)//LanL2DZ (Frisch et al. 1984; Hay and Wadt 1985) basis set. The electronic absorption wavelength and oscillator strength of complexes **1–3** in methanol solvent were calculated at the time-dependent density functional theory (TD–DFT) level (Runge and Gross 1984) with the conductor–like polarizable continuum model (CPCM) (Miertus et al. 1981). By considering SWizard (Gorelsky 2010) program, the remarkable contributions from FMOs (frontier molecular orbitals) in electronic transitions were assigned. DFT/CAM-B3LYP and ωB97XD/LanL2DZ levels in the gas phase were applied to obtain the microscopic polarizabilities (α and Δα), first- and second-order hyperpolarizabilities (β and γ). Besides, the MEP (molecular electrostatic potential) surfaces were examined by the DFT/CAM-B3LYP level.

The stability energy $E^{(2)}$ values in NBO calculations by considering q_i (the donor orbital occupancy), including ε_i and ε_j (diagonal elements), and $F(i,j)^2$ (the off-diagonal NBO Fock matrix elements) for each donor (i) and acceptor (j) were calculated the following Eq. (1) (Altürk et al. 2016, 2015; Reed and Weinhold 1983; Foster and Weinhold 1980).

$$E^{(2)} = \Delta E_{ij} = q_i \frac{F(i,j)^2}{\varepsilon_i - \varepsilon_j} \tag{1}$$

The η (chemical hardness), χ (electronegativity), S (chemical softness), ω and φ (electrophilicity and nucleophilicity index) parameters were calculated by using FMO energies. These parameters known as chemical reactivity values were calculated by the following Eq. (2)-(6) (Altürk et al. 2016; Yang and Parr 1985; Chattaraj et al. 2006).

$$\eta = \frac{\left(\mathrm{E}_{LUMO} - \mathrm{E}_{HOMO}\right)}{2} \tag{2}$$

$$\chi = -\frac{\left(\mathrm{E}_{HOMO} + \mathrm{E}_{LUMO}\right)}{2} \tag{3}$$

$$S = \frac{1}{\eta} \tag{4}$$

$$\omega = \frac{\chi^2}{2\eta} \tag{5}$$

$$\varphi = \frac{1}{\omega} \tag{6}$$

The theoretical linear optical parameters ($\overline{\alpha}$ and Δα), first- and second-order hyperpolarizability parameters (β and γ) known as nonlinear optical parameters for complexes **1–3** in gas phase were computed by using Eq. (7)–(10).

The $\overline{\alpha}$ and Δα parameters were calculated by the following Eqs. (7) and (8) (Oudar 1977; Oudar and Zyss 1982; Zhang et al. 1997; Avcı 2010, 2011),

$$\overline{\alpha} = \frac{\left(a_{xx} + a_{yy} + a_{zz}\right)}{3} \tag{7}$$

$$\Delta a = \left\{ \frac{1}{2}\left[\left(a_{xx} - a_{yy}\right)^2 + \left(a_{yy} - a_{zz}\right)^2 + \left(a_{zz} - a_{xx}\right)^2 \right] \right\}^{1/2} \tag{8}$$

in Eqs. (7) and (8), a_{xx}, a_{yy}, a_{zz} for $\overline{\alpha}$ and Δα is the Cartesian components. 1 atomic unit (a.u.) for $\overline{\alpha}$ is equal to 0.1482×10^{-24} electrostatic units (esu).

The β parameter by considering the Cartesian components of β and unit conversion ($\beta_x = \beta_{xxx} + \beta_{xyy} + \beta_{xzz}$, $\beta_y = \beta_{yyy} + \beta_{yxx} + \beta_{yzz}$, $\beta_z = \beta_{zzz} + \beta_{zyy} + \beta_{zxx}$ and 1 a.u. $= 8.6393 \times 10^{-33}$ esu) was computed by the following Eq. (9) (Oudar 1977; Oudar and Zyss 1982; Zhang et al. 1997; Avcı 2010, 2011; Dege et al. 2021),

$$\beta = \left(\beta_x^2 + \beta_y^2 + \beta_z^2\right)^{1/2} \tag{9}$$

and the γ parameter was obtained by the following Eq. (10) (Oudar 1977; Oudar and Zyss 1982; Zhang et al. 1997; Avcı 2010, 2011; Dege et al. 2021),

$$\langle\gamma\rangle = \frac{1}{5}\left[\gamma_{xxxx} + \gamma_{yyyy} + \gamma_{zzzz} + 2\left(\gamma_{xxyy} + \gamma_{xxzz} + \gamma_{yyzz}\right)\right] \tag{10}$$

in Eq. (10), $\gamma_{xxxx}, \gamma_{yyyy}, \gamma_{zzzz}, \gamma_{xxyy}, \gamma_{xxzz}$, and γ_{yyzz} are the Cartesian components of γ.

The $\chi^{(1)}$ and $\chi^{(3)}$ parameters called linear and third-order nonlinear optical susceptibility for complexes **1–3** without using the experimental equipment were obtained by using the Eq. (11) and (12) (Altürk et al. 2016; Oudar and Zyss 1982; Dege et al. 2021).

$$c^{(1)} = Nf\overline{\alpha} \tag{11}$$

$$c^{(3)} = Nf^4\gamma \tag{12}$$

In Eq. (11) and (12), f (f=(n^2+2)/3) is the local field correction factor with regard to Lorentz expression and N is the number of molecules per unit cm^3, $\overline{\alpha}$ and γ are the linear optical and third-order NLO parameters calculated by using Eq. (7) and (10), respectively.

The refractive index, *n*, was computed by using Lorentz-Lorenz Eq. (13).

$$\left(n^2 - 1\right)/\left(n^2 + 2\right) = D\overline{\alpha}/V \tag{13}$$

In Eq. (13), *V* describes the molar volume (in cm^3 units), D is a multiplier depending on Avogadro's number (N_A). By considering $\overline{\alpha}$ (in$\times 10^{-24}$ cm^3 units), *V* (in cm^3 units), and D taking values of $2.523564179\times 10^{24}$, *n* is directly calculated as dimensionless.

3 Results and discussion

3.1 The structural, vibrational, NBO characterizations, and Hirshfeld surface analysis

Table 1 depicts the crystallographic data and refinement parameters of complexes **1,2** obtained by XRD. From Table 1, the space groups are P21/c for complex **1** in the monoclinic crystal system and Ccca for complex **2** in the orthorhombic crystal system. The single crystal/optimized complex structures for complexes **1,2/3** are given in Fig. 1. The structure of the non-crystalline complex **3** was confirmed using mass spectrometry (see Fig. S1). In addition, the structures of the complexes **1–3** were optimized by DFT/ωB97XD and DFT/CAM-B3LYP methods and the bond lengths and angles, dihedral angles calculated are presented in Tables 2 and S1. The coordination around metal ions (Mn(II), Co(II), Ni(II)) of complexes **1–3** is described as a distorted octahedral geometry. The complexes **1–3** are formed by two L1 (bidentate ligand) and two isothiocyanates (monodentate ligand) ligands being coordinated to Mn(II), Co(II), Ni(II) ions. The complexes **1–3** obtained in this study act as terminal ligands.

In complexes **1–3**, five-membered chelate rings occurred by metal ions coordination over pyridine N and imine N atoms of the L_1 ligand. The M–N bond lengths between the metal ion and the pyridine N/imine N atoms of the complexes **1,2** were experimentally

Table 1 Crystal data and structure refinement parameters for complexes **1** and **2**

	Complex **1**	Complex **2**
Empirical formula	$C_{16}H_{16}MnN_6S_2$	$C_{16}H_{16}CoN_6S_2$
Formula weight	411.41	415.40
Crystal system	Monoclinic	Orthorhombic
Space group	$P2_1/c$	Ccca
Temperature	296	296
Radiation type	Mo *K*α	Mo *K*α
Wavelengh (Å)	0.71073	0.71073
Crystal size (mm)	0.63 × 0.51 × 0.31	0.72 × 0.66 × 0.52
a (Å)	12.7212(10)	14.6265(6)
b (Å)	9.2597(5)	14.6775(7)
c (Å)	16.4606(12)	19.1522(8)
α (°)	90	90
β (°)	93.077(6)	90
γ (°)	90	90
V (Å^3)	1936.2(2)	4111.6(3)
Z	4	8
F(000)	844	1704
Density (g cm^{-3})	1.411	1.342
μ (mm^{-1})	0.91	1.05
θ range (°)	2.0–32.9	2.0–30.3
Measured refls	24,305	9402
Independent refls	7089	2022
R_{int}	0.082	0.077
S	0.89	1.06
R1/wR2	0.053/0.141	0.070/0.229
max/min (eÅ^{-3})	0.67/ −0.42	0.99/ −0.76

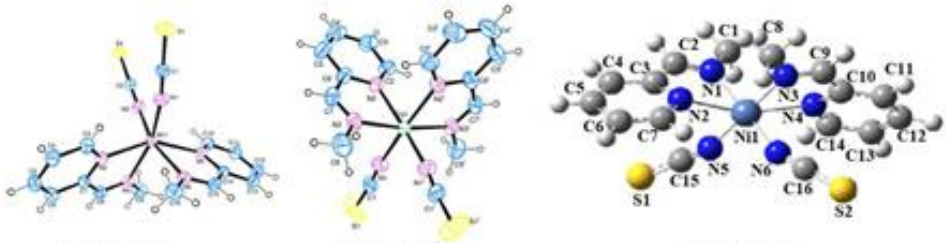

Complex **1** Complex **2** Complex **3**

Fig. 1 Single crystal structures of complex **1,2** and theoretical optimized structure of complex **3** using DFT/CAM-B3LYP level

observed as 2.2751(19)/2.321(2) and 2.165(4)/2.141(4) Å, respectively (see Table 2). These values calculated at DFT/CAM-B3LYP level corresponding to these bond lengths were obtained as 2.034/2.034, and 2.334/1.986 Å. The M–N bond lengths between the metal ion and isothiocyanate N atom of the complexes **1,2** were experimentally found to be 2.159(2) and 2.057(5) Å, respectively. The corresponding values were calculated at 1.977

Table 2 Comparison of experimental and theoretical geometric parameters for complexes **1** and **2**

Complex **1**				Complex **2**			
Parameters	XRD	ωB97XD	CAM-B3LYP		XRD	ωB97XD	CAM-B3LYP
Bond length (Å)				Bond length (Å)			
Mn1−N2	2.144(2)	1.986	1.977	Co1−N1^{i}	2.057 (5)	1.961	2.233
Mn1−N1	2.159(2)	1.986	1.977	Co1−N1	2.057 (5)	1.961	1.913
Mn1−N3	2.2751(19)	2.029	2.034	Co1−N3	2.141 (4)	2.224	1.986
Mn1−N4	2.279(2)	2.021	2.034	Co1−N3^{i}	2.141 (4)	2.224	1.965
Mn1−N5	2.2979(19)	2.029	2.034	Co1−N2	2.165 (4)	2.010	2.334
Mn1−N6	2.321(2)	2.021	2.034	Co1−N2^{i}	2.165 (4)	2.010	1.994
S2−C2	1.618(3)	1.624	1.624	N2−C2	1.325 (6)	1.331	1.324
S1−C1	1.610(3)	1.624	1.624	N2−C6	1.349 (6)	1.345	1.337
N3−C7	1.336(3)	1.349	1.349	N3−C7	1.261 (7)	1.265	1.267
N3−C3	1.338(3)	1.337	1.335	N3−C8	1.456 (8)	1.443	1.453
N5−C10	1.333(3)	1.337	1.335	N1−C1	1.107 (7)	1.174	1.169
N5−C14	1.342(3)	1.349	1.349	C6−C5	1.373 (9)	1.387	1.387
N6−C15	1.252(3)	1.277	1.275	C6−C7	1.475 (9)	1.476	1.471
N6−C16	1.462(3)	1.449	1.450	C1−S1	1.627 (6)	1.626	1.625
N4−C8	1.260(3)	1.277	1.275	C2−C3	1.374 (9)	1.387	1.391
N4−C9	1.469(3)	1.449	1.450	C5−C4	1.352 (11)	1.387	1.388
N2−C2	1.154(3)	1.175	1.171	C3−C4	1.382 (11)	1.387	1.384
N1−C1	1.146(3)	1.175	1.171				
C7−C8	1.478(4)	1.389	1.454				
Bond angles (°)				Bond angles (°)			
N2−Mn1−N1	91.50(10)	99.40	97.85	N1^{i}−Co1−N1	96.2 (3)	94.57	98.07
N2−Mn1−N3	108.18(8)	89.87	89.07	N1^{i}−Co1−N3	92.70 (19)	97.13	93.43
N1−Mn1−N3	92.05(8)	92.26	91.99	N1−Co1−N3	92.70 (18)	85.99	87.32
N2−Mn1−N4	89.02(9)	86.22	86.97	N1^{i}−Co1−N3^{i}	92.69 (18)	85.98	86.64

Table 2 (continued)

Complex **1**				Complex **2**			
Parameters	XRD	ωB97XD	CAM-B3LYP		XRD	ωB97XD	CAM-B3LYP
N1–Mn1–N4	163.90(8)	169.45	169.45	N1–Co1–N3^{i}	92.70 (19)	97.11	93.51
N3–Mn1–N4	72.54(7)	78.76	78.66	N3–Co1–N3^{i}	171.9 (2)	175.44	179.15
N2–Mn1–N5	92.21(8)	92.26	91.99	N1^{i}–Co1–N2	167.94 (17)	174.30	168.84
Dihedral angles (°)				Dihedral angles (°)			
Mn1–N3–C3–C4	178.8(2)	177.88	175.68	Co1–N2–C6–C7	1.0 (6)	4.09	7.09
Mn1–N4–C8–C7	−4.8(3)	−2.16	−2.32	Co1–N2–C6–C5	−179.2 (5)	−174.70	−171.36
Mn1–N6–C15–C14	−6.5(3)	−2.17	−2.32	Co1–N3–C7–C6	−3.1 (7)	−15.64	−5.74

and 1.913 Å by using DFT/CAM-B3LYP level, as can be seen in Table 2. Theoretical values corresponding to these bond lengths, which have no experimental counterpart for complex **3**, were calculated in a similar trend (see Table S1). In addition, theoretical bond lengths obtained by DFT/ωB97XD method in all complexes were obtained in the same direction.

The bond angles between SCN–M–NCS around the coordination in complexes **1,2** were observed as 91.50(10)° and 96.2(3)°, respectively (see Table 2). The corresponding to these bond angles were obtained as 97.85 and 98.07 by using DFT/CAM-B3LYP level. The bond angles between –C=N–M–NCS around the coordination for complexes **1,2** were found to be 89.02(9)° and 92.69(18)°, respectively. These angles were calculated at 86,97° and 86,64° by using DFT/CAM-B3LYP level. The values of the bond angles of the metal ion with pyridine, imine and isothiocyanate N atoms indicate the presence of a distorted octahedral geometric structure for complexes **1–3**. In complexes **1–3**, both the coordination around metal ions and nature of metal ions demonstrate the similarity and difference in the bond length and angles. The bond lengths and angles around the central metal ions for complex **3** are in a good agreement with previously reported values (Costes et al. 2005; Avcı et al. 2018; Mobin et al. 2006).

C−H···S type hydrogen bond interactions of **1,2** were observed between the L_1 ligand and the isothiocyanate ligand with experimentally different symmetries (see Table 3 and Fig. S2). The C1-H1A···S1 hydrogen bond interaction for complex **1** displays between S atom of the isothiocyanate ligand and methyl group of L_1 ligand. The D−H···A and H···A parameters are observed at 162° and 2.87 Å, respectively. As can be seen in Table 3, the interaction in complex **2** is observed in a similar group of the ligand as in complex **1**.

The Hirshfeld surface analysis is used as a valuable tool for investigating intermolecular interactions (McKinnon et al. 2004, 2007a, 2007b; Spackman et al. 2021; Spackman and Jayatilaka 2009; Seth et al. 2011). d_e and d_i for points on the surface define distances to the nearest atoms outside and inside. In addition, these parameters are also used to create a fingerprint graph, which is a two-dimensional summary of the intermolecular interactions in the crystal. These features are used together with the identity of those atoms, to explore the interaction of intermolecular contacts in a molecular crystal and its type (H···H, C–H···S, O–H···O, C–H···π, etc.). Besides, various functions (d_{norm}, S and C) of distance and curvature mapped on Hirshfeld surfaces can be investigated. d_{norm}, exhibited using a red–white–blue colour scheme, is negative and positive demonstrating that red and blue highlight shorter and longer contacts while white is used for contacts around the vdW separation. S, shape index, defined in terms of principal curvatures κ_1 and κ_2, ranges from −1.0 called concave through 0.0 called minimal surface to +1.0 called convex. C, curvedness, defined in terms of principal curvatures κ_1 and κ_2, ranges from −4.0 describing flat through 0.0 describing a unit sphere to +0.4 describing singular.

Table 3 Hydrogen bond interactions (Å, °) observed in complex **1** and **2**.

D−H···A	D−H	H···A	D···A	D−H···A	Symmetry codes
Complex **1**					
C16—H16C···S1^{i}	0.96	2.87	3.792(3)	162	(i) x, y + 1, z
Complex **2**					
C2—H2A···S1^{ii}	0.93	2.91	3.752(6)	151	(ii) −x + 1, −y + 1, −z + 1
C3—H3A···S1^{iii}	0.93	2.86	3.628(7)	140	(iii) x, −y + 1, z + 1/2

The Hirshfeld surfaces for complexes **1,2** mapped onto curvedness ranges from −4.0 to +0.4, shape index ranges from -1.0 to + 1.0, and d_{norm} ranges from −0.1886 to + 1.5212 (for complex **1**), −0.0980 to + 2.2630 (for complex **2**), respectively. According to the shape index map (Fig. S3), the C-H donor regions in the ring have exactly opposite curvature, shape indices of equal size and opposite sign, and are colored blue, whereas depressions can be explained as large red regions of concave curvature. It can be seen in Fig. S3 that curvature maps are typically characterized by relatively flat large green regions, separated by blue edges large positive curvature.

The d_e surface of complexes **1,2** depicts the red regions displaying the hydrogen bond acceptor, d_e is short due to the close to the hydrogen nucleus outside the surface, however, the hydrogen bond donor is much less pronounced due to the larger oxygen atom outside the surface being further away from its nucleus.

Figure 2 depicts the two-dimensional fingerprint plots. From the Hirshfeld surface analyses of complexes **1,2** appear that hydrogen–hydrogen contacts dominate and contribute 28.6% and 35.2% of overall interactions, respectively (Fig. 2). On the other hand, from Fig. 2 of the fingerprint plot, the S···H/H···S contacts contribution of 29.1% and 30.5% attributed to C−H···S interaction emerged as two sharp symmetrical spikes, respectively. Furthermore, the C···H/H···C contacts with the contribution of 26.4%/23.2% assigned as C−H···π interactions appear in the fingerprint plot in a characteristic manner displaying two broad symmetrical wings (Fig. 2). Other π···π minor interactions originated from C···C contacts for complexes **1,2** appeared in the middle of the fingerprint plot with contributions of 1.8% and 4.5%, respectively.

So as to survey the conjugative interactions, interaction among bonds, as well as the coordination geometry in the compounds, the NBO analysis of complexes **1–3** was fulfilled by using DFT/ωB97XD and DFT/CAM-B3LYP levels. In these complexes, the hyperconjugative interactions were computed at the second-order perturbation approach (Altürk et al. 2016; Reed and Weinhold 1983; Foster and Weinhold 1980). In the coordination of metal complexes, NBO analysis emerges that the lone pair electrons of metal ions interact with donor N atoms of ligands. The stabilization energy ($E^{(2)}$) values of the complex structures confirmed by the remarkable LPN → LP*M(II) hyperconjugative interactions for complexes **1–3** were presented in Table S2. These $E^{(2)}$ values calculated at DFT/CAM-B3LYP level for complexes **1–3** were obtained in the range of 63.10 and 28.28, 59.18 and 12.96, 83.39 and 14.82 kcal/mol, respectively. The other stabilization interactions, LP S → π*(N–C), π*(N–C)/(C–C) → π*(C–C)/(N–C), etc., among L_1, isothiocyanate ligands demonstrated in Table S2. In brief, the stable structures of complexes **1–3** were supported by the results of NBO analysis (Table S2).

We investigated the vibrational features of complexes **1–3** obtained from the FTIR spectra and DFT/ωB97XD and DFT/CAM-B3LYP levels. A factor of 0.96 was used to the wavenumbers obtained theoretically to get closer to FT-IR spectra, taking into account differences such as experimental and theoretical phases and anharmonic effects. It is clear from Fig. 3, Tables 4 and S3 that the assignments of vibrational modes of complexes **1–3** by considering the FTIR spectra in 4000 − 400 cm^{-1} and the results obtained with DFT levels.

The CH stretching arising from the ring, methyl, and imine groups for complexes **1–3** was observed to range from 3087 to 2859 (complex **1**), from 3073 to 2889 (complex **2**), from 3065 to 2924 (complex **3**) cm^{-1}, as expected (Varsányi 1974). Theoretical values belonging to these stretching vibrations for complexes **1,2** were obtained at the range from 3089 to 2925, and from 3076 to 2930, by using DFT/CAM-B3LYP level, respectively. According to the IR spectra of **1–3**, the stretching vibrations of the NCS ligand

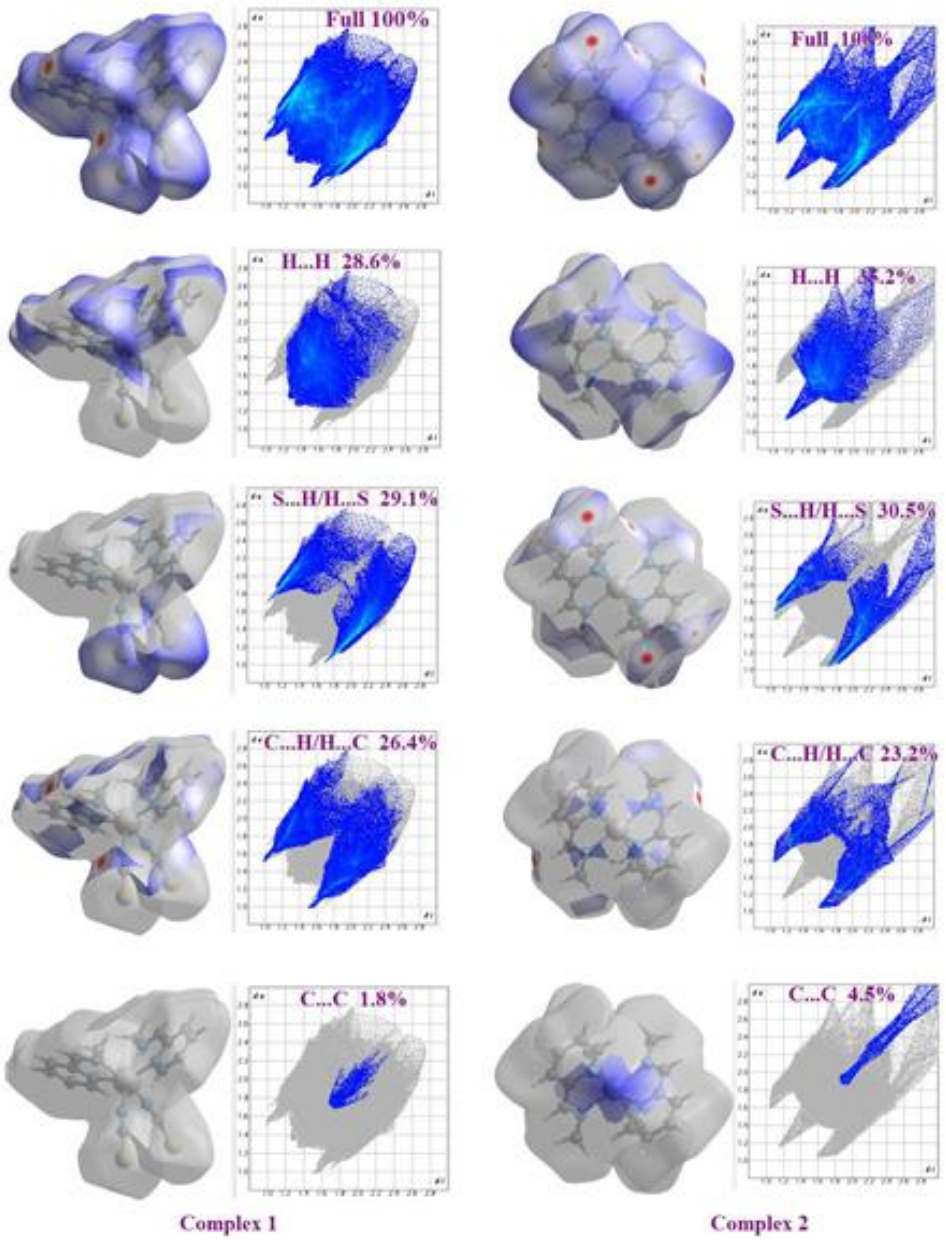

Fig. 2 2D fingerprint plots for complexes **1,2**: d_{norm} surfaces (left), all, H···H, S···H/H···S, C···H/H···C, C···C (right) contacts for each plot, indicating percentages of contacts contributed to the total Hirshfeld surface area of the complexes

were obtained in the range of 2095 and 2051 cm^{-1} and compatible with previously presented that of modes (Avcı et al. 2018; Mukherjee et al. 2000). These vibrational bands obtained at DFT/ωB97XD and DFT/CAM-B3LYP levels were found to be 2095 and 2076 cm^{-1}, and 2144 and 2076 cm^{-1} ranges, respectively. These results show the presence of the NCS ligand in complex structures. Moreover, the vibration values assigned as

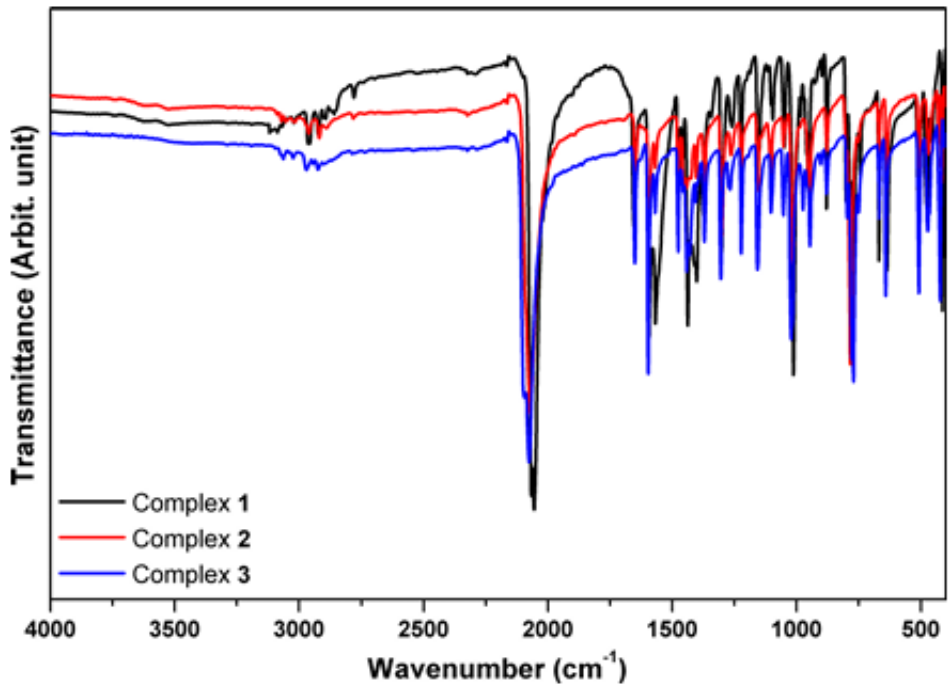

Fig. 3 Experimental IR spectra of complexes **1–3**

the stretching band of the N=C bond of Schiff base L_1 were observed at 1656, 1647 and 1650 cm^{-1}, respectively (Table 4). These results are consistent with previously reported results (Kamaal et al. 2021; Avcı 2010). The C=S stretching band of the NCS ligand in complexes **1–3** appeared within the ranges 785–751 cm^{-1} (in FTIR spectra), 819–734 cm^{-1} (in DFT/ωB97XD level), and 829–735 cm^{-1} (in DFT/CAM-B3LYP level). The vibrational bands, emerged at 1341, 1370 and 1371 cm^{-1} in FTIR spectra, and calculated at 1347, 1342 and 1361 cm^{-1} in DFT/ωB97XD level, and 1350, 1349 and 1367 cm^{-1} in DFT/CAM-B3LYP level, were assigned as the double bond CC and NC stretching vibrations belonging to the ring in complexes **1–3**. Meanwhile, the stretching vibrations of the NC bond were observed at 879 cm^{-1}, and theoretical values were computed at 871, 861 and 873 cm^{-1} (in DFT/ωB97XD level), 874, 872 and 877 cm^{-1} (in DFT/CAM-B3LYP level). Besides, the double bond CC vibrations concerning the ring in complexes **1–3** emerged at 1592, 1595 and 1596 cm^{-1} by using FTIR spectra, these vibrations were obtained at the ranges of 1619–1596 cm^{-1}, and 1611–1599 cm^{-1}, by using DFT/ωB97XD, and DFT/CAM-B3LYP levels, respectively. In addition, Table S3 demonstrates the detailed assignments of the other vibrational bands, such as in-plane/out-of-plane bending vibrations, and further vibrational modes.

3.2 The electronic spectral characterizations

Figure 4a depicts the UV–Vis absorption spectra of synthesized complexes **1–3** in the range of 200–600 nm. The absorption peaks appeared at 272.6 and 231.6 nm for complex **1**, 337.4, 279.8 and 237.7 nm for complex **2**, 281.6, 232.9 and 210.2 nm for complex **3**. It

Table 4 Selected experimental and theoretical characteristic vibration frequencies of synthesized complexes **1–3**

FT-IR (cm^{-1})	ωB97XD	CAM-B3LYP	FT-IR (cm^{-1})	ωB97XD	CAM-B3LYP	FT-IR (cm^{-1})	ωB97XD	CAM-B3LYP	Vibrational mode assignments
	6–311 + G(d,p)//LanL2DZ		6–311 + G(d,p)//LanL2DZ			6–311 + G(d,p)//LanL2DZ			
	Complex **1**		Complex **2**			Complex **3**			
3087	3089	3089	3073	3098	3076	3065	3084	3087	$\nu_{CH\ (ring)}$
3020	3077	3077	3020	3082	3062	3024	3071	3058	$\nu_{CH\ (ring)}$
2960	3004	3001	2965	3001	3017	2971	3006	3018	$\nu_{as\ (methyl)}$
2923	3014	3013	2919	2987	3001	2943	2991	2998	$\nu_{CH\ (imine)}$
2859	2916	2925	2889	2912	2930	2924	2921	2936	$\nu_{s\ (methyl)}$
2069	2095	2115	2071	2090	2133	2095	2093	2144	$\nu_{N=C\ (isothiocyanate)}$
2051	2084	2102		2076	2076	2076	2077	2127	$\nu_{N=C\ (isothiocyanate)}$
1656	1645	1650	1647	1693	1692	1650	1688	1694	$\nu_{N=C\ (imine)}$
1592	1611	1611	1595	1619	1607	1596	1596	1599	$\nu_{C=C\ (ring)}$
1341	1347	1350	1370	1342	1349	1371	1361	1367	$\nu_{C=C\ (ring)+}\ \nu_{N=C\ (ring)}$
1050	1042	1043	1050	1047	1047	1053	1037	1040	$\nu_{C=C\ (ring)}$
879	871	874	879	861	872	879	873	877	$\nu_{N=C\ (ring)}$
785	819	823	784	812	829	778	766	768	$\nu_{C=S\ (isothiocyanate)}$
771	757	762	751	754	757	771	734	735	$\nu_{C=S\ (isothiocyanate)}$

υ: Stretching; β: In-plane bending; γ: Out-of plane bending; τ: Torsion

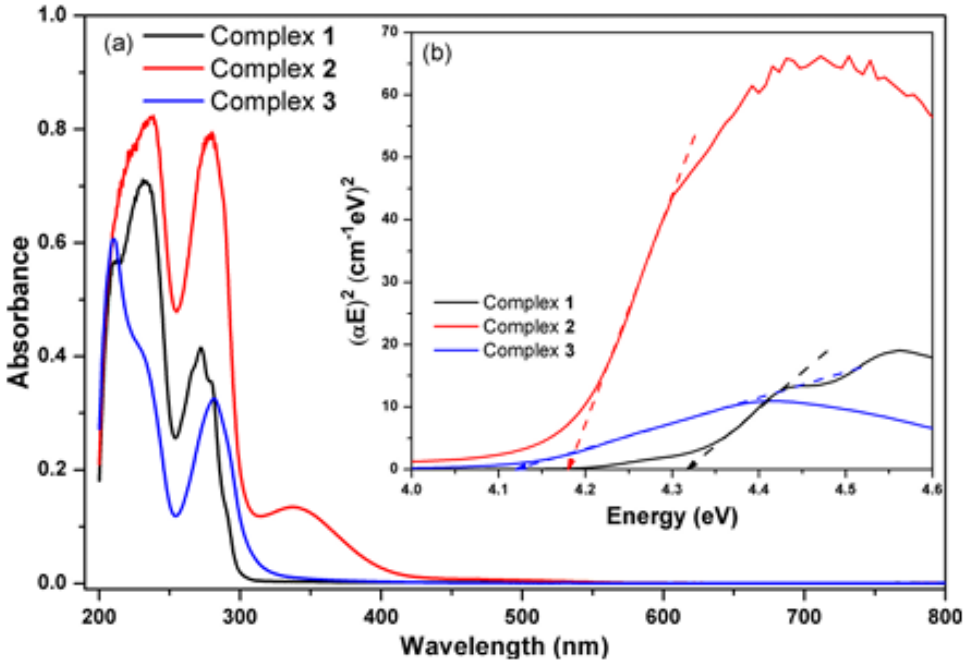

Fig. 4 **a** Experimental UV–Vis spectra and **b** the graphs of optical band gap energy for the complexes **1–3** in methanol

was determined which molecular orbitals contributed the most to the electronic transitions by using the SWizard (Gorelsky 2010) and Chemissian (Skripnikov 2016) programs (see Tables 5 and S4). Based on Table 5, Fig. 4 was presented by taking into account the occupied and unoccupied molecular orbitals that play an active role in electronic transitions. The observed absorptions for complexes **1–3** were determined as metal-to-ligand (ML)/ligand-to-metal (LM) transition, intra-ligand $\pi \rightarrow \pi^*$, and $n \rightarrow \pi^*$ transitions. The charge transitions within the ligand are clearly seen from Fig. 4 as ligand-ligand (LL) charge transfer in the high energy region.

It is well known that the enhancing contributions from the metal orbitals to the LUMO of the complex will increase the π-acceptor feature of the ligand (Gorelsky and Lever 2003). The contribution of the Mn, Co, and Ni orbitals to the HOMO/HOMOs and LUMO/LUMOs of complexes **1–3** calculated at the TD-CAM-B3LYP level changes from 4 to 58% (HOMO/HOMOs) and from 1 to 70% (LUMO/LUMOs). The contributions of the L_1 and NCS ligands orbitals to the different HOMO/HOMOs in the complexes **1–3** range from 1 to 98% and from 2 to 99% (TD-CAM-B3LYP level in methanol), respectively. At different percentages in L_1 ligand including 2-pyridyl and imine groups, and NCS ligand, HOMO contributions of L_1 ligand showing electron donor feature were found to be lower than NCS ligand, while LUMO/LUMOs contributions showing electron acceptor feature were calculated higher than NCS ligand (see Table 5). It could be said from these results that NCS ligand is a weaker π-acceptor than L_1 ligand. In complexes **1–3**, the electron density is localized on the pyridyl rings and metal ions in LUMO/LUMOs levels while the electron density is localized on the NCS ligands in HOMO level (see Fig. 5). The ML charge transfer transitions obtained at TD–CAM-B3LYP level in methanol were determined by different percentages HOMOs → LUMOs,

Table 5 Experimental and theoretical wavelength, oscillator strength and remarkable contributions for complexes **1–3**

Experimental λ (nm) (Methanol)	Methanol/TD-CAM-B3LYP/6–311 + G(d,p)// LanL2DZ		
	λ (nm)	Osc. Strength	Molecular contributions (SWizard and Chemissian programs) H: HOMO, L: LUMO, 2-pyridyl group: C_5H_4N, imine group: $CH=N-CH_3$
Complex **1**			
	426.2	0.0038	(30%) H [Mn(30%) + Pyridyl(18%) + Imine(20%) + NCS(32%)] → L α [Mn(16%) + Pyridyl(50%) + Imine(29%) + NCS(5%)]
			(16%) H − 1 [Mn(30%) + Pyridyl(32%) + Imine(17%) + NCS(21%)] → L + 1 α [Mn(41%) + Pyridyl(27%) + Imine(26%) + NCS(6%)]
272.6	273.7	0.0193	(69%) H − 3 [Mn(4%) + Pyridyl(8%) + Imine(6%) + NCS(81%)] → L α [Mn(16%) + Pyridyl(50%) + Imine(29%) + NCS(5%)]
231.6	235.3	0.0078	(45%) H[Mn(30%) + Pyridyl(18%) + Imine(20%) + NCS(32%)] → L + 4 α [Mn(70%) + Pyridyl(21%) + Imine(3%) + NCS(6%)]
			(13%) H[Mn(30%) + Pyridyl(18%) + Imine(20%) + NCS(32%)] → L + 6 α [Mn(64%) + Pyridyl(22%) + Imine(4%) + NCS(10%)]
Complex **2**			
	359.9	0.0077	(37%) H [Co(10%) + Pyridyl(26%) + Imine(25%) + NCS(40%)] → L β [Co(12%) + Pyridyl(65%) + Imine(19%) + NCS(4%)]
			(29%) H-5 [Co(44%) + Pyridyl(23%) + Imine(14%) + NCS(19%)] → L β [Co(12%) + Pyridyl(65%) + Imine(19%) + NCS(4%)]
337.4	338.5	0.0032	(26%) H-4 [Co(35%) + Pyridyl(40%) + Imine(21%) + NCS(4%)] → → L β [Co(12%) + Pyridyl(65%) + Imine(19%) + NCS(4%)]
			(28%) H-1 [Co(18%) + Pyridyl(26%) + Imine(21%) + NCS(35%)] → → L β [Co(12%) + Pyridyl(65%) + Imine(19%) + NCS(4%)]
279.8	278.1	0.0022	(40%) H [Co(18%) + Pyridyl(28%) + Imine(21%) + NCS(33%)] → L + 1 α [Co(13%) + Pyridyl(53%) + Imine(29%) + NCS(4%)]
			(28%) H-5 [Co(44%) + Pyridyl(23%) + Imine(14%) + NCS(19%)] → L + 1 α [Co(13%) + Pyridyl(53%) + Imine(29%) + NCS(4%)]
237.7	237.9	0.0103	(31%) H-7 [Co(58%) + Pyridyl(21%) + Imine(6%) + NCS(14%)] → L + 1 α [Co(13%) + Pyridyl(53%) + Imine(29%) + NCS(4%)]

Table 5 (continued)

Experimental λ (nm) (Methanol)	Methanol/TD-CAM-B3LYP/6–311 + G(d,p)// LanL2DZ		
	λ (nm)	Osc. Strength	Molecular contributions (SWizard and Chemissian programs) H: HOMO, L: LUMO, 2-pyridyl group: C_5H_4N, imine group: $CH=N-CH_3$
			(7%) H-1 [Co(4%) + Pyridyl(24%) + Imine(21%) + NCS(51%)] → L + 1 α [Co(13%) + Pyridyl(53%) + Imine(29%) + NCS(4%)]
Complex **3**			
281.6	285.1	0.0034	(64%) H-2 [Ni(37%) + Pyridyl(25%) + Imine(5%) + NCS(33%)] → L α [Ni(10%) + Pyridyl(46%) + Imine(41%) + NCS(3%)]
			(12%) H [Ni(21%) + Pyridyl(36%) + Imine(7%) + NCS(36%)] → L + 1 α [Ni(2%) + Pyridyl(55%) + Imine(37%) + NCS(6%)]
232.9	234.5	0.0006	(41%) H-4 [Ni(49%) + Pyridyl(41%) + Imine(8%) + NCS(3%)] → L + 3 α [Ni(2%) + Pyridyl(68%) + Imine(5%) + NCS(25%)]
			(11%) H-9 [Ni(25%) + Pyridyl(65%) + Imine(10%) + NCS(1%)] → L + 1 α [Ni(2%) + Pyridyl(55%) + Imine(37%) + NCS(6%)]
210.2	211.0	0.0258	(10%) H [Ni(21%) + Pyridyl(36%) + Imine(7%) + NCS(36%)] → L + 3 α [Ni(2%) + Pyridyl(68%) + Imine(5%) + NCS(25%)]
			(64%) H-2 [Ni(37%) + Pyridyl(25%) + Imine(5%) + NCS(33%)] → L + 4 α [Ni(19%) + Pyridyl(44%) + Imine(20%) + NCS(17%)]

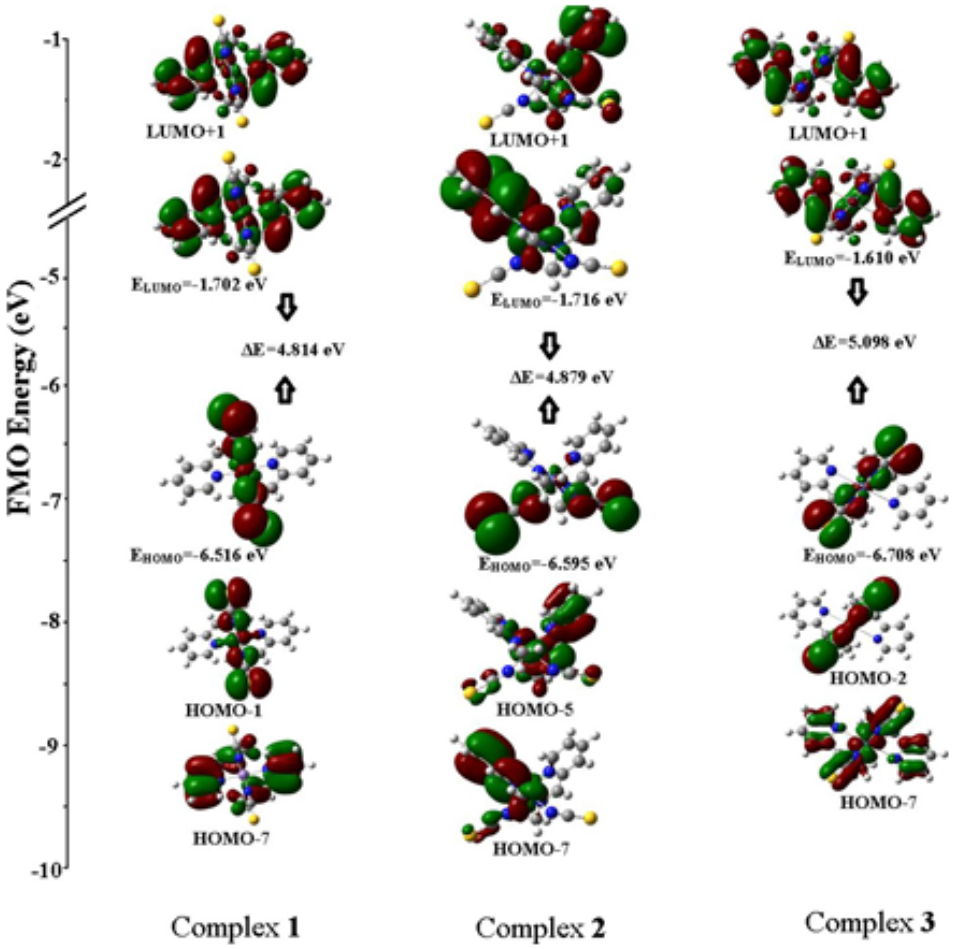

Fig. 5 FMOs and energies being the most active in electronic transition obtained by DFT/CAM-B3LYP method for complexes **1–3**

as can be seen in Table 5. For example, H-6 → L (43%) transition for complex **1** corresponds to Cd(6%), L_1(88%) including pyridyl(8%) and imine(80%)) groups, and NCS(6%) ligand in HOMO while it corresponds to pyridyl(59%) and imine(41%) in LUMO. The HOMOs → LUMOs transitions of the other complexes occurred by different percentage contribution values (see Table 5). Depending on the metal ion and its environments, the electronic transitions with the high/low oscillator strengths come out as ML/LM and LL charge transfer.

For taking into account the structure–activity relationship and physicochemical properties of biomolecules and complex systems, molecular electrostatic potential (MEP) surfaces are investigated. The MEP surfaces for **1–3** were examined by using the CAM-B3LYP/6–311 + G(d,p)//LanL2DZ level. Figure 6 depicts that the regions with the highest electron affinity in complexes **1–3** are those where the density of the red electron clouds around the isothiocyanate group is high. Besides, these negative electrostatic potential regions are related to lone pairs of electronegative atoms. The regions around the -CH groups in the ligand display the highest positive potential representing nucleophilic

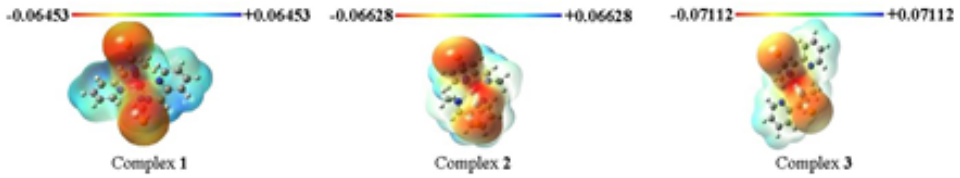

Fig. 6 Molecular electrostatic potential (MEP) surfaces for the complexes **1–3**

reactivity. These results indicate possible complex hydrogen bond interactions and more reactive regions.

To search chemical reactivity and stability as well as spectral characterization, the χ, η, S, ω, and φ parameters were computed by the energy results of frontier molecular orbital (Pearson 1986). In complexes **1–3**, the χ, η, S, ω and φ indexes calculated at CAM-B3LYP level were found to be the range of 4.511 and 3.902 eV, 3.047 eV and 2.407, 0.415 and 0.328 1/eV, 3.507 and 2.968 eV, 0.337 and 0.285 1/eV, respectively, as can be seen in Table S5. While it is clear from Table S5 that complex **2** has the smallest η and the largest ω values, it can be said that there is more electron flow and would be easily polarizable in this complex structure. The results obtained are convenient with the reported previous results (Avcı et al. 2018, 2019, 2020, 2015, 2021a; Saito et al. 1972; Mobin et al. 2006; Altürk et al. 2016, 2015).

The E_g (optical band gap energy) value is computed from the Tauc and Menth equation (Altürk et al. 2018) using the following Eq. (14).

$$(\alpha h\nu) = C(h\nu - E_g)^{1/2} \tag{14}$$

In Eq. (14), by considering d and A are the width of the cuvette (1 cm) and absorbance in the UV–Vis region, the absorption coefficient α is obtained with $\alpha = 2.303A/d$. E_g and $h\nu$ are the direct band gap energy and photon energy, in order. C is a proportionality constant concerned with the effective masses dependent on the bands. It is obviously from Fig. 4b that the E_g values for the complexes **1–3** were obtained at 4.32, 4.18, and 4.12, respectively. The gap values of HOMO–LUMO energy of complexes **1–3** calculated at CAM-B3LYP level are 4.814 eV for α spin (complex **1**), 6.095 eV (complex **2**), 5.098 eV (complex **3**). It can be stated that the obtained theoretical results are consistent with the experimental energy range values depending on the DFT method chosen.

3.3 Optical properties

Owing to likely implementations in laser technology, data storage, telecommunications, etc., the synthesis, design, and theoretical studies of new materials that may exhibit NLO properties are of great interest (Chemla and Zysss 1987; Kamada et al. 2000; Pierce 1989). Where it is not possible to experimentally investigate NLO properties for new materials, presenting a conclusion about the behavior of materials by the theoretical study is likely to be a prediction for the design and development processes of any electronic device. In this study, theoretical linear optical (LO) parameters ($\overline{\alpha}$ and Δα), first- and second-order hyperpolarizability parameters (β and γ) known as NLO parameters of synthesized complexes **1–3** were examined at DFT/ωB97XD and DFT/CAM-B3LYP levels (see Table 6).

The experimental mean n parameter in the mid-IR region of complexes **1–3** was obtained at 1.63, 1.46, and 1.50 (see Fig. S4). The experimental $\overline{\alpha}/\chi^{(1)}$ parameters for **1–3** were found

Table 6 Theoretical electric dipole moment (μ, Debye), static isotropic and anisotropic polarizability ($\overline{\alpha}$ and $\Delta\alpha, \times 10^{-24}$ esu), refractive index (n), linear optical susceptibility ($\chi^{(1)}$, in 10^{-2} esu), static first- and second-order hyperpolarizability (β, in 10^{-30} esu and γ, in 10^{-36} esu), and), third-order nonlinear optical susceptibility ($\chi^{(3)}$, in 10^{-13} esu) for complexes **1–3**

Parameter	Complex **1**		Complex **2**		Complex **3**	
	ωB97XD	CAM-B3LYP	ωB97XD	CAM-B3LYP	ωB97XD	CAM-B3LYP
	6–311 + G(d,p)		6–311 + G(d,p)		6–311 + G(d,p)	
M	12.47	14.23	14.12	15.57	11.77	13.03
M	6.20 (pNA) Cheng et al. (1991) and 4.56 (Urea) Ledoux and Zyss (1982)					
$<\alpha>$	49.75	49.45	44.62	44.64	45.08	44.59
$<\alpha_{exp}>$	5.87	4.80	4.48			
$<\alpha>$	17 (pNA) Cheng et al. (1991)					
Δα	23.51	20.31	16.64	14.98	19.35	19.92
n_{calc}	1.68	1.84	1.32	1.39	1.84	1.58
n_{exp}	1.63	1.46	1.50			
$\chi^{(1)}_{calc}$	16.91	20.20	10.49	11.65	20.23	14.95
$\chi^{(1)}_{exp}$	1.88	1.29	2.36			
$<\beta>$	51.25	54.09	14.37	17.99	9.20	9.06
$<\beta>$	9.2 (pNA) Cheng et al. (1991), 0.32 (Urea) Ledoux and Zyss (1982) and 0.13 (Urea) Adant et al. (1995)					
$<\gamma>$	636.27	580.19	58.54	75.72	63.59	60.42
$<\gamma>$	15.0 (pNA) Cheng et al. (1991) and 7 (Urea) Ledoux and Zyss (1982)					
$\chi^{(3)}$	89.85	137.14	2.67	4.45	16.51	6.82

to be $5.87\times10^{-24}/1.88\times10^{-2}$, $4.80\times10^{-24}/1.29\times10^{-2}$, and $4.48\times10^{-24}/2.36\times10^{-2}$ esu, respectively. Theoretical n values for **1–3** calculated at CAM-B3LYP level were obtained at 1.84, 1.39 and 1.58, respectively. The $\overline{\alpha}/\chi^{(1)}$ parameters for **1–3** computed at CAM-B3LYP level were obtained at $49.45\times10^{-24}/20.20\times10^{-2}$, $44.64\times10^{-24}/11.65\times10^{-2}$, and $44.59\times10^{-24}/14.95\times10^{-2}$ esu (see Table 6). Considering the results of n,$\overline{\alpha}$, and $\chi^{(1)}$ parameters in the mid-IR region, it is clear that there is coherence between experimental and theoretical results.

The computed α, β, and γ parameters were comparatively presented with the corresponding p-Nitroaniline (pNA) (Cheng et al. 1991) and urea (Ledoux and Zyss 1982; Adant et al. 1995) results used as prototype compounds. Based on DFT/CAM-B3LYP level, the mean polarizability ($\overline{\alpha}$) values of complexes **1–3** in gas phase were obtained at 49.45×10^{-24}, 44.64×10^{-24} and 44.59×10^{-24} esu, respectively. These results display that it is higher than obtained that of the polarizability of pNA (17×10^{-24} esu). The β values for complexes **1–3** in the gas phase (with DFT/CAM-B3LYP level) were found to be 54.09×10^{-30}, 17.99×10^{-30}, and 9.06×10^{-30} esu (Table 6). Similarly, the γ values of complexes **1–3** in the gas phase were obtained at 580.19×10^{-36}, 75.72×10^{-36} 60.42×10^{-36} esu (in DFT/CAM-B3LYP level). In a comparison of pNA and urea results with obtained these results, the β and γ values for complex **1** are 5.88/416.08 and 38.68/82.88 times higher than those of pNA (9.2×10^{-30} esu) (Cheng et al. 1991)/urea (0.130×10^{-30} esu) (Adant et al. 1995) and pNA (15×10^{-36} esu) (Cheng et al. 1991)/urea (7×10^{-36} esu) (Ledoux and Zyss 1982), respectively. Likewise, the static α, β, and γ parameters obtained at B3LYP/6–311 + + G(d,p) level for the synthesized 4-[(2-hydroxy-3-methoxybenzylidene) amino] benzoic acid (Kamaal et al. 2021) and dihydrated organic crystal ($TAP^{+}DNB^{-}\cdot2H_2O$) (Faizan et al. 2021) were computed at 37.4×10^{-24} and 35.72×10^{-24} for static α, 33.839×10^{-30} and 4.73×10^{-30} for static β, 167.904×10^{-36} and 32.26×10^{-36} for static γ, respectively. Regardless of the different DFT methods, the static α, β, and γ values for complex **1** are larger as compared to the static values of these compounds.

It can be noted that there are remarkable differences in NLO parameters, relating to the charge mobility in the complex, the metal ions in coordination, and its environment. In these complex structures, it is inevitable that the symmetry center around the metal ions also plays an active role in the β parameter. According to results of β and γ parameters from Table 6, complex **1** can be stated as an encouraging candidate for NLO materials (Table 6).

The extinction coefficient (k) and refractive index (n) parameters for complexes **1–3** in methanol were found to be by Eqs. (15) and (16) (Şişman and Başoğlu 2016; Erdoğan and Gündüz 2017),

$$k = \frac{\alpha\lambda}{4\pi} \tag{15}$$

$$n = \frac{1+R}{1-R} + \sqrt{\frac{4R}{(1-R)^2} - k^2} \tag{16}$$

where α, R, and λ are the absorption coefficient, reflectance and wavelength, respectively. The n values of complexes **1–3** in methanol were obtained at 2.64 at 272.6 nm, 2.13 at 337.4 nm, 2.63, at 281.6 nm, respectively (see Fig. 7a). The k values corresponding to these peaks of complexes **1–3** appear at the different peaks of 2.05×10^{-6}, 0.83×10^{-6}, and 1.68×10^{-6}, as can be seen in Fig. 7b. It can be stated that these results tend to increase and decrease similarly at different intensity maxima.

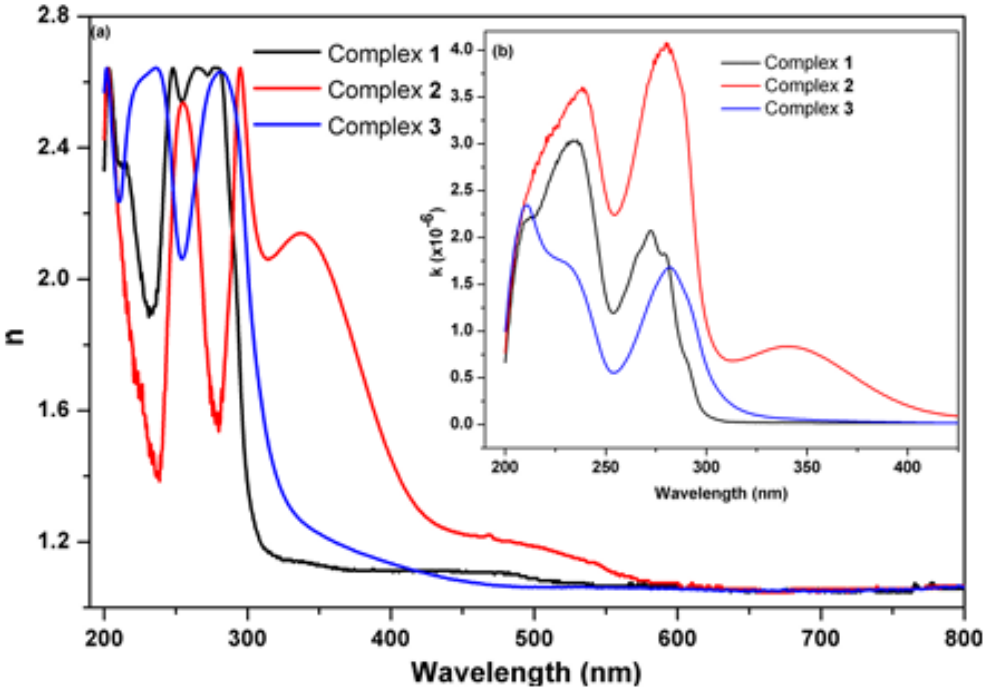

Fig. 7 **a** The refractive index n and **b** the extinction coefficient k versus λ of complexes **1–3** in methanol

The regardless of Z-scan technique (Sheik-Bahae et al. 1990; Qian et al. 2007) in this study, the third-nonlinear optical susceptibility ($\chi^{(3)}$) parameter was examined in the region in the UV–Vis region (200–600 nm). Based on the local-field polarizability model of Clausius–Mossotti, the relationship between the molar polarizability (α_p) and refractive index (n) in this region was examined by using the following Eq. (17) (El-Nahass and Farag 2012; Bharathi et al. 2017).

$$\alpha_p = \frac{3M}{4\pi N_a \rho}\left(\frac{n^2-1}{n^2+2}\right) \tag{17}$$

where M, ρ and N_a are the molecular weight, molecular density, and Avogadro number, respectively. In complexes **1–3**, the molar polarizability did not alter up to about 2.0, 2.3, and 2.8 eV, afterward, it was found to be with the increase in the energy of the photon, the polarizability values begin to increase. A similar trend was also observed in different structures (Dege et al. 2021; Avcı et al. 2021b). The maximum molar polarizabilities were obtained at 76.79×10^{-24} cm^3 versus 4.42 eV photon energy, 81.29×10^{-24} cm^3 versus 4.21 eV photon energy, 71.11×10^{-24} cm^3 versus 5.22 eV photon energy, respectively (see Fig. 8a). The $\chi^{(3)}$ parameter associated with refractive index in the UV–Vis by taking approximately 10^{-10} esu of the A parameter for all compounds regardless of frequency can be computed by using Eq. (18) (El-Nahass and Farag 2012; Bharathi et al. 2017).

$$\chi^{(3)} = \frac{A}{(4\pi)^4}\left(n^2-1\right)^4 \tag{18}$$

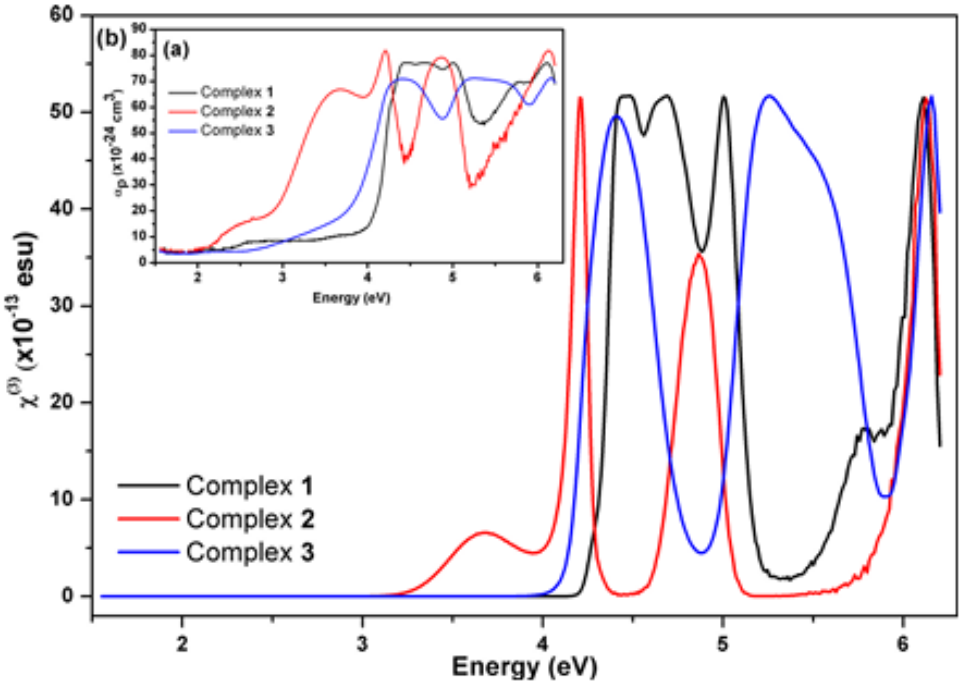

Fig. 8 **a** The molar polarizability α_p and **b** the third-order nonlinear optical susceptibility $\chi^{(3)}$ of complexes **1–3** in methanol

It could be from Fig. 8b that the $\chi^{(3)}$ values are stable until 3.18, 3.98, and 4.18 eV, and it was then observed that the $\chi^{(3)}$ started to increase with the energy of the photon. The maximum peaks for $\chi^{(3)}$ were obtained at 51.65×10^{-13}, 51.42×10^{-13}, and 51.42×10^{-13} esu corresponding to the photon energies of 4.68, 4.21, and 5.25 eV, respectively. It is clear that the same $\chi^{(3)}$ maxima values are observed at different photon energies. Besides, it has been determined that there is a similar trend in the graphs since the α_p and $\chi^{(3)}$ parameters change depending on the different strength degrees of the refractive index. It can be stated that these parameters show differences depending on the coordination environment and metal ion exchange, as well as similarities in different complex structures with similar coordination geometries (Dege et al. 2021; Şişman and Başoğlu 2016).

Owing to the importance of optical compounds and devices, the optical conductivity (σ_{opt}) associated with the absorption coefficient (α), refractive index (n), and light velocity (c) is obtained by Eq. (19) (Akinlami and Olateju 2012).

$$\sigma_{opt} = \frac{\alpha nc}{4\pi} \tag{19}$$

Figure 9 demonstrates the alternation of optical conductivity versus E of the Mn(II), Co(II), and Ni(II) complexes in methanol. It was observed that this parameter started to increase with the energy of the photon while the σ_{opt} parameter of complexes **1–3** did not change till 4.0, 2.85, and 3.69 eV, respectively. It can be reported that a similar trend is obtained with different complex structures (Dege et al. 2021; Avcı et al. 2021b). According to the estimated values n and σ_{opt} plotted versus photon energy in Figs. 7a and 9, it can be said that the constant values of n and σ_{opt} in the visible region have prospective

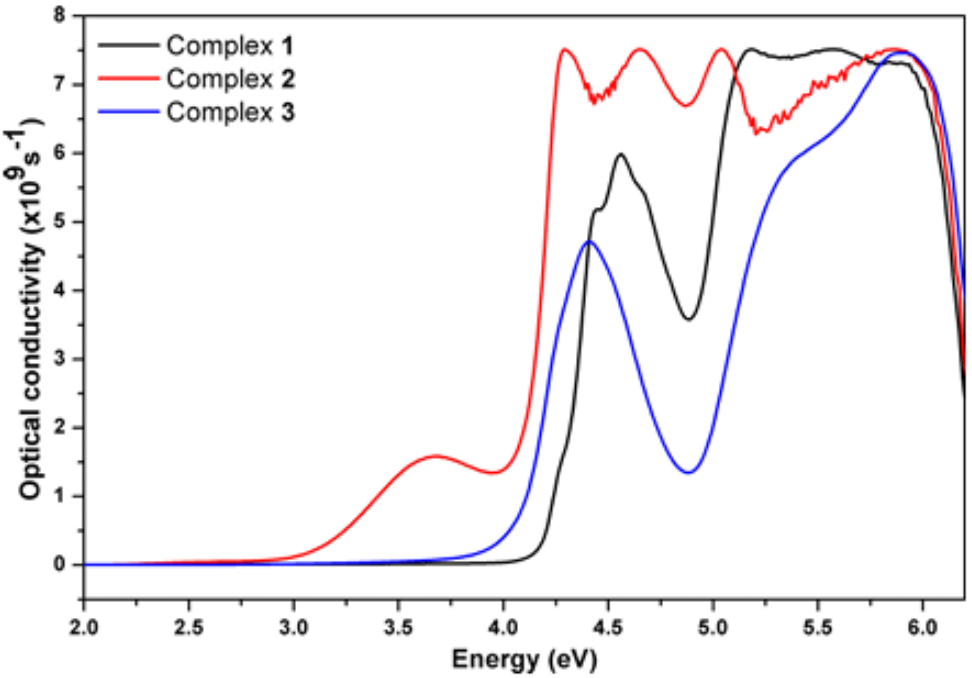

Fig. 9 **a** The optical conductivity σ_{opt} versus E of complexes **1–3** in methanol

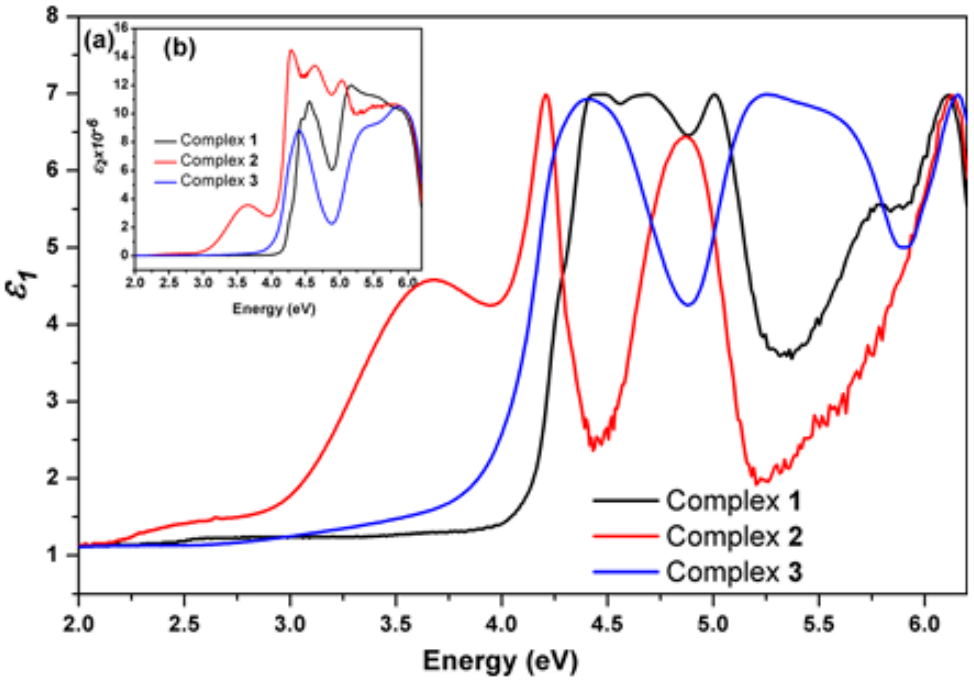

Fig. 10 **a** The real part ε_1 and **b** the imaginary part ε_2 versus E of the complexes **1–3** in methanol

implementations in a signal filter, resonator, and reflector for complexes **1–3** (Mehkoom et al. 2022a, 2021).

Figure 10 displays the variation versus photon energy of the dielectric constant including the real part ε_1 and the imaginary part ε_2 defined with Eqs. (20), (21) (Şişman and Başoğlu 2016; Erdoğan and Gündüz 2017; Urbach 1953).

$$\varepsilon_1 = n^2 - k^2 \tag{20}$$

$$\varepsilon_2 = 2nk \tag{21}$$

From Fig. 10a and b, while the real dielectric constant was stable until 2.40, 2.16, and 2.72, it was observed that the imaginary dielectric constant did not alter up to 4.05, 2.92, and 3.54. In the between 4 and 6 eV energy regions for complexes **1–3**, the same trend demonstrates with the rise in photon energy. However, the real part of the dielectric constant of complexes **1–3** is larger than the imaginary part because the extinction coefficient is lower than the refractive index of the complexes.

4 Conclusion

To investigate LO and NLO features, the *N*-(pyridin-2-ylmethylene)methanamine (L_1) and its complexes {$[Mn(L_1)_2(NCS)_2]$, (**1**), $[Co(L_1)_2(NCS)_2]$, (**2**) and $[Ni(L_1)_2(NCS)_2]$, (**3**)} were synthesized. The XRD, LC-HRMS, FT–IR, and UV–Vis spectroscopic methods for **1–3** were used to carry out structural, and spectral characterizations, as well as to examine LO and NLO features. The fingerprint plots provided the describing the intermolecular interaction types present in the crystal structures of **1,2** and the structures retrieved from CSD. Hirshfeld surface analysis was performed to describe intermolecular interactions for complexes **1,2**. In addition, it has been observed that H···H, C–H···S, and C–H…π interactions occur in fingerprint plots in areas of close contact and weakest interactions. For theoretical investigations in addition to experimental parameters, DFT/ωB97XD and DFT/CAM-B3LYP levels calculations were fulfilled. While the HOMO/HOMOs values of the L_1 ligand showing the electron donor feature were found to be lower than the NCS ligand, the higher LUMO/LUMOs values showing the electron acceptor feature were found that a much stronger π-acceptor of the L_1 ligand than the NCS ligand. The coordination around metal ions and hyperconjugative interactions for complexes **1–3** were backed up by NBO results. The experimental mean n and $\chi^{(1)}$ parameters in the mid-IR region for complex **1** were obtained at values greater than complexes **2** and **3**. Complex **1** has high values of the β and γ parameters suggesting that complex **1** can be expressed as an encouraging candidate for NLO materials. It is concluded that the experimental $\chi^{(3)}$ results obtained at the UV–Vis region for complexes **1–3** in methanol display about the same values ($\chi^{(3)} = 51.65 \times 10^{-13}$, 51.42×10^{-13}, and 51.42×10^{-13} esu, respectively) in the most maximum peaks of third-order NLO susceptibility at different photon energy (4.68, 4.21, and 5.25 eV, respectively). Although third-order NLO susceptibility, nonlinear refractive index, and absorption parameters could not be determined by the Z-scan technique for complexes **1–3** in this study, third-order NLO parameters obtained theoretically and experimentally demonstrate that complex **1** can be used to develop optoelectronic devices.

Appendix A

Crystallographic data for the structural analysis has been deposited with the Cambridge Crystallographic Data Centre, CCDC Numbers: 1990152 (complex **1**), 1,989,407 (complex **2**). Copies of this information may be obtained free of charge from the Director, CCDC, 12 Union Road, Cambridge CB2 1EZ, UK (fax: +44–1223- 336,033; e-mail: deposit@ccdc.cam.ac.uk or www: http://www.ccdc.cam.ac.uk).

Supplementary Information The online version contains supplementary material available at https://doi.org/10.1007/s11082-023-04668-1.

Author contributions DA methodology, software, formal analysis, writing-original draft, writing-review&editing. ÖÖ data curation, formal analysis, visualization. AB formal analysis, methodology, software. FS formal analysis, investigation, writing-review&editing. ÖT investigation, software. ND data curation, formal analysis, visualization. YA methodology, software.

Funding This work was supported by the Scientific Research Projects Unit of Sakarya University (Project Number: 2021-7-25-103).

Data availability The data that support the findings of this study are available from the corresponding author upon reasonable request.

Declarations

Conflict of interest The authors declare that they have no conflict of interest.

Ethical approval Not applicable.

Consent of participate Not applicable.

Consent of publish Not applicable.

References

Abdalkarim, K.A., Aziz, S.B., Abdulwahid, R.T., Alshehri, S.M., Ahamad, T., Hadi, J.M., Hussein, S.A.: Synthesis of Hg metal complex and its application to reduce the optical band gap of polymer. Arab. J. Chem. **14**, 103215 (2021)

Adant, C., Dupuis, M., Bredas, J.: Ab initio study of the nonlinear optical properties of urea: electron correlation and dispersion effects. Int. J. Quant. Chem. **56**, 497–507 (1995)

Akinlami, J.O., Olateju, I.O.: Reflection coefficient and optical conductivity of gallium nitride GaN. Semicond. Phys. Quantum Electron. Optoelectron. **15**, 281–284 (2012)

Al-Amiery, A.A.: Synthesis and antioxidant, antimicrobial evaluation, DFT studies of novel metal complexes derivate from Schiff base. Res. Chem. Intermed. **38**(3), 745–759 (2012)

Altürk, S., Tamer, Ö., Avcı, D., Atalay, Y.: Synthesis, spectroscopic characterization, second and third-order nonlinear optical properties, and DFT calculations of a novel Mn(II) complex. J. Organomet. Chem. **797**, 110–119 (2015)

Altürk, S., Avcı, D., Tamer, Ö., Atalay, Y., Şahin, O.: A cobalt(II) complex with 6-methylpicolinate: synthesis, characterization, second- and third-order nonlinear optical properties, and DFT calculations. J. Phys. Chem. Solids **98**, 71–80 (2016)

Altürk, S., Avcı, D., Başoğlu, A., Tamer, Ö., Atalay, Y., Dege, N.: Copper (II) complex with 6-methylpyridine-2-carboxyclic acid: experimental and computational study on the XRD, FT-IR and UV–Vis spectra, refractive index, band gap and NLO parameters. Spectrochim. Acta A **190**, 220–230 (2018)

Amirnasr, M., Khalaji, A.D., Falvello, L.R., Soler, T.: Synthesis, characterization, and crystal structures of $[Ag(ca_2en)(PPh_3)(X)]$ $(X = N_3, SCN)$ complexes. Polyhedron **25**, 1967–1970 (2006)

Avcı, D.: The consistency analysis of different semiempirical calculations on second- and third-order nonlinear optical properties of donor–acceptor chromophores containing α-cyan Spectrochim. Acta A **77**, 665–672 (2010)

Avcı, D.: Second and third-order nonlinear optical properties and molecular parameters of azo chromophores: semiempirical analysis. Spectrochim. Acta A **82**, 37–43 (2011)

Avcı, D., Altürk, S., Sönmez, F., Tamer, Ö., Başoğlu, A., Atalay, Y., Kurt, B.Z., Dege, N.: Three novel Cu(II), Cd(II) and Cr(III) complexes of 6−Methylpyridine−2−carboxylic acid with thiocyanate: Synthesis, crystal structures, DFT calculations, molecular docking and α-Glucosidase inhibition studies. Tetrahedron **74**, 7198–7208 (2018)

Avcı, D., Altürk, S., Sönmez, F., Tamer, Ö., Başoğlu, A., Atalay, Y., Zengin Kurt, B., Dege, N.: A novel series of mixed-ligand M(II) complexes containing 2,2′-bipyridyl as potent α-glucosidase inhibitor: synthesis, crystal structure. DFT Calculat. Mol. Dock. JBIC J. Biol. Inorg. Chem. **24**, 747–764 (2019)

Avcı, D., Altürk, S., Sönmez, F., Tamer, Ö., Başoğlu, A., Atalay, Y., Zengin Kurt, B.: Synthesis, DFT calculations and molecular docking study of mixed ligand metal complexes containing 4,4′-dimethyl-2,2′-bipyridyl as α-glucosidase inhibitors. J. Mol. Struct. **1205**, 127665 (2020)

Avcı, D., Altürk, S., Sönmez, F., Tamer, Ö., Başoğlu, A., Atalay, Y., Zengin Kurt, B., Dege, N.: Synthesis, spectral properties, in vitro α-glucosidase inhibitory activity and quantum chemical calculations of novel mixed-ligand M(II) complexes containing 1,10-phenanthroline. Appl. Organomet. Chem. **34**, e5412 (2020)

Avcı, D., Altürk, S., Sönmez, F., Tamer, Ö., Başoğlu, A., Atalay, Y., Zengin Kurt, B., Dege, N.: Novel metal complexes containing 6-methylpyridine-2-carboxylic acid as potent α-glucosidase inhibitor: synthesis, crystal structures. DFT Calculat. Mol. Dock. Mol. Div. **25**, 171–189 (2021)

Avcı, D., Saeedi, Y., Başoğlu, A., Dege, N., Altürk, S., Tamer, Ö., Atalay, Y.: Novel Mn(II) and Zn(II) complexes of 6-bromopicolinic acid as a potential optical material: synthesis, spectral characterizations, linear, and nonlinear optical properties and density functional theory calculations. Appl. Organomet. Chem. **35**, e6125 (2021b)

Barquín, M., Cocera, N., Gonźalez Garmendia, M.J., Larrínaga, L., Pinilla, E., Seco, J.M., Torres, M.R.: Acetato and formato copper(II) complexes with 4,4'-dimethyl-2,2'-bipyridine and 5,5'-dimethyl-2,2'-bipyridine: synthesis, crystal structure, magnetic properties and EPR results. A new 1D polymeric water chain. Inorgan. Chim. Acta **363**, 127–133 (2010)

Bharathi, M.D., Ahila, G., Mohana, J., Chakkaravarthi, G., Anbalagan, G.: Synthesis, crystal structure, growth, optical and third order nonlinear optical studies of $8HQ_2C_5N$ single crystal-an efficient third-order nonlinear optical material. Mater. Chem. Phys. **192**, 215–227 (2017)

Chai, J.-D., Head-Gordon, M.: Long-range corrected hybrid density functionals with damped atom-atom dispersion corrections. Phys. Chem. Chem. Phys. **10**, 6615–6620 (2008)

Chattaraj, P.K., Sarkar, U., Ro, D.R.: Electrophilicity Index. Chem. Rev. **106**(6), 2065–2091 (2006)

Chemla, D.S., Zysss, J.: Nonlinear Optical Properties of Organic Molecules and Crystals. Academic Press, Orlando, FL (1987)

Cheng, L.T., Tam, W., Stevenson, S.H., Meredith, G.R., Rikken, G., Marder, S.R.: Experimental investigations of organic molecular nonlinear optical polarizabilities. 1. Methods and results on benzene and stilbene derivatives. J. Phys. Chem. **95**, 10631–10643 (1991)

Constable, E.C., Steel, P.J.: N, N'-Chelating biheteroaromatic ligands; a survey. Coord. Chem. Rev. **93**(2), 205–223 (1989)

Costes, J.P., Lamère, J.F., Lepetit, C., Lacroix, P.G., Dahan, F.: Synthesis, crystal structures, and nonlinear optical (NLO) properties of new schiff-base nickel(II) complexes. Toward a new Type of molecular switch? Inorganic Chemistry **44**(6), 1973–1982 (2005)

da Silva, M.A.V.R., da Silva, M.D.M.C.R., Monte, M.J.S., Gonçalves, J.M., Fernandes, É.M.R.: Energetics of metal–ligand binding in copper (II) and nickel (II) complexes of two Schiff bases. J. Chem. Soc. Dalton Trans. **7**, 1257–1262 (1997)

Dege, N., Özge, Ö., Avcı, D., Başoğlu, A., Sönmez, F., Yaman, M., Tamer, Ö., Atalay, Y., Zengin Kurt, B.: Concentration effects on optical properties, DFT, crystal characterization and α-glucosidase activity studies: Novel Zn(II) complex. Spectrochim. Acta A **262**, 120072 (2021)

Derkowska-Zielinskaa, B., Barwiolek, M., Cassagne, C., Boudebs, G.: Nonlinear optical study of Schiff bases using Z-scan technique. Opt. Laser Technol. **124**, 105968 (2020)

Driessen, W., De Graaff, R., Parlevliet, F., Reedijk, J., De Vos, R.: Transition metal compounds of the tridentate pyrazole substituted amine ligand bis (2-(3,5-dimethyl-1-pyrazolyl) ethyl) ethylamine (ddae). X-ray structures of $[Co(ddae)(NO_3)_2]$, $[Cu(ddae)(NO_3)(H_2O)](NO_3)$ and $[Cu(ddae)(Cl)_2]C_2H_5OH$. Inorgan. Chim. Acta **216**, 43–49 (1994)

El-Nahass, M.M., Farag, A.A.M.: Structural, optical and dispersion characteristics of nanocrystalline GaN films prepared by MOVPE. Opt. Laser Technol. **44**, 497–503 (2012)

Erdoğan, E., Gündüz, B.: Optoelectronic parameters of TBADN organic molecule: new aspect to solution technique. Opt. Laser Technol. **91**, 130–137 (2017)

Faizan, M., Mehkoom, M., Afroz, Z., Rodrigues, V.H.N., Afzal, S.M., Ahmad, S.: Experimental and computational investigation of novel dihydrated organic single crystal of 2,4,6-triaminopyrimidine and 3,5-dintrobenzoic acid: Linear and nonlinear optical response with limiting performance. J. Solid State Chem. **300**, 122255 (2021)

Foster, J.P., Weinhold, F.: Natural hybrid orbitals. J. Am. Chem. Soc. **102**, 7211–7218 (1980)

Frisch, M.J., Pople, J.A., Binkley, J.S.: Self-consistent molecular orbital methods 25. Supplementary functions for Gaussian basis set. J. Chem. Phys. **80**, 3265–3269 (1984)

Gaussian 16, Revision C.01, M. J. Frisch, G. W. Trucks, H. B. Schlegel, G. E. Scuseria, M. A. Robb, J. R. Cheeseman, G. Scalmani, V. Barone, G. A. Petersson, H. Nakatsuji, X. Li, M. Caricato, A. V. Marenich, J. Bloino, B. G. Janesko, R. Gomperts, B. Mennucci, H. P. Hratchian, J. V. Ortiz, A. F. Izmaylov, J. L. Sonnenberg, D. Williams-Young, F. Ding, F. Lipparini, F. Egidi, J. Goings, B. Peng, A. Petrone, T. Henderson, D. Ranasinghe, V. G. Zakrzewski, J. Gao, N. Rega, G. Zheng, W. Liang, M. Hada, M. Ehara, K. Toyota, R. Fukuda, J. Hasegawa, M. Ishida, T. Nakajima, Y. Honda, O. Kitao, H. Nakai, T. Vreven, K. Throssell, J. A. Montgomery, Jr., J. E. Peralta, F. Ogliaro, M. J. Bearpark, J. J. Heyd, E. N. Brothers, K. N. Kudin, V. N. Staroverov, T. A. Keith, R. Kobayashi, J. Normand, K. Raghavachari, A. P. Rendell, J. C. Burant, S. S. Iyengar, J. Tomasi, M. Cossi, J. M. Millam, M. Klene, C. Adamo, R. Cammi, J. W. Ochterski, R. L. Martin, K. Morokuma, O. Farkas, J. B. Foresman, and D. J. Fox, Gaussian, Inc., Wallingford CT, 2016.

GaussView, Version 6.1, R. Dennington, T.A. Keith, J.M. Millam, Semichem Inc., Shawnee Mission, KS, (2016)

Ghani, U.: Re-exploring promising a-glucosidase inhibitors for potential development into oral anti-diabetic drugs: finding needle in the haystack. Eur. J. Med. Chem. **103**, 133–162 (2015)

Ghosh, S., Roy, N., Singh, T.S., Chattopadhyay, N.: Photophysics of a coumarin based Schiff base in solvents of varying polarities. Spectrochim. Acta Part A Mol. Biomol. Spectrosc. **188**, 252–257 (2018)

Glendening, E.D., Reed, A.E., Carpenter, J.E., Weinhold, F.: NBO Version3.1, TCI, University of Wisconsin, Madison, 1998.

Gollapalli, M., Taha, M., Javid, M.T., Almandil, N.B., Rahim, F., Wadood, A., Mosaddik, A., Ibrahim, M., Alqahtani, M.A., Bamarouf, Y.A.: Synthesis of benzothiazole derivatives as a potent α−glucosidase inhibitör. Bioorg. Chem. **85**, 33–48 (2019)

Gorelsky, S.I.: *SWizard Program, Revision 4.5*, University of Ottawa, Ottawa, Canada, 2010, http://www.sg.chem.net/.

Gorelsky, S.I., Lever, A.B.P.: The electronic structure and spectra of [Ru(NH3)4(LL)]2+ (LL = bpy, bpz, bqdi) studied by density functional theory and INDO/S. Charge transfer character of electronic transitions and their solvatochromism. Can. J. Anal. Sci. Spectr. **48**(1), 93–105 (2003)

Habib, M., Karmakar, T.K., Aromí, G., Ribas-Ariño, J., Fun, H.-K., Chantrapromma, S., Chandra, S.K.: A versatile series of nickel(II) complexes derived from tetradentate imine/pyridyl ligands and various pseudohalides: azide and cyanate compared. Inorg. Chem. **47**(10), 4109–4117 (2008)

Hay, P.J., Wadt, W.R.: Ab initio effective core potentials for molecular calculations. Potentials for the transition metal atoms Sc to Hg. J. Chem. Phys. **82**, 270–283 (1985)

Iqbal, M.S., Khan, A.H., Loothar, B.A., Bukhari, I.H.: Effect of derivatization of sulfamethoxazole and trimethoprim with copper and zinc on their medicinal value. Med. Chem. Res. **18**(1), 31–42 (2009)

Kamaal, S., Mehkoom, M., Ali, A., Afzal, S.M., Alam, M.J., Ahmad, S., Ahmad, M.: Potential third-order nonlinear optical response facilitated by intramolecular charge transfer in a simple schiff base molecule: experimental and theoretical exploration. ACS Omega **6**, 6185–6194 (2021)

Kamada, K., Ueda, M., Nagao, H., Tawa, K., Sugino, T., Shmizu, Y., Ohta, K.: Molecular design for organic nonlinear optics: polarizability and hyperpolarizabilities of furan homologues investigated by ab initio molecular orbital method. J. Phys. Chem. A **104**(20), 4723–4734 (2000)

Kanwal, A., Parveen, B., Ashraf, R., Haider, N., Ali, K.G.: A review on synthesis and applications of some selected Schiff bases with their transition metal complexes. J. Coord. Chem. **75**, 2533–2556 (2022)

Khan, A., Sarkar, S., Sarkar, D.: Bactericidal activity of 2-nitroimidazole against activereplicating stage of *Mycobacterium bovis* BCG and *M. tuberculosis* with intracellular efficacy in THP-1 macrophage. Int. J. Antimicrob. Agents **32**(1), 40–45 (2008)

Lacroix, P.G.: Second-order optical nonlinearities in coordination chemistry: the case of bis(salicylaldiminato)metal schiff base complexes. Eur. J. Inorg. Chem. **2001**, 339–348 (2001)

Lacroix, P.G., Bella, S.D.: Ledoux, synthesis and second-order nonlinear optical properties of new copper(II), nickel(II), and zinc(II) schiff-base complexes. Toward a role of inorganic chromophores for second harmonic generation. Chem. Mater. **8**, 541–545 (1996)

Ledoux, I., Zyss, J.: Influence of the molecular environment in solution measurements of the second-order optical susceptibility for urea and derivatives. Chem. Phys. **73**, 203–213 (1982)

Li, L., Liao, D., Liu, S., Jiang, Z., Yan, S.: A one-dimensional chain compound $[Cu(im2\text{-}py)(SCN)_2]_n$ exhibiting strong ferromagnetic coupling. Inorg. Chem. Commun. **6**, 225–228 (2003)

Liu, C.-G., Qiu, Y.-Q., Sun, S.-L., Chen, H., Li, N., Su, Z.-M.: DFT study on second-order nonlinear optical properties of a series of mono Schiff-base M(II) (M = Ni, Pd, Pt) complexes. Chem. Phys. Lett. **429**, 570–574 (2006)

McKinnon, J.J., Spackman, M.A., Mitchell, A.S.: Novel tools for visualizing and exploring intermolecular interactions in molecular crystals. Acta Cryst. **B60**, 627–668 (2004)

McKinnon, J.J., Jayatilaka, D., Spackman, M.A.: Towards quantitative analysis of intermolecular interactions with Hirshfeld surfaces. Chem. Commun. **37**, 3814–3816 (2007)

McKinnon, J.J., Fabbiani, F.P.A., Spackman, M.A.: Comparison of polymorphic molecular crystal structures through Hirshfeld surface analysis. Cryst. Growth Des. **7**, 755–769 (2007b)

Mehkoom, M., Faizan, M., Afzal, S.M., Ahmad, S.: Z-scan screening of proton-shifted monohydrated organic salt: the linear, nonlinear, and optical limiting characteristics for photonic applications. J. Mater. Sci. Mater. Electron. **32**, 28750–28764 (2021)

Mehkoom, M., Afzal, S.M., Ahmad, S., Khan, S.A.: The new pyrazoline derivative 5-(3,4-Dimethoxyphenyl)-3-(2,5-dimethyl-thiophene-3-yl),-4,5-dihydro-pyrazole-1-carbothioic acid amide (DDPA) as an advisable candidate for optical linearity, nonlinearity, and limiting performance. J. Mol. Liq. **345**, 117018 (2022)

Mehkoom, M., Ali, A., Alam, M.J., Ali, F., Afzal, S.M., Ahmad, S.: Intramolecular charge transfer-based linear and nonlinear optical properties of a D–π–A–π–D type organic chromophore: experimental and computational approach. J. Nonlinear Opt. Phys. Mater. **31**(02), 2250006 (2022)

Miertus, S., Scrocco, E., Tomasi, J.: Electrostatic interaction of a solute with a continuum. A direct utilizaion of Ab initiomolecular potentials for the prevision of solvent effects. J. Chem. Phys. **55**, 117–129 (1981)

Mobin, S.M., Saini, A.K., Mishra, V., Chaudhary, A.: A series of new heteroleptic Hg (II) complexes: synthesis, crystal structures and photophysical properties. Polyhedron **110**, 131–141 (2006)

Mukherjee, P.S., Maji, T.K., Mostafa, G., Mallah, T., Chaudhuri, N.R.: The first structurally alternating copper(II) chain with alternate single end-on and end-to-end azido bridging: a synthesis, crystal structure, and low-temperature magnetic study. Inorg. Chem. **39**, 5147–5150 (2000)

Oudar, J.L.: Optical nonlinearities of conjugated molecules. Stilbene derivatives and highly polar aromatic compounds. J. Chem. Phys. **67**, 446–457 (1977)

Oudar, J.L., Zyss, J.: Relations between microscopic and macroscopic lowest-order optical nonlinearities of molecular crystals with one-or two-dimensional units. Phys. Rev. A **26**, 2028–2048 (1982)

Pearson, R.G.: Absolute electronegativity and hardness correlated with molecular orbital theory. Proc. Nati. Acad. Sci. USA **83**, 8440–8441 (1986)

Petrus, M.L., Bouwer, R.K.M., Lafont, U., Murthy, D.H.K., Kist, R.J.P., Böhm, M.L., Olivier, Y., Savenije, T.J., Siebbeles, L.D.A., Greenhamd, N.C., Dingemans, T.J.: Conjugated poly(azomethine)s via simple one-step polycondensation chemistry: synthesis, thermal and optoelectronic properties. Polym. Chem. **4**, 4182–4191 (2013)

Pierce, B.M.: A theoretical analysis of third-order nonlinear optical properties of linear polyenes and benzene. J. Chem. Phys. **91**(2), 791–811 (1989)

Qian, Y., Xiao, G., Wang, G., Lin, B., Cui, Y., Sun, Y.: Synthesis and Z-scan measurements of third-order optical nonlinearity in push–pull molecules with dihydroxylethyl amino donor and nitro acceptor. Dyes Pigm. **75**, 218–224 (2007)

Reed, A.E., Weinhold, F.: Natural bond orbital analysis of near-Hartree–Fock water dimer. J. Chem. Phys. **78**, 4066–4073 (1983)

Richmond, T.G., Kelson, E.P., Arif, A.M.: Mechanism of formation of coordination polymers: a structural model for polymer chain growth. J. Am. Chem. Soc. **110**(7), 2334–2335 (1988)

Runge, E., Gross, E.K.U.: Density-functional theory for time-dependent systems. Phys. Rev. Lett. **52**, 997–1000 (1984)

Saito, Y., Takemoto, J., Hutchinson, B., Nakamoto, K.: Infrared studies of coordination compounds containing low-oxidation-state metals I Tris (2,2'-bipyridine) and tris (1,10-phenanthroline) complexes. Inorg. Chem. **11**(9), 2003–2011 (1972)

Sarkar, S., Biswas, S., Liao, M.-S., Kar, T., Aydogdu, Y., Dagdelen, F., Mostafa, G., Chattopadhyay, A.P., Yap, G.P.A., Xie, R.-H., Khan, A.T., Dey, K.: An attempt towards coordination supramolecularity from Mn(II), Ni(II) and Cd(II) with a new hexadentate $[N_4O_2]$ symmetrical Schiff base ligand: syntheses, crystal structures, electrical conductivity and optical properties. Polyhedron **27**, 3359–3370 (2008)

Seth, S.K., Sarkar, D., Roy, A., Kar, T.: Insight into supramolecular self-assembly directed by weak interactions in acetophenone derivatives: crystal structures and Hirshfeld surface analyses. CrystEngComm **13**, 6728–6741 (2011)
Sheik-Bahae, M., Said, A.A., Wei, T.-H., Hagan, D.J., Van Stryland, E.W.: Sensitive measurement of optical nonlinearities using a single beam. IEEE J. Quantum Electron. **26**, 760–769 (1990)
Şişman, İ, Başoğlu, A.: Effect of Se content on the structural, morphological and optical properties of Bi_2Te_3–ySey thin films electrodeposited by under potential deposition technique. Mater. Sci. Semicond. Process. **54**, 57 (2016)
Skripnikov, L.: Chemissian: software to analyze spectra, build density maps and molecular orbitals, Version 4.43, (2016)
Sönmez, F., Güneşli, Z., Zengin Kurt, B., Gazioğlu, I., Avcı, D., Küçükislamoğlu, M.: Synthesis, antioxidant activity and SAR study of novel spiro-isatin-based Schiff bases. Mol. Div. **23**, 829–844 (2019)
Spackman, M.A., Jayatilaka, D.: Hirshfeld surface analysis. CrystEngComm **11**, 19–32 (2009)
Spackman, P.R., Turner, M.J., McKinnon, J.J., Wolff, S.K., Grimwood, D.J., Jayatilaka, D., Spackman, M.A.: *CrystalExplorer*: a program for Hirshfeld surface analysis, visualization and quantitative analysis of molecular crystals. J. Appl. Cryst. **54**, 1006–1011 (2021)
Uddin, E., Bitu, N.A., Asraf, A., Hossen, F., Mohapatra, R.K., Zahan, Md.K.E.: An updated perspective of nano schiff base complexes: synthesis catalytic, electrochemical, optical, crystalline features and pharmacological activities. Rev. Adv. Chem. **12**(1), 57–95 (2022)
Urbach, F.: The long-wavelength edge of photographic sensitivity and of the electronic absorption of solids. Phys. Rev. **92**, 1324 (1953)
Varsányi, G.: Assignments for Vibrational Spectra of Seven Hundred Benzene Derivatives. Halsted Press, Ultimo (1974)
Xia, L., Xia, Y.-F., Huang, L.-R., Xiao, X., Lou, H.-Y., Liu, T.-J., Pan, W.-D., Luo, H.: Benzaldehyde Schiff bases regulation to the metabolism, hemolysis, and virulence genes expression in vitro and their structure–microbicidal activity relationship. Eur. J. Med. Chem. **97**(83), 93 (2015)
Yanai, T., Tew, D.P., Handy, N.C.: A new hybrid exchange-correlation functional using Coulomb attenuating method (CAM-B3LYP). Chem. Phys. Lett. **393**(1–3), 51–57 (2004)
Yang, W., Parr, R.G.: Hardness, softness, and the fukui function in the electronic theory of metals and catalysis. Proc. Nati. Acad. Sci. USA **82**, 6723–6726 (1985)
Yang, L.-J., Liu, Q.-L., Wang, M.-X., Gu, L.-S., Luo, Y.-H., Sun, B.-W.: Complexation of different transition metals with 4,4'-dimethyl-2,2'-bipyridine: crystal structure, UV spectra and Hirshfeld surfaces. Spectrochim. Acta Part A Mol. Biomol. Spectrosc. **166**, 1–7 (2016)
Zhang, Y., Zhao, C.-Y., Fang, W.-H., You, X.-Z.: A molecular design view on the first hyperpolarizability of salicylideneaniline derivatives. Chem. Acc. **96**, 129–134 (1997)

Authors and Affiliations

Davut Avcı[1] · Özgen Özge[1,2] · Adil Başoğlu[1] · Fatih Sönmez[3] · Ömer Tamer[1] · Necmi Dege[4] · Yusuf Atalay[1]

[1] Department of Physics, Faculty of Science, Sakarya University, 54187 Serdivan, Sakarya, Turkey

[2] Health Vocational School, Cappadocia University, 50400 Ürgüp, Nevşehir, Turkey

[3] Pamukova Vocational High School, Sakarya University of Applied Sciences, 54055 Pamukova, Sakarya, Turkey

[4] Department of Physics, Faculty of Science, Ondokuz Mayıs University, 55139 Samsun, Turkey

Synthesis, crystal structures, and DFT calculations: Novel Mn(II), Co(II) and Ni(II) complexes of *N*-(pyridin-2-ylmethylene)methanamine with isothiocyanate as promising optical materials

Davut Avcı[1], Özgen Özge[1,2], Adil Başoğlu[1], Fatih Sönmez[3], Ömer Tamer[1], Necmi Dege[4], Yusuf Atalay[1]

[1]*Sakarya University, Faculty of Science, Department of Physics, 54187, Sakarya, Turkey*
[2]*Cappadocia University, Health Vocational School, Ürgüp, 50400, Nevşehir, Turkey*
[3]*Sakarya University of Applied Sciences, Pamukova Vocational High School, 54055, Sakarya, Turkey*
[4]*Ondokuz Mayıs University, Faculty of Science, Department of Physics, 55139, Samsun, Turkey*

Supplementary Material

X-ray structure determination

In order to determine suitable single crystal structure and data collection of complexes **1,2**, a Stoe IPDS II diffractometer having Mo–Kα (λ=0.71073 Å) radiation at 296 K was used. The detailed crystal structure parameters are given in Table 1. The crystal structure was solved by direct methods using SHELXT [1] and refined by full-matrix least-squares methods on F^2 using SHELXL-97 [1]. The hydrogen atoms bonding to carbon atoms were located from different maps and then processed as riding atoms with C−H distances of 0.96 Å. Water H atoms were located in a difference map refined freely. Molecular diagrams were composed using MERCURY [2]. Supramolecular analyses were fulfilled and the diagrams were prepared with the aid of PLATON [3].

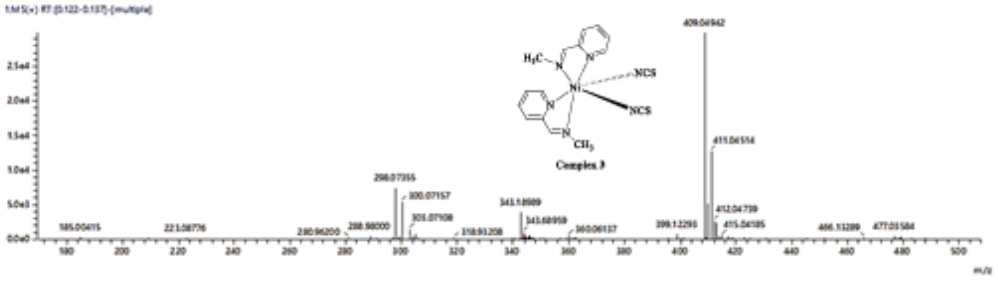

Figure S1. The mass spectrum of the complex **3**.

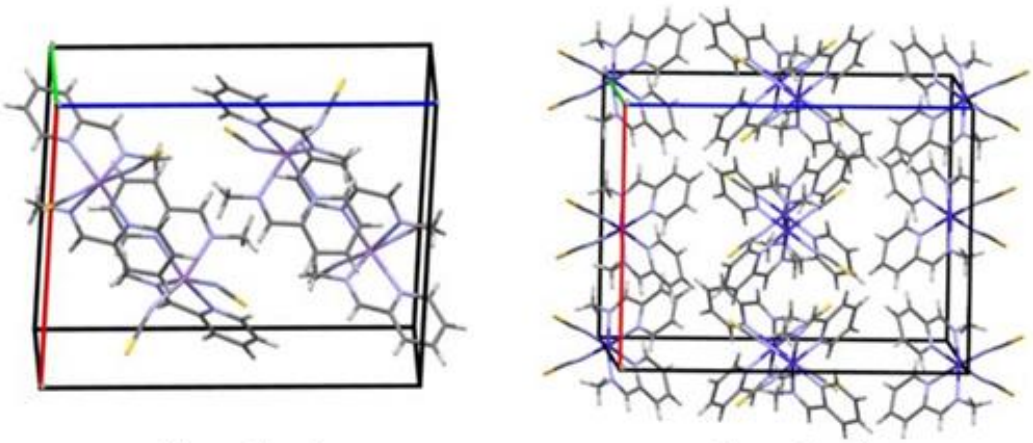

Complex **1** Complex **2**

Figure S2. The crystal packing structures of complexes **1**and **2**.

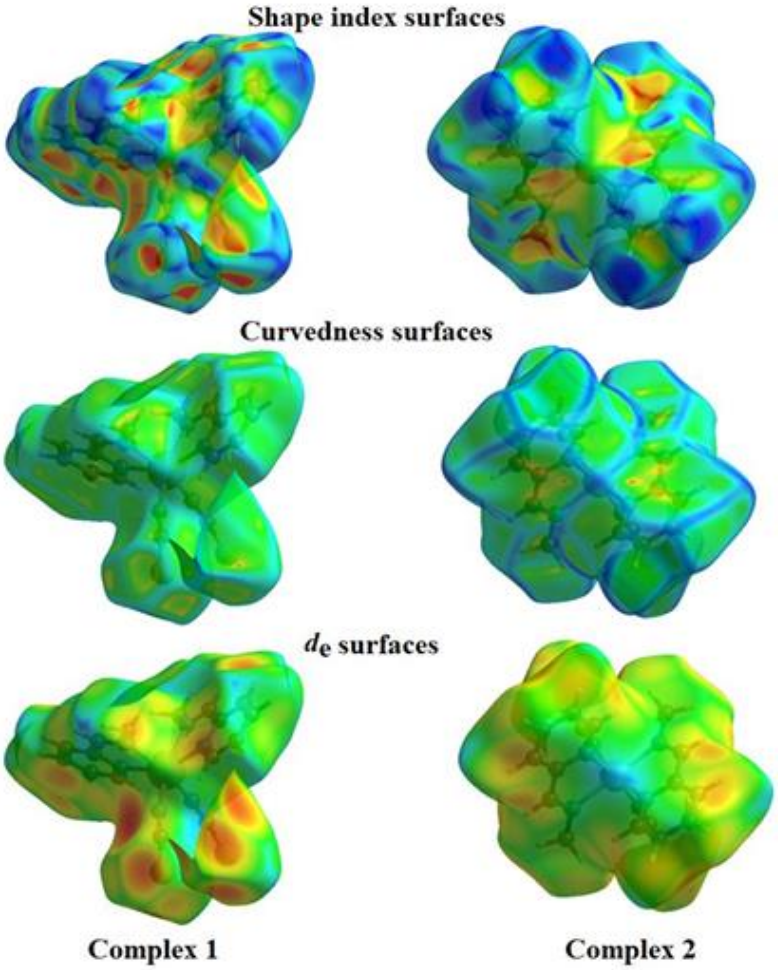

Figure S3. Representations of Hirshfeld surface mapped over shape index, curvedness, de for complexes **1** and **2**.

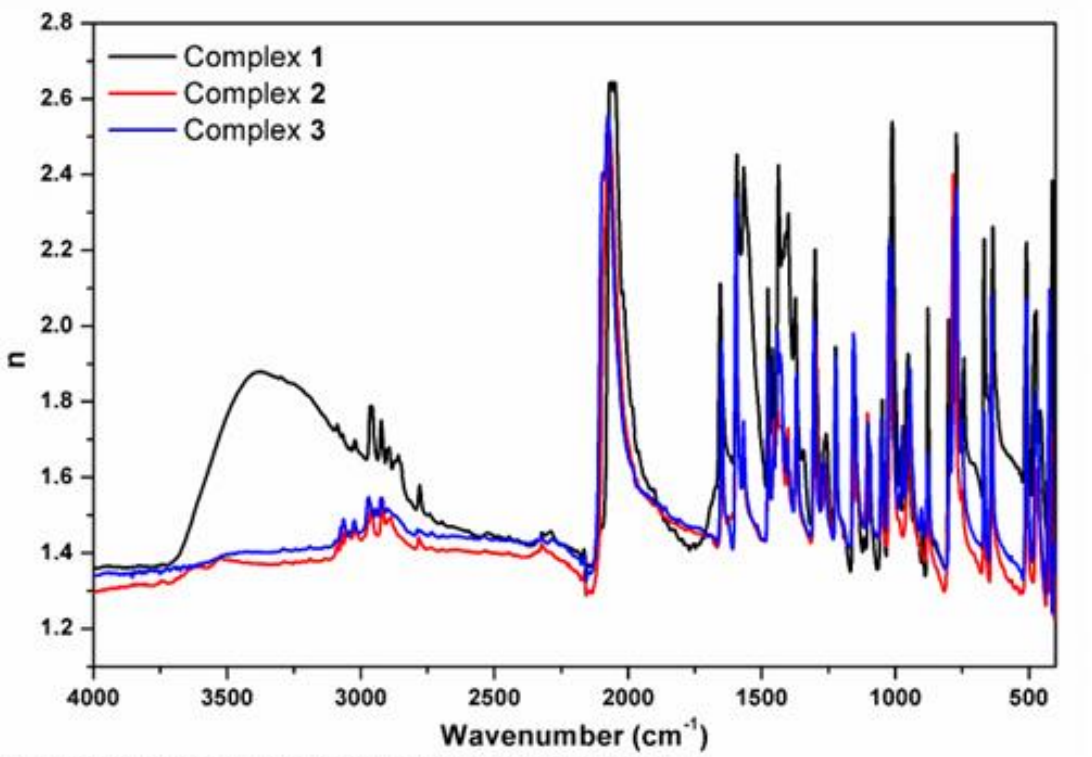

Figure S4. The refractive index (*n*) versus wavenumber of complexes **1-3**.

Table S1. Comparison of experimental and theoretical geometric parameters for complexes **3**.

Complex **3**		
Parameters	ωB97XD	CAM-B3LYP
Bond length (Å)		
Ni1–N6	1.883	1.861
Ni1–N5	1.884	1.861
Ni1–N4	2.575	2.732
Ni1–N3	1.949	1.939
Ni1–N2	2.575	2.732
Ni1–N1	1.949	1.939
S2–C16	1.623	1.623
S1–C15	1.623	1.623
N4–C14	1.325	1.324
N4–C10	1.335	1.335
N1–C2	1.272	1.270
N1–C1	1.454	1.457
N3–C9	1.272	1.270
N3–C8	1.454	1.457
N2–C7	1.325	1.324
N2–C3	1.335	1.335
N5–C15	1.175	1.169
C10–C9	1.474	1.471
N6–C16	1.175	1.169
C3–C2	1.474	1.471
Bond angles (°)		
N6– Ni1–N5	94.94	94.21
N6– Ni1–N4	93.73	85.68
N5– Ni1–N4	96.13	104.80
N6– Ni1–N3	86.83	86.67
N5– Ni1–N3	170.50	176.64
N4– Ni1–N3	74.42	72.01
N6– Ni1–N2	96.13	104.80
Dihedral angles (°)		
Ni1–N4–C10–C11	157.95	153.44
i1–N3–C9–C10	5.01	6.96
Ni1–N1–C2–C3	5.01	6.96
Ni1–N4–C10–C9	-19.86	-24.52
Ni1–N4–C14–C13	-146.78	-138.04

Table S2. Second–order perturbation theory analysis of Fock matrix on NBO basis for complexes **1-3**.

Donor (*i*)	Acceptor (j)	$E^{(2)}$ (kcal/mol)	Donor (*i*)	Acceptor (j)	$E^{(2)}$ (kcal/mol)	Donor (*i*)	Acceptor (j)	$E^{(2)}$ (kcal/mol)	Donor (*i*)	Acceptor (j)	$E^{(2)}$ (kcal/mol)
Complex **1**						Complex **2**					
ωB97XD/LanL2DZ			CAM-B3LYP/LanL2DZ			ωB97XD/6–311G+(d,p)//LanL2DZ			CAM-B3LYP/6–311G+(d,p)//LanL2DZ		
LP(1)N4	LP*(4)Mn1	34.50	LP(1)N4	LP*(7)Mn1	28.28	LP(1)N2	LP*(8)Co1	22.22	LP(1)N2	LP*(8)Co1	12.96
LP(1)N3	LP*(4)Mn1	49.26	LP(1)N3	LP*(4)Mn1	40.55	LP(1)N3	LP*(9)Co1	19.78	LP(1)N3	LP*(4)Co1	25.09
LP(1)N6	LP*(4)Mn1	34.52	LP(1)N6	LP*(7)Mn1	28.26	LP(1)N1	LP*(4)Co1	40.28	LP(1)N1	LP*(4)Co1	59.18
LP(1)N5	LP*(5)Mn1	49.26	LP(1)N5	LP*(4)Mn1	40.55	LP(1)$N2^{i}$	LP*(8)Co1	22.25	LP(1)$N2^{i}$	LP*(7)Co1	28.10
LP(1)N2	LP*(4)Mn1	65.62	LP(1)N2	LP*(3)Mn1	63.08	LP(1)$N3^{i}$	LP*(9)Co1	19.79	LP(1)$N3^{i}$	LP*(4)Co1	29.85
LP(1)N1	LP*(4)Mn1	65.54	LP(1)N1	LP*(3)Mn1	63.10	LP(1)$N1^{i}$	LP*(4)Co1	40.32	LP(1)$N1^{i}$	LP*(6)Co1	30.22
LP(2)S2	π*(N2-C2)	34.01	LP(2)S2	σ*(N2-C2)	20.21	LP(2)S1	π*(N1-C1)	26.19	LP(2)S1	π*(N1-C1)	31.15
LP(2)S1	π*(N1-C1)	34.02	LP(2)S1	σ*(N1-C1)	20.25	LP(2)$S1^{i}$	π*($N1^{i}$-$C1^{i}$)	26.19	LP(2)$S1^{i}$	π*($N1^{i}$-$C1^{i}$)	28.52
π*(N3-C7)	π*(N4-C8)	32.55	π*(N3-C7)	π*(N4-C8)	52.94	π*(N2-C5)	π*(N3-C7)	18.39	π*(N2-C5)	π*(N3-C7)	36.58
π*(N3-C7)	π*(C3-C4)	35.75	π*(N3-C7)	π*(C3-C4)	34.04	π*(N2-C5)	π*(C2-C3)	48.49	π*(N2-C5)	π*(C2-C3)	68.26
π*(N3-C7)	π*(C6-C5)	56.25	π*(N3-C7)	π*(C6-C5)	55.37	π*(N2-C5)	π*(C5-C4)	58.90	π*(N2-C5)	π*(C5-C4)	80.42
π*(N5-C14)	π*(N6-C15)	32.54	π*(N5-C14)	π*(N6-C15)	52.95	π*($N2^{i}$ –$C6^{i}$)	π*($N3^{i}$-$C7^{i}$)	18.38	π*($N2^{i}$ –$C6^{i}$)	π*($N3^{i}$-$C7^{i}$)	29.40
π*(N5-C14)	π*(C10-C11)	35.75	π*(N5-C14)	π*(C10-C11)	34.04	π*($N2^{i}$ –$C6^{i}$)	π*($C2^{i}$-$C3^{i}$)	48.50	π*($N2^{i}$ –$C6^{i}$)	π*($C2^{i}$-$C3^{i}$)	47.33
π*(N5-C14)	π*(C13-C12)	56.26	π*(N5-C14)	π*(C13-C12)	55.37	π*($N2^{i}$ –$C6^{i}$)	π*($C5^{i}$-$C4^{i}$)	58.90	π*($N2^{i}$ –$C6^{i}$)	π*($C5^{i}$-$C4^{i}$)	54.16
π*(C6-C5)	π*(C3-C4)	151.34	π*(C6-C5)	π*(C3-C4)	142.12						
Complex **3**											
ωB97XD/6–311G+(d,p)//LanL2DZ			CAM-B3LYP/6–311G+(d,p)//LanL2DZ								
LP(1)N6	LP*(6)Ni1	73.17	LP(1)N6	LP*(5) Ni1	83.36						
LP(1)N5	LP*(6) Ni1	73.17	LP(1)N5	LP*(5) Ni1	83.39						
LP(1)N4	LP*(9) Ni1	21.53	LP(1)N4	LP*(9) Ni1	14.82						
LP(1)N3	LP*(5) Ni1	53.48	LP(1)N3	LP*(5) Ni1	50.34						
LP(1)N1	LP*(5) Ni1	53.48	LP(1)N1	LP*(5) Ni1	50.34						
LP(1)N2	LP*(9) Ni1	21.53	LP(1)N2	LP*(9) Ni1	14.82						
LP(2)S2	π*(N6-C16)	65.51	LP(2)S2	π*(N6-C16)	48.54						
LP(2)S1	π*(N5-C15)	65.51	LP(2)S1	π*(N5-C15)	48.46						
π*(C3-C4)	π*(N2-C7)	29.17	π*(C3-C4)	π*(N2-C7)	26.17						
π*(C3-C4)	π*(N1-C2)	20.51	π*(C3-C4)	π*(N1-C2)	19.36						
π*(C3-C4)	π*(C6-C5)	34.13	π*(C3-C4)	π*(C6-C5)	29.61						
π*(C10-C11)	π*(N4-C14)	29.17	π*(C10-C11)	π*(N4-C14)	26.17						
π*(C10-C11)	π*(N3-C9)	20.51	π*(C10-C11)	π*(N3-C9)	19.36						
π*(C10-C11)	π*(C13-C12)	34.13	π*(C10-C11)	π*(C13-C12)	29.61						

[2] Hyperconjugative interaction energy (stabilization energy).

Table S3. Experimental and theoretical characteristic vibration frequencies of synthesized complexes **1-3**.

FT-IR (cm^{-1})	ωB97XD	CAM-B3LYP	FT-IR (cm^{-1})	ωB97XD	CAM-B3LYP	FT-IR (cm^{-1})	ωB97XD	CAM-B3LYP	Vibrational mode assignments
	LanL2DZ			6-311+G(d,p)//LanL2DZ			6-311+G(d,p)//LanL2DZ		
	Complex **1**			Complex **2**		Complex **3**			
3087	3089	3089	3073	3098	3076	3065	3084	3087	$\nu_{CH\ (ring)}$
3020	3077	3077	3020	3082	3062	3024	3071	3058	$\nu_{CH\ (ring)}$
2960	3004	3001	2965	3001	3017	2971	3006	3018	$\nu_{as\ (methyl)}$
2923	3014	3013	2919	2987	3001	2943	2991	2998	$\nu_{CH\ (imine)}$
2859	2916	2925	2889	2912	2930	2924	2921	2936	$\nu_{s\ (methyl)}$
2069	2095	2115	2071	2090	2133	2095	2093	2144	$\nu_{N=C\ (isothiocyanate)}$
2051	2084	2102		2076	2076	2076	2077	2127	$\nu_{N=C\ (isothiocyanate)}$
1656	1645	1650	1647	1693	1692	1650	1688	1694	$\nu_{N=C\ (imine)}$
	1641	1646		1692	1674		1686	1692	$\nu_{N=C\ (imine)}$
1592	1611	1611	1595	1619	1607	1596	1596	1599	$\nu_{C=C\ (ring)}$
1565	1561	1567	1565	1583	1581	1568	1586	1589	$\nu_{C=C\ (ring)}$
1478	1456	1460	1477	1468	1474	1476	1466	1470	$\beta_{HCC\ (methyl)}$
1459	1442	1445	1450	1445	1445	1458	1447	1444	$\beta_{HCC(ring)}$
1438	1429	1433	1441	1431	1440	1441	1425	1428	$\beta_{HCH\ (methyl)}$
1401	1425	1426	1404	1419	1411	1430	1422	1420	$\beta_{HCC\ (ring)}$
1341	1347	1350	1370	1342	1349	1371	1361	1367	$\nu_{C=C\ (ring)+}\ \nu_{N=C\ (ring)}$
1301	1282	1282	1303	1287	1290	1304	1297	1295	$\nu_{N=C\ (ring)+}\ \beta_{HCC(ring)}$
1257	1248	1239	1263	1257	1254	1268	1266	1254	$\nu_{C=C\ (ring)+}\ \beta_{HCC\ (ring)}$
1224	1212	1216	1224	1211	1220	1222	1204	1211	$\beta_{HCC\ (ring)}$
1096	1095	1095	1105	1102	1104	1103	1104	1091	$\tau_{\ HCCC\ (ring)+}\ \tau_{\ CCCC\ (ring)}$
1050	1042	1043	1050	1047	1047	1053	1037	1040	$\nu_{C=C\ (ring)}$
1012	1021	1017	1014	1016	1012	1021	1023	1017	$\tau_{\ HCCC\ (ring)+}\ \tau_{\ CCCC\ (ring)}$
952	999	1002	948	927	939	946	941	946	$\tau_{\ HCCN\ (imine)}$
879	871	874	879	861	872	879	873	877	$\nu_{N=C\ (ring)}$
785	819	823	784	812	829	778	766	768	$\nu_{C=S\ (isothiocyanate)}$
771	757	762	751	754	757	771	734	735	$\nu_{C=S\ (isothiocyanate)}$
667	658	661	669	659	667	668	663	667	$\beta_{NCC\ (ring)}$
634	634	634	639	636	641	642	615	618	$\beta_{CNC\ (ring)+}\ \beta_{CCC\ (ring)}$
510	517	520	508	509	511	508	509	518	$\tau_{\ CCCC\ (ring)}$
413	406	404	416	433	424	422	417	421	$\tau_{\ CCCC\ (ring)}$

υ: Stretching; β: In-plane bending; γ: Out-of plane bending; τ: Torsion.

Table S4 Experimental and theoretical wavelength, oscillator strength and remarkable contributions for complexes **1-3**.

Experimental λ (nm) (Methanol)	Methanol			
	λ (nm)	Osc. Strength	Molecular orbital contributions H: HOMO, L: LUMO	
Complex **1**				
	TD-ωB97XD/6-311+G(d,p)//LanL2DZ			
	572.6	0.0345	H→L β (78%)	H-1→L+1 β (8%)
272.6	270.9	0.0016	H→L+2 α (22%)	H-4→L β (6%)
	248.5	0.4190	H-7→L α (20%)	H-6→L+1 β (19%)
231.6	234.6	0.0050	H-6→L+1 α (15%)	H-5→L β (13%)
	TD-CAM-B3LYP/6-311+G(d,p)//LanL2DZ			
	426.2	0.0038	H→L α (30%)	H-1→L+1 α (16%)
272.6	273.7	0.0193	H-3→L α (69%)	
231.6	235.3	0.0078	H→L+4 α (45%)	H→L+6 α (13%)
Complex **2**				
	TD-ωB97XD/6-311+G(d,p)//LanL2DZ			
	441.5	0.0015	H→L α (82%)	
337.4	332.4	0.0086	H-1→L β (55%)	H-5→L β (30%)
279.8	276.3	0.0003	H-4→L α (54%)	H-9→L α (12%)
237.7	237.4	0.0611	H-4→L+1 β (14%)	H-5→L β (12%)
	TD-CAM-B3LYP/6-311+G(d,p)//LanL2DZ			
	359.9	0.0077	H→L β (37%)	H-5→L β (29%)
337.4	338.5	0.0032	H-4→L β (26%)	H-1→L β (28%)
279.8	278.1	0.0022	H→L+1 α (40%)	H-5→L+1 α (28%)
237.7	237.9	0.0103	H-7→L+1 α (31%)	H-1→L+1 α (7%)
Complex **3**				
	TD-ωB97XD/6-311+G(d,p)//LanL2DZ			
281.6	282.5	0.0077	H-2→L α (58%)	H-7→L α (17%)
232.9	233.5	0.0056	H-1→L+1 α (51%)	H-3→L α (19%)
210.2	212.4	0.0158	H-5→L+2 α (79%)	H-5→L+1 α (5%)
	TD-CAM-B3LYP/6-311+G(d,p)//LanL2DZ			
281.6	285.1	0.0034	H-2→L α (64%)	H→L+1 α (12%)
232.9	234.5	0.0006	H-4→L+3 α (41%)	H-9→L+1 α (11%)
210.2	211.0	0.0258	H→L+3 α (10%)	H-2→L+4 α (64%)

Table S5. Theoretical global chemical reactivity descriptors for complexes **1-3**.

Parameter (unit)	Complex **1**				Complex **2**				Complex **3**	
	ωB97XD		CAM-B3LYP		ωB97XD		CAM-B3LYP		ωB97XD	CAM-B3LYP
	α spin	β spin	α spin	β spin	α spin	β spin	α spin	β spin	α spin	α spin
E_{HOMO} (eV)	-7.146	-6.670	-6.516	-6.145	-7.311	-7.264	-7.559	-7.499	-7.443	6.708
E_{LUMO} (eV)	-1.052	-1.081	-1.702	-1.690	-0.932	-0.930	-1.464	-1.451	-0.968	-1.610
ΔE (eV)	6.094	5.589	4.814	4.455	6.379	6.334	6.095	6.048	6.475	5.098
Electronegativity (χ, eV)	4.099	3.875	4.109	3.917	4.122	4.097	4.511	4.475	4.205	4.159
Chemical hardness (η, eV)	3.047	2.794	2.407	2.227	3.190	3.167	3.047	3.024	3.237	2.549
Chemical softness (S, 1/eV)	0.328	0.358	0.415	0.449	0.313	0.316	0.328	0.331	0.309	0.392
Electrophilic index (ω, eV)	2.757	2.687	3.507	3.445	2.663	2.650	3.339	3.311	2.731	3.393
Nucleophilic index (φ, 1/eV)	0.362	0.372	0.285	0.290	0.376	0.377	0.299	0.302	0.366	0.295

References

[1] G.M. Sheldrick, SHELXT – integrated space-group and crystal-structure determination, Acta Cryst A71 (2015) 3–8.
[2] C.F. Macrae, P.R. Edgington, P.McCabe, E. Pidcock, G.P. Shields, R. Taylor,M. Towler, J. van de Streek, Mercury Visualization and Analysis of Crystal Structures, J. Appl. Crystallogr. 39 (2006) 453–457.
[3] A.L. Spek, Structure validation in chemical crystallography, Acta Cryst. D65 (2009) 148–155.

EK B. Özge, Ö., Avcı, D., Sönmez, F., Tamer, Ö., Dege, N., Başoğlu, A., Atalay, Y., & Zengin Kurt, B. (2023). Synthesis, DFT calculations, α-glucosidase inhibitor activity, and docking studies on Schiff base metal complexes containing isothiocyanate. Applied Organometallic Chemistry, 37(5), e7084. https://doi.org/10.1002/aoc.7084

Received: 5 December 2022 | Revised: 20 February 2023 | Accepted: 16 March 2023

DOI: 10.1002/aoc.7084

FULL PAPER

Applied Organometallic Chemistry WILEY

Synthesis, DFT calculations, α-glucosidase inhibitor activity, and docking studies on Schiff base metal complexes containing isothiocyanate

Özgen Özge[1,2] | Davut Avcı[1] | Fatih Sönmez[3] | Ömer Tamer[1] | Necmi Dege[4] | Adil Başoğlu[1] | Yusuf Atalay[1] | Belma Zengin Kurt[5]

[1]Faculty of Science, Department of Physics, Sakarya University, Sakarya, Turkey

[2]Health Vocational School, Cappadocia University, Nevşehir, Turkey

[3]Pamukova Vocational High School, Sakarya University of Applied Sciences, Sakarya, Turkey

[4]Faculty of Science, Department of Physics, Ondokuz Mayıs University, Samsun, Turkey

[5]Faculty of Pharmacy, Department of Pharmaceutical Chemistry, Bezmialem Vakif University, Istanbul, Turkey

Correspondence
Davut Avcı, Faculty of Science, Department of Physics, Sakarya University, 54187, Sakarya, Turkey.
Email: davci@sakarya.edu.tr

Funding information
Scientific Research Projects Unit of Sakarya University, Grant/Award Number: 2021-7-25-103

Diabetes is one of the fastest growing global health crises of the 21st century. One of the current therapeutic approaches used in the treatment of diabetes involves the suppression of carbohydrate hydrolyzing enzymes such as α-glucosidase. In this context, α-glucosidase inhibitors are important in the treatment and prevention of diabetes. For this reason, new Schiff base complexes including isothiocyanate {$[Cd(L_1)_2(NCS)_2]$, (**1**), $[Zn(L_1)_2(NCS)_2]$, (**2**), $[Cu(L_1)_2(NCS)_2]$, (**3**), $[Ag(L_1)(NCS)_2]$, (**4**), $[Hg(L_1)_2(NCS)Cl]$, (**5**); L_1: *N*-(pyridin-2-ylmethylene)methanamine} were synthesized to investigate α-glucosidase inhibitor potentials. The IC_{50} values of complexes **1–5** were found at 0.2376 ± 0.82 and 251.403 ± 2.54-μM range. Among these complexes, complex **5** has the highest α-glucosidase inhibitor property. The spectral investigations for the complexes **1/2–5** characterized by XRD/LC-HRMS were performed by UV–Vis and FT–IR spectra. Furthermore, the TD-DFT/DFT calculations were fulfilled by using CAM-B3LYP and ωB97XD/6–311+G(d,p)//LanL2DZ levels to obtain optimum complex structures, spectral, linear and nonlinear optical properties for **1–5**. According to obtained theoretical nonlinear optical results, complex **3** is a strong indicator in terms of microscopic nonlinear optical (NLO) properties. The docking studies of these complexes were examined to display the target protein interactions with these complexes.

KEYWORDS
DFT//CAM-B3LYP/ωB97XD; metal ions; *N*-(pyridin-2-ylmethylene)methanamine; XRD, electronic spectra; α-Glucosidase

1 | INTRODUCTION

Diabetes, a metabolic and non-communicable chronic disease, is one of the five leading causes of death in the world with multiple etiologies.[1,2] This disease is a clinical syndrome of social economic significance characterized by hyperglycemia owing to relative insulin deficiency.[3,4] Type 1 and Type 2 diabetes mellitus, T1DM and T2DM, are known as types of this disease. The autoimmune annihilation of β-cells is the main cause of T1DM[5,6] while the second type, T2DM, is complex in nature, due to damaged environmental and genetic factors, insulin resistance and secretion.[6–8]

α-Glucosidase converts the disaccharides to monosaccharides in the gut and retards digestion and absorption of carbohydrates as a consequence of suppression of excessive insulin secretion and postprandial hyperglycemia.[9,10] It is known that regulating or controlling

α-glucosidase activity can obstruct diseases giving rise to the differentiation of nerve cells, immune responses, metabolic disorders, viral infections, and tumor metastases.[11–19] The α-glucosidase inhibitory activity acts a significant role in the effect of oral antidiabetic drugs (OAD) therapy on non-insulin-dependent T2DM.[20] Miglitol, voglibose, genistein, and acarbose are commonly known and used types of α-glucosidase inhibitors.[10]

The azomethine (imine) moiety (-C=N-) is one of the important groups of organic compounds and this group is widely used in the design and synthesis of molecules with biological properties.[21,22] Molecules containing imine group are known for their diverse pharmacological effects such as antibacterial, antimalarial, and anti-inflammatory, as well as they are used as starting compounds, catalysts, and organic synthesis intermediates.[23,24] In addition, azomethine groups are known as very effective ligands in organometallic chemistry because of their forming chelates and strong coordination with metal ions.[25–27] Therefore, synthesis of azomethine-containing coordination compounds has been a major focus due to their potential biological activities.[28,29] Antipathogenic activities of ligand systems containing azomethine group were investigated and these compounds were determined more effective to be in the structure of complexes.[30] Similarly, some drugs have been found to have greater activity in the complexes of transition metals.[31]

Recent advances in medicinal chemistry play a significant role in the DM treatment of metal complexes. In designing new therapeutic drugs, complexes of transition metal have been observed to be forceful in the treatment of this chronic disorder that cannot be countered by pure organic compounds. It was determined that Zn^{2+}, Cd^{2+}, and Hg^{2+} belonging to the 2B group encouraged glucose-carrying activity in rat adipocytes.[32] Some Ag(I) complexes containing imine group were synthesized as α-glucosidase inhibitors by Zheng and Ma in 2015 and 2016,[20,33] and it was reported that the –NH group and Ag(I) ion were very important for the inhibitory activity. In 2017,[4] the IC_{50} value of the Zn complex containing N_2O_2 was found at the mM level against α-glucosidase. In the study of the synthesis and activity reported by Philip et al in 2017,[34] IC_{50} values against α-glucosidase enzyme for the metal (II) complexes were obtained at millimolar level. From these results, it is seen that the best inhibition value is obtained for the Cu (II) complex. The IC_{50} values of some transition metal complexes containing pyridine derivatives could not be determined in metal complexes of chromium, manganese, cobalt, and nickel, while IC_{50} values of the other metal complexes were calculated between 0.22 and 0.92 mM.[35–37] IC_{50} values against α-glucosidase for different metal complexes with mixed ligand containing 6-methylpyridine-2-carboxylic acid were determined at varying micromolar levels.[38–44] In the studies given above, it has been observed that metal complexes of ligands containing both heteroatoms and azomethine group inhibited the α-glucosidase enzyme. It is known that complexes of heteroatom-containing molecules are analog to some substrate with enzyme complexes in our body in terms of structural, spectroscopic and catalytic properties,[45–48] not only synthesis and design of different coordination complexes of nitrogen-containing heterocyclic structures/pseudohalides (such as *N*-(pyridin-2-ylmethylene)methanamine, 2,2′-bipyridyl, 1,10-phenanthroline, thiocyanate, isothiocyanate, and azide), but also the investigation of their physicochemical properties such as nonlinear optics, catalysis, luminescence are of great importance in terms of examining biological and pharmaceutical activities.[38–44,49–62] Besides, the pseudohalides, NCS/SCN, and N_3 were reported to coordinate with metal ions in both bridging and terminal modes.[58–62] Considering the results obtained in the literature and our previous studies, it was seen that the α–glucosidase inhibitory activities of the complexes including Hg, Cd, Mn, Ag, Co, Cu, Ni, and Zn metals were at the micromolar level.[4,8,34–44]

The present study is considered in order to design and synthesize more effective α-glucosidase inhibitors than those above. In this context, to examining α-glucosidase activities of synthesized complexes, experimental and computational investigations of their electronic features are of great importance in terms of revealing structure–activity relationships and inhibition mechanisms. We synthesized novel series of metal complexes (**1–5**) containing *N*-(pyridin-2-ylmethylene)methanamine and isothiocyanate. While the crystal Cd (II) structure (**1**) was defined by XRD method, the structures of other complexes (**2–5**) were described by LC-HRMS and FT–IR spectra. α-Glucosidase inhibitory activity studies of **1–5** were performed. The experimental and theoretical investigations of electronic spectral behavior of **1–5** were fulfilled. Besides, so as to specify the target protein interactions with ligands and interpret in vitro α-glucosidase activity results, docking analysis was fulfilled.

2 | EXPERIMENTAL AND CALCULATION PROCEDURES

2.1 | Physical equipment

The structure of the synthesized L_1 ligand was confirmed using the Varian Infinity Plus NMR spectrometer. The structures of the single crystals of synthesized complexes of sufficient size were elucidated using the data obtained from the STOE brand IPDS (II) Imaging Plate model diffraction device. For the complexes obtained, FT–IR spectra were taken with Perkin Elmer UATR–TWO (Perkin

Elmer Spectrum–two equipped with ATR) spectrophotometer in the range of 4000–400 cm^{-1}. The structures of the non-crystalline complexes were confirmed using the SHIMADZU LCMS-9030 model triple quadrupole liquid chromatograph mass spectrometer. UV–Vis absorption spectra in the 900- to 200-nm range were studied using the SHIMADZU UV–2600 UV–Vis spectrophotometer. The Leco CHNS-932 instrument was used for elemental analyses of the synthesized complexes.

The method of crystal structure[63–65] for complex **1** is given in the supporting information.

2.2 | Materials and synthesis of the N-(pyridin-2-ylmethylene)methanamine (L_1) and complexes 1–5 {$[Cd(L_1)_2(NCS)_2]$, (1), $[Zn(L_1)_2(NCS)_2]$, (2), $[Cu(L_1)_2(NCS)_2]$, (3), $[Ag(L_1)(NCS)_2]$, (4), $[Hg(L_1)_2(NCS)Cl]$, (5)}

All chemical reagents were bought from Sigma-Aldrich and used without any specific re-handling. 2-Pyridinecarboxaldehyde, methylamine solution purum (33% in absolute ethanol), potassium thiocyanate, cadmium (II) acetate (Cd $[OCOCH_3]_2$), zinc acetate dihydrate (Zn $[CH_3COO]_2{\cdot}2H_2O$), copper (II) nitrate trihydrate (Cu $[NO_3]_2{\cdot}3H_2O$), silver nitrate ($AgNO_3$) mercury (II) chloride ($HgCl_2$). The synthesis methods of the *N*-(pyridin-2-ylmethylene)methanamine and complexes **1–5** are given in Scheme 1.

Synthesis of the *N*-(pyridin-2-ylmethylene)methanamine: 0.1 mol of 2-pyridine carboxaldehyde was dissolved in 10 mL of ethanol and 2 drops of triethylamine were dropped on it. The solution was cooled by taking it into an ice bath, and 0.1 mol of methylamine (33% ethanol solution) was added to it and stirred in an ice bath for 30 min, and at room temperature for 3.5 h. The alcohol in the mixture was evaporated in the evaporator and 100 mL of chloroform was added to this mixture. This solution was washed three times with 25 mL of water. The organic phase was dried with anhydrous $MgSO_4$, filtered and evaporated in the evaporator. The *N*-(pyridin-2-ylmethylene)methanamine (L_1) was obtained as dark yellow oil and its structure was confirmed by ^1H and ^{13}C NMR spectra (Figure S1). ^1H NMR ($CDCl_3$, 300 MHz)

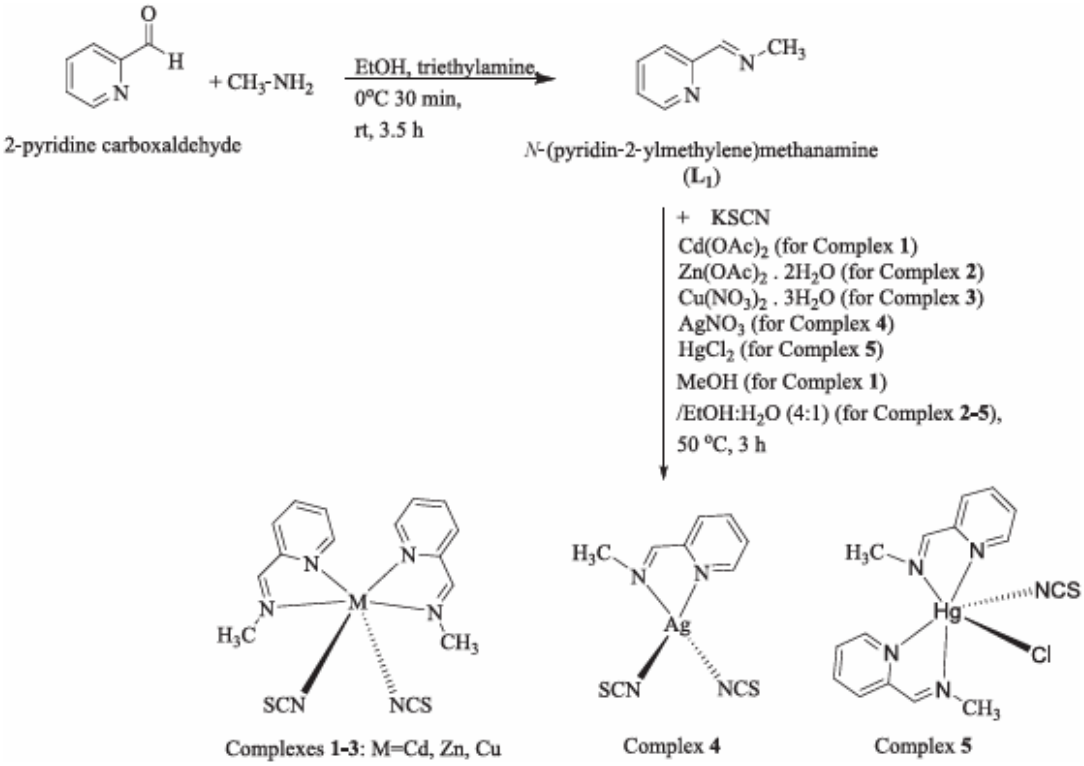

SCHEME 1 Synthesis of complexes **1–5**.

δ/ppm: 8.40–8.43 (1H, dt, $J_1 = 0.9$ Hz, $J_2 = 5.0$ Hz), 8.17 (1H, d, $J = 1.4$ Hz), 7.72–7.75 (1H, dd, $J_1 = 0.9$ Hz, $J_2 = 7.9$ Hz), 7.48–7.54 (1H, td, $J_1 = 1.4$ Hz, $J_2 = 6.1$ Hz), 7.06–7.10 (1H, m), 3.34 (3H, d, $J = 1.8$ Hz). ^{13}C NMR ($CDCl_3$, 75 MHz) δ/ppm: 163.4, 154.4, 149.4, 136.7, 124.8, 121.1, 48.2.

Synthesis of the complex **1**: Solution of 1-mmol metal salt (Cd $(OCOCH_3)_2$) for complex **1** in 10-mL methanol, *N*-(pyridin-2-ylmethylene)methanamine (L_1) prepared in 10-mL MeOH (2 mmol) was added to this solution and stirred at 50°C for about 15 min. Potassium thiocyanate (2 mmol) solution prepared in 10-mL MeOH was added onto the solution. The mixture was stirred at 50°C for 3 h, then left to evaporate at room temperature. Complex products in crystalline form were obtained in about 7–10 days. The structure of the product was confirmed by XRD. The complex **1** was obtained as colorless single crystal in prism-shaped.

Synthesis of the complexes **2–5**: 1 mmol metal salts (Zn $(CH_3COO)_2{\cdot}2H_2O$ for complex **2**, Cu $(NO_3)_2{\cdot}3H_2O$ for complex **3**, $AgNO_3$ for complex **4**, and $HgCl_2$ for complex **5**) were added to the potassium thiocyanate (2 mmol) solution prepared in ethanol (10 mL). *N*-(pyridin-2-ylmethylene)methanamine (L_1) (2 mmol for complexes **2,3,5**/1 mmol for complex **4**) solution prepared in ethanol (10 mL) was added onto the solution. By adding 5 mL of distilled water to the solution, this mixture was stirred at 50°C for 3 h, then filtered and left to evaporate at room temperature. Complex **2–5** products in powder form were obtained in about 7–10 days as yellow-orange, green, dark brown, charcoal color, respectively. The structures of these products were verified by mass spectroscopy. Anal. Calc. for $C_{16}H_{16}N_6S_2Zn$ (complex **2**): C, 45.56; H, 3.82; N, 19.92; S, 15.20; Zn, 15.50. Found: C, 46.22; H, 3.65; N, 19.22; S, 15.95. Calculated exact mass (m/z): 420.0169 ($C_{16}H_{16}N_6S_2Zn$); found: LC-HRMS (m/z): 439.0663 ($[M + H_2O]^+$) for complex **2**. Anal. Calc. for $C_{16}H_{16}CuN_6S_2$ (complex **3**): C, 45.75; H, 3.84; Cu, 15.13; N, 20.01; S, 15.27. Found: C, 46.80; H, 3.46; N, 20.89; S, 15.85. Calculated exact mass (m/z): 419.0174 ($C_{16}H_{16}CuN_6S_2$); found: LC-HRMS (m/z): 442.3024 ($[M + Na]^+$) for complex **3**. Anal. Calc. for $C_9H_8AgN_4S_2$ (complex **4**): C, 31.41; H, 2.34; Ag, 31.34; N, 16.28; S, 18.63. Found: C, 31.12; H, 2.54; N, 15.96; S, 15.98. Calculated exact mass (m/z): 342.9241 ($C_9H_8AgN_4S_2$); found: LC-HRMS (m/z): 341.8191 ($[M]^+$) for complex **4**. Anal. Calc. for $C_{15}H_{16}ClHgN_5S$ (complex **5**): C, 33.71; H, 3.02; Cl, 6.63; Hg, 37.53; N, 13.10; S, 6.00. Found: C, 34.05; H, 2.85; N, 13.75; S, 6.25. Calculated exact mass (m/z): 535.0521 ($C_{15}H_{16}ClHgN_5S$); found: LC-HRMS (m/z): 530.0269 ($[M\text{-}5H]^+$) for complex **5**. Figures S2–S5 display the HRMS spectra of complexes **2–5**.

2.3 | α-Glucosidase inhibition assay

By considering the previous studies,[38–40,66] α-glucosidase inhibitory activities for complexes **1–5** were investigated. The method of α-glucosidase inhibitory activity is given in the supporting information. The α-glucosidase inhibition values of complexes **1–5** were determined by taking A_c and A_s displaying the absorbance of the control and samples in the following equation.

$$\text{Glucosidase inhibition}\% = [(A_c - A_s)/A_c]\text{x}100$$

The Graphpad Software was applied to calculate IC_{50} values for complexes **1–5**.

2.4 | Computational procedure

The analysis of the structural, spectral, and nonlinear optical features were performed by using by the Gaussian 16, Revision C.01,[67] and GaussView 6[68] program. To perform the optimized complex structures, vibrational wavenumbers, and natural bond orbital (NBO) analysis of the complexes **2,3** in the ground state, the CAM-B3LYP[69] and ωB97XD methods[70] with 6-311+G (d,p)//LanL2DZ[71,72] basis set were used. The same properties for the complexes **1,4,5** were evaluated by using DFT/CAM-B3LYP and ωB97XD/LanL2DZ levels. The electronic absorption wavelength and oscillator strength of complexes **1–5** in MeOH were calculated at the time-dependent DFT (TD–DFT) level[73] with the conductor-like polarizable continuum model (CPCM).[74] The SWizard[75] program was used to determine remarkable contributions in electronic transitions. DFT/CAM-B3LYP and ωB97XD/LanL2DZ levels in gas phase were applied to obtain the microscopic polarizabilities (α and Δα), first- and second-order hyperpolarizabilities (β and γ). The DFT/CAM-B3LYP level was also applied to examine the MEP (molecular electrostatic potential) surfaces.

The stability energy $E^{(2)}$ in NBO calculations was obtained by using Equation (1)

$$E^{(2)} = \Delta E_{ij} = q_i \frac{F(i,j)^2}{\varepsilon_i - \varepsilon_j} \quad (1)$$

In Equation (1), $F(i,j)^2$ is the off-diagonal NBO Fock matrix elements, ε_i and ε_j are diagonal elements, and q_i is the donor orbital occupancy for each donor (i) and acceptor (j).[76–79]

The molecular parameters computed from the HOMO and LUMO energies are the chemical hardness (η), electronegativity (χ), chemical softness (S), electrophilicity

(ω), and nucleophilicity (φ) index. These parameters were calculated as follows (Equations (2)–(6))[76,80,81]:

$$\eta = \frac{(E_{LUMO} - E_{HOMO})}{2} \quad (2)$$

$$\chi = -\frac{(E_{HOMO} + E_{LUMO})}{2} \quad (3)$$

$$S = \frac{1}{\eta} \quad (4)$$

$$\omega = \frac{\chi^2}{2\eta} \quad (5)$$

$$\varphi = \frac{1}{\omega} \quad (6)$$

The theoretical microscopic electric dipole moment (μ), linear optical parameters ($\overline{\alpha}$ and $\Delta\alpha$) described as the mean and anisotropy of polarizability, first- and second-order hyperpolarizability parameters (β and γ) for complexes **1–5** in gas phase were computed by using Equations (7)–(10).[82–85]

$$\overline{\alpha} = \frac{(a_{xx} + a_{yy} + a_{zz})}{3} \quad (7)$$

$$\Delta\alpha = \left\{\frac{1}{2}\left[(a_{xx} - a_{yy})^2 + (a_{yy} - a_{zz})^2 + (a_{zz} - a_{xx})^2\right]\right\}^{1/2} \quad (8)$$

In Equations (7) and (8), the Cartesian components of $\overline{\alpha}$ and $\Delta\alpha$ are a_{xx}, a_{yy}, and a_{zz}. 1 a.u. of $\overline{\alpha}$ is converted to 0.1482×10^{-24} esu.

The theoretical β and γ parameters, known as first- and second-order hyperpolarizability parameters, were computed with Equations (9) and (10),[82–85]

$$\beta = \left(\beta_x^2 + \beta_y^2 + \beta_z^2\right)^{1/2} \quad (9)$$

$$< \gamma > = \frac{1}{5}\left[\gamma_{xxxx} + \gamma_{yyyy} + \gamma_{zzzz} + 2\left(\gamma_{xxyy} + \gamma_{xxzz} + \gamma_{yyzz}\right)\right] \quad (10)$$

In Equation (9), the Cartesian components of β are $\beta_x = \beta_{xxx} + \beta_{xyy} + \beta_{xzz}$, $\beta_y = \beta_{yyy} + \beta_{yxx} + \beta_{yzz}$, $\beta_z = \beta_{zzz} + \beta_{zyy} + \beta_{zxx}$. To obtain β in esu unit, 1 a.u. $= 8.6393 \times 10^{-33}$ esu conversion is used.

2.5 | Docking procedure

The investigations of the interactions between target protein (the template structure *Saccharomyces cerevisiae* isomaltase [PDBID: 3A4A]) and synthesized complexes **1–5** were performed by using the AutoDock4 program[86] implemented via the graphical user interface AutoDockTools (ADT1.4.6).[87] By using optimized structures of complexes **1–5** and genistein obtained at the DFT/CAM-B3LYP method, the binding energies and estimated inhibition constants of the complexes were obtained with docking results. 2-D and 3-D structures demonstrating interactions between amino acid residues and ligands of complexes **3–5** were visualized Discovery Studio 4.0 program.[88] The detailed docking procedure is also presented in supporting information.

3 | RESULTS AND DISCUSSION

3.1 | The structural and vibrational characterizations of the synthesized complexes

From the ^{1}H NMR spectra, the signals of NH and CH protons of imine were detected at 8.43 and 8.17 ppm, respectively, and also the signals of aromatic hydrogens were between 7.06 and 7.75 ppm. The signals for protons of methyl were observed at 3.34 ppm. From the ^{13}C NMR spectra, the signals of imine carbon can be seen at 163.4 ppm and the signals of aromatic carbons were between 121.1–154.4 ppm. Also, the signal relating to methyl carbon can be observed at 48.2 ppm.

The crystallographic data of complex **1** were obtained by XRD (see Table 1). Table 1 shows that the space groups are P21/c for complex **1** in the monoclinic crystal system. Figure 1 demonstrates the crystal structure of complex **1** and optimized structures of complexes **2–5**. The structures of the non-crystalline complexes were confirmed using mass spectrometry (see Figures S2–S5). In addition, the structures of the complexes **1–5** were optimized and their bond lengths and angles, dihedral angles were calculated by DFT/ωB97XD and DFT/CAM-B3LYP methods (Tables 2 and S1). The coordination around metal ions (Cd (II), Zn (II), Cu (II) and Hg (II)) of complexes **1–3,5** is described as a distorted octahedral geometry whereas the coordination of Ag(I) ion in complex **4** is defined as a distorted tetrahedral geometry. The complexes **1–3** are formed by two L_1 (bidentate ligand) and two isothiocyanates (monodentate ligand) ligands being coordinated to Cd (II), Zn (II) and Cu (II) ions. Complex **5** comprises Hg (II) ion coordinated by two L_1, a chloride, and an isothiocyanate ligand. On the other hand, complex **4** is comprised of Ag(I) ion coordinated by a L_1 and two isothiocyanate ligands. It is compatible with the coordination geometry of Ag(I) coordinated to the different ligands.[58,89–91] The L_1 and NCS in the complexes **1–5** obtained in this study act as terminal ligands.

TABLE 1 Crystal data and structure refinement parameters for complex **1**.

Empirical formula	$C_{16}H_{16}CdN_6S_2$
Formula weight	468.87
Crystal system	Monoclinic
Space group	$P2_1/c$
Temperature	296
Radiation type	Mo $K\alpha$
Wavelengh (Å)	0.71073
Crystal size (mm)	0.75 × 0.62 × 0.47
a (Å)	12.8634 (8)
b (Å)	9.3026 (4)
c (Å)	16.4441 (10)
α (°)	90
β (°)	93.282 (5)
γ (°)	90
V (Å^3)	1964.52 (19)
Z	4
F(000)	936
Density (g cm^{-3})	1.585
μ (mm^{-1})	1.34
θ range (°)	2.0–33.0
Measured refls.	23,339
Independent refls.	7185
R_{int}	0.040
S	1.04
R1/wR2	0.037/0.089
max/min (eÅ^{-3})	0.43/−1.24

In complexes **1–5**, five-membered chelate rings are occurred by the coordination of pyridine N and imine N atoms of the L_1 ligand to metal ions. The M-N bond lengths between the metal ion and the pyridine N/imine N atoms of the complex **1** were experimentally observed as 2.381(19)/2.4089(18) Å (see Table 2). These values calculated at DFT/CAM-B3LYP level corresponding to these bond lengths were obtained as 2.423/2.468 Å. The Cd-N bond length between the metal ion and isothiocyanate N atom of the complex **1** was experimentally found to be 2.265(2) Å. The corresponding value was calculated at 2.222 Å by using DFT/CAM-B3LYP level (Table 2). Theoretical values corresponding to these bond lengths, which have no experimental counterpart for complexes **2–5**, were calculated in a similar trend (see Table S1). In addition, theoretical bond lengths obtained by DFT/ωB97XD method in all complexes were obtained in the same direction.

For complex **1**, the N-Cd-N bond angle between Cd ion and isothiocyanate N atoms around the coordination was observed as 91.77 (9)° (see Table 2). This value calculated at DFT/CAM-B3LYP level corresponding to the bond angle was obtained as 115.23°. The bond angle between the imine N, Cd ion, and isothiocyanate N around the coordination for complex **1** was found to be 89.08(8)° (with XRD), 81.24° (with DFT/CAM-B3LYP level), respectively. The calculated values of bond angles of the metal ion with pyridine, imine and isothiocyanate N atoms indicate the presence of a distorted octahedral geometric structure for complexes **1–3,5**. In the similarity and difference in the bond length and angles, both the coordination around metal ions of complexes **1–5** and the nature of metal ions play important role. In complexes **2–5**, the geometrical parameters around the central metal ions are in a good agreement with previously reported values.[38,44]

For complex **1**, C–H···S type hydrogen bond interactions were observed between the L_1 ligand and the isothiocyanate ligand with experimentally different symmetries. The crystal packing structure of complex **1** is given in Figure S6. In complex **1**, the C1-H1A···S1 hydrogen bond interaction displays between S atom of the isothiocyanate ligand and methyl –CH group of L_1 ligand. The H···A and D–H···A parameters are observed at 2.84 Å and 165°, respectively.

NBO analyses for **1–5** were fulfilled by using DFT/ωB97XD and DFT/CAM-B3LYP levels, so as to survey the interactions among molecular bonding and coordination geometry around the metal ions in the complex structures. In these complexes, the hyperconjugative interactions were computed at the second-order perturbation approach.[76,78,79] In the coordination environment around central Cd (II), Zn (II), Cu (II), Ag(I), and Hg (II) ions, the hyperconjugative interactions are a substantial role between the lone pair electron (n) of metal ions and N atoms. The stabilization energy ($E^{(2)}$) values of the complex structures confirmed by the remarkable LPN → LP*M (II) hyperconjugative interactions for complexes **1–5** were presented in Tables 3 and S2. These $E^{(2)}$ values calculated at DFT/CAM-B3LYP level for complexes **1–5** were obtained in the range of 31.85 and 16.81, 47.30 and 22.62, 20.05 and 11.29, 18.30 and 5.13, 29.73 and 9.81 kcal/mol, respectively. The other stabilization interactions, LP S → π*(N-C), π*(N-C)/(C-C) → π*(C-C)/(N-C), etc., between L_1 and isothiocyanate ligands were demonstrated in Table S2. In brief, the stable structures of complexes **1–5** were supported by the NBO results (Tables 3 and S2).

The vibrational frequencies for complexes **1–5** were examined by FTIR and obtained at DFT/ωB97XD and DFT/CAM-B3LYP levels. The multiplier of 0.96 was

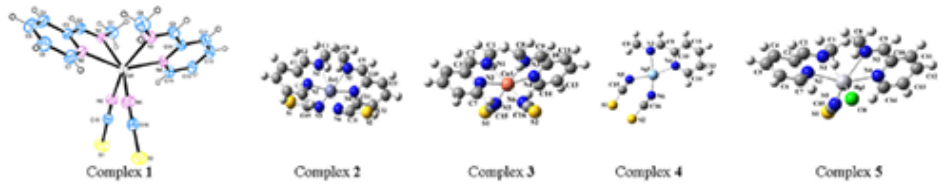

FIGURE 1 Single crystal structure of complex **1** and theoretical optimized structures of complexes **2–5** using DFT/CAM-B3LYP level.

TABLE 2 Comparison of experimental and theoretical geometric parameters for complex **1**.

Parameters	XRD	ωB97XD	CAM-B3LYP
Bond length (Å)			
Cd1–N6	2.248(2)	2.221	2.222
Cd1–N5	2.265(2)	2.221	2.222
Cd1–N4	2.3511(18)	2.423	2.423
Cd1–N3	2.3599(19)	2.463	2.468
Cd1–N2	2.3808(19)	2.423	2.423
Cd1–N1	2.4089(18)	2.463	2.468
S2–C16	1.613(2)	1.676	1.676
S1–C15	1.610(3)	1.676	1.676
N4–C14	1.328(3)	1.347	1.346
N4–C10	1.342(3)	1.357	1.355
N1–C2	1.246(3)	1.283	1.282
N1–C1	1.457(3)	1.463	1.464
N3–C9	1.259(3)	1.283	1.282
N3–C8	1.451(3)	1.463	1.464
N2–C7	1.325(3)	1.347	1.346
N2–C3	1.347(3)	1.357	1.355
N5–C15	1.135(3)	1.193	1.191
C10–C9	1.467(3)	1.484	1.481
N6–C16	1.150(3)	1.193	1.191
Bond angles (°)			
N6–Cd1–N5	91.77(9)	115.04	115.23
N6–Cd1–N4	110.10(7)	105.77	103.06
N5–Cd1–N4	91.52(8)	89.033	87.67
N6–Cd1–N3	89.08(8)	82.26	81.24
N5–Cd1–N3	161.42(8)	155.67	154.46
N4–Cd1–N3	70.82(7)	69.08	68.95
N6–Cd1–N2	91.15(7)	89.03	87.67
Dihedral angles (°)			
Cd1–N4–C10–C11	177.00(18)	179.48	175.52
Cd1–N3–C9–C10	3.6(3)	7.95	9.81
Cd1–N1–C2–C3	4.7(3)	7.95	9.80
Cd1–N4–C10–C9	−1.5(2)	−0.04	−3.35
Cd1–N4–C14–C13	−178.33(18)	−179.77	−175.38

TABLE 3 Second-order perturbation theory analysis of Fock matrix on NBO basis for complex **1**.

Donor (*i*)	Acceptor (j)	$E^{(2)}$ (kcal/mol)	Donor (*i*)	Acceptor (j)	$E^{(2)}$ (kcal/mol)
ωB97XD/LanL2DZ			CAM-B3LYP/LanL2DZ		
LP(1)N6	LP*(6)Cd1	31.49	LP(1)N6	LP*(6)Cd1	31.85
LP(1)N5	LP*(6)Cd1	31.49	LP(1)N5	LP*(6)Cd1	31.86
LP(1)N4	LP*(9)Cd1	16.84	LP(1)N4	LP*(9)Cd1	16.81
LP(1)N3	LP*(6)Cd1	14.40	LP(1)N3	LP*(6)Cd1	13.61
LP(1)N1	LP*(6)Cd1	14.40	LP(1)N1	LP*(6)Cd1	13.61
LP(1)N2	LP*(9)Cd1	16.84	LP(1)N2	LP*(9)Cd1	16.81
LP(2)S2	π*(N6-C16)	75.86	LP(2)S2	π*(N6-C16)	57.39
LP(2)S1	π*(N5-C15)	75.86	LP(2)S1	π*(N5-C15)	57.26
π*(N4-C14)	π*(C10-C11)	108.20	π*(N4-C14)	π*(C10-C11)	105.29
π*(N4-C14)	π*(C13-C12)	107.10	π*(N4-C14)	π*(C13-C12)	107.14
π (C10-C11)	π*(N3-C9)	18.78	π(C10-C11)	π*(N3-C9)	17.88
π*(C3-C4)	π*(N1-C2)	18.78	π*(C3-C4)	π*(N1-C2)	17.88
π*(N2-C7)	π*(C3-C4)	108.20	π*(N2-C7)	π*(C3-C4)	105.29
π*(N2-C7)	π*(C6-C5)	107.10	π*(N2-C7)	π*(C6-C5)	107.12
π(C13-C12)	π*(N4-C14)	53.86	π(C13-C12)	π*(N4-C14)	18.75

applied to theoretically the wavenumbers to get closer to FT–IR spectra. Figure 2 and Tables 4 and S3 display the experimental IR spectra and vibrational mode assignments, as well as characteristic vibrational wavenumbers for complexes **1–5** in the range of 4000–400 cm^{-1}. The CH stretching is attributed to the ring, methyl and imine groups for complexes **1–5** were observed at the range of 3086 and 2854 (complex **1**), 3078 and 2852 (complex **2**), 3064 and 2849 (complex **3**), 3006 and 2801 (complex **4**), 3052 and 2849 (complex **5**) cm^{-1}, as expected.[92] The corresponding theoretical values to stretching vibrations for complexes **1-5** were obtained at the range from 3127 to 2933, from 3089 to 2914, and from 3085 to 2922, from 3129 to 2930, and from 3110 to 2928 cm^{-1} by using DFT/CAM-B3LYP level, respectively. The IR spectra of **1–5** exhibit bands in the 2134 and 2004 cm^{-1} range, corresponding to the NC stretching vibrations of the NCS, which match to those previously reported.[38,59] These vibrational bands calculated at DFT/ωB97XD and DFT/CAM-B3LYP levels were obtained at 2089 and 2023 cm^{-1}, and 2110 and 2036 cm^{-1} ranges, respectively. These bands demonstrate the presence of the NCS ligand in complex structures. Furthermore, the vibrational bands for complexes **1–5** located at 1661, 1658, 1650, 1764, and 1722 cm^{-1}, respectively, exhibit the stretching vibrations of the N=C bond of the L_1 (see Table 4). These results are consistent with previously reported ones.[38,59] In complexes **1–5**, the experimental and theoretical C=S stretching band of the NCS ligand appeared within the ranges 784–739 cm^{-1} (in FTIR spectra), 803–730 cm^{-1} (in DFT/ωB97XD level), and 809–734 cm^{-1} (in DFT/CAM-B3LYP level). The double bond CC and NC stretching vibrations of the ring were found to be ranged from 1373 to 1339 cm^{-1} (in FTIR spectra), from 1418 to 1307 cm^{-1} (in DFT/ωB97XD level), and from 1417 to 1303 cm^{-1} (in DFT/CAM-B3LYP level). At the same time, the stretching vibrations of the NC bond were observed at 880–823 cm^{-1} range, and theoretical values were found within the ranges 888–858 cm^{-1} (in DFT/ωB97XD level) and 873–860 cm^{-1} (in DFT/CAM-B3LYP level). The double bond CC vibrations belonging to the ring emerged at 1604–1566 cm^{-1} ranges, 1610–1585 cm^{-1}, and 1612–1586 cm^{-1}, by using FTIR spectra, DFT/ωB97XD, and DFT/CAM-B3LYP levels, respectively (see Table S3). Moreover, the detailed assignments of the

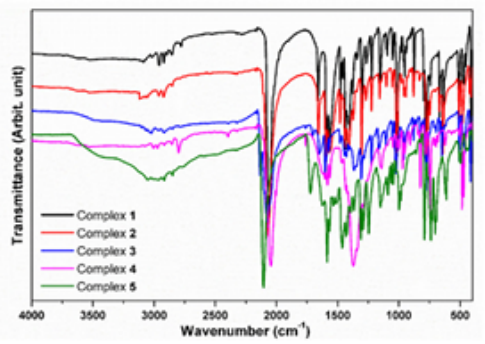

FIGURE 2 Experimental IR spectra of complexes **1–5**.

TABLE 4 Selected experimental and theoretical characteristic vibration frequencies of synthesized complexes **1–5**.

FT-IR (cm^{-1})	ωB97XD LanL2DZ	CAM-B3LYP	FT-IR (cm^{-1})	ωB97XD 6-311+G(d,p)// LanL2DZ	CAM-B3LYP	FT-IR (cm^{-1})	ωB97XD 6-311+G(d,p)// LanL2DZ	CAM-B3LYP	Vibrational mode assignments
Complex **1**			Complex **2**			Complex **3**			
3086	3139	3127	3078	3082	3089	3064	3086	3085	υ_{CH} (ring)
3015	3122	3112	3056	3074	3073	3021	3061	3064	υ_{CH} (ring)
2961	3020	3027	2962	2980	2989	2963	2993	2999	υ_{as} (methyl)
2918	2994	2995	2922	2953	2973	2916	2975	2978	υ_{CH} (imine)
2854	2925	2933	2852	2900	2914	2849	2912	2922	υ_{s} (methyl)
2070	2058	2066	2108	2085	2079	2134	2089	2110	$\upsilon_{N=C}$ (isothiocyanate)
2057	2050	2058	2067	2073	2068	2076	2072	2094	$\upsilon_{N=C}$ (isothiocyanate)
1661	1687	1688	1658	1708	1707	1650	1697	1699	$\upsilon_{N=C}$ (imine)
1588	1604	1605	1598	1610	1612	1600	1603	1603	$\upsilon_{C=C}$ (ring)
1339	1307	1303	1343	1348	1351	1346	1354	1356	$\upsilon_{C=C}$ (ring)+ $\upsilon_{N=C}$ (ring)
1052	1046	1044	1052	1041	1042	1054	1039	1041	$\upsilon_{C=C}$ (ring)
876	861	862	880	888	869	880	869	873	$\upsilon_{N=C}$ (ring)
783	792	795	774	764	768	784	803	809	$\upsilon_{C=S}$ (isothiocyanate)
774	747	764	769	741	744	775	764	769	$\upsilon_{C=S}$ (isothiocyanate)
Complex **4**			Complex **5**						
	LanL2DZ			6-311+G(d,p)//LanL2DZ					
3006	3130	3129	3052	3116	3110				υ_{CH} (ring)
2973	3117	3110	3009	3108	3105				υ_{CH} (ring)
2916	3032	3030	2959	3047	3046				υ_{as} (methyl)
2854	2988	2993	2919	2982	2985				υ_{CH} (imine)
2801	2924	2930	2849	2920	2928				υ_{s} (methyl)
2045	2053	2069	2105	2048	2063				$\upsilon_{N=C}$ (isothiocyanate)
2004	2023	2036							$\upsilon_{N=C}$ (isothiocyanate)
1764	1687	1690	1722	1694	1695				$\upsilon_{N=C}$ (imine)
1604	1602	1603	1586	1603	1603				$\upsilon_{C=C}$ (ring)
1373	1418	1417	1310	1313	1311				$\upsilon_{C=C}$ (ring)+ $\upsilon_{N=C}$ (ring)
1046	1041	1041	1048	1043	1043				$\upsilon_{C=C}$ (ring)
823	860	860	858	858	860				$\upsilon_{N=C}$ (ring)
784	788	792							$\upsilon_{C=S}$ (isothiocyanate)
746	756	761	739	730	734				$\upsilon_{C=S}$ (isothiocyanate)

Note: υ: stretching; β: in-plane bending; γ: out-of-plane bending; τ: torsion.

other vibrational bands, such as in-plane/out-of-plane bending vibrations, for complexes **1–5** are presented in Table S3.

3.2 | The electronic spectral properties

The UV–Vis spectra for synthesized complexes **1–5** are displayed in Figure 3 in the range of 200–600 nm. The absorption peaks emerged at 279.2 and 232.9 nm for complex **1**, 277.6, 236.2 and 207.1 nm for complex **2**, 387.8, 284.9, and 229.8 nm for complex **3**, 261.2 and 228.8 nm for complex **4**, 321.5 and 228.8 nm for complex **5**. By using the SWizard[75] and Chemissian[93] programs, it was determined which molecular orbitals come from the greatest contributions to electronic transitions (see Tables 5 and S4). According to Table 5, Figure 4 is formed by considering the occupied and unoccupied molecular

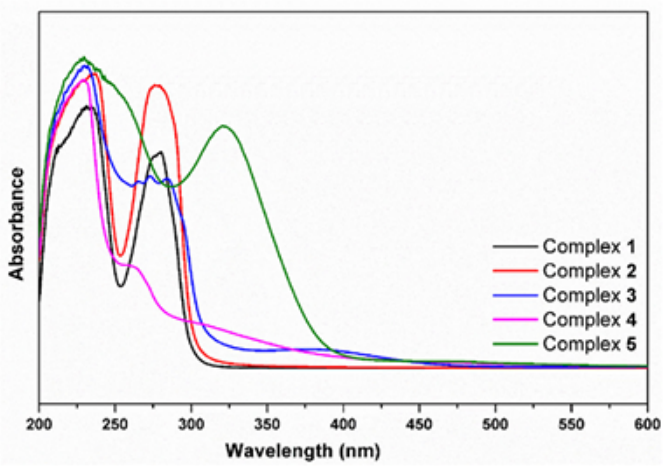

FIGURE 3 Experimental UV–Vis spectra in methanol for complexes **1–5**.

orbitals that play an active role in electronic transitions. The observed absorptions for complexes **1–5** were determined to be due to metal-to-ligand/ligand-to-metal transition, intra-ligand $\pi \rightarrow \pi^*$, and $n \rightarrow \pi^*$ transitions. In the electronic configuration of Zn (II), Cd (II) and Hg (II) ions, $d \rightarrow d$ electronic transition is not expected since the d-orbitals are completely filled. Therefore, no absorption showing this transition has been observed both theoretically and experimentally at higher wavelengths. The charge transitions within the ligand are clearly seen from Figure 4 as ligand–ligand charge transfer in the high energy region.

It is reported that the rising contributions from metal orbitals to the LUMO of the complex can increase the π-acceptor feature of the ligand.[94] The contribution of the Cd, Zn, Cu, Ag, and Hg orbitals to the HOMO/HOMOs and LUMO/LUMOs of complexes **1–5** calculated at the TD-CAM-B3LYP level change from 2% to 38% (HOMO/HOMOs) and from 1% to 29% (LUMO/LUMOs). The orbital contributions of the L_1 and NCS ligands to the different LUMO/LUMOs in the synthesized complexes (except for complex **4**) range from 67% to 100% and from 0% to 11% (TD-CAM-B3LYP level in methanol), respectively. At different percentages in L_1 ligand including 2-pyridyl and imine groups, and NCS ligand, the LUMO/LUMOs contributions showing electron acceptor feature were calculated higher than NCS ligand (see Table 5). It could be said from these results that L_1 ligand is much stronger π-acceptor than NCS ligand. In complexes **1–5**, the electron density is localized in the pyridyl rings and metal ions in LUMO/LUMOs levels while the electron density is localized in the NCS ligands in HOMO level (see Figure 4). The MLCT (metal-to-ligand charge transfer) transitions obtained at TD–CAM-B3LYP level in methanol were determined by different percentages HOMOs→LUMOs, as can be seen in Table 5. For example, H-6 → L (43%) transition for complex **1** corresponds to Cd(6%), L_1(88%) including pyridyl(8%) and imine(80%) groups, and NCS(6%) ligand in HOMO while it corresponds to pyridyl(59%) and imine(41%) in LUMO. The HOMOs→LUMOs transitions of the other complexes occurred by different percentage contribution values (see Table 5). Depending on the metal ion and its environments, the electronic transitions with the high/low oscillator strengths come out as ligand-to-metal/metal-to-ligand, and ligand-to-ligand charge transfer.

Molecular electrostatic potential (MEP) surfaces have been taken into account to investigate the structure–activity relationship (SAR) of biomolecules and complex systems. The MEP surfaces for complexes **1–5** were obtained with CAM-B3LYP/6–311+G(d,p)//LanL2DZ level. It is clear from Figure 5 that the regions with the highest electron affinity of complexes **1–5** are where the density of the red electron clouds around the isothiocyanate group. In addition, these negative electrostatic potential (ESP) regions are associated with lone pairs of electronegative atoms. The regions with the highest positive potential representing the nucleophilic reactivity were found around the -CH groups in the ligand. These results point out that more reactive regions of the complexes and their hydrogen bond interactions may occur.

To investigate chemical stability and reactivity as well as spectroscopic properties, the χ, η, S, ω, and φ index parameters were obtained from the frontier molecular orbital (FMO) energies.[95] The χ, η, S, ω, and φ indexes of complexes **1–5** for α spin calculated by using CAM-

TABLE 5 Experimental and theoretical wavelength, oscillator strength, and remarkable contributions for complexes **1–5**.

	Methanol/TD-CAM-B3LYP/6-311+G(d,p)//LanL2DZ		
Experimental λ (nm) (Methanol)	**λ (nm)**	**Osc. Strength**	Molecular contributions (SWizard and Chemissian programs) H: HOMO, L: LUMO, 2-pyridyl: C_5H_4N, imine group: CH=N−CH_3
Complex **1**			
279.2	274.0	0.0024	(43%) H−6 [Cd(6%)+Pyridyl(8%)+Imine(80%)+NCS(6%)]→L [Pyridyl(59%)+Imine(41%)] (28%) H−7 [Cd(7%)+Pyridyl(59%)+Imine(32%)+NCS(2%)]→L+1 [Pyridyl(61%)+Imine(38%)]
	261.0	0.0062	(51%) H [NCS(99%)]→L [Pyridyl(%59)+Imine(41%)] (30%) H−2 [NCS(98%)]→L [Pyridyl(%59)+Imine(41%)]
232.9	235.7	0.0119	(25%) H−10 [Imine(5%)+Pyridyl(93%)]→L+1 [Pyridyl(61%)+Imine (38%)] (23%) H−6 [Cd(6%)+Pyridyl(8%)+Imine(80%)+NCS(6%)]→L+1 [Pyridyl(61%)+Imine(38%)]
Complex **2**			
277.6	269.9	0.0058	(41%) H [Zn(15%)+Pyridyl(13%)+Imine(2%)+NCS(71%)]→L α [Zn (8%)+Pyridyl(57%)+Imine(32%)+NCS(3%)] (21%) H-6[Zn(7%)+Pyridyl(27%)+Imine(58%)+NCS(8%)]→L α [Zn (8%)+Pyridyl(57%)+Imine(32%)+NCS(3%)]
236.2	231.6	0.0065	(34%) H-6[Zn(7%)+Pyridyl(27%)+Imine(58%)+NCS(8%)]→L+1 α [Zn(4%)+Pyridyl(57%)+Imine(34%)+NCS(5%)] (26%) H-7[Zn(5%)+Pyridyl(81%)+Imine(12%)+NCS(2%)]→→L α [Zn(8%)+Pyridyl(57%)+Imine(32%)+NCS(3%)]
207.1	207.1	0.0006	(37%) H-2 [Zn(38%)+Pyridyl(26%)+Imine(18%)+NCS(19%)]→L+3 α [Zn(2%)+Pyridyl(80%)+Imine(11%)+NCS(7%)] (14%) H [Zn(15%)+Pyridyl(13%)+Imine(2%)+NCS(71%)]→L+3 α [Zn(2%)+Pyridyl(80%)+Imine(11%)+NCS(7%)]
Complex **3**			
387.8	398.0	0.0001	(19%) H-6 [Cu(2%)+Pyridyl(76%)+Imine(20%)+NCS(2%)]→L+1 β [Cu(16%)+Pyridyl(46%)+Imine(34%)+NCS(4%)] (18%) H-4 [Cu(5%)+Pyridyl(63%)+Imine(29%)+NCS(3%)]→L+1 α [Cu(3%)+Pyridyl(49%)+Imine(40%)+NCS(8%)]
284.9	287.0	0.0002	(40%) H-7 [Cu(18%)+Pyridyl(13%)+Imine(53%)+NCS(16%)]→L α [Cu(15%)+Pyridyl(46%)+Imine(35%)+NCS(4%)] (16%) H-4 [Cu(21%)+Pyridyl(64%)+Imine(13%)+NCS(2%)]→L+2 β [Cu(3%)+Pyridyl(48%)+Imine(38%)+NCS(11%)]
229.8	233.7	0.0011	(36%) H-4 [Cu(21%)+Pyridyl(64%)+Imine(13%)+NCS(2%)]→L+4 β [Cu(14%)+Pyridyl(63%)+Imine(13%)+NCS(10%)] (13%) H-9 [Cu(18%)+Pyridyl(64%)+Imine(10%)+NCS(7%)]→L+3 β [Cu(29%)+Pyridyl(59%)+Imine(8%)+NCS(4%)]
Complex **4**			
	530.6	0.3212	(94%) H-2 [Ag(10%)+Pyridyl(1%)+NCS(88%)]→L β [Ag(2%)+NCS (98%)]
261.2	262.1	0.0227	(30%) H-13 [Ag(3%)+ NCS(96%)]→L β [Ag(2%)+NCS(98%)] (8%) H-4 [Ag(37%)+Pyridyl(31%)+Imine(12%)+NCS(20%)]→L+1 β [Ag(1%)+Pyridyl(59%)+Imine(39%)+NCS(1%)]
228.8	229.0	0.0017	(14%) H-1 [Ag(20%)+Pyridyl(10%)+Imine(11%)+NCS(59%)]→L +10 β [Ag(1%)+Pyridyl(1%)+NCS(98%)] (9%) H-2 [Ag(10%)+Pyridyl(1%)+NCS(88%)]→L+9 α [Ag(31%) +Pyridyl(5%)+Imine(3%)+NCS(60%)]

(Continues)

TABLE 5 (Continued)

Experimental λ (nm) (Methanol)	Methanol/TD-CAM-B3LYP/6-311+G(d,p)//LanL2DZ		
	λ (nm)	Osc. Strength	Molecular contributions (SWizard and Chemissian programs) H: HOMO, L: LUMO, 2-pyridyl: C_5H_4N, imine group: CH=N−CH_3
Complex **5**			
321.5	285.3	0.0009	(21%) H-7 [Hg(10%)+Pyridyl(53%)+Imine(34%)+NCS(3%)]→L+1 α [Hg(1%)+Pyridyl(61%)+Imine(38%)] (16%) H-8 [Hg(5%)+Pyridyl(11%)+Imine(74%)+NCS(1%)+Cl (10%)]→L α [Hg(1%)+Pyridyl(58%)+Imine(41%)]
	251.7	0.0062	(47%) H [Imine(1%)+NCS(99%)]→L α [Hg(1%)+Pyridyl(58%) +Imine(41%)] (27%) H [Imine(1%)+NCS(99%)]→L+1 α [Hg(1%)+Pyridyl(61%) +Imine(38%)]
228.8	228.3	0.0101	(73%) H-3 [Hg(3%)+Pyridyl(5%)+Imine(2%)+NCS(2%)+Cl(88%)]→ L+1 α [Hg(1%)+Pyridyl(61%)+Imine(38%)] (10%) H-3 [Hg(3%)+Pyridyl(5%)+Imine(2%)+NCS(2%)+Cl(88%)]→ L α [Hg(1%)+Pyridyl(58%)+Imine(41%)]

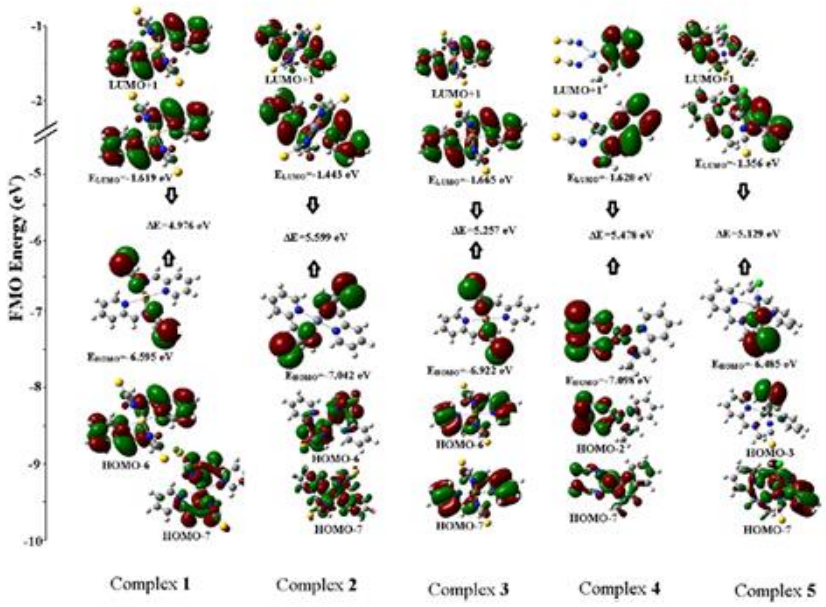

FIGURE 4 FMOs and energies being the most active in electronic transition obtained by DFT/CAM-B3LYP method for complexes **1–5**.

B3LYP level were obtained at the range of 4.359 and 3.902 eV, 2.799 eV and 2.488, 0.402 and 0.357 1/eV, 3.505 and 2.968 eV, 0.337 and 0.285 1/eV, respectively (see Table S5). According to these results, complex **1** has the smallest η and the largest ω values, so it can be said that there is more electron flow and this complex can be easily polarizable. The obtained results are well consistent with the reported ones.[38–44,76,77]

The values of optical band gap energy are found from the Tauc and Menth equation[96] by using Equation (11).

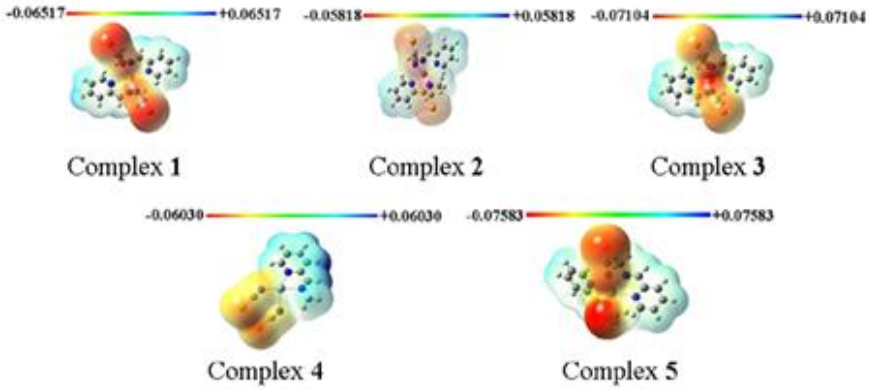

FIGURE 5 Molecular electrostatic potential (MEP) surfaces for the complexes **1–5**.

FIGURE 6 The graphs of optical band gap energy for the complexes **1–5**.

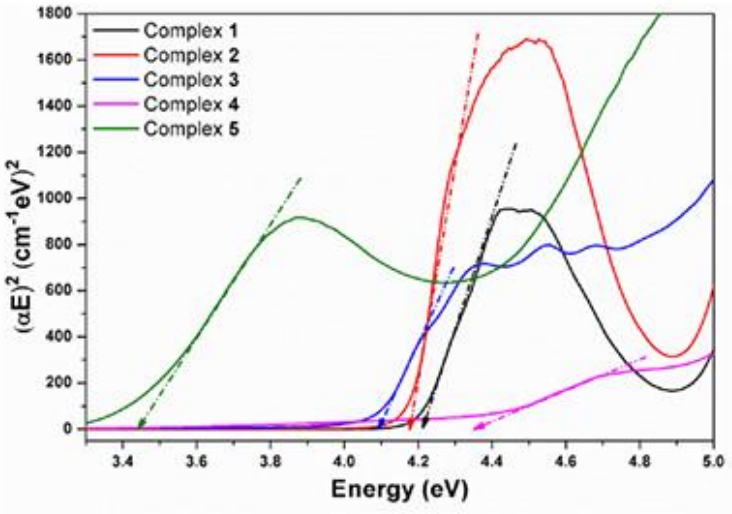

$$(\alpha h\nu) = C\left(h\nu - E_g\right)^{1/2} \tag{11}$$

In Equation (11), the α called as the absorption coefficient is obtained by $\alpha = 2.303A/d$, A and d are the absorbance in the UV–Vis region and width of the cuvette (1 cm), respectively. $h\nu$ and E_g are the photon energy and direct band gap energy, in order. C is a proportionality constant concerned with the effective masses dependent on the bands. It is obviously seen from Figure 6 that the E_g values for complexes **1–5** were obtained at 4.21, 4.19, 4.09, 4.35, and 3.44, respectively. The HOMO-LUMO energy gap values for **1–5** calculated at CAM-B3LYP level are 4.976 eV for α spin (complex **1**), 5.599 eV for α spin (complex **2**), 5.257 eV (complex **3**), 5.478 eV (complex **4**) and 5.129 eV for α spin (complex **5**). These results exhibit that the experimental and theoretical energy gap values are coherent.

3.3 | NLO properties

Owing to potential applications in telecommunications, laser technology, data storage, and electrochemical sensors, the synthesis, design and theoretical studies of new materials that may exhibit NLO (nonlinear optical) features draw attention.[97–99] Considering the design and development processes of any electronic device, when the experimental investigation of NLO properties for new materials is not possible, a foresight about the behavior of materials can be obtained by theoretical study. In this

regard, the linear optical (LO) and second-/third-order NLO parameters of the synthesized complexes **1–5** were computed at DFT/ωB97XD and DFT/CAM-B3LYP levels (see Table 6).

Theoretical α, β, and γ parameters were given comparatively the corresponding results of p-Nitroaniline (pNA)[100] and urea[101,102] used as prototype compounds. By using DFT/CAM-B3LYP level, the mean polarizability ($\overline{\alpha}$) values of complexes **1–5** in gas phase were computed at the range of 29.0×10^{-24} and 44.60×10^{-24} esu. These results display that it is higher than obtained that of the polarizability of pNA (17×10^{-24} esu). The β values for complexes **1–5** in the gas phase were obtained at 8.52×10^{-30}–10.80×10^{-30} esu ranges, as can be seen in Table 6 (in DFT/CAM-B3LYP level). Similarly, the γ values for complexes **1–5** in the gas phase were found within the ranges 30.44×10^{-36}–81.26×10^{-36} esu (in DFT/CAM-B3LYP level). In comparison of pNA and urea results with these results obtained, the β and γ values for complex **3** are about 1.17/83.08 and 5.42/11.61 times higher than those of pNA (9.2×10^{-30} esu)[100]/urea (0.130×10^{-30} esu)[102] and pNA (15×10^{-36} esu)[100]/urea (7×10^{-36} esu),[101] respectively. According to results, complex **3** is a powerful indicator in terms of microscopic NLO properties. The observed differences in NLO parameters could be interpreted associating with the charge mobility in the complex, metal ions in coordination, and its environment. Besides, the symmetry center around metal ions for the β parameter in these complex structures plays an efficient role.

The obtained β and γ results exhibit that complex **3** can be stated as an encouraging candidate for NLO materials (Table 6).

3.4 | α-Glucosidase inhibition activity

The IC_{50} values of the synthesized complexes **1–5** against α-glucosidase were determined at the range of 0.2376 ± 0.82 and 251.403 ± 2.54 μM (see Table 7). While the complex **5** ($IC_{50} = 0.2376 \pm 0.82$ μM) has the strongest inhibitory activity against α-glucosidase, the lowest inhibition value of 251.403 ± 2.54 μM was obtained for complex **2**. The complex **5** ($IC_{50} = 0.2376 \pm 0.82$ μM) was found to be 52.77 times more effective than genistein ($IC_{50} = 12.54 \pm 0.43$ μM), used as a standard in this study.

Considering Table 7, the following points for SAR could be deduced:

- The coordination of complexes **1–3,5** including metal ions (Cd (II), Zn (II), Cu (II), and Hg (II)) was described as a distorted octahedral geometry while the coordination of Ag(I) ion in complex **4** was defined as a distorted tetrahedral geometry. The complex **5** ($IC_{50} = 0.2376 \pm 0.82$ μM) containing Hg ion has the best inhibitory activity compared to complexes containing other metal ions with similar coordination. On the other hand, activity values of other complexes **1–3** were obtained at 214.80 ± 3.36, 251.403 ± 2.54, and 5.618 ± 1.22 μM, respectively. Compared α-glucosidase activities of complexes **1** ($IC_{50} = 214.80 \pm 3.36$ μM) and **2** ($IC_{50} = 251.403 \pm 2.54$ μM), the difference can be interpreted that the atomic diameter of Zn metal is lower than that of Cd. It is concluded that in the comparison of complexes **3** ($IC_{50} = 5.618 \pm 1.22$ μM) with **2** ($IC_{50} = 251.403 \pm 2.54$ μM), the exchanging of Cu with Zn having fully occupied d orbitals significantly reduced α-glucosidase inhibition due to the increase of

TABLE 6 Theoretical electric dipole moment (μ, Debye), static isotropic and anisotropic polarizability ($\overline{\alpha}$ and $\Delta\alpha$, $\times 10^{-24}$ esu), and static first- and second-order hyperpolarizability (β, $\times 10^{-30}$ esu, and γ, $\times 10^{-36}$ esu) for complexes **1–5**.

	Complex 1		Complex 2		Complex 3		Complex 4		Complex 5	
	ωB97XD	CAM-B3LYP	ωB97XD	CAM-B3LYP	ωB97XD	CAM-B3LYP	ωB97XD	CAM-B3LYP	ωB97XD	CAM-B3LYP
Parameter	**LanL2DZ**		**6–311 + G(d,p)**		**6–311 + G(d,p)**		**LanL2DZ**		**LanL2DZ**	
μ	13.94	14.09	10.95	9.32	12.09	12.71	13.92	13.75	12.84	12.95
μ	6.20 (pNA)[100] and 4.56 (Urea)[101]									
<α>	36.99	37.11	42.95	43.13	44.63	44.60	29.34	29.00	34.45	34.56
<α>	17 (pNA)[100]									
$\Delta\alpha$	24.47	20.58	18.28	17.84	20.43	19.20	17.82	18.58	18.74	18.99
<β>	9.26	10.03	6.57	8.62	9.83	10.80	11.99	7.25	7.82	8.52
<β>	9.2 (pNA),[100] 0.32 (Urea)[101] and 0.13 (Urea)[102]									
<γ>	39.30	42.13	51.77	52.66	81.03	81.26			28.17	30.44
<γ>	15.0 (pNA)[100] and 7 (Urea)[101]									

TABLE 7 In vitro inhibition IC_{50} values (μM) for α–glucosidase of complexes **1–5** and ligands.

Ligand/Complex	IC_{50} (μM)[a]
N-(pyridin-2-ylmethylene)methanamine (**L_1**)	Not active
Potassium thiocyanate (KSCN)	Not active
Complex **1** $[Cd(L_1)_2(NCS)_2]$	214.80 ± 3.36
Complex **2** $[Zn(L_1)_2(NCS)_2]$	251.403 ± 2.54
Complex **3** $[Cu(L_1)_2(NCS)_2]$	5.618 ± 1.22
Complex **4** $[Ag(L_1)(NCS)_2]$	34.735 ± 1.76
Complex **5** $[Hg(L_1)_2(NCS)Cl]$	0.2376 ± 0.82
Genistein	12.54 ± 0.43

[a]IC_{50} values represent the means ± S.E.M. of three parallel measurements ($p < 0.05$).

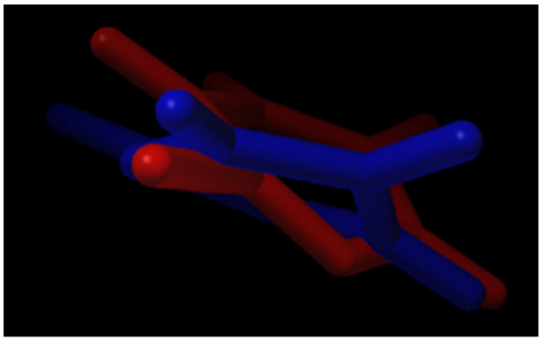

FIGURE 7 Superimpose of the native alpha-D-glucose ligand (red) versus re-docked co-crystallized ligand (blue) binding modes of the alpha-D-glucose.

the π-conjugation effect of L_1 ligand including 2-pyridyl and imine groups.

- According to the metal ions of similar group, the complex **5** containing Hg ion demonstrated the best inhibition effect compared to complexes **1,2** containing Cd (II) and Zn (II) ions. It could be shown for this reason that the atomic diameter of Hg is larger than that of Zn and Cd, and the Hg complex, unlike the Zn and Cd complex, is coordinated with an isothiocyanate ligand and a chloride instead of two isothiocyanate ligands.
- It could be deduced that the variation in the IC_{50} values of the complexes depends on the role of metal ion and its coordination environment.

The reported IC_{50} values for triazine-triazole, chromone-based benzohydrazide and chromone hydrazone derivatives against α-glucosidase were observed in the range from 11.63 ± 0.15 to 37.44 ± 0.35, 4.51 ± 0.09 to 27.21 ± 0.83, and 20.1 ± 0.19 μM to 45.7 ± 0.23 μM, respectively.[103–105] In the study of Tripath et al. in 2014,[8] α-glucosidase inhibition values for $[Co(en)_3]\cdot SO_4$ and $[Co(en)_3]\cdot 2Cl$ complexes were reported as 927.89 and 784.12 μM. In 2017,[4] the IC_{50} value of α − glucosidase inhibition for the Zn complex containing N_2O_2 was found to be 0.23 mM. Philip et al in 2017,[34] IC_{50} values against α − glucosidase enzyme for the metal (II) complexes were obtained between 0.1471 and 0.2320 mM. Furthermore, the IC_{50} values in some transition metal complexes containing pyridine derivatives could not be determined in metal complexes of chromium, manganese, cobalt, and nickel, while it was calculated between 0.22 and 0.92 mM in other metal complexes.[35–37] On the other hand, α-glucosidase inhibitor activity studies of different metal complexes with mixed ligand including 6-methylpicolinic acid synthesized in previous studies by our group, IC_{50} values were found to vary between 0.161 and >600 μM.[38–44] The IC_{50} values obtained for the Cu (II), Cd (II) and Cr (III) complexes with 6-methylpicolinic acid and isothiocyanate were reported at 8.02, 240.08, and >600 μM,[38] respectively. Considering on the IC_{50} values for the Cd, Zn, Cu, Ag, and Hg complexes bearing *N*-(pyridin-2-ylmethylene)methanamine and isothiocyanate, the complex **5** $[Hg(L_1)_2(NCS)Cl]$ was determined to have the highest inhibitory activity. Besides, it is obvious that complex **5** (IC_{50} = 0.2376 μM) is the best α-glucosidase inhibitor compared with previous studies.[20,37–40,57,106] Therefore, it can be stated that metal complexes containing the imine group tend to increase the inhibition of α-glucosidase.

The reported IC_{50} values for Hg (II) and Cu (II) complexes against α-glucosidase were 0.184 ± 0.015 and 1.685 ± 0.02 μM, while the IC_{50} values of them for the cytotoxicity study on healthy cell line were found to be 24.141 ± 1.039 and 53.435 ± 1.120 μM, respectively, in the our reported studies.[40,106] According to these results, the inhibition concentrations are 131.20 and 31.71 times lower than the concentrations where they exert cytotoxic effects, and considering these values, it can be said that the toxic effects of the Hg and Cu complexes on healthy cells are negligible. Therefore, the toxic effects of mercury, known as heavy metal, in complex structures on living cells are negligible, and their use as an α–glucosidase inhibitor can be considered appropriate. However, metal ions at high concentrations are toxic, but metal complexes have many advantages such as highly selective combination with the active site of the enzyme and modulating the conformation of the enzyme by binding the residue near the active site of the enzyme.[20]

3.5 | Molecular docking

In order to identify the ligand-protein interactions of the complexes **1–5**, the target protein (*S. cerevisiae* isomaltase

TABLE 8 Protein-ligand interactions and distance values for complexes **1–5** and genistein.

Substrate	Receptor	Interaction	Distance (Å)	K_i (μM)	Binding energy (kcal/mol)
Complex **1**				531.4	−4.47
NCS	PHE-494	Pi-Sulfur	5.10		
NCS	SER-490	Conventional H-Bond	3.13		
L_1	LYS-566	Pi-Sigma	3.78		
Imine-C	TYR-560	Carbon H-Bond	3.43		
Methyl-C	ASN-489	Carbon H-Bond	3.48		
L_1	PRO-488	Pi-Alkyl	5.39		
Complex **2**				704.84	−4.3
NCS	ASN-153	Conventional H-Bond	3.77		
NCS	LEU-226	Conventional H-Bond	3.59		
L_1-C	GLY-225	Carbon H-Bond	3.46		
L_1	LYS-141	Pi-Alkyl	5.01		
L_1	PRO-152	Pi-Alkyl	5.02		
L_1	PRO-139	Pi-Alkyl	5.22		
Complex **3**				63.44	−5.73
NCS	TYR-303	Pi-Sulfur	5.62		
NCS	HIS-280	Pi-Sulfur	4.69		
NCS	PHE-303	Pi-Sulfur	4.60		
L_1	TYR-158	Pi-Pi Stacked	4.03		
NCS	HIS-280	Conventional H-Bond	3.64		
L_1	ARG-315	Pi-Alkyl	3.84		
Complex **4**				190.81	−5.07
NCS	PHE-314	Pi-Sulfur	5.94		
NCS	TYR-316	Pi-Sulfur	5.02		
NCS	ASN-415	Conventional H-Bond	3.37		
NCS	TYR-158	Conventional H-Bond	2.88		
NCS	GLU-411	Conventional H-Bond	3.24		
NCS	SER-311	Conventional H-Bond	3.35		
L_1	SER-240	Pi-Donor	3.98		
L_1	TYR-158	Pi-Pi Stacked	4.23		
Imine-C	ASP-242	Carbon H-Bond	3.40		
L_1	LYS-156	Pi-Alkyl	5.06		
Complex **5**				33.49	−6.11
NCS	PHE-321	Pi-Sulfur	5.41		
NCS	PHE-360	Pi-Sulfur	4.88		
NCS	PHE-360	Conventional H-Bond	3.51		
NCS	TRP-326	Pi-Donor	4.12		
Methyl-C	PHE-321	Pi-Sigma	3.73		
Imine-C	PHE-321	Carbon H-Bond	3.17		
L_1	LYS-523	Pi-Alkyl	4.49		
Genistein				22.06	−6.35
C=O (benzopyran-4-one)	ILE-272	Conventional H-Bond	2.73		
CO (5-hydroxy-benzopyran-4-one)	SER-298	Conventional H-Bond	2.45		

TABLE 8 (Continued)

Substrate	Receptor	Interaction	Distance (Å)	K_i (μM)	Binding energy (kcal/mol)
CO (7-hydroxy-benzopyran-4-one)	LEU-297	Conventional H-Bond	3.29		
CO (7-hydroxy-benzopyran-4-one)	SER-291	Conventional H-Bond	2.88		
CO (7-hydroxy-benzopyran-4-one)	ALA-292	Conventional H-Bond	3.14		
Phenyl	ARG-263	Pi-Alkyl	4.19		
Phenyl	ILE-272	Pi-Alkyl	5.25		

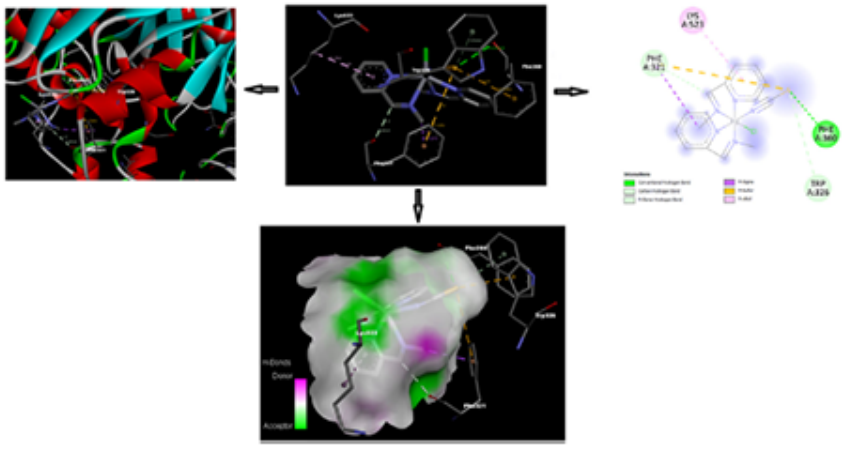

FIGURE 8 3D- and 2D-structures, and H-bond interactions between amino acid residues and ligands of the most active complex **5**.

[PDBID: 3A4A]) was selected as rigid and molecular docking study was carried out by the AutoDock4 program[86] implemented via the graphical user interface AutoDockTools (ADT1.4.7).[87] In the study conducted to determine that the selected docking parameters were acceptable, the conformation Root Mean Square Deviation (RMSD) value of the native alpha-D-glucose ligand (red) and re-docked co-crystallized ligand (blue) were compared in terms of structural alignment, as shown in Figure 7. The RMSD value obtained at 0.446 Å indicates that the selected docking parameters are acceptable.[107,108] Optimized parameters were used to dock for complexes **1–5** and genistein into the active site of the α-glucosidase homology model.

The docking results were used to explain the binding energies and estimated inhibition constants of the complexes. 2-D and 3-D structures demonstrating interactions between ligands of complexes **3–5** and amino acid residues were visualized Discovery Studio 4.0 program.[88]

According to the docking results of genistein, used as a standard inhibitor, and complexes **1–5**, the binding energy values were obtained at −6.35, −4.47, −4.3, −5.73, −5.07, and −6.11 kcal/mol, respectively. The estimated inhibition constants (K_i) corresponding to these binding energy values were found to be 22.06, 531.4, 704.84, 63.44, 190.81, and 33.49 μM, respectively (Table 8). Complex **5** ($IC_{50} = 0.2376 \pm 0.82$ μM), which showed the strongest inhibitory activity against α-glucosidase, was obtained at the lowest K_i value (33.49 μM) and binding energy (−6.11 kcal/mol), according to the docking results. It is concluded from in vitro results that the Complex **5** > Complex **3** > Complex **4** > Complex **2** > Complex **1** ranking of the best inhibitory property was supported by the docking results. From in vitro and docking results, it can be stated that the binding affinity for complex **5** is better than other complexes. Moreover, the docking results display that interaction with the enzyme active site indirectly/directly affects α-glucosidase inhibitor activity depending on the coordination environment. Figures 8, S7, and S8 show the two- and three-dimensional molecular docking diagram of **3–5** with amino acid residues of the target protein, such as some hydrogen bonding, van der Waals and pi-alkyl interactions. According to the docking results of complex **3** $[Cu(L_1)_2(NCS)_2]$ and complex **5** $[Hg(L_1)_2(NCS)Cl]$, it was observed that there were the conventional hydrogen

bond/pi-sulfur interactions between isothiocyanate and amino acid residues HIS-280/TYR-158, PHE-303 for complex **3**, PHE-360/PHE-321 for complex **5**. These complexes demonstrate that the pi-alkyl interactions are the between L_1 ligand, including 2-pyridyl and imine groups, and amino acid residues ARG-315 for complex **3** and LYS-523 for complex **5** (see Table 8). Apart from these interactions, the pi-pi stacked interaction for complex **3** emerged while the interactions for complex **5** appeared as carbon hydrogen bond, pi-donor hydrogen bond, and pi-sigma (see Figures 8 and S7). Similar interactions for complex **4** were detected among the different/same amino acid residues, as can be seen in Figure S8 and Table 8. Conventional hydrogen bond and pi-alkyl interactions for genistein were depicted at distances of 2.72 and 5.25 Å between amino acid residues ILE-272 and the C=O group of benzopyran-4-one and phenyl ring (Table 8). It was observed that there was the similar trend between the predicted inhibition constant and in vitro inhibition results. Furthermore, whether the electron density is localized or delocalized in the molecule is related to the donor and acceptor properties of the molecule, it can be said that these properties may cause similarities and differences in interactions with amino acid residues in the enzyme active site of the molecule.

The inhibition mechanism of α-glucosidase is explained by the fact that the enzymatic hydrolysis of glucosidases occurs through the interaction of the covalent glycosyl-enzyme intermediate in the literatures.[109–111] According to these studies on the inhibition mechanism of glucosidases and our docking studies, it is considered that the hydrolysis of isothiocyanate/imine moieties can occur as a result of interaction between enzyme active site and complexes. Moreover, the metal complexes are generally non-competitive inhibitors against α-glucosidase according to the reported enzyme kinetic studies.[20,33,112] We consider that the synthesized complexes **1–5** can be non-competitive inhibitors as similar to literature.

4 | CONCLUSION

To examine α-glucosidase inhibitory activity, the *N*-(pyridin-2-ylmethylene)methanamine (L_1) and complexes **1–5** {$[Cd(L_1)_2(NCS)_2]$, (**1**), $[Zn(L_1)_2(NCS)_2]$, (**2**), $[Cu(L_1)_2(NCS)_2]$, (**3**), $[Ag(L_1)(NCS)_2]$, (**4**), $[Hg(L_1)_2(NCS)Cl]$, (**5**)} were synthesized, and the XRD, LC-HRMS, FT–IR and UV–Vis spectroscopic methods for complexes **1–5** were applied to confirm structural and spectral characterization. The IC_{50} values against α-glucosidase for **1–5** were found at 0.2376- and 251.403-μM range. The lowest α-glucosidase inhibition value was determined for complex **5**, while a remarkable inhibition value was obtained for complex **3**. These effects were supported by docking results demonstrating protein-ligand interaction. Additionally, to detect the detailed spectral and structural features, as well as to relate the corresponding experimental results, DFT/ωB97XD and DFT/CAM-B3LYP levels calculations were carried out. While the HOMO/HOMOs values of the L_1 ligand showing the electron donor feature were found to be lower than those of the NCS ligand, the higher LUMO/LUMOs values showing the electron acceptor feature were found that much stronger π-acceptor of the L_1 ligand than the NCS ligand. The stable coordination geometries between lone pair electrons of N atoms and metal ions in **1–5** were verified by NBO results. While complex **3** has an IC_{50} value of 5.618 μM against α-glucosidase, the results of the β and γ parameters suggest that complex **3** can be expressed as an encouraging candidate for NLO materials. By considering in vitro/docking and NLO results, in this study with metal complexes of L_1 and NCS ligands, complex **5** may be an alternative drug candidate for T2DM, as well as complex **3** may be a candidate for NLO material.

AUTHOR CONTRIBUTIONS

Özgen Özge: Data curation, formal analysis, and visualization. **Davut Avcı**: Methodology, software, formal analysis, writing-original draft, and writing-review & editing. **Fatih Sönmez**: Formal analysis, investigation, writing-review & editing. **Ömer Tamer**: Investigation and software. **Necmi Dege**: Data curation, formal analysis, and visualization. **Adil Başoğlu**: Formal analysis, methodology, and software. **Yusuf Atalay**: Methodology and software. **Belma Zengin Kurt**: Formal analysis.

ACKNOWLEDGMENTS

This work was supported by the Scientific Research Projects Unit of Sakarya University (Project Number: 2021-7-25-103).

CONFLICT OF INTEREST STATEMENT

The authors declare that they have no known competing financial interests or personal relationships that could have appeared to influence the work reported in this paper.

DATA AVAILABILITY STATEMENT

The data that support the findings of this study are available from the corresponding author upon reasonable request.

REFERENCES

[1] S. Wild, K. Roglic, A. Green, R. Sicree, H. King, *Diabetes Care* **2004**, *27*, 1047.
[2] E. A. Alam, *Res. J. Recent Sci.* **2012**, *1*(ISC-2011), 398.
[3] C. N. Aguwa, *Therapeutic Basis for Clinical Pharmacy in the Tropics*, 3rd ed., SNAAP Press Ltd., Enugu **2004** 125.

[4] K. Balan, P. Ratha, G. Prakash, P. Viswanathamurthi, S. Adisakwattana, T. Palvannan, *Arab. J. Chem.* **2017**, *10*, 732.
[5] H. E. Thomas, T. W. Kay, *Diabetes/Metab. Res. Rev.* **2000**, *16*(4), 251.
[6] H. Iwahashi, N. Itoh, K. Yamagata, A. Imagawa, H. Nakajima, K. Tomita, M. Moriwaki, M. Waguri, K. Yamamoto, J. Miyagawa, M. Namba, T. Hanafusa, Y. Matsuzawa, *Cytokines Cell. Mol. Ther.* **1998**, *4*(1), 45.
[7] M. Kumari, S. Jain, *Res. J. Recent Sci.* **2012**, *1*(12), 70.
[8] I. P. Tripath, M. M. Kumar, T. Ruchita, M. Chinmayi, K. Arti, S. Laxmikant, D. Atul, S. U. Kumar, P. K. Bhihari, *Res. J. Chem. Sci.* **2014**, *4*(6), 13.
[9] R. Rhabasa-Lhoret, J. L. Chiasson, Alpha-glucosidase inhibitors, in *International Textbook of Diabetes Mellitus*, 3rd ed. (Eds: R. A. Defronzo, E. Ferrannini, H. Keen, P. Zimmet), John Wiley, UK **2004**.
[10] R. Miyazaki, H. Yasui, Y. Yoshikawa, *Open J. Inorg. Chem.* **2016**, *6*(2), 114.
[11] Y. P. Zhu, L. J. Yin, Y. Q. Cheng, K. Yamaki, Y. Mon, Y. C. Su, L. T. Li, *Food Chem.* **2008**, *109*(4), 737.
[12] J. Naowaboot, P. Pannangpetch, V. Kukongviriyapan, U. Kukongviriyapan, S. Nakmareong, A. Itharat, *Nutr. Res.* **2009**, *29*(8), 602.
[13] B. C. Raju, A. K. Ashok, J. A. Kumar, A. Z. Ali, S. B. Agawane, G. Saidachary, K. Madhusudana, *Bioorg. Med. Chem.* **2010**, *18*(1), 358.
[14] Y. Yao, W. Sang, M. Zhou, G. Ren, *J. Agric. Food Chem.* **2010**, *58*(2), 770.
[15] C. R. Bertozzi, L. L. Kiessling, *Science* **2001**, *291*, 2357.
[16] S. Horii, H. Fukase, T. Matsuo, Y. Kameda, N. Asano, K. Matsui, *J. Med. Chem.* **1986**, *29*(6), 1038.
[17] A. L. Floris, L. L. Peter, P. Reinier, H. L. Eloy, E. R. Guy, W. Chris, *Diabetes Care* **2005**, *28*, 154.
[18] B. Fernandes, U. Sagman, N. Auger, M. Demetrio, J. W. Dennis, *Cancer Res.* **1991**, *51*(2), 718.
[19] S. Ogawa, A. Maruyama, T. Odagiri, H. Yuasa, H. Hashimoto, *Eur. J. Org. Chem.* **2001**, *2001*(5), 967.
[20] J. Zheng, L. Ma, *Bioorg. Med. Chem. Lett.* **2015**, *25*, 2156.
[21] A. Khan, S. Sarkar, D. Sarkar, *Int. J. Antimicrob. Agents* **2008**, *32*(1), 40.
[22] M. S. Iqbal, A. H. Khan, B. A. Loothar, I. H. Bukhari, *Med. Chem. Res.* **2009**, *18*(1), 31.
[23] K. A. Abdalkarim, S. B. Aziz, R. T. Abdulwahid, S. M. Alshehri, T. Ahamad, J. M. Hadi, S. A. Hussein, *Arab. J. Chem.* **2021**, *14*, 103215.
[24] M. L. Petrus, R. K. M. Bouwer, U. Lafont, D. H. K. Murthy, R. J. P. Kist, M. L. Böhm, Y. Olivier, T. J. Savenije, L. D. A. Siebbeles, N. C. Greenhamd, T. J. Dingemans, *Polym. Chem.* **2013**, *4*, 4182.
[25] S. Ghosh, N. Roy, T. S. Singh, N. Chattopadhyay, *Spectrochim. Acta, Part a* **2018**, *188*, 252.
[26] L. Xia, Y.-F. Xia, L.-R. Huang, X. Xiao, H.-Y. Lou, T.-J. Liu, W.-D. Pan, H. Luo, *Eur. J. Med. Chem.* **2015**, *97*, 83.
[27] F. Sönmez, Z. Güneşli, B. Zengin Kurt, I. Gazioğlu, D. Avcı, M. Küçükislamoğlu, *Mol. Diversity* **2019**, *23*, 829.
[28] M. A. V. R. da Silva, M. D. M. C. R. da Silva, M. J. S. Monte, J. M. Gonçalves, É. M. R. Fernandes, *J. Chem. Soc., Dalton Trans.* **1997**, *7*, 1257.
[29] A. A. Al-Amiery, *Res. Chem. Intermed.* **2012**, *38*(3), 745.
[30] M. C. Rodríguez-Argüelles, P. Tourón-Touceda, R. Cao, A. M. García-Deibe, P. Pelagatti, C. Pelizzi, F. Zani, *J. Inorg. Biochem.* **2009**, *103*(1), 35.
[31] Z. L. You, D. H. Shi, C. Xu, Q. Zhang, H. L. Zhu, *Eur. J. Med. Chem.* **2008**, *43*(4), 862.
[32] M. Ueda, F. W. Robinson, M. M. Smith, T. Kono, *J. Biol. Chem.* **1984**, *259*(15), 9520.
[33] J.-W. Zheng, L. Ma, *Chin. Chem. Lett.* **2016**, *27*(2), 283.
[34] J. E. Philip, M. Shahid, M. R. Prathapachandra Kurup, M. P. Velayudhan, *J. Photochem. Photobiol. B: Biol.* **2017**, *175*, 178.
[35] Y. Yoshikawa, E. Ueda, K. Kawabe, H. Miyake, T. Takino, H. Sakurai, Y. Kojima, *J. Biol. Inorg. Chem.* **2002**, *7*, 68.
[36] N. Yasumatsu, Y. Yoshikawa, Y. Adachi, H. Sakurai, *Bioorg. Med. Chem.* **2007**, *15*, 4917.
[37] Y. Yoshikawa, R. Hirata, H. Yasui, H. Sakurai, *Biochimie* **2009**, *91*, 1339.
[38] D. Avcı, S. Altürk, F. Sönmez, Ö. Tamer, A. Başoğlu, Y. Atalay, B. Z. Kurt, N. Dege, *Tetrahedron* **2018**, *74*, 7198.
[39] D. Avcı, S. Altürk, F. Sönmez, Ö. Tamer, A. Başoğlu, Y. Atalay, B. Zengin Kurt, N. Dege, *Appl. Organomet. Chem.* **2019**, *33*, e4935.
[40] D. Avcı, S. Altürk, F. Sönmez, Ö. Tamer, A. Başoğlu, Y. Atalay, B. Zengin Kurt, N. Dege, *J. Biol. Inorg. Chem.* **2019**, *24*, 747.
[41] D. Avcı, S. Altürk, F. Sönmez, Ö. Tamer, A. Başoğlu, Y. Atalay, B. Zengin Kurt, N. Dege, *J. Mol. Struct.* **2019**, *1197*, 645.
[42] D. Avcı, S. Altürk, F. Sönmez, Ö. Tamer, A. Başoğlu, Y. Atalay, B. Zengin Kurt, N. Dege, *Appl. Organomet. Chem.* **2020**, *34*, e5412.
[43] D. Avcı, S. Altürk, F. Sönmez, Ö. Tamer, A. Başoğlu, Y. Atalay, B. Zengin Kurt, *J. Mol. Struct.* **2020**, *1205*, 127665.
[44] D. Avcı, S. Altürk, F. Sönmez, Ö. Tamer, A. Başoğlu, Y. Atalay, B. Zengin Kurt, N. Dege, *Mol. Diversity* **2021**, *25*, 171.
[45] E. C. Constable, P. J. Steel, *Coord. Chem. Rev.* **1989**, *93*(2), 205.
[46] W. Driessen, R. De Graaff, F. Parlevliet, J. Reedijk, R. De Vos, *Inorg. Chim. Acta* **1994**, *216*, 43.
[47] M. Gollapalli, M. Taha, M. T. Javid, N. B. Almandil, F. Rahim, A. Wadood, A. Mosaddik, M. Ibrahim, M. A. Alqahtani, Y. A. Bamarouf, *Bioorg. Chem.* **2019**, *85*, 33.
[48] U. Ghani, *Eur. J. Med. Chem.* **2015**, *103*, 133.
[49] K. D. Demadis, S. D. Katarachia, *Phosphorus, Sulfur Silicon Relat. Elem.* **2004**, *179*(3), 627.
[50] J. Monot, M. Petit, S. M. Lane, I. Guisle, J. Léger, C. Tellier, D. R. Talham, B. Bujoli, *J. Am. Chem. Soc.* **2008**, *130*(19), 6243.
[51] J. Umeda, M. Suzuki, M. Kato, M. Moriya, W. Sakamoto, T. Yogo, *J. Power Sources* **2010**, *195*(18), 5882.
[52] Y. Saito, J. Takemoto, B. Hutchinson, K. Nakamoto, *Inorg. Chem.* **1972**, *11*(9), 2003.
[53] V. Amani, N. Safari, H. R. Khavasi, *Polyhedron* **2007**, *26*(15), 4257.
[54] S. M. Mobin, A. K. Saini, V. Mishra, A. Chaudhary, *Polyhedron* **2006**, *110*, 131.
[55] L.-J. Yang, Q.-L. Liu, M.-X. Wang, L.-S. Gu, Y.-H. Luo, B.-W. Sun, *Spectrochim. Acta, Part a* **2016**, *166*, 1.

[56] M. Barquín, N. Cocera, M. J. Gonźalez Garmendia, L. Larrinaga, E. Pinilla, J. M. Seco, M. R. Torres, *Inorg. Chim. Acta* **2010**, *363*, 127.

[57] C. M. Santos, M. Freitas, E. Fernandes, *Eur. J. Med. Chem.* **2018**, *157*, 1460.

[58] M. Amirnasr, A. D. Khalaji, L. R. Falvello, T. Soler, *Polyhedron* **2006**, *25*, 1967.

[59] M. Habib, T. K. Karmakar, G. Aromí, J. Ribas-Ariño, H.-K. Fun, S. Chantrapromma, S. K. Chandra, *Inorg. Chem.* **2008**, *47*(10), 4109.

[60] L. Li, D. Liao, S. Liu, Z. Jiang, S. Yan, *Inorg. Chem. Commun.* **2003**, *6*, 225.

[61] P. S. Mukherjee, T. K. Maji, G. Mostafa, T. Mallah, N. R. Chaudhuri, *Inorg. Chem.* **2000**, *39*, 5147.

[62] T. G. Richmond, E. P. Kelson, A. M. Arif, *J. Am. Chem. Soc.* **1988**, *110*(7), 2334.

[63] G. M. Sheldrick, *Acta Cryst.* **2015**, *A71*, 3.

[64] C. F. Macrae, P. R. Edgington, P. McCabe, E. Pidcock, G. P. Shields, R. Taylor, M. Towler, J. van de Streek, *J. Appl. Crystallogr.* **2006**, *39*, 453.

[65] A. L. Spek, *Acta Cryst.* **2009**, *D65*, 148.

[66] H. Sun, W. Ding, X. Song, D. Wang, M. Chen, K. Wang, Y. Zhang, P. Yuan, Y. Ma, R. Wang, *Bioorg. Med. Chem. Lett.* **2017**, *27*(15), 3226.

[67] M. J. Frisch, G. W. Trucks, H. B. Schlegel, G. E. Scuseria, M. A. Robb, J. R. Cheeseman, G. Scalmani, V. Barone, G. A. Petersson, H. Nakatsuji, X. Li, M. Caricato, A. V. Marenich, J. Bloino, B. G. Janesko, R. Gomperts, B. Mennucci, H. P. Hratchian, J. V. Ortiz, A. F. Izmaylov, J. L. Sonnenberg, D. Williams-Young, F. Ding, F. Lipparini, F. Egidi, J. Goings, B. Peng, A. Petrone, T. Henderson, D. Ranasinghe, V. G. Zakrzewski, J. Gao, N. Rega, G. Zheng, W. Liang, M. Hada, M. Ehara, K. Toyota, R. Fukuda, J. Hasegawa, M. Ishida, T. Nakajima, Y. Honda, O. Kitao, H. Nakai, T. Vreven, K. Throssell, J. A. Montgomery Jr., J. E. Peralta, F. Ogliaro, M. J. Bearpark, J. J. Heyd, E. N. Brothers, K. N. Kudin, V. N. Staroverov, T. A. Keith, R. Kobayashi, J. Normand, K. Raghavachari, A. P. Rendell, J. C. Burant, S. S. Iyengar, J. Tomasi, M. Cossi, J. M. Millam, M. Klene, C. Adamo, R. Cammi, J. W. Ochterski, R. L. Martin, K. Morokuma, O. Farkas, J. B. Foresman, D. J. Fox, *Gaussian 16, Revision C.01*, Gaussian, Inc., Wallingford CT **2016**.

[68] R. Dennington, T. A. Keith, J. M. Millam, *GaussView, Version 6.1*, Semichem Inc., Shawnee Mission, KS **2016**.

[69] T. Yanai, D. P. Tew, N. C. Handy, *Chem. Phys. Lett.* **2004**, *393*(1–3), 51.

[70] J.-D. Chai, M. Head-Gordon, *Phys. Chem. Chem. Phys.* **2008**, *10*, 6615.

[71] M. J. Frisch, J. A. Pople, J. S. Binkley, *J. Chem. Phys.* **1984**, *80*, 3265.

[72] P. J. Hay, W. R. Wadt, *J. Chem. Phys.* **1985**, *82*, 270.

[73] E. Runge, E. K. U. Gross, *Phys. Rev. Lett.* **1984**, *52*, 997.

[74] S. Miertus, E. Scrocco, J. Tomasi, *J. Chem. Phys.* **1981**, *55*, 117.

[75] S. I. Gorelsky, *SWizard Program, Revision 4.5*, University of Ottawa, Ottawa, Canada **2010** http://www.sg.chem.net/

[76] S. Altürk, D. Avcı, Ö. Tamer, Y. Atalay, O. Şahin, *J. Phys. Chem. Solids* **2016**, *98*, 71.

[77] S. Altürk, Ö. Tamer, D. Avcı, Y. Atalay, *J. Organomet. Chem.* **2015**, *797*, 110.

[78] A. E. Reed, F. Weinhold, *J. Chem. Phys.* **1983**, *78*, 4066.

[79] J. P. Foster, F. Weinhold, *J. Am. Chem. Soc.* **1980**, *102*, 7211.

[80] W. Yang, R. G. Parr, *Proc. Nati. Acad. Sci. U.S.a.* **1985**, *82*, 6723.

[81] P. K. Chattaraj, U. Sarkar, D. R. Ro, *Chem. Rev.* **2006**, *106*(6), 2065.

[82] J. L. Oudar, *J. Chem. Phys.* **1977**, *67*, 446.

[83] J. L. Oudar, J. Zyss, *Phys. Rev. a* **1982**, *26*, 2028.

[84] Y. Zhang, C.-Y. Zhao, W.-H. Fang, X.-Z. You, *Theor. Chem. Acc.* **1997**, *96*, 129.

[85] D. Avcı, *Spectrochim. Acta a* **2011**, *82*, 37.

[86] G. M. Morris, R. Huey, W. Lindstrom, M. F. Sanner, R. K. Belew, D. S. Goodsell, A. J. Olson, *J. Comput. Chem.* **2009**, *30*, 2785.

[87] F. Michel, *J. Mol. Graphics Modell.* **1999**, *17*, 57.

[88] D. Systèmes, *Dassault Systèmes Biovia:* San Diego, CA, USA **2016**.

[89] H. Tong-Liang, D. Wen-Ping, H. Bo-Wen, J.-R. Li, B. Xian-He, R. Cao, *CrystEngComm* **2008**, *10*, 1037.

[90] H. Wu, F. Wang, F. Shi, Z. Yang, H. Zhang, H. Peng, *Transition Met. Chem.* **2015**, *40*, 555.

[91] Y. Xu, H. Wu, H. Zhang, S. O. Aderinto, Z. Yang, *J. Coord. Chem.* **2016**, *69*(19), 2988.

[92] G. Varsányi, *Assignments for vibrational spectra of seven hundred benzene derivatives*, Vol. 1, Halsted Press **1974**.

[93] L. Skripnikov, *Chemissian: software to analyze spectra, build density maps and molecular orbitals*, Version 4.43, **2016**.

[94] S. I. Gorelsky, A. B. P. Lever, *Can. J. Anal. Sci. Spectrosc.* **2003**, *48*(1), 93.

[95] R. G. Pearson, *Proc. Nati. Acad. Sci. U.S.a.* **1986**, *83*, 8440.

[96] S. Altürk, D. Avcı, A. Başoğlu, Ö. Tamer, Y. Atalay, N. Dege, *Spectrochim. Acta a* **2018**, *190*, 220.

[97] D. S. Chemla, J. Zysss, *Nonlinear Optical Properties of Organic Molecules and Crystals*, Academic Press, Orlando, FL **1987**.

[98] K. Kamada, M. Ueda, H. Nagao, K. Tawa, T. Sugino, Y. Shmizu, K. Ohta, *J. Phys. Chem. A* **2000**, *104*(20), 4723.

[99] B. M. Pierce, *J. Chem. Phys.* **1989**, *91*(2), 791.

[100] L. T. Cheng, W. Tam, S. H. Stevenson, G. R. Meredith, G. Rikken, S. R. Marder, *J. Phys. Chem.* **1991**, *95*, 10631.

[101] I. Ledoux, J. Zyss, *Chem. Phys.* **1982**, *73*, 203.

[102] C. Adant, M. Dupuis, J. Bredas, *Int. J. Quantum Chem.* **1995**, *56*, 497.

[103] G. Wang, Z. Peng, J. Wang, X. Li, J. Li, *Eur. J. Med. Chem.* **2017**, *125*, 423.

[104] M. Fan, W. Yang, Z. Peng, Y. He, G. Wang, *Bioorg. Chem.* **2023**, *131*, 106276.

[105] G. Wang, M. Chen, J. Wang, Y. Peng, L. Li, Z. Xie, B. Deng, S. Chen, W. Li, *Bioorg. Med. Chem. Lett.* **2017**, *27*, 2957.

[106] D. Avcı, S. Altürk, F. Sönmez, Ö. Tamer, A. Başoğlu, Y. Atalay, B. Zengin Kurt, D. Öztürk, N. Dege, *Appl. Organomet. Chem.* **2019**, *33*(3), e4725.

[107] A. Korkmaz, E. Bursal, *Chem. Biodiversity* **2022**, *19*, e202200140.

[108] A. Korkmaz, G. Kurtay, E. Kaya, E. Bursal, *J. Biomol. Struct. Dyn.*, 1. https://doi.org/10.1080/07391102.2022.2116600
[109] G. J. Davies, L. Mackenzie, A. Varrot, M. Dauter, A. M. Brzozowski, M. Schülein, S. G. Withers, *Biochemistry* **1998**, *37*(34), 11707.
[110] C. S. Rye, S. G. Withers, *Curr. Opin. Chem. Biol.* **2000**, *4*, 573.
[111] J. D. McCarter, S. G. Withers, *J. Am. Chem. Soc.* **1996**, *118*, 241.
[112] Y. Wang, L. Ma, Z. Li, Z. Du, Z. Liu, J. Qin, X. Wang, Z. Huang, L. Gu, A. S. C. Chen, *FEBS Lett.* **2004**, *576*, 46.

SUPPORTING INFORMATION

Additional supporting information can be found online in the Supporting Information section at the end of this article.

How to cite this article: Ö. Özge, D. Avcı, F. Sönmez, Ö. Tamer, N. Dege, A. Başoğlu, Y. Atalay, B. Z. Kurt, *Appl Organomet Chem* **2023**, e7084. https://doi.org/10.1002/aoc.7084

Synthesis, DFT calculations, α-glucosidase inhibitor activity, and docking studies on Schiff base metal complexes containing isothiocyanate

Özgen Özge[1,2], Davut Avcı[1], Fatih Sönmez[3], Ömer Tamer[1], Necmi Dege[4], Adil Başoğlu[1], Yusuf Atalay[1], Belma Zengin Kurt[5]

[1]*Sakarya University, Faculty of Arts and Sciences, Department of Physics, 54187, Sakarya, Turkey*
[2]*Cappadocia University, Health Vocational School, Ürgüp, 50400, Nevşehir, Turkey*
[3]*Sakarya University of Applied Sciences, Pamukova Vocational High School, 54055, Sakarya, Turkey*
[4]*Ondokuz Mayıs University, Faculty of Arts and Sciences, Department of Physics, 55139, Samsun, Turkey*
[5]*Bezmialem Vakif University, Faculty of Pharmacy, Department of Pharmaceutical Chemistry, 34093 Istanbul, Turkey*

Supplementary Material

X-ray structure determination

In order to determine suitable single crystal structure and data collection of complex **1**, a Stoe IPDS II diffractometer having Mo–Kα (λ=0.71073 Å) radiation at 296 K was used. The detailed crystal structure parameters are given in Table 1. The crystal structure was solved by direct methods using SHELXT [1] and refined by full-matrix least-squares methods on F^2 using SHELXL-97 [1]. The hydrogen atoms bonding to carbon atoms were located from different maps and then processed as riding atoms with C−H distances of 0.96 Å. Water H atoms were located in a difference map refined freely. Molecular diagrams were composed using MERCURY [2]. Supramolecular analyses were fulfilled and the diagrams were prepared with the aid of PLATON [3].

α-Glucosidase inhibition assay

By using p−nitrophenyl−α−D−glucopyranoside (pNGP, Sigma, N1377) as the substrate, the α−glucosidase from Saccharomyces cerevisiae (Sigma, G5003) was determined as the target protein. The compounds and genistein were dissolved in DMSO. The enzyme and the substrate were dissolved in potassium phosphate buffer (0.05 M, pH 6.8). The enzymatic reaction mixture composed of α-glucosidase (0.02 U, 20 µL), substrate (1.25 mM, 30 µL), test compounds (10 µL) and potassium phosphate buffer (140 µL) was incubated at 37 °C for 30 min. After 30 min of incubation, the absorbance of yellow colour produced due to the formation of p-nitrophenol was measured using Synergy H1 (BioTek, USA) 96-well microplate reader at 405 nm. All experiments were performed in triplicates. The surveying of α−glucosidase inhibition activity for the complexes **1-5** was fulfilled by basing on our previously reported study [4-7],

Glucosidase inhibition = $[(A_c-A_s)/A_c]x100$

where A_c is the absorbance of control and A_s is the absorbance of samples, respectively. The calculation of IC_{50} values was performed by using Graphpad Software.

Docking procedure

In order to investigate the protein-ligand interactions of the synthesized complexes **1-5**, the target protein (S. *cerevisiae* isomaltase (PDBID: 3A4A)) provided from the Protein Data Bank was selected as rigid and molecular docking study was carried out by the AutoDock4 [8] program implemented via the graphical user interface AutoDockTools (ADT1.5.7) [9]. The pdb files were generated for complexes **1-5** and genistein optimized at CAM-B3LYP level (in Gaussian 16W program) to use in docking. ADT1.5.7 was used to add Kollman charges, identify rotatable bonds, and join non-polar hydrogen atoms to carbon atoms. All calculations for complex-target flexible docking were performed using the Lamarckian genetic algorithm (LGA) method [10]. Grid and docking parameter file, PDBQT format for target and ligand (target.pdbqt, ligand.pdbqt) using AutoDock 4.2 were prepared. AutoGrid 4 was provided the determination of docking area. The grid box dimensions were determined as different points to cover the target binding site and accommodate complexes **1-5** and genistein to move freely. 3D affinity grid centered around the complexes **1-5** and and genistein binding site with a 1.0 Å (complexes **1,2,4** and genistein), 0.903 Å (complexes **3**), and 0.861 Å (complexes **5**) grid point spacing was calculated for each of the following atom types: (a) receptor (protein): A (aromatic C), C, Ca, HD, N, OA, SA and (b) ligand: A, C, NA, N, SA, as well as Cd for complex **1**, Zn for complex **2**, Cu for complex **3**, Ag for complex **4**, Cl and Hg for complex **5**, only A and OA for genistein, e (electrostatic), and d (desolvation). Further docking parameters were used as: Population size: 150, mutation rate: 0.02, elitism: 1, crossover rate: 0.8, local search rate: 0.06, and energy evaluations: 2,500,000. Final docked conformations were achieved within a 2 Å root mean square deviation (RMSD) tolerance.

Complex **1**: grid points in xyz: 60, 60, 60 and grid box center in xyz: 21.831, -0.612, 18.719
Complex **2**: grid points in xyz: 60, 60, 60 and grid box center in xyz: 21.831, -0.612, 18.719
Complex **3**: grid points in xyz: 80, 94, 80 and grid box center in xyz: 21.276, -0.752, 18.634
Complex **4**: grid points in xyz: 60, 60, 60 and grid box center in xyz: 21.835, -0.612, 18.716
Complex **5**: grid points in xyz: 80, 98, 80 and grid box center in xyz: 21.276, -0.752, 18.634
Genistein: grid points in xyz: 60, 60, 60 and grid box center in xyz: 21.831, -0.612, 18.719

The docking results obtained here were used to explain the relative performance of the stabilization and binding energy of the complexes. 2-D and 3-D structures demonstrating interactions between amino acid residues and ligands of complexes **3-5** were visualized Discovery Studio 4.0 program [11].

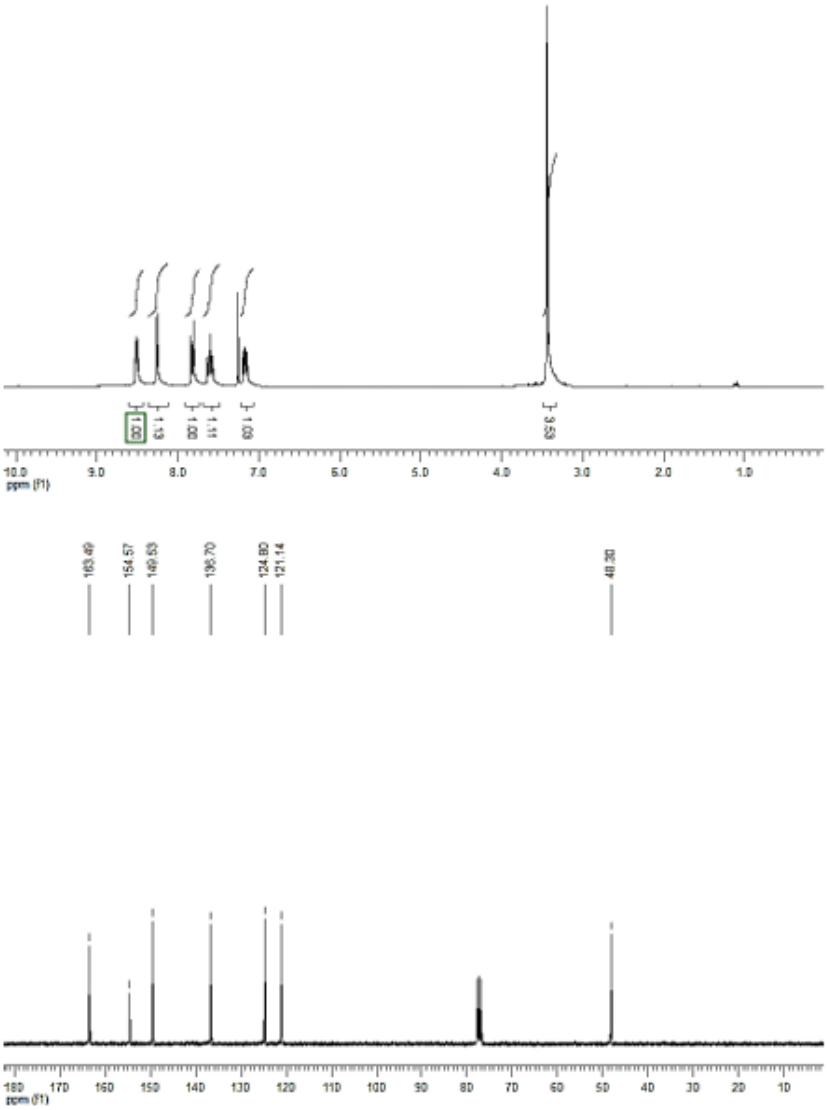

Figure S1. The ^{1}H and ^{13}C NMR spectra (in $CDCl_3$) of *N*-(pyridin-2-ylmethylene)methanamine (L_1).

5

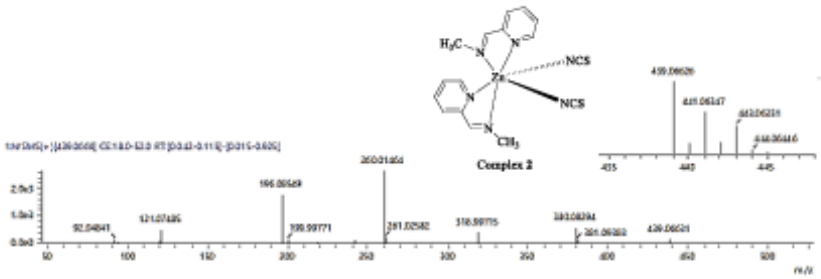

Figure S2. The mass spectrum of the complex **2**.

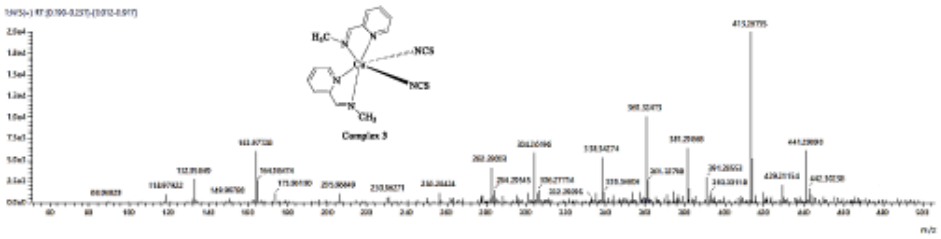

Figure S3. The mass spectrum of the complex **3**.

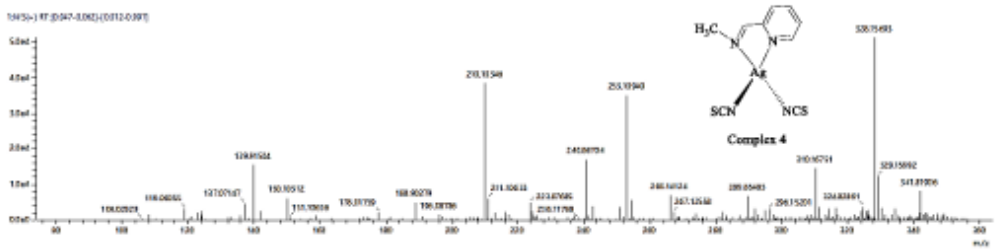

Figure S4. The mass spectrum of the complex **4**.

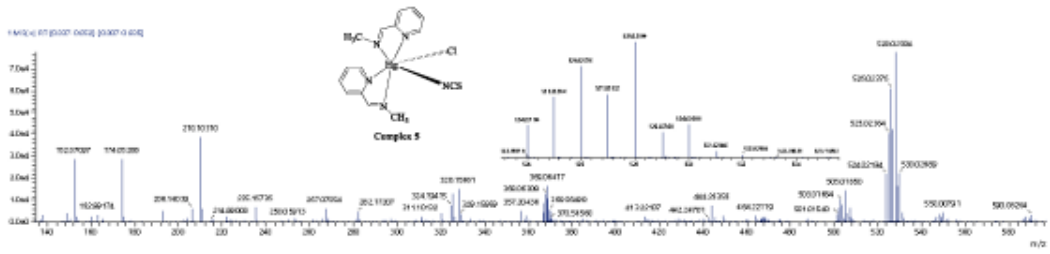

Figure S5. The mass spectrum of the complex **5**.

9

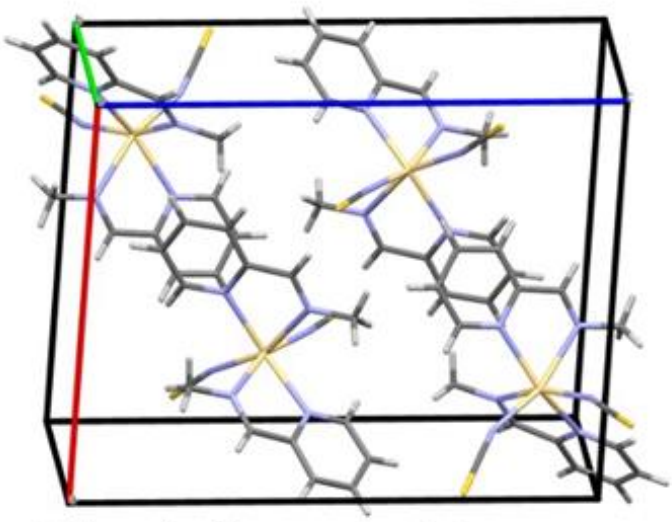

Figure S6. The crystal packing structure of complex **1**.

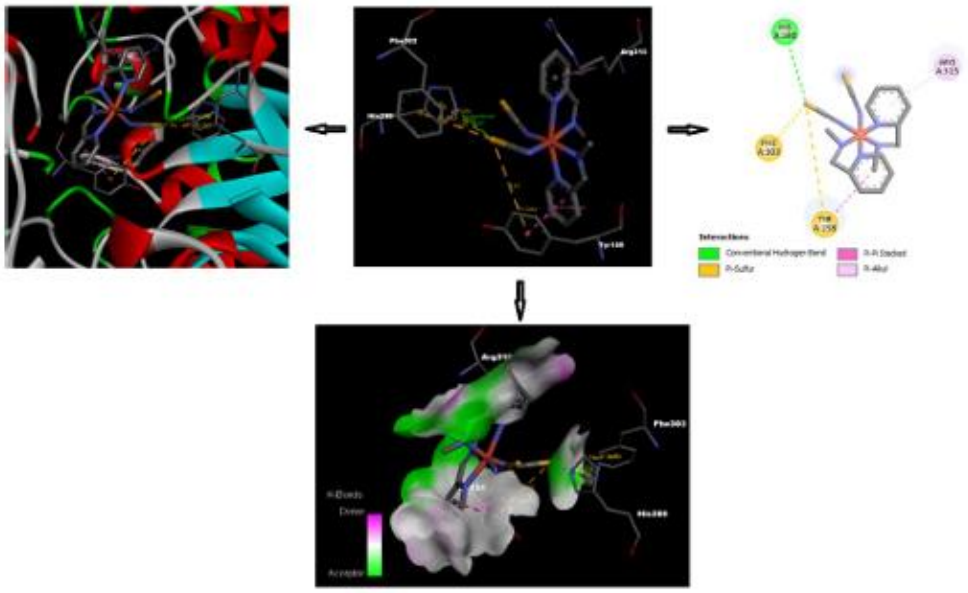

Figure S7. 3D- and 2D-structures, and H-bond interactions between amino acid residues and ligands of the most active complex **3**.

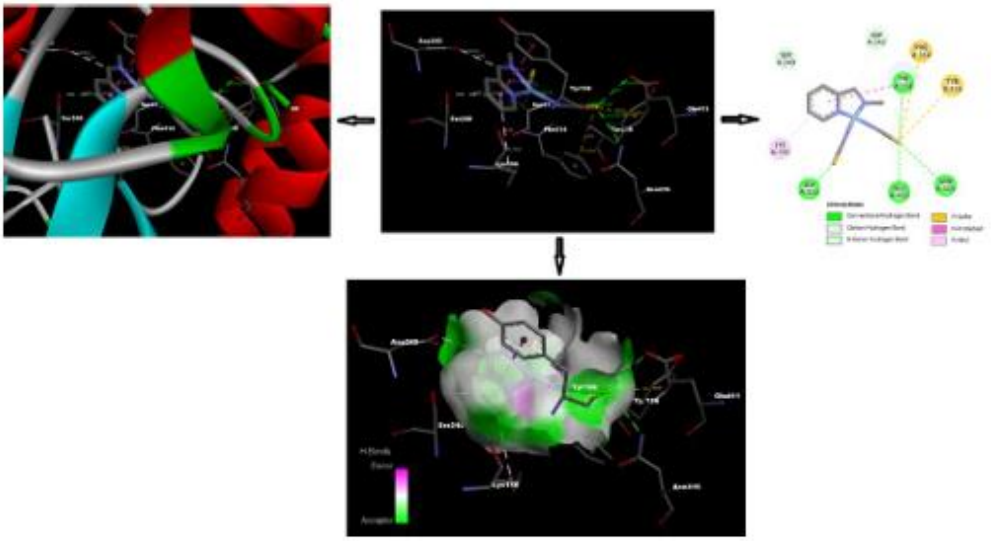

Figure S8. 3D- and 2D-structures, and H-bond interactions between amino acid residues and ligands of the most active complex **4**.

Table S1. Comparison of experimental and theoretical geometric parameters for complexes **2-5**.

Complex **2**			Complex **3**		
Parameters	ωB97XD	CAM-B3LYP	Parameters	ωB97XD	CAM-B3LYP
Bond length (Å)					
Zn1–N6	2.012	2.042	Cu1–N6	1.971	1.961
Zn1–N5	2.012	2.042	Cu1–N5	1.971	1.961
Zn1–N4	2.213	2.198	Cu1–N4	2.393	2.409
Zn1–N3	2.353	2.327	Cu1–N3	2.111	2.110
Zn1–N2	2.213	2.198	Cu1–N2	2.393	2.410
Zn1–N1	2.353	2.327	Cu1–N1	2.111	2.111
S2–C16	1.623	1.621	S2–C16	1.626	1.626
S1–C15	1.623	1.621	S1–C15	1.626	1.626
N4–C14	1.329	1.327	N4–C14	1.326	1.325
N4–C10	1.339	1.337	N4–C10	1.336	1.335
N1–C2	1.262	1.262	N1–C2	1.267	1.265
N1–C1	1.444	1.445	N1–C1	1.449	1.451
N3–C9	1.262	1.262	N3–C9	1.267	1.265
N3–C8	1.444	1.445	N3–C8	1.449	1.451
N2–C7	1.329	1.327	N2–C7	1.326	1.325
N2–C3	1.339	1.337	N2–C3	1.336	1.335
N5–C15	1.176	1.175	N5–C15	1.175	1.171
N6–C16	1.176	1.175	N6–C16	1.175	1.171
Bond angles (°)					
N6– Zn1–N5	111.88	111.22	N6– Cu1–N5	100.31	100.15
N6– Zn1–N4	99.81	94.84	N6– Cu1–N4	97.70	97.72
N5– Zn1–N4	93.56	91.89	N5– Cu1–N4	93.32	92.17
N6– Zn1–N3	84.64	83.69	N6– Cu1–N3	86.26	85.83
N5– Zn1–N3	160.39	159.98	N5– Cu1–N3	166.34	165.36
N4– Zn1–N3	72.52	72.99	N4– Cu1–N3	73.82	73.70
N6– Zn1–N2	93.56	91.90	N6– Cu1–N2	93.32	92.15
Dihedral angles (°)					
Zn1–N4–C10–C11	177.58	170.79	Cu1–N4–C10–C11	169.93	169.18
Zn1–N3–C9–C10	9.04	12.54	Cu1–N3–C9–C10	6.82	6.76
Zn1–N1–C2–C3	9.04	12.54	Cu1–N1–C2–C3	6.82	6.78
Zn1–N4–C10–C9	-2.45	-8.36	Cu1–N4–C10–C9	-9.26	-9.36
Zn1–N4–C14–C13	-177.76	-170.41	Cu1–N4–C14–C13	-167.19	-166.01

Table S1. Continued

Complex **4**			Complex **5**		
Parameters	ωB97XD	CAM-B3LYP	Parameters	ωB97XD	CAM-B3LYP
Bond length (Å)					
Ag1–N6	2.214	2.193	Hg1–Cl1	2.590	2.598
Ag1–N5	2.448	2.457	Hg1–N5	2.319	2.304
Ag1–N4	2.421	2.435	Hg1–N4	2.552	2.551
Ag1–N3	2.347	2.316	Hg1–N3	2.535	2.545
S2–C16	1.694	1.696	Hg1–N2	2.514	2.519
S1–C15	1.700	1.702	Hg1–N1	2.610	2.597
N4–C14	1.346	1.345	S1–C15	1.679	1.680
N4–C10	1.356	1.355	N4–C14	1.347	1.345
N3–C9	1.283	1.281	N4–C10	1.356	1.354
N3–C8	1.463	1.462	N1–C2	1.283	1.281
N5–C15	1.189	1.187	N1–C1	1.463	1.463
N6–C16	1.187	1.184	N3–C9	1.282	1.281
			N3–C8	1.461	1.462
			N2–C7	1.347	1.345
			N2–C3	1.354	1.353
			N5–C15	1.194	1.191
Bond angles (°)					
N6–Ag1–N5	87.94	87.18	Cl1–Hg1–N5	121.12	120.28
N6– Ag1–N4	124.57	124.12	Cl1–Hg1–N4	115.41	110.76
N5– Ag1–N4	132.02	132.94	N5– Hg1–N4	85.27	84.51
N6– Ag1–N3	157.67	158.90	Cl1– Hg1–N3	85.60	82.99
N5– Ag1–N3	90.90	90.38	N5– Hg1–N3	148.16	148.41
N4– Ag1–N3	71.26	71.58	N4– Hg1–N3	66.37	66.29
			Cl1– Hg1–N2	89.28	87.76
Dihedral angles (°)					
Ag1–N4–C10–C11	-177.19	-176.91	Hg1–N4–C10–C11	-176.06	176.67
Ag1–N3–C9–C10	10.30	9.97	Hg1–N3–C9–C10	8.81	12.61
Ag1–N4–C10–C9	3.24	3.56	Hg1–N1–C2–C3	11.47	10.31
Ag1–N4–C14–C13	176.41	175.98			

Table S2. Second–order perturbation theory analysis of Fock matrix on NBO basis for complexes **2**-**5**.

Donor (*i*)	Acceptor (j)	$E^{(2)}$ (kcal/mol)	Donor (*i*)	Acceptor (j)	$E^{(2)}$ (kcal/mol)
Complex **2**					
ωB97XD/6–311G+(d,p)/LanL2DZ			CAM-B3LYP/6–311G+(d,p)/LanL2DZ		
LP(1)N6	LP*(6)Zn1	54.45	LP(1)N6	LP*(6) Zn1	47.29
LP(1)N5	LP*(6)Zn1	54.45	LP(1)N5	LP*(6) Zn1	47.30
LP(1)N4	LP*(9) Zn1	35.00	LP(1)N4	LP*(9) Zn1	33.96
LP(1)N3	LP*(6) Zn1	21.94	LP(1)N3	LP*(6) Zn1	22.62
LP(1)N1	LP*(6) Zn1	21.94	LP(1)N1	LP*(6) Zn1	22.62
LP(1)N2	LP*(9) Zn1	35.00	LP(1)N2	LP*(9) Zn1	33.96
LP(2)S2	π*(N6-C16)	78.15	LP(2)S2	π*(N6-C16)	66.68
LP(2)S1	π*(N5-C15)	78.15	LP(2)S1	π*(N5-C15)	66.68
π*(N4-C14)	π*(C10-C11)	152.62	π*(N4-C14)	π*(C10-C11)	126.60
π*(N4-C14)	π*(C13-C12)	150.28	π*(N4-C14)	π*(C13-C12)	148.42
π*(N2-C7)	π*(C3-C4)	152.62	π*(N2-C7)	π*(C3-C4)	126.61
π*(N2-C7)	π*(C6-C5)	150.28	π*(N2-C7)	π*(C6-C5)	148.42
Complex **3**					
ωB97XD/6–311G+(d,p)/LanL2DZ			CAM-B3LYP/6–311G+(d,p)/LanL2DZ		
LP(1)N6	LP*(6)Cu1	31.07	LP(1)N6	LP*(5) Cu1	11.29
LP(1)N5	LP*(6) Cu1	31.07	LP(1)N5	LP*(5) Cu1	11.29
LP(1)N4	LP*(9)Cu1	15.53	LP(1)N4	LP*(7) Cu1	14.68
LP(1)N3	LP*(8) Cu1	13.76	LP(1)N3	LP*(6) Cu1	20.05
LP(1)N1	LP*(8)Cu1	13.75	LP(1)N1	LP*(6) Cu1	20.05
LP(1)N2	LP*(9) Cu1	15.52	LP(1)N2	LP*(7) Cu1	14.64
LP(2)S2	π*(N6-C16)	37.38	LP(2)S2	π*(N6-C16)	33.12
LP(2)S1	π*(N5-C15)	37.38	LP(2)S1	π*(N5-C15)	33.12
π*(N4-C10)	π*(N3-C9)	34.84	π*(N4-C10)	π*(N3-C9)	39.18
π*(N4-C10)	π*(C14-C13)	56.09	π*(N4-C10)	π*(C14-C13)	58.22
π*(N4-C10)	π*(C11-C12)	88.50	π*(N4-C10)	π*(C11-C12)	92.02
π*(N2-C3)	π*(N1-C2)	34.84	π*(N2-C3)	π*(N1-C2)	39.21
π*(N2-C3)	π*(C7-C6)	56.10	π*(N2-C3)	π*(C7-C6)	58.25
π*(N2-C3)	π*(C4-C5)	88.51	π*(N2-C3)	π*(C4-C5)	92.07
Complex **4**					
ωB97XD/LanL2DZ			CAM-B3LYP/LanL2DZ		
LP(1)N6	LP*(6)Ag1	17.39	LP(1)N6	LP*(6)Ag1	18.30
LP(1)N5	LP*(8)Ag1	9.87	LP(1)N5	LP*(8)Ag1	9.76
LP(1)N4	LP*(6) Ag1	5.60	LP(1)N4	LP*(6) Ag1	5.13
LP(1)N3	LP*(6) Ag1	8.96	LP(1)N3	LP*(6) Ag1	9.48
LP(2)S2	π*(N6-C16)	26.98	LP(2)S2	π*(N6-C16)	24.95
LP(2)S1	π*(N5-C15)	28.47	LP(2)S1	π*(N5-C15)	25.96
π*(N4-C10)	π*(N3-C9)	26.32	π*(N4-C10)	π*(N3-C9)	29.94
π*(N4-C10)	π*(C14-C13)	45.78	π*(N4-C10)	π*(C14-C13)	47.44
π*(N4-C10)	π*(C11-C12)	61.04	π*(N4-C10)	π*(C11-C12)	62.23
Complex **5**					
LP(1)Cl1	LP*(6)Hg1	9.87	LP(1)Cl1	LP*(6)Hg1	9.81
LP(1)N5	LP*(6) Hg1	28.70	LP(1)N5	LP*(6) Hg1	29.73
LP(1)N4	LP*(6)Hg1	14.75	LP(1)N4	LP*(6)Hg1	14.07
LP(1)N3	LP*(6)Hg1	16.54	LP(1)N3	LP*(6)Hg1	15.37
LP(1)N1	LP*(6)Hg1	12.17	LP(1)N1	LP*(8)Hg1	12.29
LP(1)N2	LP*(7)Hg1	16.66	LP(1)N2	LP*(7)Hg1	15.89
LP(2)S1	π*(N5-C15)	72.62	LP(2)S1	π*(N5-C15)	65.16
LP(4)Cl1	LP*(6)Hg1	56.20	LP(4)Cl1	LP*(6)Hg1	51.46
π(C10-C11)	π*(N4-C14)	30.01	π(C10-C11)	π*(N4-C14)	25.91
π(C10-C11)	π*(N3-C9)	18.46	π(C10-C11)	π*(N3-C9)	17.60
π(C3-C4)	π*(N1-C2)	18.46	π(C3-C4)	π*(N1-C2)	17.53
π(C3-C4)	π*(N2-C7)	30.18	π(C3-C4)	π*(N2-C7)	25.79

[2] Hyperconjugative interaction energy (stabilization energy).

Table S3. Experimental and theoretical characteristic vibration frequencies of synthesized complexes **1-5**.

FT-IR (cm^{-1})	ωB97XD	CAM-B3LYP	FT-IR (cm^{-1})	ωB97XD	CAM-B3LYP	FT-IR (cm^{-1})	ωB97XD	CAM-B3LYP	Vibrational mode assignments
	LanL2DZ			6-311+G(d,p)//LanL2DZ			6-311+G(d,p)//LanL2DZ		
	Complex **1**			Complex **2**		Complex **3**			
3086	3139	3127	3078	3082	3089	3064	3086	3085	$\nu_{CH\ (ring)}$
3015	3122	3112	3056	3074	3073	3021	3061	3064	$\nu_{CH\ (ring)}$
2961	3020	3027	2962	2980	2989	2963	2993	2999	$\nu_{as\ (methyl)}$
2918	2994	2995	2922	2953	2973	2916	2975	2978	$\nu_{CH\ (imine)}$
2854	2925	2933	2852	2900	2914	2849	2912	2922	$\nu_{s\ (methyl)}$
2070	2058	2066	2108	2085	2079	2134	2089	2110	$\nu_{N=C\ (isothiocyanate)}$
2057	2050	2058	2067	2073	2068	2076	2072	2094	$\nu_{N=C\ (isothiocyanate)}$
1661	1687	1688	1658	1708	1707	1650	1697	1699	$\nu_{N=C\ (imine)}$
	1686	1688		1707	1707		1695	1697	$\nu_{N=C\ (imine)}$
1588	1604	1605	1598	1610	1612	1600	1603	1603	$\nu_{C=C\ (ring)}$
1566	1603	1587	1571	1587	1589	1568	1589	1590	$\nu_{C=C\ (ring)}$
1477	1482	1474	1480	1469	1473	1479	1469	1472	$\beta_{HCC\ (methyl)}$
1457	1475	1468	1457	1441	1446	1445	1451	1448	$\beta_{HCC(ring)}$
1438	1461	1450	1440	1427	1433	1429	1428	1431	$\beta_{HCH\ (methyl)}$
1401	1432	1430	1408	1422	1425	1409	1424	1425	$\beta_{HCC\ (ring)}$
1339	1307	1303	1343	1348	1351	1346	1354	1356	$\nu_{C=C\ (ring)+}\ \nu_{N=C\ (ring)}$
1304	1279	1275	1304	1285	1291	1308	1293	1297	$\nu_{N=C\ (ring)+}\ \beta_{HCC(ring)}$
1265	1233	1234	1269	1264	1256	1284	1268	1258	$\nu_{C=C\ (ring)+}\ \beta_{HCC\ (ring)}$
1222	1171	1163	1225	1208	1212	1225	1205	1208	$\beta_{HCC\ (ring)}$
1095	1120	1119	1102	1102	1101	1107	1102	1105	$\tau_{HCCC\ (ring)+}\ \tau_{CCCC\ (ring)}$
1052	1046	1044	1052	1041	1042	1054	1039	1041	$\nu_{C=C\ (ring)}$
1013	1001	1000	1016	1014	1017	1022	1021	1012	$\tau_{HCCC\ (ring)+}\ \tau_{CCCC\ (ring)}$
951	954	964	958	938	941	958	941	950	$\tau_{HCCN\ (imine)}$
876	861	862	880	888	869	880	869	873	$\nu_{N=C\ (ring)}$
783	792	795	774	764	768	784	803	809	$\nu_{C=S\ (isothiocyanate)}$
774	747	764	769	741	744	775	764	769	$\nu_{C=S\ (isothiocyanate)}$
667	663	663	670	659	663	667	662	664	$\beta_{NCC\ (ring)}$
634	636	632	639	631	633	650	621	623	$\beta_{CNC\ (ring)+}\ \beta_{CCC\ (ring)}$
508	516	519	508	508	506	508	503	508	$\tau_{CCCC\ (ring)}$
409	423	425	411	414	418	414	406	409	$\tau_{CCCC\ (ring)}$

Table S3. Continued

FT-IR (cm^{-1})	ωB97XD 6-311+G(d,p)//LanL2DZ	CAM-B3LYP 6-311+G(d,p)//LanL2DZ	FT-IR (cm^{-1})	ωB97XD 6-311+G(d,p)//LanL2DZ	CAM-B3LYP 6-311+G(d,p)//LanL2DZ	Vibrational mode assignments
Complex **4**				Complex **5**		
3006	3130	3129	3052	3116	3110	$\nu_{CH\ (ring)}$
2973	3117	3110	3009	3108	3105	$\nu_{CH\ (ring)}$
2916	3032	3030	2959	3047	3046	$\nu_{as\ (methyl)}$
2854	2988	2993	2919	2982	2985	$\nu_{CH\ (imine)}$
2801	2924	2930	2849	2920	2928	$\nu_{s\ (methyl)}$
2045	2053	2069				$\nu_{N=C\ (isothiocyanate)}$
2004	2023	2036	2105	2048	2063	$\nu_{N=C\ (isothiocyanate)}$
1764	1687	1690	1722	1694	1695	$\nu_{N=C\ (imine)}$
			1626	1687	1690	$\nu_{N=C\ (imine)}$
1604	1602	1603	1586	1603	1603	$\nu_{C=C\ (ring)}$
1584	1585	1586	1566	1602	1602	$\nu_{C=C\ (ring)}$
1563	1480	1473	1536	1482	1473	$\beta_{HCC\ (methyl)}$
1469	1470	1469	1463	1476	1471	$\beta_{HCC(ring)}$
1460	1452	1443	1430	1459	1447	$\beta_{HCH\ (methyl)}$
1434	1430	1428	1420	1430	1428	$\beta_{HCC\ (ring)}$
1373	1418	1417	1367	1280	1274	$\nu_{C=C\ (ring)}+\ \nu_{N=C\ (ring)}$
1340	1304	1301	1310	1313	1311	$\nu_{N=C\ (ring)}+\ \beta_{HCC(ring)}$
1290	1277	1272	1290	1280	1273	$\nu_{C=C\ (ring)}+\ \beta_{HCC\ (ring)}$
1254	1231	1231	1247	1233	1233	$\beta_{HCC\ (ring)}$
1091	1101	1097	1090	1102	1098	$\tau_{HCCC\ (ring)}+\ \tau_{CCCC\ (ring)}$
1046	1041	1041	1048	1043	1043	$\nu_{C=C\ (ring)}$
1016	1025	1034	998	1008	1017	$\tau_{HCCC\ (ring)}+\ \tau_{CCCC\ (ring)}$
998	1005	1003	983	1000	999	$\tau_{HCCN\ (imine)}$
823	860	860	858	858	860	$\nu_{N=C\ (ring)}$
784	788	792				$\nu_{C=S\ (isothiocyanate)}$
746	756	761	739	730	734	$\nu_{C=S\ (isothiocyanate)}$
698	691	690	693	663	663	$\beta_{NCC\ (ring)}$
623	627	627	613	643	630	$\beta_{CNC\ (ring)}+\ \beta_{CCC\ (ring)}$
507	515	518	506	518	522	$\tau_{CCCC\ (ring)}$
404	418	422	412	420	424	$\tau_{CCCC\ (ring)}$

υ: Stretching; β: In-plane bending; γ: Out-of plane bending; τ: Torsion.

Table S4. Experimental and theoretical wavelength, oscillator strength and remarkable contributions for complexes **1-5**.

Experimental λ (nm) (Methanol)	Methanol			
	λ (nm)	Osc. Strength	Molecular orbital contributions H: HOMO, L: LUMO	
Complex **1**				
	TD-ωB97XD/ LanL2DZ			
279.2	272.1	0.0016	H−7→L α (43%)	H−6→L+1 α (39%)
	239.0	0.0076	H→L α (66%)	H−2→L α (23%)
232.9	233.2	0.0171	H−2→L α (31%)	H−1→L+1 α (29%)
	TD-CAM-B3LYP/LanL2DZ			
279.2	274.0	0.0024	H−6→L α (43%)	H−7→L+1 α (28%)
	261.0	0.0062	H→L α (51%)	H−2→L α (30%)
232.9	235.73	0.0119	H−10→L+1 α (25%)	H−6→L+1 α (23%)
Complex **2**				
	TD-ωB97XD/6-311+G(d,p)//LanL2DZ			
277.6	269.2	0.0046	H-6→L α (48%)	H-7→L+1 α (21%)
	245.3	0.0372	H→L α (46%)	H-2→L α (10%)
236.2	236.4	0.0012	H-1→L α (32%)	H-6→L+1 α (17%)
207.1	207.8	0.0010	H-2→L+14 α (15%)	H-1→L+18 α (10%)
	TD-CAM-B3LYP/6-311+G(d,p)//LanL2DZ			
277.6	269.9	0.0058	H→L α (%41)	H-6→L α (%28)
	258.9	0.0873	H→L α (%41)	H-6→L α (%23)
236.2	231.6	0.0065	H-6→L+1 α (%34)	H-7→L α (%26)
207.1	207.1	0.0006	H-2→L+3 α (%37)	H→L+3 α (%14)
Complex **3**				
	TD-ωB97XD/6-311+G(d,p)//LanL2DZ			
387.8	383.2	0.0001	H-6→L+1 β (19%)	H-7→L α (19%)
	330.5	0.0030	H→L β (91%)	H-18→L β (4%)
284.9	276.9	0.0041	H-4→L+1 α (28%)	H-6→L α (11%)
	257.1	0.3019	H→L+1 β (19%)	H→L α (11%)
229.8	231.9	0.0053	H-3→L+1 α (55%)	H-3→L+2 β (18%)
	TD-CAM-B3LYP/6-311+G(d,p)//LanL2DZ			
387.8	398.0	0.0001	H-6→L+1 β (19%)	H-4→L+1 α (18%)
	341.7	0.0055	H→L β (93%)	H-18→L β (3%)
284.9	287.0	0.0002	H-7→L α (40%)	H-4→L+2 β (16%)
	254.9	0.5053	H-6→L β (20%)	H-4→L α (19%)
229.8	233.7	0.0011	H-4→L+4 β (36%)	H-9→L+3 α (13%)
Complex **4**				
	TD-ωB97XD/LanL2DZ			
	544.7	0.3239	H→L β (96%)	
261.2	262.2	0.0255	H-5→L α (20%)	H-4→L+1 β (18%)
228.8	227.5	0.0116	H-6→L+1 β (20%)	H→L+3 α (10%)
	TD-CAM-B3LYP/LanL2DZ			
	530.6	0.3212	H-2→L β (94%)	
261.2	262.1	0.0227	H-13→L β (30%)	H-4→L+1 β (8%)
228.8	229.0	0.0017	H-1→L+10 β (14%)	H-2→L+9 β (9%)
Complex **5**				
	TD-ωB97XD/LanL2DZ			
321.5	285.3	0.0009	H-7→L+1 α (21%)	H-8→L α (16%)
	251.7	0.0062	H→L α (47%)	H→L+1 α (27%)
228.8	228.3	0.0101	H-3→L+1 α (73%)	H-3→L α (10%)
	TD-CAM-B3LYP/LanL2DZ			
321.5	285.3	0.0009	H-7→L+1 α (21%)	H-8→L α (16%)
	251.7	0.0062	H→L α (47%)	H→L+1 α (27%)
228.8	228.3	0.0101	H-3→L+1 α (73%)	H-3→L α (10%)

Table S5. Theoretical global chemical reactivity descriptors for complexes **1-5**.

Parameter (unit)	Complex **1**		Complex **2**		Complex **3**				Complex **4**				Complex **5**	
	ωB97XD	CAM-B3LYP	ωB97XD	CAM-B3LYP	ωB97XD		CAM-B3LYP		ωB97XD		CAM-B3LYP		ωB97XD	CAM-B3LYP
	α spin	α spin	α spin	α spin	α spin	β spin	α spin	β spin	α spin	β spin	α spin	β spin	α spin	α spin
E_{HOMO} (eV)	-7.300	-6.595	-7.612	-7.042	-7.542	-7.517	-6.922	-6.904	-7.624	-7.833	-7.098	-7.259	-7.160	-6.485
E_{LUMO} (eV)	-1.017	-1.619	-0.957	-1.443	-1.035	-1.032	-1.665	-1.660	-1.006	-1.996	-1.620	-2.458	-0.776	-1.356
ΔE (eV)	6.283	4.976	6.655	5.599	6.507	6.485	5.257	5.244	6.618	5.837	5.478	4.801	3.192	5.129
Electronegativity (χ, eV)	4.159	4.107	4.285	4.242	4.289	4.275	4.293	4.282	4.315	4.914	4.359	4.859	3.968	3.902
Chemical hardness (η, eV)	3.142	2.488	3.328	2.799	3.253	3.243	2.629	2.622	3.309	2.918	2.739	2.400	1.596	2.565
Chemical softness (S, 1/eV)	0.318	0.402	0.300	0.357	0.307	0.308	0.380	0.381	0.302	0.342	0.365	0.417	0.627	0.390
Electrophilic index (ω, eV)	2.753	3.390	2.759	3.214	2.827	2.818	3.505	3.496	2.813	4.138	3.469	4.918	4.933	2.968
Nucleophilic index (φ, 1/eV)	0.363	0.295	0.362	0.311	0.354	0.355	0.285	0.286	0.355	0.242	0.288	0.203	0.203	0.337

References

[1] G.M. Sheldrick, SHELXT – integrated space-group and crystal-structure determination, Acta Cryst A71 (2015) 3–8.
[2] C.F. Macrae, P.R. Edgington, P.McCabe, E. Pidcock, G.P. Shields, R. Taylor,M. Towler, J. van de Streek, Mercury Visualization and Analysis of Crystal Structures, J. Appl. Crystallogr. 39 (2006) 453–457.
[3] A.L. Spek, Structure validation in chemical crystallography, Acta Cryst. D65 (2009) 148–155.
[4] D. Avcı, S. Altürk, F. Sönmez, Ö. Tamer, A. Başoğlu, Y. Atalay, B.Z. Kurt, N. Dege, Three novel Cu(II), Cd(II) and Cr(III) complexes of 6-Methylpyridine-2-carboxylic acid with thiocyanate: Synthesis, crystal structures, DFT calculations, molecular docking and α-Glucosidase inhibition studies, Tetrahedron 74 (2018) 7198–7208.
[5] D. Avcı, S. Altürk, F. Sönmez, Ö. Tamer, A. Başoğlu, Y. Atalay, B.Z. Kurt, N. Dege, A novel series of M(II) complexes of 6-methylpyridine-2-carboxylic acid with 4(5) methylimidazole: Synthesis, crystal structures, α-glucosidase activity, density functional theory calculations and molecular docking. Appl. Organometal. Chem. 33 (2019) e4935.
[6] D. Avcı, S. Altürk, F. Sönmez, Ö. Tamer, A. Başoğlu, Y. Atalay, B. Zengin Kurt, N. Dege, A novel series of mixed-ligand M(II) complexes containing 2,2′-bipyridyl as potent α-glucosidase inhibitor: synthesis, crystal structure, DFT calculations, and molecular docking, JBIC J. Biolog. Inorg. Chem. 24 (2019) 747–764.
[7] D. Avcı, S. Altürk, F. Sönmez, Ö. Tamer, A. Başoğlu, Y. Atalay, B. Zengin Kurt, N. Dege, Novel Cu(II), Co(II) and Zn(II) metal complexes with mixed-ligand: Synthesis, crystal structure, α-glucosidase inhibition, DFT calculations, and molecular docking, J. Mol. Struct. 1197 (2019) 645–655.
[8] G.M. Morris, R. Huey, W. Lindstrom, M.F. Sanner, R.K. Belew, D.S. Goodsell, and A.J. Olson, Autodock4 and AutoDockTools4: automated docking with selective receptor flexibility, J. Comput. Chem. 30 (2009) 2785-2791.
[9] Michel F. Sanner, Python: A Programming Language for Software Integration and Development. J. Mol. Graphics Mod. 17 (1999) 57-61.
[10] G.M. Morris, D.S. Goodsell, R.S. Halliday, R. Huey, W.E. Hart, R.K. Belew, A.J. Olson, Automated Docking Using a Lamarckian Genetic Algorithm and and Empirical Binding Free Energy Function, J. Comput. Chem. 19(14) (1998) 1639-1662.
[11] D. Systèmes, Dassault Systèmes Biovia: San Diego, CA, USA 2016.

EK C. Avcı, D., Özge, Ö., Sönmez, F., Başoğlu, A., Tamer, Ö., & Atalay, Y. (2024). Novel schiff base-azide metal complexes: Synthesis, spectral, nonlinear optics, and DFT studies. Materials Science in Semiconductor Processing, 179, 108523. https://doi.org/10.1016/j.mssp.2024.108523

Materials Science in Semiconductor Processing 179 (2024) 108523

Contents lists available at ScienceDirect

Materials Science in Semiconductor Processing

journal homepage: www.elsevier.com/locate/mssp

Novel schiff base-azide metal complexes: Synthesis, spectral, nonlinear optics, and DFT studies

Davut Avcı [a,*], Özgen Özge [a,b], Fatih Sönmez [c], Adil Başoğlu [a], Ömer Tamer [a], Yusuf Atalay [a]

[a] Sakarya University, Faculty of Science, Department of Physics, 54187, Sakarya, Turkey
[b] Cappadocia University, Health Vocational School, Ürgüp, 50400, Nevşehir, Turkey
[c] Sakarya University of Applied Sciences, Pamukova Vocational High School, 54055, Sakarya, Turkey

ARTICLE INFO

Keywords:
Schiff base
Azide
Mn/Ni/Co ions
Spectral elucidation
NLO
TD/DFT levels

ABSTRACT

In order to enhance nonlinear optics (NLO)-based technologies, current research focuses on the design and synthesis of coordination materials. In this context, to investigate spectral and theoretical linear optical (LO)/nonlinear optical (NLO) behaviors, novel metal complexes including azide {[$Mn(L_1)_2(N_3)_2$], (**9**), [$Ni(L_1)_2(N_3)$], (**10**), [$Co_2(L_1)_2(N_3)_2]\cdot 2H_2O$, (**11**); L_1: *N*-(pyridin-2-ylmethylene)methanamine} were synthesized. The vibrational and electronic spectral features of complexes **9–11** were investigated by UV–Vis and FT–IR spectra. Depending on the central metal ion and coordination geometries of complexes, the microscopic static nonlinear behaviors were examined by using the CAM-B3LYP/and ωB97XD/6–311 + G (d,p)//LanL2DZ levels of density functional theory (DFT). Furthermore, the vibrational and electronic properties of complexes **9–11** based on the same levels of time-dependent/density functional theory (TD-DFT/DFT) were surveyed. Additionally, the theoretical $\chi^{(1)}$, $\chi^{(2)}$, and $\chi^{(3)}$ parameters, known as linear optical, second-, and third-order nonlinear optical susceptibility tensors, as well as linear, second-, and third-order polarization parameters ($P^{(1)}$, $P^{(2)}$, and $P^{(3)}$) for complexes **9–11** were examined. The greatest $<\beta(0; 0,0)>$ value for complex **10** found to be 262.55×10^{-30} esu using CAM-B3LYP level is 820.5 and 2019.6 times higher than the urea findings (0.32×10^{-30} esu and 0.130×10^{-30} esu). The $<\gamma(0; 0,0,0)>$ results indicate that complex **9** having the highest value obtained at 2216.40×10^{-36} esu using CAM-B3LYP level is 47.76 and 316.63 times greater than those of pNA (15×10^{-36} esu) and urea (7×10^{-36} esu), respectively. Complexes **10** and **9** demonstrated promising microscopic second-order and third-order NLO features, respectively. Our research is anticipated to provide insight into NLO materials that may have applications in optoelectronics and telecommunication field.

1. Introduction

There are numerous studies on complex structures where an ion or cluster of molecules is coordinated to a metal ion by Schiff base because metal complexes play essential roles in many sectors, including medicines [1–3], industrial chemistry [4,5], and optoelectronic technology [6–8]. It was reported that the chelation of Schiff bases with metal ions significantly affected nonlinear optical and biological properties such as anti-bacterial, anti-fungal, and anti-diabetic [9–16]. In terms of these properties, Schiff bases containing –C=N imine groups and Schiff base-based metal complexes, in which different ligands containing lone pair electrons of N, O, and S atoms, have been synthesized [17–22]. The imine groups that combine with metal ions to create chelates have a significant affinity for transition metal ions, which is another reason why Schiff bases are regarded as superior ligands. Due to the possibility of conjugation between two aromatic rings made possible by the presence of this imine group, resonance stabilization on the whole molecule is expected to rise. It would be expected that high electron conjugation enhances the structure-property interactions of the synthesized molecules and makes the generated radical more stable.

In coordination chemistry, a number of studies are carried out on metal complexes containing the azido ($-N_3$) ligand [13,19–21,23]. In these metal complexes, their structural, spectral, magnetic, and optical properties have been taken into consideration due to their different reactivity and potential applications in various field [24–26]. The azide ion has a high degree of coordination flexibility, which can also participate in the formation of monodentate, bidentate or multidentate complexes that can bind to metal centers via nitrogen atoms. In this way,

* Corresponding author.
E-mail address: davci@sakarya.edu.tr (D. Avcı).

https://doi.org/10.1016/j.mssp.2024.108523
Received 15 March 2024; Received in revised form 1 May 2024; Accepted 8 May 2024
Available online 12 May 2024

azide ions contribute to the formation of coordination compounds with trigonal, bent, or bridge coordination [13,19–23,29,30]. In this context, the synthesis of new coordination compounds containing azido ligands is not only remarkable in terms of structure and properties due to their possible applications in fields such as optoelectronics and telecommunications, but also contributes to pioneering new studies.

It is known that nonlinear optics, which started with the discovery of the laser and found its place in different applications today, is still one of the active fields of study. NLO materials have a nonlinear response to an electric field, causing different optical phenomena such as the creation of light at new frequencies or changing the optical properties of the material [28]. However, in order for new materials to contribute to this field, the synthesis of nonlinear optical (NLO) motifs containing organic, inorganic, or transition metal complexes has become interesting due to their possible applications in technology. Thanks to the structural properties of organic ligands and the different electronic properties of the metal ions, metal-organic coordination compounds showing NLO properties have been widely studied [6,7,14,28–35]. According to the findings of these investigations, the asymmetric charge distribution in ground and excited states, as well as the placement of electron donating and withdrawing groups at the extreme points of the conjugated system, significantly increased both linear and nonlinear optical characteristics. Organic compounds that induce molecular charge transfer and in which delocalized π electrons can move freely between electron-donating and withdrawing groups located on opposite sides of the molecule can be used to create coordination compounds without centers of symmetry. In this way, delocalized orbitals of electrons within molecular units can be distributed over the whole molecule, creating faster and greater polarizability. Coordination of transition metal ions with organic molecules provides greater electronic transition and metal-to-ligand or ligand-to-metal charge transfer with the addition of more energy sublevels; leading to intramolecular electron delocalization and hence larger NLO properties. In recent years, especially in telecommunication and optoelectronic technology, the examination of NLO features has attracted attention in various application areas such as frequency switching, optical modulation, optical focusing, optical communication, and optical switching. Due to these applications, great importance is given to metal complexes such as nickel, copper, and zinc, additionally these metal complexes can create exciting properties in semiconductor applications [8]. When the results obtained in the literature and previous studies are examined, it is seen that complexes containing Mn, Co, Ni, Cu, Zn, Cd, Hg and Pb metal ions are used effectively in the investigations of non-linear parameters [6–8,11,17,18,36]. Therefore, within the scope of this study, it has been observed that the inductive electron support of the alkyl group such as methyl of the Schiff base ligand and the electron support of the nitrogen atom of the azide ligand contribute to both the formation of complex structures with different coordination geometries with selected metal ions and nonlinear optical activity. In addition, it is predicted that it efforts the nonlinear optical properties in complex structures containing metal ions, heterocyclic structures and azomethine groups, depending on the coordination environment. When experimental studies are not possible, DFT methods are used extensively to systematically explore the second-/third-order nonlinear optical (NLO) features [36–44]. Considering these studies, it is inevitable that the synthesis of new more effective NLO compounds will continue to be an important research topic today.

The uses of various DFT models are significant in terms of investigating different properties of materials such as structural, vibrational, electronic, and non-linear optical properties, and providing harmony with experimental results. A selected DFT method may not provide the best fit and results in examining every structure-property relationship [6,7,14,16,36]. Taking into consideration, the developed exchange-correlation functionals, selection of appropriate functionals for coordination compounds, and inclusion of solvent effects show that the compatibility of DFT with experimental results will further increase in examining these compounds in terms of structure-property relationships [36,44–47]. CAM-B3LYP (Handy and coworkers' long range corrected version of B3LYP using the Coulomb-attenuating method) [48] and ωB97XD (the last functional containing empirical dispersion and long-range corrections suggested by Head-Gordon and co-workers) [49,50] functionals can reliably predict the structural and spectroscopic properties of coordination compounds as well as charge transfer interactions and their use in examining more molecular properties are among the reasons for choosing these methods.

To develop and produce useful NLO material, new metal complexes (**9–11**) including *N*-(pyridin-2-ylmethylene)methanamine (L_1) and azido (-N_3) ligands were synthesized as the outcome of our continuous research. The characterizations of these complex structures (**9–11**) were fulfilled by the mass (LC-HRMS), powder XRD and FTIR spectra. Structure-activity relationships were determined by examining the theoretical microscopic NLO and electronic properties of the synthesized complexes using experimental and DFT methods. Additionally, the structure-property relationships of the coordination compounds were comprehensively investigated using the DFT/ωB97XD and DFT/CAM-B3LYP functionalities.

2. Experimental and computational details

2.1. Spectroscopic measurement tools

The Varian Infinity Plus NMR spectrometer was utilized to define the structure of the synthesized the *N*-(pyridin-2-ylmethylene)methanamine (L_1) ligand. The structures of new metal complexes (**9–11**) were determined by using the SHIMADZU LCMS-9030 model triple quadrupole liquid chromatograph mass spectrometer. The FT–IR spectra in the 4000–400 cm^{-1} range for complexes **9–11** were recorded at the PerkinElmer UATR–TWO (PerkinElmer Spectrum–two equipped with ATR) spectrophotometer. Electronic absorption wavelengths (UV–Vis spectra) in the range of 900–200 nm were obtained with the SHIMADZU UV–2600 UV–Vis spectrophotometer. The photoluminescence (PL) spectra were recorded with the HITACHI F-2710 in the wavelength region 220–800 nm. The elemental analyses of the synthesized complexes **9–11** were performed by using the CHNS-932 (Leco) elemental analyzer. The particle sizes of the synthesized complexes **9–11** were obtained by using a Rigaku D/max 2200 PC X-ray diffractometer with Cu Kα ($\lambda = 1.54059$ Å) radiation in the operating voltage of 40 kV and current of 30 mA, and the scanning 2°/min.

2.2. Materials and synthesis of the N-(pyridin-2-ylmethylene) methanamine (L_1) and complexes 9–11 {[Mn (L_1)$_2$(N_3)$_2$], (9), [Ni (L_1)$_2$(N_3)], (10), [Co_2(L_1)$_2$(N_3)$_2$]·2H_2O, (11)}

2-Pyridinecarboxaldehyde, methylamine solution purum (33 % in absolute ethanol), sodium azide, manganese (II) acetate tetrahydrate ($Mn(OAc)_2{\cdot}4H_2O$), nickel (II) acetate tetrahydrate ($Ni(OAc)_2{\cdot}4H_2O$), cobalt (II) acetate tetrahydrate ($Co(OAc)_2{\cdot}4H_2O$) reagents purchased from Sigma-Aldrich were utilized without any special reprocessing. Scheme 1 depicts the synthesis methods of complexes **9–11**. In Supplementary data, the synthesis and NMR spectra of the *N*-(pyridin-2-ylmethylene)methanamine is provided (Fig. S1).

Synthesis of complexes **9–11**: 1 mmol of corresponding metal salts ($Mn(OAc)_2{\cdot}4H_2O$)/($Ni(OAc)_2{\cdot}4H_2O$)/($Co(OAc)_2{\cdot}4H_2O$) were added to *N*-(pyridin-2-ylmethylene)methanamine (L_1) (2 mmol) dissolved in 15 mL of ethanol. Twenty minutes later, 2 mmol NaN_3 dissolved in 5 mL water was added to this solution. The mixture was stirred for 3 h at room temperature before being let to evaporate. It took around 7–10 days to acquire complex compounds in powder form. The structures of complexes **9–11** were confirmed by the mass spectroscopy (LC-HRMS). Complex **9**: Anal. Calc. For $C_{14}H_{16}MnN_{10}$: C, 44.33; H, 4.25; N, 36.93; found: C, 44.72; H, 4.54; N, 35.78. Calculated exact mass (*m/z*): 379.0940 ($C_{14}H_{16}MnN_{10}$); found: LC-HRMS (*m/z*): 383.0881 ($[M+3H]^+$). Complex **10**: Anal. Calc. For $C_{14}H_{16}N_7Ni$: C, 49.31; H, 4.73;

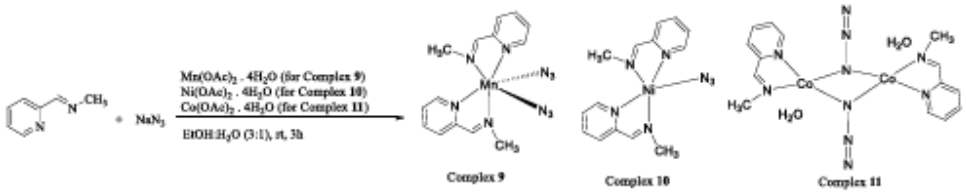

Scheme 1. Synthesis of complexes **9**–**11**.

N, 28.75; found: C, 49.86; H, 4.84; N, 28.25. Calculated exact mass (*m*/*z*): 340.0821 ($C_{14}H_{16}N_7Ni$); found: LC-HRMS (*m*/*z*): 343.0697 ($[M+2H]^+$). Complex **11**: Anal. Calc. For $C_{14}H_{20}Co_2N_{10}O_2$: C, 35.16; H, 4.22; N, 29.29; found: C, 35.65; H, 4.52; N, 28.68. Calculated exact mass (*m*/*z*): 478.0435 ($C_{14}H_{20}Co_2N_{10}O_2$); found: LC-HRMS (*m*/*z*): 478.1207 ($[M]^+$). The mass (LC-HRMS) spectra are presented in Supplementary data (see Figs. S2–S4).

2.3. Computational details

The Gaussian 16 Revision C.01 [51] and GaussView 6 [52] programs were applied to explore the characteristics of structural, spectral (vibrational and electronic), and nonlinear optics (NLO). For complexes **9**–**11**, the optimized complex structures, results of vibrational frequencies, and natural bond orbital (NBO) were obtained at the CAM-B3LYP [48] and ωB97XD methods [49,50] with 6-311 + G (d, p)//LanL2DZ [53,54] basis set in the ground state. To examine electronic absorption wavelengths (λ) and oscillator strengths of these complexes in MeOH, TD–DFT (time-dependent DFT) levels [55] with the CPCM (conductor-like polarizable continuum model) [56] were utilized. The remarkable contributions in electronic transitions were defined by using the SWizard [57] and Chemissian [58] programs. The microscopic static polarizabilities (α and Δα), first– and second–order hyperpolarizabilities (β and γ) parameters displaying the LO/NLO features were investigated using the same DFT levels. Furthermore, to investigate further electronic and optoelectronic parameters, the external electric field (*E*), the permittivity of the vacuum (ε_0), the relative permittivity of the medium (ε_r), the electric susceptibility (χ_e), the electric displacement (*D*), and polarization (*P*), the theoretical $\chi^{(1)}$, $\chi^{(2)}$, and $\chi^{(3)}$ parameters, known as linear optical, second-, and third-order nonlinear optical susceptibility tensors, as well as linear, second-, and third-order polarization parameters ($P^{(1)}$, $P^{(2)}$, and $P^{(3)}$) were obtained by using equations 11–21. Considering the frontier molecular orbital (FMO: the highest occupied molecular orbital (HOMO) and lowest unoccupied molecular orbital (LUMO)) energies, the molecular parameters describing chemical reactivity (χ (electronegativity), η (chemical hardness), *S* (chemical softness), ω (electrophilicity), φ (nucleophilicity)) were examined by the same DFT levels. Lastly, the investigations of MEP (molecular electrostatic potential) surfaces for complexes **9**–**11** were performed by using the DFT/CAM-B3LYP level.

Equation (1) was utilized in the NBO computations to obtain the stability energy ($E^{(2)}$) values.

$$E^{(2)} = \Delta E_{ij} = q_i \frac{F(i,j)^2}{\varepsilon_i - \varepsilon_j} \tag{1}$$

Where q_i is the donor orbital occupancy for each donor (i) and acceptor (j), $F(i,j)^2$ is the off-diagonal NBO Fock matrix elements, ε_i and ε_j are diagonal elements [42,59].

The chemical hardness (η), electronegativity (χ), chemical softness (*S*), electrophilicity (ω), and nucleophilicity (φ) index calculated from the HOMO and LUMO energies exhibit the molecular characteristics. These parameters were computed using equations (2)–(6) [6,60].

$$\eta = \frac{(E_{LUMO} - E_{HOMO})}{2} \tag{2}$$

$$\chi = -\frac{(E_{HOMO} + E_{LUMO})}{2} \tag{3}$$

$$S = \frac{1}{\eta} \tag{4}$$

$$\omega = \frac{\chi^2}{2\eta} \tag{5}$$

$$\varphi = \frac{1}{\omega} \tag{6}$$

For complexes **9**–**11** in gas phase, the theoretical microscopic electric dipole moment (μ), linear optical parameters ($\overline{\alpha}$ and Δα), which are characterized as the mean and anisotropy of polarizability, and second– and third–order nonlinear optical parameters (β and γ), which are characterized as first– and second–order hyperpolarizability, were calculated using equations (7)–(10) [30,32].

$$\overline{\alpha} = \frac{(a_{xx} + a_{yy} + a_{zz})}{3} \tag{7}$$

$$\Delta\alpha = \left\{\frac{1}{2}\left[(a_{xx} - a_{yy})^2 + (a_{yy} - a_{zz})^2 + (a_{zz} - a_{xx})^2\right]\right\}^{1/2} \tag{8}$$

Where equations (7) and (8), the a_{xx}, a_{yy}, a_{zz} are the Cartesian components of the $\overline{\alpha}$ and Δα For $\overline{\alpha}$, 1 atomic unit (a.u.) was multiplied by 0.1482×10^{-24} to obtain the electrostatic unit (esu).

The theoretical first– and second–order hyperpolarizability (β and γ) parameters were calculated by using equations (9) and (10) [30,32].

$$\beta = \left(\beta_x^2 + \beta_y^2 + \beta_z^2\right)^{1/2} \tag{9}$$

$$< \gamma > = \frac{1}{5}\left[\gamma_{xxxx} + \gamma_{yyyy} + \gamma_{zzzz} + 2\left(\gamma_{xxyy} + \gamma_{xxzz} + \gamma_{yyzz}\right)\right] \tag{10}$$

Where equation (9), $\beta_x = \beta_{xxx} + \beta_{xyy} + \beta_{xzz}$, $\beta_y = \beta_{yyy} + \beta_{yxx} + \beta_{yzz}$, $\beta_z = \beta_{zzz} + \beta_{zyy} + \beta_{zxx}$ are the Cartesian components of β. For β, 1 atomic unit (a.u.) was multiplied by 8.6393×10^{-33} to obtain the electrostatic unit (esu).

Furthermore, considering the E (the external electric field), ε_0 and ε_r (the permittivity of the vacuum and the relative permittivity of the medium), and χ_e (the electric susceptibility), the physical parameters electric displacement (D) and polarization (P) were calculated by the following eqs. (11) and (12).

$$D = \varepsilon_0 E + P = \varepsilon_0 \varepsilon_r E = \varepsilon_0 (1 + \chi_e) E \tag{11}$$

$$P = \varepsilon_0 \chi_e E = \varepsilon_0 (\varepsilon_r - 1) E \tag{12}$$

In eq. (12), χ_e (the electric susceptibility) is taken as $\varepsilon_r - 1$.

The refractive index (n) is computed by the following eq. (13).

$$n = \sqrt{(1 + \chi_e)} = \sqrt{\varepsilon_r} \tag{13}$$

On the other hand, the evaluations of NLO parameters in terms of optoelectronic and electronic features were performed by using eq. (14)–(21).

$$E = \mu/\overline{\alpha} \tag{14}$$

$$P = \mu/V \tag{15}$$

In eqs. (14) and (15), μ, $\overline{\alpha}$, and V are the electric dipole moment, average isotropic polarizability, and volume of the compound, respectively.

The theoretical $\chi^{(1)}$, $\chi^{(2)}$, and $\chi^{(3)}$ parameters, known as linear optical, second-, and third-order nonlinear optical susceptibility tensors, were obtained by using eqs. (16), (18) and (20) [61–64].

$$\chi^{(1)} = \overline{\alpha}/\varepsilon_0 V \tag{16}$$

$$P^{(1)} = \varepsilon_0 \chi^{(1)} E \tag{17}$$

$$\chi^{(2)} = \beta/2\varepsilon_0 V \tag{18}$$

$$P^{(2)} = \varepsilon_0 \chi^{(2)} E^2 \tag{19}$$

$$\chi^{(3)} = \gamma/6\varepsilon_0 V \tag{20}$$

$$P^{(3)} = \varepsilon_0 \chi^{(3)} E^3 \tag{21}$$

Using the following equation (22), the E_g (optical band gap energy) value is calculated using the Tauc and Menth equation [6].

$$(\alpha h\nu) = C(h\nu - E_g)^{1/2} \tag{22}$$

In eq. (22), the absorption coefficient α is found by equation of $\alpha = 2.303A/d$ by taking into account d and A depicting the width of the cuvette (1 cm) and absorbance in the UV–Vis region. Direct band gap energy is abbreviated E_g, while photon energy is abbreviated $h\nu$. C is a proportionality constant that has to do with the bands' dependent effective masses.

The refractive index (n) parameters for complexes **9**–**11** in methanol were calculated by equation (23) by considering the reflectance (R) [65,66],

$$n = \frac{1+\sqrt{R}}{1-\sqrt{R}} \tag{23}$$

In this work, the third-order nonlinear optical susceptibility ($\chi^{(3)}$) parameter was investigated in the UV–Vis range (200–600 nm), regardless of the Z-scan approach [67,68]. Equation (24) may be used to get the $\chi^{(3}$ parameter, which is related to the refractive index in the UV–Vis, by taking about 10^{-10} esu of the A parameter for all compounds irrespective of frequency [69–71].

$$\chi^{(3)} = \frac{A}{(4\pi)^4}(n^2-1)^4 \tag{24}$$

3. Results and discussion

3.1. The structural characterizations of the synthesized complexes

The structure of *N*-(pyridin-2-ylmethylene)methanamine (L_1) was determined by ^{1}H and ^{13}C NMR spectra. In ^{1}H NMR spectrum given in Fig. S1, the aromatic proton signals for L_1 emerged at the range of 7.44 and 7.93 ppm, aromatic CH neighbor pyridine-N and CH protons belonging to imine were observed at 8.61 and 8.33 ppm, respectively. The aromatic carbon signals for the L_1 ligand appeared at the range of 120.89 and 163.84 ppm in ^{13}C NMR spectra given in Fig. S1. The carbon signal belonging to imine in L_1 ligand was observed at 154.81 ppm (in Fig. S1). Besides, the structures of complexes **9**–**11** were confirmed by the mass spectra given in Figs. S2–S4. The optimized structures (obtained at DFT/CAM-B3LYP) of complexes **9**–**11** are presented in Fig. 1. The geometrical parameters belonging to the bond lengths and angles, and dihedral angles given in Table S1 were obtained by using DFT/ωB97XD and DFT/CAM-B3LYP levels.

Complex **9** [Mn $(L_1)_2(N_3)_2$] consists of the coordination of two L_1 and two azido ligands with the Mn ion, while complex **10** [Ni$(L_1)_2(N_3)$] is comprised of two L_1 ligands and one azido ligand with the Ni ion. Thus, complex **9** has a six-coordinated with distorted octahedral geometry whereas complex **10** has a five-coordinated with distorted trigonal bipyramidal geometry.

A versatile ligand, the azide anion may assemble binuclear complexes by binding to transition metal atoms in a variety of coordination ways [72]. Similarly, complex **11** [$(Co)_2$ $(L_1)_2(N_3)_2$]·$2H_2O$, forming a tetrahedral bridge with two Co(II) ions over the N atoms of two azido ligands, consists of the coordination of two L_1 and two azido ligands with Co(II) ion, and the uncoordinated two water molecules. So, complex **11** has a four-coordinated with distorted tetrahedral geometry.

The coordination geometries of synthesized complexes **9**–**11** are consistent with the complexes Co(II), Mn(II), and Cu(II) coordinated with different ligands and azido ligand [19–21,26,27].

Theoretical some geometrical parameters of complexes **9**–**11** are tabulated in Table S1. The coordination of N atoms of L_1 ligand with metal ions forms five-membered chelate rings defined by the M(metal)–N bond lengths. The Mn1/Ni1/Co1–N2/N4 bond distances of complexes **9**–**11** were calculated at 1.969/1.959, 2.151/2.062, and 1.925/1.873 Å by using DFT/CAM-B3LYP level, respectively. The same bond lengths reported in different complex structures were obtained at the average 2.2 Å for Mn complexes, and the average 1.9–2.2 Å range for Co complexes [19–21,26,27]. On the other hand, the Mn1/Ni1/Co1–N6/N7 bond distances defined by the M(metal)–N (azido ligand) bond lengths were found to be 1.942/2.031, 2.069, and 1.969/1.966 Å by the same DFT level, respectively. The distortion along the axial direction is displayed by the N–M–N bond angles belonging to the Mn/Ni/Co with N atoms of L_1 and N_3 ligands. The N–M–N bond angles for complexes **9**–**11** were computed at the range of 155.7 and 178.3° with DFT/CAM-B3LYP level. Additionally, the N2–M–N5/N3–M–N4 bond angles formed by N atoms of L_1 ligand with metal ions demonstrating five-membered chelate rings for complexes **9**–**11** were obtained at 80.48/77.68, 78.04/80.79, and 52.57/82.54° with DFT/CAM-B3LYP level, respectively. The N–M–N angles defining the imine/pyridine *N*-metal ion-azido N in the coordination environment observed at values greater or less than 90° indicate the distorted geometry of the complexes **9**–**11**. Besides, the Co1–N6–Co2/Co1–N6–Co2 bond angles for complex **11** show that the two N_3^- anions provide the bridge between the cobalt ions in coordination.

Considering the coordination environment/geometry differences, the theoretical geometric parameter results of the complexes are consistent with the previous ones [6,14,19–21,26,27].

Natural bond orbital (NBO) analysis is used to demonstrate intra-/inter-molecular bonds, charge transfer in molecular systems, or conjugative interactions [42,73,74]. The second-order perturbation method is used to compute the hyperconjugative interactions [59,75]. The large $E^{(2)}$ energy value obtained from NBO results shows that the interactions between electron acceptors and electron donors are more intense and intra- and inter-molecular charge transitions are high. Table S2 depicts the NBO calculation results of the synthesized complexes **9**–**11**. The interactions between LP(n) of nitrogen orbital pairs and LP*(n) of M(II) (Mn, Ni, Co) assigned as the $n \rightarrow n^*$ interactions display the coordination environment around the metal ions in complexes **9**–**11**. By using DFT/CAM-B3LYP level, $E^{(2)}$ values of these interactions were computed at the range from 9.85 to 63.21, from 16.73 to 44.75, and from 14.09 to 76.28, respectively (Table S2). The other remarkable interactions show stabilization within the L_1 ligand possessing the π-conjugation. The interactions between bonding and antibonding orbitals represent charge transfer (CT) interactions that cause the system to stabilize.

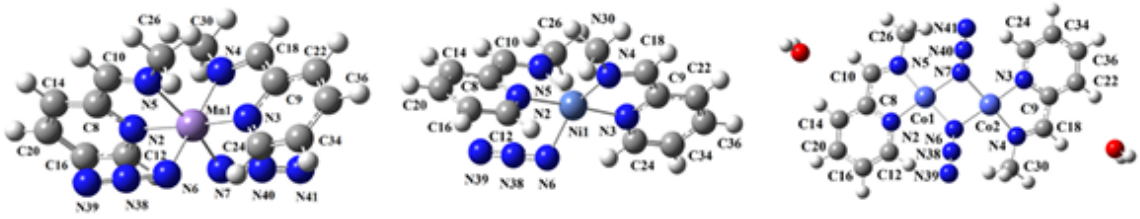

Fig. 1. Theoretical optimized structures of complexes **9**–**11** obtained at DFT/CAM-B3LYP level.

3.2. IR analysis of the synthesized complexes

The FTIR spectra demonstrate the wavenumbers in the range of 4000−400 cm^{-1} for the synthesized complexes **9**–**11** (see Fig. 2). In addition to the fact that the calculations were made in the gas phase, considering situations such as the lack of basis set and electron correlation effect, the theoretical vibrational frequencies obtained at DFT/ωB97XD/and DFT/CAM-B3LYP/6-311 + G (d,p)//LanL2DZ levels were multiplied by 0.96 to bring the results closer to the experimental results. Tables S1 and S3 present the assignments of experimental and corresponding theoretical characteristic vibrational wavenumbers. The IR spectra of the complexes and the free ligands were compared to identify the coordination sites that may be involved in chelation. The position and/or intensities of some guide peaks in the spectra of the ligands are expected to change after chelation. The $\nu_{CH(ring)}$, $\nu_{CH(imine)}$ and $\nu_{CH(methyl)}$ stretching modes were observed at 2967–3082 cm^{-1} range for free L_1 ligands, while the corresponding stretching modes appeared at the range from 2852 to 3098 cm^{-1} for complex **9**, from 2892 to 3056 cm^{-1} for complex **10**, from 2927 to 3123 cm^{-1} for complex **11**. It is stated that this band was shifted to higher or lower wavenumbers in the complexes, depending on the coordination with metal ions. These results are coherent with the previous ones for the Schiff base metal complexes [1,2,6,13,14,16]. The corresponding ones for complexes **9**–**11** obtained at DFT/ωB97XD were found at 2897–3082 cm^{-1} range, 2891–3060 cm^{-1} range, and 2921–3118 cm^{-1} range, respectively (see Tables S1 and S3). It has been observed that the azide NN bond stretching vibration, which occurs on average at 2100 cm^{-1}, generally shifts to lower wave numbers in the synthesized complexes. As can be seen in Fig. 2, the experimental IR spectra of three complexes exhibit the ν_{NN} asymmetric stretching characteristic band demonstrating the coordination with N_3 emerged at 2059 cm^{-1} for complex **9**, 2111 cm^{-1} for complex **10**, 2015 and 2002 cm^{-1} for complex **11**. The other characteristic band assigned as the $\nu_{NN\ (azide)}$ symmetric stretching mode appeared at 1305, 1338, and 1341 cm^{-1} is attributed to the coordination of the Mn/Ni/Co ions with the N atom of the azide. These asymmetric/symmetric bands show the existence of several azido groups and the azido bridges. These findings are compatible with the modes reported in several complexes [19–21,26,27]. The corresponding theoretical asymmetric/symmetric bands for complexes **9**–**11** were computed at 2079–2127/1341-1345, and 2087–2160/1338-1349 cm^{-1} ranges, using DFT/ωB97XD and DFT/CAM-B3LYP levels, respectively. Furthermore, $\upsilon_{C=N(imine)}$ stretching vibration in the free L_1 ligand was observed at 1592 cm^{-1}. It was observed that this band shifted to higher wavenumbers in complexes **9**–**11**. This shift indicates the involvement of the imine group of L_1 ligand in the coordination (M–N). The experimental $\nu_{C=N(imine)}$ stretching vibrational modes for complexes **9**–**11** were observed at 1656, 1653, and 1681 cm^{-1}, and corresponding theoretical modes were obtained at 1664, 1680, and 1607 cm^{-1} (with DFT/ωB97XD level), respectively (Tables S1 and S3). Likewise, the $\nu_{NC(imine\text{-}methyl)}$ stretching mode belonging to the N–CH_3 bond for free L_1 ligand was observed at 1017 cm^{-1}, this vibrational mode for complexes **9**–**11** emerged at 1017, 1024, and 1021 cm^{-1}, and the corresponding values computed at DFT/ωB97XD and DFT/CAM-B3LYP levels were found at the range of 1022, 1024, and 1020 cm^{-1}, 1019, 1021, and 1017 cm^{-1}, respectively. On the other hand, the $\nu_{CC(ring)}$ stretching mode belonging to free L_1 ligand emerged at 1567 cm^{-1}. This mode attributed to the ring C=C bond for complexes **9**–**11** appeared at the ranges 1596–1637 cm^{-1} in FTIR spectra and was calculated at 1530–1592 cm^{-1} by using DFT/ωB97XD level, and 1533–1591 cm^{-1} by using DFT/CAM-B3LYP level (see Tables S1 and S3). These findings agree with comparable group frequency values in various topologies in the earlier research [6,14,19–21,26,27]. For complexes **9**–**11**, the ν_{CC} and ν_{CN} stretching modes belonging to the ring of the L_1 ligand were observed at 1223, 1228, and 1233 cm^{-1}, while the corresponding theoretical modes were obtained at 1224, 1223, and 1250 cm^{-1} with DFT/ωB97XD level, and 1246, 1227, and 1246 cm^{-1} with DFT/CAM-B3LYP level, respectively (Table S3). These vibrational modes were assigned as 1281 cm^{-1} for free L_1 ligand, and it is seen that these modes were obtained at the lower wave numbers depending on the coordination in complexes **9**–**11**. Moreover, the $\beta_{HCC\ (ring)}$ in-plane bending modes for free L_1 ligand were observed at 1425/1332/1087 cm^{-1}, while these IR bands appeared at 1408/1286/1051, 1400/1299/1047, and 1407/1284/1051 cm^{-1} for complexes **9**–**11** from the FTIR spectra, respectively. Theoretical these bands were calculated at 1415/1285/1042, 1411/1318/1042, and 1431/1281/1046 cm^{-1} with DFT/CAM-B3LYP level. The bands observed at 511, 513 and 514 cm^{-1} for complexes **9**–**11** can be due to M–N (MnN/NiN/CoN) bond stretching vibration modes, respectively. The corresponding theoretical bands were obtained at 504, 510 and 507 cm^{-1} with DFT/CAM-B3LYP level (see Tables S1 and S3). These results are consistent with reported Schiff base metal complexes [76–78]. The M–N (MnN/NiN/CoN) bond stretching vibration modes of L_1 and azide ligand, which were not recorded in the experimental IR spectra, were

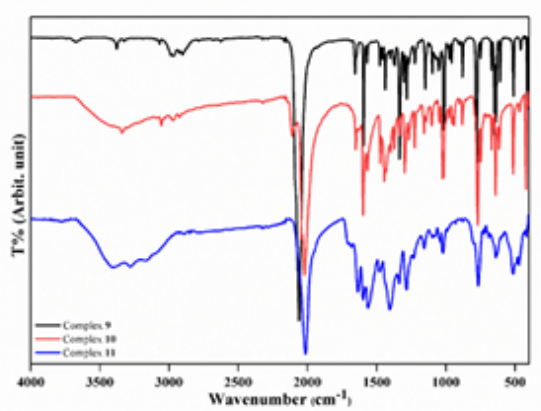

Fig. 2. FTIR spectra of complexes **9**–**11**.

theoretically calculated in the range of 389–287 cm^{-1} and are given in Table 1. In addition, Fig. 2 and Table S3 show the additional stretching, in-plane, and torsion vibrational modes associated with the ring, azide, imine, and methyl groups.

As a result, in the experimental and theoretical IR characterization of **9**–**11** complexes, bond stretching modes and other vibration modes that provide coordination formation are presented in comparison with the modes of free L1 and azide ligands.

3.3. Powder XRD analysis

The powder XRD samples of the complexes **9**–**11** were recorded at the $2\theta = 5–70^{\circ}$ range and their spectra are given in Fig. 3. According to the powder XRD spectra, the sharp peaks demonstrating their crystalline structure were observed for complexes **9**–**11**. Scherrer's formula (eq. (25)) [79,80] was used to calculate d_{XRD} (the average crystallite sizes) of the complexes **9**–**11**.

$$d_{XRD} = 0.9\lambda / \beta Cos\theta \quad (25)$$

In eq. (25), λ is the wavelength of Cu Kα radiation (1.54059 Å), θ and β are the Braggs reflection angle and full width at half maximum, respectively. The d_{XRD} values were found to be 26.45, 23.34 and 33.96 nm for manganese, nickel and cobalt complexes, respectively. The findings show that the crystallite size is within nano-scale range.

3.4. Analysis of the electronic absorption spectra, electronic transitions, and photoluminescence spectra

The UV–Vis absorption spectra and the plot of experimental E_g (optical band gap energy) in MeOH of synthesized complexes **9**–**11** are presented in Fig. 4a and b. Considering theoretical analysis in TD-DFT/ωB97XD and TD-DFT/CAM-B3LYP levels, the wavelengths, oscillator strengths, as well as FMOs contributions to electronic transitions were computed. In addition, the SWizard [57] and Chemissian [58] programs were used to describe the molecular orbitals and atoms/functional groups that make important contributions to electronic transitions. Based on Fig. 4a, three absorption peaks emerged in bridge-structured complex **11**, while two maximum absorption peaks appeared in complexes **9** and **10**. For complex **11**, the absorption peaks were observed at 337.7, 268.7, and 207.3 nm, while the absorption peaks were detected at 263.7, 202.7 nm for complex **9**, and 280.9 and 226.1 nm for complex **10**, respectively (see Table 2). These peaks were ascribed to $n\rightarrow\pi^*$ transitions, ligand-to-metal/metal-to-ligand, and intra-ligand $\pi\rightarrow\pi^*$. The charge transitions within the ligand, as well as the transitions from ligands to metal ion/metal ion to ligands, are evident in Fig. 5.

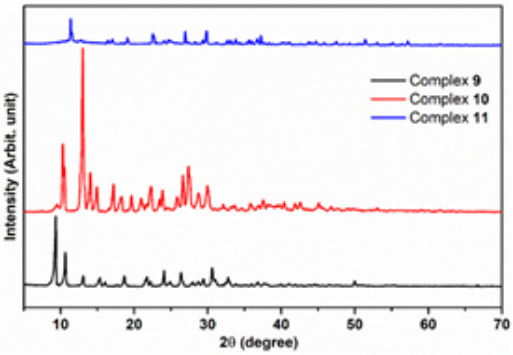

Fig. 3. Powder XRD spectra for the complexes **9**–**11**.

The photoluminescence spectra of synthesized complexes **9**–**11** in MeOH were recorded using the excitation wavelengths at 255, 291 and 307 nm and the emission spectra were obtained in the ranges of 280 nm–480 nm (see Fig. 6). These complexes are comprised of L_1 (*N*-(pyridin-2-ylmethylene)methanamine) and azido ligands with π-bonds and resonance structure. This statement affects emission wavelength peaks detected 319 nm for complex **9**, 303 and 374 nm for complex **10**, and 309 and 392 nm for complex **11**. Due to the Stokes shift of the excitation spectrum at the same electronic transition, the absorption of the excitation band gap energy directly occurs as the band gap energy difference in the range of 22.1–54.3 nm. Using the formula $E_g = hc/(\lambda_e)$, where λ_e is the fluorescence wavelength, the energy band gap was computed at 3.32 and 3.16 eV for complexes **10** and **11**, respectively. In particular, a

Table 1
Experimental and theoretical selected characteristic vibration frequencies of synthesized complexes **9**–**11** and L_1 ligand.

FT-IR (cm^{-1})	FT-IR (cm^{-1})	ωB97XD	CAM-B3LYP	FT-IR (cm^{-1})	ωB97XD	CAM-B3LYP	FT-IR (cm^{-1})	ωB97XD	CAM-B3LYP	Vibrational mode assignments
		6-311 + G (d,p)// LanL2DZ			6-311 + G (d,p)// LanL2DZ			6-311 + G (d,p)// LanL2DZ		
L_1 ligand	Complex 9			Complex 10			Complex 11			
3070	3098	3082	3083	3056	3060	3061	3123	3118	3127	ν_{CH} (ring)
3053	3032	3045	3046	3029	3015	3018	3163	3052	3054	ν_{CH} (imine)
2994	2975	2962	2963	2972	2967	2956	3000	3002	3004	ν_{as} (methyl)
2967	2926	2920	2928	2925	2913	2921	2977	2921	2928	ν_{s} (methyl)
	2059	2127	2136	2111	2079	2087	2015	2157	2160	ν_{NN} (azide)
1592	1656	1664	1666	1653	1680	1683	1681	1607	1608	$\nu_{C=N}$ (imine)
1567	1627	1615	1616	1631	1614	1614	1637	1581	1584	$\nu_{C=C}$ (ring)
	1596	1592	1591	1598	1582	1583	1597	1561	1551	$\nu_{C=N}$ (imine)
1425	1408	1421	1415	1400	1408	1411	1407	1424	1431	β_{HCC} (ring)
	1305	1345	1338	1338	1352	1349	1341	1341	1343	ν_{NN} (azide)
1373	1286	1286	1285	1299	1318	1318	1284	1277	1281	β_{HCC} (ring)
1281	1223	1224	1246	1228	1223	1227	1233	1250	1246	ν_{CN} (ring) + ν_{CC} (ring)
1017	1017	1022	1019	1024	1024	1021	1021	1020	1017	ν_{NC} (imine-methyl)
		675	672		664	664	588	567	572	β_{NNN} (azide)
	648	670	605					565	570	β_{NNN} (azide)
	609	600	676					712	711	$\tau_{NNNMta/Ni/Co}$
		595	597	614	604	608	631	659	700	$\tau_{NNNMta/Ni/Co}$
	511	501	504	513	507	510	514	511	507	$\nu_{MetN/NiN/CoN}$ (imine)
		376	377		334	337		389	369	$\nu_{MetN/NiN/CoN}$ (azide)
		358	362		287	296		323	324	$\nu_{MetN/NiN/CoN}$ (ring)

ν: Stretching; β: In-plane bending; γ: Out-of-plane bending; τ: Torsion.

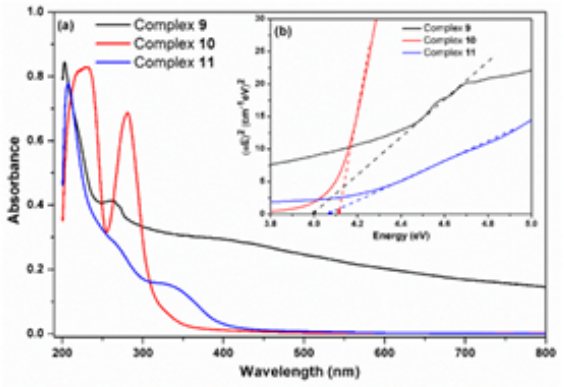

Fig. 4. (A) Experimental UV–Vis spectra and **(b)** the plots of optical band gap energy for the complexes **9**–**11** in methanol.

drastic change was observed in the PL spectrum of complex **11**. It can be explained that the reason is that complex **11** has a more rigid molecular conformation due to its dinuclear bridged structure. The possible applications in the production of blue LEDs are verified by the PL spectra.

Large metal orbital contributions to the LUMO in complex structures have been shown to boost the ligand's π-acceptor property [81]. The results of TD-CAM-B3LYP level display the metal orbital contributions in HOMO/HOMOs and LUMO/LUMOs for complexes **9**–**11** obtained at the range from 0 % to 62 %, and from 0 % to 16 %, respectively. The LUMO/LUMOs contributions of the L_1 including 2-pyridyl and imine groups, and azido (-N_3) ligands for complex **9**/**10** change between 56 % and 99 %/58 % and 98 % (in L_1), 0 % and 11 %/0 % and 36 % (in N_3), respectively, whereas those of contributions of the L_1 for complex **11** having bridge-structure vary 12 %–98 % range (in L_1), 2 %–87 % range (in N_3), seen in Table 2. It is deduced that the L_1 ligand has more electron acceptor properties for complexes **9** and **10** according to the LUMO/-LUMOs contributions.

The crucial ligand-to-ligand charge transfer (LLCT), and metal-to-ligand/ligand-to-metal charge transfer (MLCT/LMCT) transitions are displayed in Table 2. For complex **9**/**10**, the 83 %/82 % contribution in HOMO→LUMO β-spin state depicts the MLCT transition obtained at the contributions of Mn (61 %), L_1 (27 %) and N_3 (12 %) ligands/Ni(32 %), L_1 (63 %) and N_3 (5 %) ligands in HOMO, and Mn (4 %), L_1 (87 %) and N_3 (9 %) ligands/Ni(2 %), L_1 (93 %) and N_3 (5 %) ligands in LUMO. These transitions absorption wavelength obtained at 640.9/726.3 nm (f = 0.0326/f = 0.0027) occurred predominantly from metals to the L_1 ligand. For complex **11**, the absorption wavelength obtained at 608.7 nm (f = 0.2914) demonstrates the contribution of 23 % HOMO→LUMO contribution changing from Co(43 %), L_1 (54 %) and N_3 (3 %) ligands in HOMO to L_1 (12 %) and N_3 (87 %) ligands in LUMO. This MLCT transition is dominantly attributed from metal to N_3 ligand. Considering the metal ions and their environments, the other significant contributions and further the percentage of HOMOs→LUMOs transitions are given in Tables S2 and S4.

Considering Fig. 5, it could be stated that the electron density for complexes **9** and **11** is predominantly localized on the Mn/Co ion and azido ligand in HOMO α-states, while that of these complexes is localized on the L_1 ligands in LUMO α-states. For complex **10**, it was observed that a delocalized density on the Ni ion, L_1, and azido ligands at the HOMO α-state, while a localized density occurs on the L_1 ligand on one side at the LUMO α-state. On the other hand, it can be stated that the electron density is localized on the metal ions and L_1 ligands for the HOMO β-states of complexes **9** and **10**, and on the L_1 ligands for the LUMO β-states. These results for complexes **9** and **10** exhibit that the L_1 ligand has more π-acceptor features.

Table 2
Experimental and theoretical wavelengths, oscillator strengths, and major contributions for complexes **9**–**11**.

Experimental λ (nm) (Methanol)	Methanol/TD-CAM-B3LYP/6-311 + G (d,p)//LanL2DZ		
	λ (nm)	Osc. Strength	Molecular contributions (SWizard and Chemissian programs) H: HOMO, L: LUMO, 2-pyridyl: C_5H_4N, imine group: CH=N–CH_3
Complex **9**			
	640.9	0.0326	(83 %) H [Mn (61 %) + Pyridyl (16 %) + Imine (11 %) + N_3 (12 %)]→L β [Mn (4 %) + Pyridyl (46 %) + Imine (41 %) + N_3 (9 %)] (10 %) H-1 [Mn (8 %) + Pyridyl (21 %) + N_3 (70 %)]→L+1 β [Mn (19 %) + Pyridyl (63 %) + Imine (17 %)]
263.7	260.6	0.0163	(12 %) H-5 [Mn (6 %) + Pyridyl (61 %) + Imine (13 %) + N_3 (20 %)]→L β [Mn (4 %) + Pyridyl (46 %) + Imine (41 %) + N_3 (9 %)] (6 %) H-6 [Mn (37 %) + Pyridyl (38 %) + Imine (15 %) + N_3 (10 %)]→L+1 α [Mn (4 %) + Pyridyl (42 %) + Imine (43 %) + N_3 (11 %)]
	248.9	0.2105	(22 %) H-1 [Mn (8 %) + Pyridyl (21 %) + N_3 (70 %)]→L+4 β [Mn (34 %) + Pyridyl (48 %) + Imine (8 %) + N_3 (10 %)] (13 %) H-6 [Mn (37 %) + Pyridyl (38 %) + Imine (15 %) + N_3 (10 %)]→ L+1 α [Mn (4 %) + Pyridyl (42 %) + Imine (43 %) + N_3 (11 %)]
202.7	213.4	0.1758	(20 %) H-2 [Mn (6 %) + Pyridyl (20 %) + Imine (24 %) + N_3 (49 %)]→L+5 β [Mn (8 %) + Pyridyl (71 %) + Imine (14 %) + N_3 (7 %)] (15 %) H-3 β [Mn (62 %) + Pyridyl (15 %) + Imine (7 %) + N_3 (16 %)]→L+3 β [Pyridyl (13 %) + Imine (86 %)]
Complex **10**			
	726.3	0.0027	(82 %) H [Ni(32 %) + Pyridyl (30 %) + Imine (33 %) + N_3 (5 %)]→L β [Ni(2 %) + Pyridyl (71 %) + Imine (22 %) + N_3 (5 %)] (7 %) H-2 [Ni(34 %) + Pyridyl (24 %) + Imine (2 %) + N_3 (40 %)]→L β [Ni(2 %) + Pyridyl (71 %) + Imine (22 %) + N_3 (5 %)]
280.9	281.1	0.0074	(28 %) H-2 [Ni(46 %) + Pyridyl (35 %) + Imine (7 %) + N_3 (12 %)]→L+3 α [Ni (13 %) + Pyridyl (54 %) + Imine (4 %) + N_3 (29 %)] (13 %) H-3 [Ni(36 %) + Pyridyl (32 %) + Imine (5 %) + N_3 (27 %)]→L+3 β [Ni(16 %) + Pyridyl (52 %) + Imine (6 %) + N_3 (26 %)]
	243.2	0.1358	(24 %) H [Ni(12 %) + Pyridyl (62 %) + Imine (14 %) + N_3 (12 %)] →L+8 α [Pyridyl (58 %) + Imine (40 %)] (7 %) H-7 [Pyridyl (38 %) + Imine (4 %) + N_3 (57 %)]→L β [Ni(2 %) + Pyridyl (71 %) + Imine (22 %) + N_3 (5 %)]
226.1	230.8	0.0290	(10 %) H [Ni(12 %) + Pyridyl (62 %) + Imine (14 %) + N_3 (12 %)]→L+17 α [Ni (2 %) + Pyridyl (59 %) + Imine (3 %) + N_3 (36 %)] (7 %) H [Ni(12 %) + Pyridyl (62 %) + Imine (14 %) + N_3 (12 %)]→L α [Ni(10 %) + Pyridyl (39 %) + Imine (20 %) + N_3 (31 %)]
Complex **11**			
	608.7	0.2914	(23 %) H [Co(43 %) + Pyridyl (40 %) + Imine (14 %) + N_3 (3 %)]→L α [Pyridyl (10 %) + Imine (2 %) + N_3 (87 %)] (28 %) H-1 [Co(10 %) + Pyridyl (16 %) + Imine (2 %) + N_3 (72 %)]→L+1 α [Co (16 %) + Pyridyl (60 %) + Imine (17 %) + N_3 (7 %)]

(continued on next page)

Table 2 (*continued*)

Experimental λ (nm) (Methanol)	Methanol/TD-CAM-B3LYP/6-311 + G (d,p)//LanL2DZ		
	λ (nm)	Osc. Strength	Molecular contributions (SWizard and Chemissian programs) H: HOMO, L: LUMO, 2-pyridyl: C_5H_4N, imine group: CH=N–CH_3
337.7	328.7	0.1294	(36 %) H-5 [Co(28 %) + Pyridyl (14 %) + Imine (2 %) + N_3 (56 %)]→L+2 α [Pyridyl (57 %) + Imine (24 %) + N_3 (18 %)] (31 %) H-3 [Co(34 %) + Pyridyl (13 %) + Imine (2 %) + N_3 (51 %)]→ L+3 α [Pyridyl (53 %) + Imine (2 %) + N_3 (44 %)]
268.7	263.3	0.0206	(27 %) H-8 [Co(5 %) + Pyridyl (18 %) + Imine (7 %) + N_3 (70 %)]→L α [Pyridyl (10 %) + Imine (2 %) + N_3 (87 %)] (8 %) H-1 [Co(10 %) + Pyridyl (16 %) + Imine (2 %) + N_3 (72 %)]→L+2 α [Pyridyl (57 %) + Imine (24 %) + N_3 (18 %)]
	250.4	0.4697	(45 %) H-10 [Co(6 %) + Pyridyl (65 %) + Imine (25 %) + N_3 (4 %)] →L α [Pyridyl (10 %) + Imine (2 %) + N_3 (87 %)] (31 %) H-9 [Co(3 %) + Pyridyl (55 %) + Imine (21 %) + N_3 (21 %)] →L+1 α [Co(16 %) + Pyridyl (60 %) + Imine (17 %) + N_3 (7 %)]
207.3	213.8	0.0359	(14 %) H-2 [Co(27 %) + Pyridyl (15 %) + Imine (5 %) + N_3 (53 %)]→L+11 α [Pyridyl (45 %) + Imine (53 %) + N_3 (2 %)] (7 %) H-1 [Co(10 %) + Pyridyl (16 %) + Imine (2 %) + N_3 (72 %)]→L+19 α [Co(4 %) + Pyridyl (29 %) + Imine (7 %) + N_3 (60 %)]

3.5. Analysis of the MEP and global reactivity parameters

Many chemical systems' structure-activity relationships (SARs) may be understood using MEP (molecular electrostatic potential) surfaces. The electron density is connected to these surfaces. On the MEP surface, the areas that are red and yellow represent spaces with negative charges whereas the parts that are blue represent positively charged regions with low electron densities. Green areas represent neutral environments without any potential [82]. DFT/CAM-B3LYP level was utilized to define MEP surfaces of complexes **9**–**11** (see Fig. 7). As it is clear from Fig. 7, for complexes **9**–**11**, the dense reddish electron clouds around the azido ligand are the areas of highest electron density associated with the lone pairs of electronegative atoms. The –CH groups in the L_1 ligand,

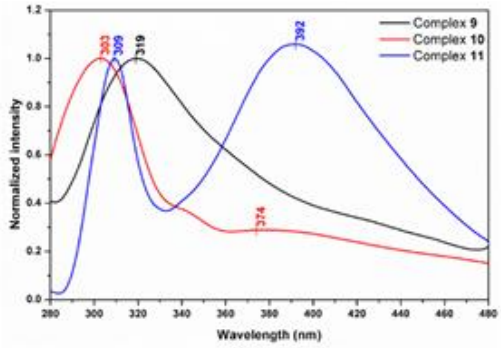

Fig. 6. Photoluminescence emission spectra of complexes **9**–**11** in methanol.

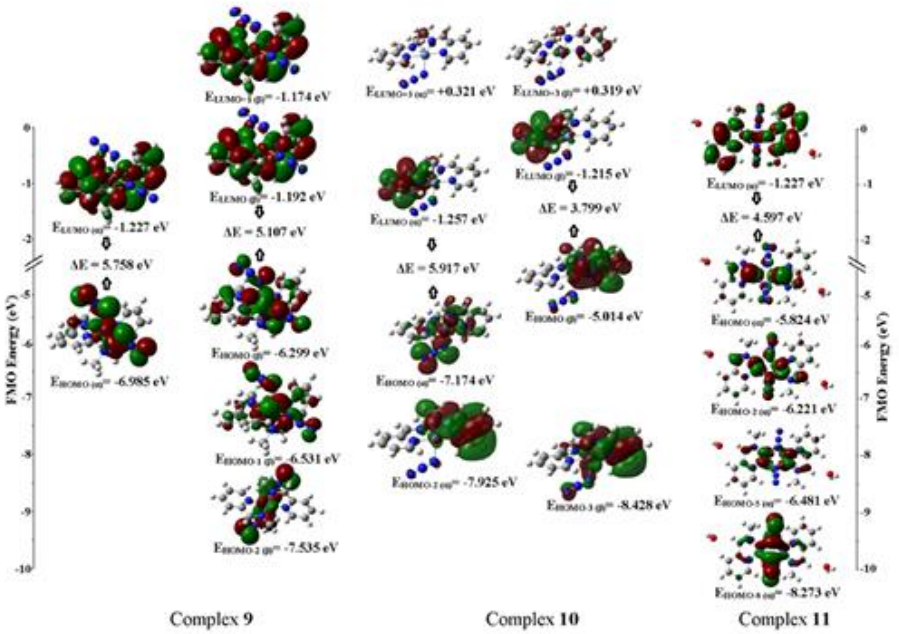

Fig. 5. FMOs and their energies that contribute the most to the electronic transition obtained by the DFT/CAM-B3LYP method in methanol for complexes **9**–**11**.

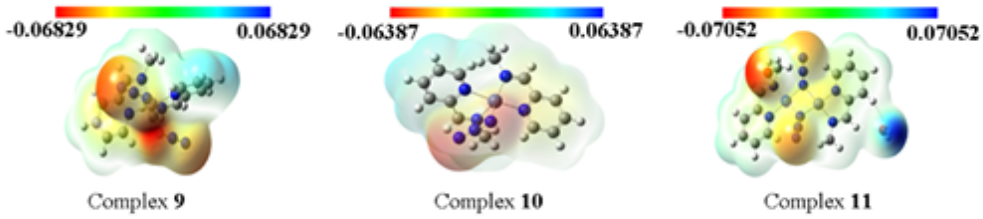

Fig. 7. Molecular electrostatic potential (MEP) surfaces for the complexes **9**–**11**.

which have the largest positive potential, were found to be regions where nucleophilic reactivity was presented. In this context, reactive parts were revealed in these complexes.

As described in section 2.3, molecular parameters (χ, S, ω, and φ) known as global reactivity parameters given in the computational procedure were computed by using FMO energy values and tabulated in Table S5. Chemical systems' resistance to alter their electronic distribution is known as chemical hardness (η). The chemical reactivity and stability of systems are associated with the parameters η, χ, S. It is clear from Fig. 4b that the experimental E_g (optical band gap energy) values of complexes **9**–**11** were found to be 3.99, 4.11, and 4.06 eV, respectively. The corresponding theoretical energy gap values of these complexes in α-spin level calculated at the DFT/CAM-B3LYP level were obtained at 5.442, 5.340, and 4.577 eV, in order. For complexes **9**–**11**, χ, η, S, ω, and φ parameters in α-spin state calculated at the DFT/CAM-B3LYP level were obtained at 3.126–4.354 eV range, 2.289–2.721 eV range, 0.368–0.437 1/eV range, 2.135–3.484 eV range, and 0.287–0.468 1/eV range, respectively (see Table S5). In this method, χ, η, and ω values were obtained in the order from smallest to largest: complex **11**<complex **10**<complex **9**. The smallest values were obtained in complex **11**, which has coordination in a bridged structure. Low η values show that intraligand charge transfer (ILCT) occurs in these complexes. These findings are consistent with those that have already been published in various structures [6,60]. The fact that the chemical softness values calculated in complexes **9**–**11** are greater than 0.301 eV indicate that these structures can be considered as more polarizable units and, as a result, may have sufficient NLO behavior. It can be noted that these results are comparable to different organic compounds reported previously [83]. Additionally, the calculated results can be stated that the examined compounds have sufficient molecular parameters (χ, S, ω, and φ) values required to exhibit NLO response.

Binding energy is also used in the analysis of the optoelectronic properties of the compounds examined. The excitation separation is stronger the lower the binding energy owing to higher energy states. The binding energy computed by using equation (26) includes the HOMO-LUMO (ΔE) energy gap difference and the first excitation E_{exc} minimum energy value, being mostly taken as the first singlet excited state energy of the $S_0 \rightarrow S_1$ transition [83,84].

$$E_b = \Delta E - E_{exc} \tag{26}$$

While a bigger E_b is preferred in electroluminescent devices like LEDs to ensure that charge recombination predominates, a smaller E_b is desirable in photovoltaic devices to permit the quick separation of charges [85]. The binding energies obtained at DFT/CAM-B3LYP level are estimated in descending order, as follows: Complex **9** (3.172 eV) < Complex **11** (2.560) < Complex **10** (2.012). These results were obtained at a level comparable to previous findings in different structures [83,86]. According to these findings, compound **10** has the lowest binding energy, indicating that it may cause greater excitation dissociation in the higher energy state, while the newly developed complexes may have potential optical activity and be applied in various NLO applications. Furthermore, considering that high binding energies are advised for electroluminescent devices, we believe these results are important.

3.6. The analysis of LO/NLO parameters

Due to its prospective uses in optoelectronic and telecommunication technologies, such as optical modulation, optical communication, optical switching, data storage, and processing, the synthesis of NLO (nonlinear optics) materials and related research have received a great deal of attention [29,30,32–35]. When practical investigation of the NLO properties of newly synthesized compounds is not feasible, the response of molecules to these features is calculated using theoretical NLO studies. Considering this, theoretical investigations of $\overline{\alpha}$ and Δα (LO parameters), β and γ (NLO parameters) of the synthesized complexes **9**–**11** were performed at DFT/ωB97XD and DFT/CAM-B3LYP levels in gas phase by using equations (7)–(10) [30,32]. The obtained results are given in Table 3 in comparison with the results of *p*-nitroaniline (pNA) [87] and urea [88,89], which are referenced as prototype compounds. Furthermore, to investigate further electronic and optoelectronic parameters, the external electric field (E), the permittivity of the vacuum (ε_0), the relative permittivity of the medium (ε_r), the electric susceptibility (χ_e), the physical parameters electric displacement (D), and polarization (P) were considered for complexes **9**–**11**. As it is known, the energy difference between HOMO and LUMO affects the polarizability of molecules. It has been reported that compounds with smaller energy ranges and lower hardness parameters (especially organic compounds) can have high hyperpolarizability values [62,83,86]. As a result, these parameters can also be evaluated quantitatively for Schiff-based metal complexes, giving an idea of the NLO activity.

The theoretical $\chi^{(1)}$, $\chi^{(2)}$, and $\chi^{(3)}$ parameters, known as linear optical, second-, and third-order nonlinear optical susceptibility tensors, as well as linear, second-, and third-order polarization parameters ($P^{(1)}$, $P^{(2)}$, and $P^{(3)}$) were obtained by using equations (11)–(21). The *E*, *P*, and *D* values were theoretically obtained at the range of 3.88–7.22 × 10^9 V/m, 4.45–7.86 × 10^{-2} C/m^2, and 7.88–14.45 × 10^{-2} C/m^2, respectively (see Table 3). By considering the mid-IR region, the experimental average *n* values of complexes **9**–**11** were calculated at 1.29, 1.65, and 1.54, respectively, while the corresponding theoretical *n* values were obtained at the range from 1.49 to 1.62 b y using DFT/ωB97XD and DFT/CAM-B3LYP levels. It can be stated that it is consistent within possible errors arising from experimental measurements and theoretical approaches.

Based on the plot of the third-order nonlinear optical susceptibility ($\chi^{(3)}$) parameter versus the photon energy in the UV–Vis region (200–600 nm), the $\chi^{(3)}$ parameter was evaluated in this work regardless of the use of experimental Z-scan technique [67,68]. Since the $\chi^{(3)}$ parameter varies depending on the refractive index, a graph of refractive index versus wavelength is given in Fig. 8. It is seen from Fig. 9 that the $\chi^{(3)}$ values of complexes **10** and **11** start to increase from 3.60 to 3.22 eV of the photon energy, while $\chi^{(3)}$ value of complex **9** starts to increase at 1.42 eV. For complexes **9**–**11**, the maximum $\chi^{(3)}$ values were observed at 51.82 × 10^{-13} esu versus the photon energies of 4.45, 4.18, and 5.17 eV, respectively. According to Fig. 8, for complexes **9**–**11**, the maximum *n* values appeared at 2.65 for 237.74, 251.29, and 277.09 nm. The shifts in *n* and $\chi^{(3)}$ parameters are influenced by different/similar metal ions in complex structures with varying coordination geometries, just as these

Table 3
Average electric field (E), electric polarization (P), electric displacement (D), relative dielectric constant (ε_r), average electric susceptibility (χ_e), refractive index (n), first-order linear, second-, and third-order nonlinear optical susceptibility ($\chi^{(1)}$, $\chi^{(2)}$ in 10^{-12} m/V, and $\chi^{(3)}$ in 10^{-22} m^2/V^2), electric dipole moment (μ, Debye), average static isotropic and anisotropic polarizability (<α(0; 0)>, in 10^{-24} esu, and Δα(0; 0), in 10^{-24} esu), static first- and second-order hyperpolarizabilities (<β(0; 0,0)>, in 10^{-30} esu, and <γ(0; 0,0,0)>, in 10^{-36} esu) for complexes **9**–**11**.

Parameter	Complex 9		Complex 10		Complex 11	
	ωB97XD	CAM-B3LYP	ωB97XD	CAM-B3LYP	ωB97XD	CAM-B3LYP
	6-311 + G (d,p)					
E (× 10^9 V/m)	5.80	7.22	5.63	5.69	3.84	3.88
P (× 10^{-2} C/m^2)	6.65	7.86	7.08	6.58	5.49	4.45
D (× 10^{-2} C/m^2)	11.78	14.25	12.07	11.61	8.89	7.88
ε_r	2.30	2.23	2.42	2.31	2.61	2.29
χ_e	1.30	1.23	1.42	1.31	1.61	1.29
n	1.52	1.49	1.56	1.52	1.62	1.51
$\chi^{(1)}$	1.30	1.23	1.42	1.31	1.61	1.29
$P^{(1)}$ (× 10^{-2} C/m^2)	6.65	7.86	7.08	6.58	5.49	4.45
$\chi^{(2)}$	61.19	49.98	147.88	159.36	6.39	5.35
$P^{(2)}$ (× 10^{-4} C/m^2)	182.26	230.69	415.03	456.83	8.34	7.13
$\chi^{(3)}$	29.35	109.05	−142.72	−154.02	10.67	8.98
$P^{(3)}$ (× 10^{-4} C/m^2)	50.70	363.40	−225.51	−251.22	5.35	4.64
μ	8.83	11.16	7.33	7.40	7.04	7.11
μ	6.20 (pNA) [87] and 4.56 (Urea) [88]					
<α(0; 0)>	45.67	46.34	39.04	39.02	54.97	54.93
<α>	17 (pNA) [87]					
Δα(0; 0)	31.92	35.26	27.14	26.83	35.67	36.54
<β(0; 0,0)>	129.29	112.95	243.64	262.55	13.05	13.62
<β>	9.2 (pNA) [87], 0.32 (Urea) [88] and 0.13 (Urea) [89]					
<γ(0; 0,0,0)>	557.67	2216.40	−2114.81	−2282.22	195.93	205.46
<γ>	15.0 (pNA) [87] and 7 (Urea) [88]					

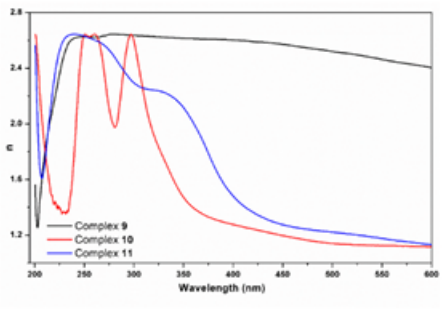

Fig. 8. The refractive index (n) versus λ of complexes **9**–**11** in methanol.

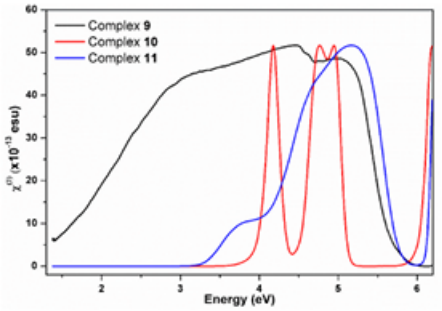

Fig. 9. The third-order nonlinear optical susceptibility $\chi^{(3)}$ of complexes **9**–**11** in methanol.

parameters change based on the metal ion exchange in various coordination structures with similar coordination geometries [70,71,90].

The DFT/CAM-B3LYP level indicates the mean static polarizability (α(0; 0)) values of complexes **9**–**11** in the gas phase obtained at 46.34 × 10^{-24}, 39.02 × 10^{-24}, and 54.93 × 10^{-24} esu exhibited higher than that of pNA (17 × 10^{-24} esu) [82]. The increase in polarization tendency was observed in the order complex **10**<complex **9**<complex **11**. It is seen that this polarization tendency is related to molecular mass. Theoretical $\chi^{(1)}$ linear optical parameters of complexes **9**–**11** were computed at the 1.23–1.61 range. On the other hand, the <β(0; 0,0)> parameters of complexes **9**–**11** in the DFT/ωB97XD and/CAM-B3LYP levels were computed at 129.29 × 10^{-30}, 243.64 × 10^{-30}, and 13.05 × 10^{-30} esu, and 112.95 × 10^{-30}, 262.55 × 10^{-30}, and 13.62 × 10^{-30} esu, respectively (see Table 3). Among the complexes, complex **10** has the highest value of <β(0; 0,0)>, this value (262.55 × 10^{-30} esu) based on CAM-B3LYP level is 820.5 and 2019.6 times greater than the urea results (0.32 × 10^{-30} esu [88] and 0.130 × 10^{-30} esu [89]) and 28.5 times greater than the pNA result (9.2 × 10^{-30} esu [87]). All calculated <β(0; 0,0)> values are greater than the referenced results. The $\chi^{(2)}$ parameter associated with β of complexes **9**–**11** was obtained at the range from 5.35 to 159.36 p.m./V. The $P^{(2)}$ parameter for complexes **9**–**11** was computed at the range from 7.13 × 10^{-4} to 456.83 × 10^{-4} C/m^2. These results change in a similar trend to the static first-order hyperpolarizability ones in order of complex **11**<complex **9**<complex **10**. These outcomes demonstrate that the highest value was obtained for complex **10** as in β parameters. As for the <γ(0; 0,0,0)> results in the gas phase obtained at the same levels for complexes **9**–**11**, complex **9** has the highest value of <γ(0; 0,0,0)>. The obtained value (2216.40 × 10^{-36} esu) based on CAM-B3LYP level is 147.76 and 316.63 times greater than that of pNA (15 × 10^{-36} esu) [87] and urea (7 × 10^{-36} esu) [88]. The $\chi^{(3)}$ parameter linked with γ of complexes **9**–**11** was found at the range of −154.06 and 109.05 m^2/V^2. The $P^{(3)}$ parameter for complexes **9**–**11** was computed at the range from −251.22 × 10^{-4} to 363.40 × 10^{-4} C/m^2 (see Table 3). The outcomes of $\chi^{(2)}/\beta$ and $\chi^{(3)}/\gamma$ indicate that complexes **10** and **9** are highly effective in terms of second- and third-NLO

characteristics, respectively. In the DFT/CAM-B3LYP level, the energy gap (ΔE) and η values were obtained in the increasing order values as complex **11**<complex **10**<complex **9**. Although the Co ions of complex **11** in the bridged structure have a center of symmetry around them, β and especially γ results were obtained remarkably. It is clear from Table 3 that the linear azide anion has a dramatic effect on the geometry, γ sign, and magnitude of the complex **10**. On the other hand, it has been reported that a negative gamma value may physically correspond to state in which molecular polarization will decrease with increasing laser intensity [29]. The impacts of the metal ion and its coordination environment on the structure were seen in the variations in the computed NLO parameters, considering the electronic structure of the complexes. However, when these effects are considered, a direct or inverse proportional relationship between these parameters with energy band gaps and the hardness parameters cannot be obtained.

The results obtained from this research may shed light on electronic devices that have the potential to be produced or designed.

4. Conclusion

Experimental and theoretical spectral properties, as well as theoretical nonlinear optical features on the *N*-(pyridin-2-ylmethylene) methanamine (L_1) and complexes **9**–**11** {[Mn $(L_1)_2(N_3)_2$], (**9**), [Ni $(L_1)_2(N_3)$], (**10**), $[Co_2(L_1)_2(N_3)_2]\cdot 2H_2O$, (**11**)} synthesized, and characterized by mass (LC-HRMS), powder XRD and FT–IR spectra were investigated. Considering the electronic spectral results, the L_1 ligand has more electron acceptor properties for complexes **9** and **10** according to the LUMO/LUMOs contributions. Based on CAM-B3LYP level, the χ, η, and ω values were obtained in the order from smallest to largest: complex **11**<complex **10**<complex **9**. The smallest values were obtained in complex **11**, which has coordination in a bridged structure. The increase in polarization tendency was observed in the order of complex **10**<complex **9**<complex **11**. Among the complexes, complex **10** has the highest value of $<\beta(0;0,0)>$, this value (262.55×10^{-30} esu) based on CAM-B3LYP level is 820.5 and 2019.6 times greater than the urea results (0.32×10^{-30} esu and 0.130×10^{-30} esu) and 28.5 times greater than the pNA result (9.2×10^{-30} esu). It can be thought that the noncentrosymmetric structure of complex **10** containing Ni ion allows this parameter to be high. The highest value of $<\gamma(0;0,0,0)>$ for complex **9** obtained at 2216.40×10^{-36} esu based on CAM-B3LYP level is 147.76 and 316.63 times greater than those of pNA (15×10^{-36} esu) and urea (7×10^{-36} esu). The results of β and γ indicate that complexes **10** and **9** are highly effective in terms of microscopic second- and third-NLO characteristics, respectively. It is observed that these outcomes were supported by the results of $\chi^{(2)}$ and $\chi^{(3)}$ parameters. The linear azide anion has a dramatic effect on the geometry, γ sign, and magnitude of the complex **10**. The NBO findings between the lone pair electrons of N atoms and metal ions validated the coordination geometries of complexes **9**–**11**. Among the Schiff base-azide Mn/Ni/Co complexes, complexes **9** and **10** can be suggested as candidates for NLO material. All of the outcomes reached here are especially significant since they serve as a starting point for future nonlinear optical investigations of Schiff base-based metal complexes.

Author contributions

Yusuf Atalay: Software, Methodology. Davut Avcı: Writing – review & editing, Writing – original draft, Software, Methodology, Formal analysis. Özgen Özge: Visualization, Formal analysis, Data curation. Fatih Sönmez: Writing – review & editing, Investigation, Formal analysis. Adil Başoğlu: Formal analysis. Ömer Tamer: Software, Investigation

Declaration of competing interest

The authors declare that they have no known competing financial interests or personal relationships that could have appeared to influence the work reported in this paper.

Data availability

The authors do not have permission to share data.

Acknowledgements

This work was supported by the Scientific Research Projects Unit of Sakarya University, Turkey (Project Number: 2021-7-25-103).

Appendix A. Supplementary data

Supplementary data to this article can be found online at https://doi.org/10.1016/j.mssp.2024.108523.

References

[1] J.-W. Zheng, L. Ma, Silver(I) complexes of 2,4-dihydroxybenzaldehyde–amino acid Schiff bases–Novel noncompetitive α-glucosidase inhibitors, Bioorg. Med. Chem. Lett 25 (2015) 2156–2161.
[2] J.-W. Zheng, L. Ma, Assessment of silver(I) complexes of salicylaldehyde derivatives–histidine Schiff base as novel α-glucosidase inhibitors, Chin. Chem. Lett. 27 (2) (2016) 283–286.
[3] R.V. Sakthivel, P. Sankudevan, P. Vennila, G. Venkatesh, S. Kaya, G. Serdaroğlu, Experimental and theoretical analysis of molecular structure, vibrational spectra and biological properties of the new Co(II), Ni(II) and Cu(II) Schiffbase metal complexes, J. Mol. Struct. 1233 (2021) 130097.
[4] S. Nagar, S. Raizada, N. Tripathee, A review on various green methods for synthesis of Schiff base ligands and their metal complexes, Results Chem. 6 (2023) 101153.
[5] V.K. Juyal, A. Pathak, M. Panwar, S.C. Thakuri, O. Prakash, A. Agrwal, V. Nand, Schiff base metal complexes as a versatile catalyst: a review, J. Organomet. Chem. 999 (2023) 122825.
[6] D. Avcı, Ö. Özge, A. Başoğlu, F. Sönmez, Ö. Tamer, N. Dege, Y. Atalay, Synthesis, crystal structures, and DFT calculations: novel Mn(II), Co(II) and Ni(II) complexes of *N*-(pyridin-2-ylmethylene)methanamine with isothiocyanate as promising optical materials, Opt. Quant. Electron. 55 (2023) 408.
[7] S. Kamaal, M. Mehkoom, A. Ali, S.M. Afzal, M.J. Alam, S. Ahmad, M. Ahmad, Potential third-order nonlinear optical response facilitated by intramolecular charge transfer in a simple schiff base molecule: experimental and theoretical exploration, ACS Omega 6 (2021) 6185–6194.
[8] A. Irfan, A.G. Al-Sehemi, M.A. Assiri, S. Ullah, Exploration the effect of metal and electron withdrawing groups on charge transport and optoelectronic nature of schiff base Ni(II), Cu(II) and Zn(II) complexes at molecular and solid-state bulk scales, Mater. Sci. Semicond. Process. 107 (2020) 104855.
[9] K.B. Manjunatha, S. Supriya, S.S. Nawaz, P. Ranjan, T. Chakraborty, P. Poornesh, R. Dileep, Nonlinear optical and quantum chemical studies of Palladium benzimidazole Schiff base complex, Mater. Sci. Semicond. Process. 151 (2022) 107012.
[10] S. Di Bella, A. Colombo, C. Dragonetti, S. Righetto, D. Roberto, Zinc(II) as a versatile template for efficient dipolar and octupolar second-order nonlinear optical molecular materials§, INORGA 6 (2018) 133.
[11] H. Ali, A. Anjum, D. Goswami, Investigating the third-order nonlinear optical properties of a Schiff base (DBAP) and its Co/Cu metal complex using Z-scan and DFT methodology, J. Mol. Struct. 1307 (2024) 138039.
[12] L.H. Abdel-Rahman, A.M. Abu-Dief, H. Moustafa, A.A.H. Abdel-Mawgoud, Design and nonlinear optical properties (NLO) using DFT approach of new Cr(III), VO(II), and Ni(II) chelates incorporating tri-dentate imine ligand for DNA interaction, antimicrobial, anticancer activities and molecular docking studies, Arab. J. Chem. 13 (2020) 649–670.
[13] M. Montazerozohori, S. Mojahedi Jahromi, A. Masoudiasl, P. McArdle, Nano structure zinc (II) Schiff base complexes of a N_3-tridentate ligand as new biological active agents: spectral, thermal behaviors and crystal structure of zinc azide complex, Spectrochim. Acta 138 (2015) 517–528.
[14] Ö. Özge, D. Avcı, F. Sönmez, Ö. Tamer, N. Dege, A. Başoğlu, Y. Atalay, B. Zengin Kurt, Synthesis, DFT calculations, α-glucosidase inhibitor activity, and docking studies on Schiff base metal complexes containing isothiocyanate, Appl. Organomet. Chem. 37 (2023) e7084.
[15] O.A. El-Gammal, F.Sh Mohamed, G.N. Rezk, A.A. El-Bindary, Structural characterization and biological activity of a new metal complexes based of Schiff base, J. Mol. Liq. 330 (2021) 115522.
[16] Y. Deswal, S. Asija, A. Dubey, L. Deswal, D. Kumar, D.K. Jindal, J. Devi, Cobalt(II), nickel(II), copper(II) and zinc(II) complexes of thiadiazole based Schiff base ligands: synthesis, structural characterization, DFT, antidiabetic and molecular docking studies, J. Mol. Struct. 1253 (2022) 132266.
[17] A.A. Abdel Aziz, F.M. Elantabli, H. Moustafa, S.M. El-Medani, Spectroscopic, DNA binding ability, biological activity, DFT calculations and non linear optical properties (NLO) of novel Co(II), Cu(II), Zn(II), Cd(II) and Hg(II) complexes with ONS Schiff base, J. Mol. Struct. 1141 (2017) 563–576.

[18] H. Moustafa, G.G. Mohamed, S. Elramly, Spectroscopic studies, Density Functional Theory calculations, and non-linear optical properties of binuclear Fe(III), Co(II), Ni(II), Cu(II), and Zn(II) complexes of OONN Schiff base ligand, J. Chin. Chem. Soc. 67 (2020) 1783–1793.

[19] A. Lehleh, A. Beghidja, C. Beghidja, O. Mentré, R. Welter, Synthesis, crystal structure and thermal decomposition of Cu(II), Co(II), Mn(II) complexes with hetero-ligands containing cysteic acid, 4,4′-dimethyl-2,2′-bipyridine and azide, C. R. Chimie 14 (2011) 462–470.

[20] Li-Y. Wang, B. Zhao, Chen-X. Zhang, Dai-Z. Liao, Zong-H. Jiang, Shi-P. Yan, The first azide($\mu_{1,1}$)-bridged binuclear cobalt(II)-Imino nitroxide complex with ferromagnetic behavior, Inorg. Chem. 42 (2003) 5804–5806.

[21] Y.-Q. Wang, Q. Yue, Y. Qi, K. Wang, Q. Sun, E.-Q. Gao, Manganese (II), iron (II), and mixed-metal metal–organic frameworks based on chains with mixed carboxylate and azide bridges: magnetic coupling and slow relaxation, Inorg. Chem. 52 (2013) 4259–4268.

[22] T. Vijayan, J. Kim, M. Azam, S.I. Al-Resayes, A. Stalin, B.S. Kannan, A. Jayamani, A. Ayyakannu, S. Nallathambi, Influence of co-ligand on the biological properties of Schiff base metal complexes: synthesis, characterization, cytotoxicity, and antimicrobial studies, Appl. Organomet. Chem. 36 (2021) e6542.

[23] Y. Song, C. Massera, O. Roubeau, P. Gamez, A.M.M. Lanfredi, J. Reedijk, An unusual open cubane structure in a $\mu_{1,1}$-azido- and alkoxo-bridged tetranuclear copper(II) complex, $[Cu_4L_2(\mu_{1,1}\text{-}N_3)_2]\cdot 5H_2O$ (H_2L = *N,N*-(2-Hydroxylpropane-1,3-diyl)bis-salicylideneimine), Inorg. Chem. 43 (2004) 6842–6847.

[24] J. Hou, X. Liu, J. Shen, G. Zhao, P.G. Wang, The impact of click chemistry in medicinal chemistry, Expet Opin. Drug Discov. 7 (6) (2012) 489–501.

[25] P. Gao, L. Sun, J. Zhou, X. Li, P. Zhan, X. Liu, Discovery of novel anti-HIV agents via Cu(I)-Catalyzed azide-alkyne cycloaddition (CuAAC) click chemistry-based approach, Expet Opin. Drug Discov. 11 (9) (2016) 857–871.

[26] C. Pastor-Ramírez, R. Zamorano-Ulloa, H. Vazquez-Lima, S. Hernández-Anzaldo, Y. Reyes-Ortega, Synthesis and magneto-structural study of distorted octahedral Co^{II} complexes with picolinamide and azide ($\mu_{1,1}$)-Bridge, ChemistrySelect 6 (2021) 1394–1403.

[27] M. Villanueva, J.L. Mesa, M.K. Urtiaga, R. Cortés, L. Lezama, M.I. Arriortua, T. Rojo, A new alternating ferro- and antiferromagnetic, one-dimensional manganese(II) azide complex, $[Mn(dpa)(N_3)_2]_2$ crystal structure and spectroscopic and magnetic properties, Eur. J. Inorg. Chem. (2001) 1581–1586.

[28] P.N. Prasad, D.J. Williams, Introduction to Nonlinear Optical Effects in Molecules and Polymers, Wiley, New York, 1991, pp. 120–131.

[29] F. Meyers, S.R. Marder, B.M. Pierce, J.L. Brédas, Electric field modulated nonlinear optical properties of donor-acceptor polyenes: sum-over-states investigation of the relationship between molecular polarizabilities (α, β, and γ) and bond length alternation, J. Am. Chem. Soc. 116 (1994) 10703–10714.

[30] J.L. Oudar, J. Zyss, Relations between microscopic and macroscopic lowest-order optical nonlinearities of molecular crystals with one-or two-dimensional units, Phys. Rev. A 26 (1982) 2028–2048.

[31] B.M. Pierce, A theoretical analysis of third-order nonlinear optical properties of linear polyenes and benzene, J. Chem. Phys. 91 (2) (1989) 791–811.

[32] D. Avci, Second and third-order nonlinear optical properties and molecular parameters of azo chromophores: semiempirical analysis, Spectrochim. Acta 82 (2011) 37–43.

[33] D.S. Chemla, J. Zysss, Nonlinear Optical Properties of Organic Molecules and Crystals, Academic Press, Orlando, FL, 1987.

[34] M. Faizan, M. Mehkoom, Z. Afroz, V.H.N. Rodrigues, S.M. Afzal, S. Ahmad, Experimental and computational investigation of novel dihydrated organic single crystal of 2,4,6-triaminopyrimidine and 3,5-dintrobenzoic acid: linear and nonlinear optical response with limiting performance, J. Solid State Chem. 300 (2021) 122255.

[35] M. Mehkoom, S.M. Afzal, S. Ahmad, S.A. Khan, The new pyrazoline derivative 5-(3,4-Dimethoxyphenyl)-3-(2,5-dimethyl-thiophene-3-yl),-4,5-dihydro-pyrazole-1-carbothioic acid amide (DDPA) as an advisable candidate for optical linearity, nonlinearity, and limiting performance, J. Mol. Liq. 345 (2022) 117018.

[36] Y. Yao, Y. Zhang, X. Li, Y.-Q. Qiu, The second-order NLO property of a photoswitchable heteroditpioc ion-pair receptor based on 2-pyridyl acylhydrazone linking with 2,6-pyridine bisamide: the impacts of metal cations and anions, J. Mol. Graph. Model. 100 (2020) 107652.

[37] D. Aggoun, Z. Messasma, B. Bouzerafa, R. Berenguer, E. Morallon, Y. Ouennoughi, A. Ourari, Synthesis, characterization and DFT investigation of new metal complexes of Ni(II), Mn(II) and VO(IV) containing N,O-donor Schiffbase ligand, J. Mol. Struct. 1231 (2021) 129923.

[38] S. Hussain, S. Muhammad, S.H. Talib, M. Akkurt, A. Mahsud, Z. Yang, H. Wang, Z. Lu, Nonlinear optical properties of novel crystalline complexes of cobalt (II) and nickel (II) with 4-bromo-3-methyl-1H-pyrazole: combined experimental and computational study, J. Mol. Struct. 1296 (2024) 136834.

[39] D. Avcı, S. Altürk, F. Sönmez, Ö. Tamer, A. Başoğlu, Y. Atalay, B.Z. Kurt, N. Dege, Three novel Cu(II), Cd(II) and Cr(III) complexes of 6−Methylpyridine−2−carboxylic acid with thiocyanate: synthesis, crystal structures, DFT calculations, molecular docking and α-Glucosidase inhibition studies, Tetrahedron 74 (2018) 7198–7208.

[40] D. Avcı, S. Altürk, F. Sönmez, Ö. Tamer, A. Başoğlu, Y. Atalay, B. Zengin Kurt, N. Dege, A novel series of mixed-ligand M(II) complexes containing 2,2′-bipyridyl as potent α-glucosidase inhibitor: synthesis, crystal structure, DFT calculations, and molecular docking, JBIC, J. Biol. Inorg. Chem. 24 (2019) 747–764.

[41] D. Avcı, S. Altürk, F. Sönmez, Ö. Tamer, A. Başoğlu, Y. Atalay, B. Zengin Kurt, N. Dege, Synthesis, spectral properties, in vitro α-glucosidase inhibitory activity and quantum chemical calculations of novel mixed-ligand M(II) complexes containing 1,10-phenanthroline, Appl. Organomet. Chem. 34 (2020) e5412.

[42] S. Altürk, D. Avcı, Ö. Tamer, Y. Atalay, O. Şahin, A cobalt(II) complex with 6-methylpicolinate: synthesis, characterization, second- and third-order nonlinear optical properties, and DFT calculations, J. Phys. Chem. Solid. 98 (2016) 71–80.

[43] D. Avcı, S. Altürk, F. Sönmez, Ö. Tamer, A. Başoğlu, Y. Atalay, B. Zengin Kurt, Synthesis, DFT calculations and molecular docking study of mixed ligand metal complexes containing 4,4′-dimethyl-2,2′-bipyridyl as α-glucosidase inhibitors, J. Mol. Struct. 1205 (2020) 127665.

[44] D. Avcı, S. Altürk, F. Sönmez, Ö. Tamer, A. Başoğlu, Y. Atalay, B. Zengin Kurt, N. Dege, Novel metal complexes containing 6-methylpyridine-2-carboxylic acid as potent α-glucosidase inhibitor: synthesis, crystal structures, DFT calculations, and molecular docking, Mol. Divers. 25 (2021) 171–189.

[45] A. Benmohammed, D. Hadji, A. Guendouzi, Y. Mouchaal, A. Djafri, A. Khelil, Synthesis, characterization, linear and NLO properties of novel N-(2,4-Dinitrobenzylidene)-3-Chlorobenzenamine schiff base: combined experimental and DFT calculations, J. Electron. Mater. 50 (2021) 5282–5293.

[46] M. Lashanizadegan, H.A. Ashari, M. Sarkheil, M. Anafcheh, S. Jahangiry, New Cu (II), Co(II) and Ni(II) azo-Schiff base complexes: synthesis, characterization, catalytic oxidation of alkenes and DFT study, Polyhedron 200 (2021) 115148.

[47] H. Kargar, M. Ashfaq, M. Fallah-Mehrjardi, R. Behjatmanesh-Ardakani, K. S. Munawar, M.N. Tahir, Synthesis, crystal structure, spectral characterization, theoretical and computational studies of Ni(II), Cu(II) and Zn(II) complexes incorporating Schiff base ligand derived from 4-(diethylamino)salicylaldehyde, Inorg. Chim. Acta. 536 (2022) 120878.

[48] T. Yanai, D.P. Tew, N.C. Handy, A new hybrid Exchange-correlation functional using the Coulomb-attenuating method (CAM-B3LYP), Chem. Phys. Lett. 393 (2004) 51–57.

[49] J.-D. Chai, M. Head-Gordon, Systematic optimization of long-range corrected hybrid density functionals, J. Chem. Phys. 128 (2008) 084106.

[50] J.-D. Chai, M. Head-Gordon, Long-range corrected hybrid density functionals with damped atom-atom dispersion corrections, Phys. Chem. Chem. Phys. 10 (2008) 6615–6620.

[51] Gaussian 16 Revision C.01, M.J. Frisch, G.W. Trucks, H.B. Schlegel, G.E. Scuseria, M.A. Robb, J.R. Cheeseman, G. Scalmani, V. Barone, G.A. Petersson, H. Nakatsuji, X. Li, M. Caricato, A.V. Marenich, J. Bloino, B.G. Janesko, R. Gomperts, B. Mennucci, H.P. Hratchian, J.V. Ortiz, A.F. Izmaylov, J.L. Sonnenberg, D. Williams-Young, F. Ding, F. Lipparini, F. Egidi, J. Goings, B. Peng, A. Petrone, T. Henderson, D. Ranasinghe, V.G. Zakrzewski, J. Gao, N. Rega, G. Zheng, W. Liang, M. Hada, M. Ehara, K. Toyota, R. Fukuda, J. Hasegawa, M. Ishida, T. Nakajima, Y. Honda, O. Kitao, H. Nakai, T. Vreven, K. Throssell, J. A. Montgomery Jr., J.E. Peralta, F. Ogliaro, M.J. Bearpark, J.J. Heyd, E. N. Brothers, K.N. Kudin, V.N. Staroverov, T.A. Keith, R. Kobayashi, J. Normand, K. Raghavachari, A.P. Rendell, J.C. Burant, S.S. Iyengar, J. Tomasi, M. Cossi, J. M. Millam, M. Klene, C. Adamo, R. Cammi, J.W. Ochterski, R.L. Martin, K. Morokuma, O. Farkas, J.B. Foresman, D.J. Fox, Gaussian, Inc., 2016. Wallingford CT.

[52] R. Dennington, T.A. Keith, J.M. Millam, GaussView, Version 6.1, Semichem Inc., Shawnee Mission, KS, 2016.

[53] M.J. Frisch, J.A. Pople, J.S. Binkley, Self-consistent molecular orbital methods 25. Supplementary functions for Gaussian basis set, J. Chem. Phys. 80 (1984) 3265–3269.

[54] P.J. Hay, W.R. Wadt, Ab initio effective core potentials for molecular calculations. Potentials for the transition metal atoms Sc to Hg, J. Chem. Phys. 82 (1985) 270–283.

[55] E. Runge, E.K.U. Gross, Density-functional theory for time-dependent systems, Phys. Rev. Lett. 52 (1984) 997–1000.

[56] S. Miertus, E. Scrocco, J. Tomasi, Electrostatic interaction of a solute with a continuum. A direct utilizaion of Ab initiomolecular potentials for the prevision of solvent effects, J. Chem. Phys. 55 (1981) 117–129.

[57] **S.I. Gorelsky, SWizard Program, Revision 4.5, University of Ottawa, Ottawa, Canada, 2010.** http://www.sg.chem.net/.

[58] L. Skripnikov, Chemissian: Software to Analyze Spectra, Build Density Maps and Molecular Orbitals, 2016, Version 4.43.

[59] J.P. Foster, F. Weinhold, Natural hybrid orbitals, J. Am. Chem. Soc. 102 (1980) 7211–7218.

[60] R.G. Pearson, Absolute electronegativity and hardness correlated with molecular orbital theory, Proc. Natl. Acad. Sci. USA 83 (1986) 8440–8441.

[61] H. Reis, M.G. Papadopoulos, P. Calaminici, K. Jug, A.M. Koster, Calculation of macroscopic linear and nonlinear optical susceptibilities for the naphthalene, anthracene and meta-nitroaniline crystals, Chem. Phys. 261 (2000) 359–371.

[62] R.F.N. Rodrigues, L.R. Almeida, F.G.d. Santos, P.S.C. Jr, W.C.d. Souza, K. S. Moreira, G.L.B.d. Aquino, C. Valverde, H.B. Napolitano, B. Baseia, Solid state characterization and theoretical study of non-linear optical properties of a Fluoro-N-Acylhydrazide derivative, PLoS One 12 (4) (2017).

[63] P. Noudem, D. Fouejio, C.D.D. Mveme, S.S. Zekeng, F. Tchangnwa Nya, G.W. Ejuh, Hartree-Fock and DFT studies of the optoelectronic, thermodynamic, structural and nonlinear optical properties of photochromic polymers containing styrylquinoline fragments, Mater. Chem. Phys. 281 (2022) 125883.

[64] R.W. Boyd, Nonlinear Optics, third ed., Academic Press, 2008.

[65] İ. Şişman, A. Başoğlu, Effect of Se content on the structural, morphological and optical properties of $Bi_2Te_{3-y}Se_y$ thin films electrodeposited by under potential deposition technique, Mater. Sci. Semicond. Process. 54 (2016) 57.

[66] E. Erdoğan, B. Gündüz, Optoelectronic parameters of TBADN organic molecule: new aspect to solution technique, Opt Laser. Technol. 91 (2017) 130–137.

[67] M. Sheik-Bahae, A.A. Said, T.-H. Wei, D.J. Hagan, E.W. Van Stryland, Sensitive measurement of optical nonlinearities using a single beam, IEEE J. Quant. Electron. 26 (1990) 760–769.

[68] Y. Qian, G. Xiao, G. Wang, B. Lin, Y. Cui, Y. Sun, Synthesis and Z-scan measurements of third-order optical nonlinearity in push–pull molecules with dihydroxylethyl amino donor and nitro acceptor, Dyes Pigments 75 (2007) 218–224.
[69] M.M. El-Nahass, A.A.M. Farag, Structural, optical and dispersion characteristics of nanocrystalline GaN films prepared by MOVPE, Opt Laser. Technol. 44 (2012) 497–503.
[70] M.D. Bharathi, G. Ahila, J. Mohana, G. Chakkaravarthi, G. Anbalagan, Synthesis, crystal structure, growth, optical and third order nonlinear optical studies of $8HQ_2C_5N$ single crystal-An efficient third-order nonlinear optical material, Mater. Chem. Phys. 192 (2017) 215–227.
[71] D. Avcı, Y. Saeedi, A. Başoğlu, N. Dege, S. Altürk, Ö. Tamer, Y. Atalay, Novel Mn(II) and Zn(II) complexes of 6-bromopicolinic acid as a potential optical material: synthesis, spectral characterizations, linear, and nonlinear optical properties and density functional theory calculations, Appl. Organomet. Chem. 35 (2021) e6125.
[72] G. Manca, J. Cano, E. Ruiz, Exchange interactions in azido-bridged ligand Ni^{II} complexes: a theoretical analysis, Inorg. Chem. 48 (7) (2009) 3139–3144.
[73] F. Weinhold, C. Landis, Valency and Bonding: A Natural Bond Orbitaldonor–Acceptor Perspective, Cambridge University Press, Cambridge, 2005.
[74] A.E. Reed, F. Weinhold, Natural bond orbital analysis of near-Hartree–Fock water dimer, J. Chem. Phys. 78 (1983) 4066–4073.
[75] E.D. Glendening, A.E. Reed, J.E. Carpenter, F. Weinhold, NBO Version3.1, TCI, University of Wisconsin, Madison, 1998.
[76] M.S. Nair, R.S. Joseyphus, Synthesis and characterization of Co(II), Ni(II), Cu(II) and Zn(II) complexes of tridentate Schiff base derived from vanillin and DL-α-aminobutyric acid, Spectrochim. Acta 70 (2008) 749–753.
[77] M.L. Sundararajan, T. Jeyakumar, J. Anandakumaran, B.K. Selvan, Synthesis of metal complexes involving Schiff base ligand with methylenedioxymoiety: spectral, thermal, XRD and antimicrobial studies, Spectrochim. Acta 131 (2014) 82–93.
[78] A. Varshney, A.P. Mishra, Synthesis, spectral characterization, computational studies, antifungal, DNA interaction, antioxidant and fluorescence property of novel Schiff base ligand and its metal chelates, Spectrochim. Acta 297 (2023) 122765.
[79] B.E. Warren, X-Ray Diffraction, Dover, New York, 1990, p. 253.
[80] P. Kavitha, M. Saritha, K.L. Reddy, Synthesis, structural characterization, fluorescence, antimicrobial, antioxidant and DNA cleavage studies of Cu(II) complexes of formyl chromone Schiff bases, Spectrochim. Acta 102 (2013) 159–168.
[81] S.I. Gorelsky, A.B.P. Lever, The electronic structure and spectra of $[Ru(NH_3)_4(LL)]^{2+}$ (LL = bpy, bpz, bqdi) studied by density functional theory and INDO/S. Charge transfer character of electronic transitions and their solvatochromism, Can. J. Anal. Sci. Spectrosc. 48 (1) (2003) 93–105.
[82] F.J. Luque, M. Orozco, P.K. Bhadane, S.R. Gadre, SCRF calculation of the effect of water on the topology of the molecular electrostatic potential, J. Phys. Chem. 97 (1993) 9380–9384.
[83] M. Khalid, M.U. Khan, Eisha-tul Razia, Z. Shafiq, M.M. Alam, M. Imran, M. S. Akram, Exploration of efficient electron acceptors for organic solar cells: rational design of indacenodithiophene based non-fullerene compounds, Sci. Rep. 11 (2021) 19931.
[84] A. Dkhissi, Excitons in organic semiconductors, Synth. Met. 161 (13–14) (2011) 1441–1443.
[85] L. Zhu, Y. Yi, L. Chen, Z. Shuai, Exciton binding energy of electronic polymers: a first principles study, J. Theor. Comput. Chem. 7 (4) (2008) 517–530.
[86] M. Khalid, ·S. Naseer, ·M.S. Tahir, I. Shafiq, K.S. Munawar, S.F. de Alcântara Morais, A.A.C. Braga, A theoretical approach towards designing of banana shaped non-fullerene chromophores using efficient acceptors moieties: exploration of their NLO response properties, Opt. Quant. Electron. 55 (2023) 258.
[87] L.T. Cheng, W. Tam, S.H. Stevenson, G.R. Meredith, G. Rikken, S.R. Marder, Experimental investigations of organic molecular nonlinear optical polarizabilities. 1. Methods and results on benzene and stilbene derivatives, J. Phys. Chem. 95 (1991) 10631–10643.
[88] I. Ledoux, J. Zyss, Influence of the molecular environment in solution measurements of the second-order optical susceptibility for urea and derivatives, Chem. Phys. 73 (1982) 203–213.
[89] C. Adant, M. Dupuis, J. Brédas, Ab initio study of the nonlinear optical properties of urea: electron correlation and dispersion effects, Int. J. Quant. Chem. 56 (1995) 497–507.
[90] N. Dege, Ö. Özge, D. Avcı, A. Başoğlu, F. Sönmez, M. Yaman, Ö. Tamer, Y. Atalay, B. Zengin Kurt, Concentration effects on optical properties, DFT, crystal characterization and α-glucosidase activity studies: novel Zn(II) complex, Spectrochim. Acta 262 (2021) 120072.

Supplementary data

Novel Schiff base-azide metal complexes: Synthesis, spectral, nonlinear optics, and DFT studies

Davut Avcı[1*], Özgen Özge[1,2], Fatih Sönmez[3], Adil Başoğlu[1], Ömer Tamer[1], Yusuf Atalay[1]

[1]*Sakarya University, Faculty of Science, Department of Physics, 54187, Sakarya, Turkey*
[2]*Cappadocia University, Health Vocational School, Ürgüp, 50400, Nevşehir, Turkey*
[3]*Sakarya University of Applied Sciences, Pamukova Vocational High School, 54055, Sakarya, Turkey*

Contents

The synthesis of the *N*-(pyridin-2-ylmethylene)methanamine (L_1)

0.1 mol of 2-pyridine carboxaldehyde was dissolved in 10 mL of ethanol and 2 drops of triethylamine were added on it. The solution was cooled by taking it into an ice bath, and 0.1 mol of methylamine (33% ethanol solution) was added to it and stirred in an ice bath for 30 minutes, and at room temperature for 3.5 hours. The alcohol in the mixture was evaporated under the vacuum and 100 mL of chloroform was added to this mixture. This solution was washed three times with 25 mL of water. The organic phase was dried with anhydrous $MgSO_4$, filtered and evaporated under the vacuum. The *N*-(pyridin-2-ylmethylene)methanamine (L_1) was obtained as dark yellow oil and its structure was confirmed by ^1H and ^{13}C NMR spectra. ^1H NMR (DMSO-d_6, 300 MHz) δ/ppm: 8.61 (1H, dd, J_1 = 1.2 Hz, J_2 = 4.7 Hz), 8.33 (1H, s), 7.82-7.93 (2H, m), 7.44 (1H, td, J_1 = 1.2 Hz, J_2 = 5.0 Hz), 3.47 (3H, s). ^{13}C NMR (DMSO-d_6, 75 MHz) δ/ppm: 163.84, 154.81, 150.00, 137.57, 125.73, 120.89, 48.14.

2

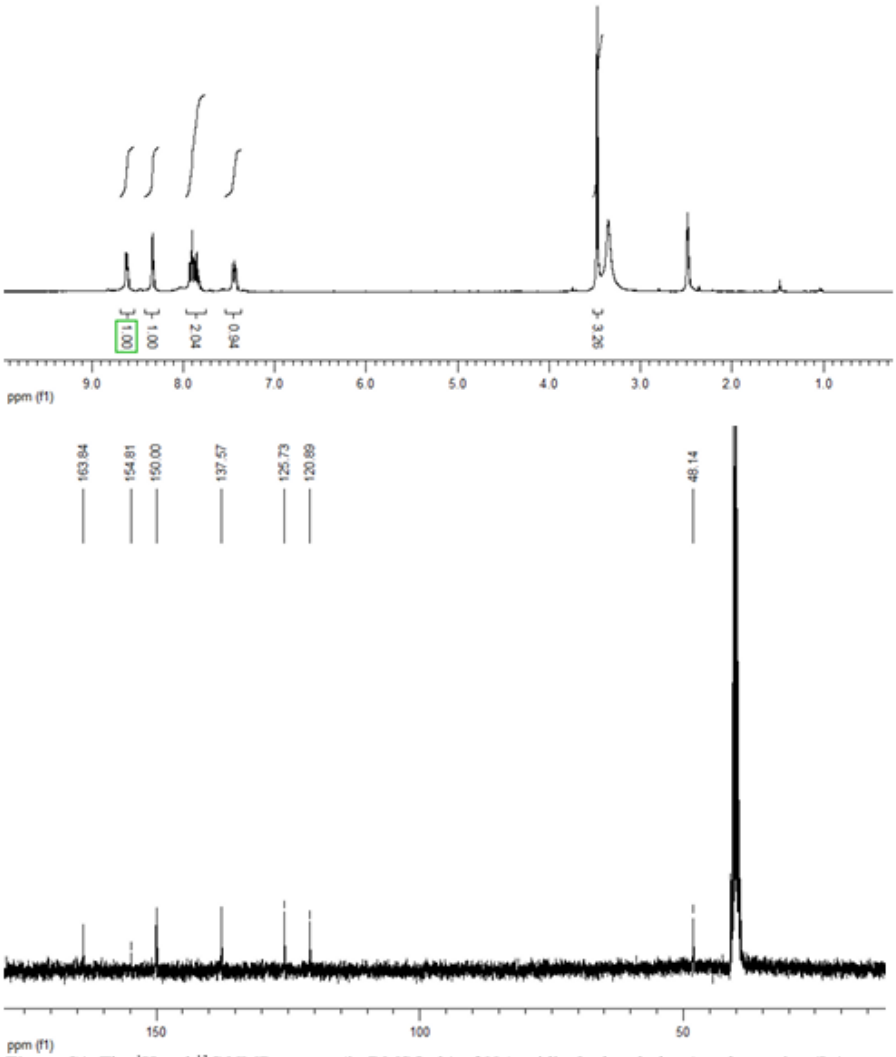

Figure S1. The ^{1}H and ^{13}C NMR spectra (in DMSO-d_6) of *N*-(pyridin-2-ylmethylene)methanamine (L_1).

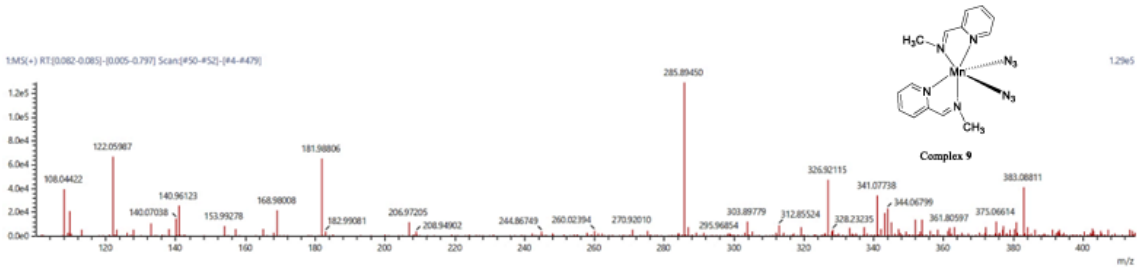

Figure S2. The mass spectrum of the complex **9**.

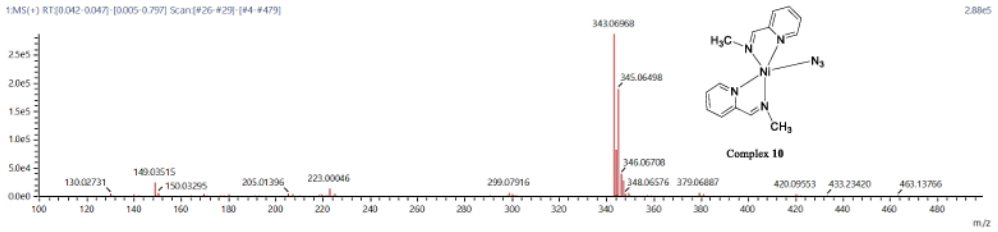

Figure S3. The mass spectrum of the complex **10**.

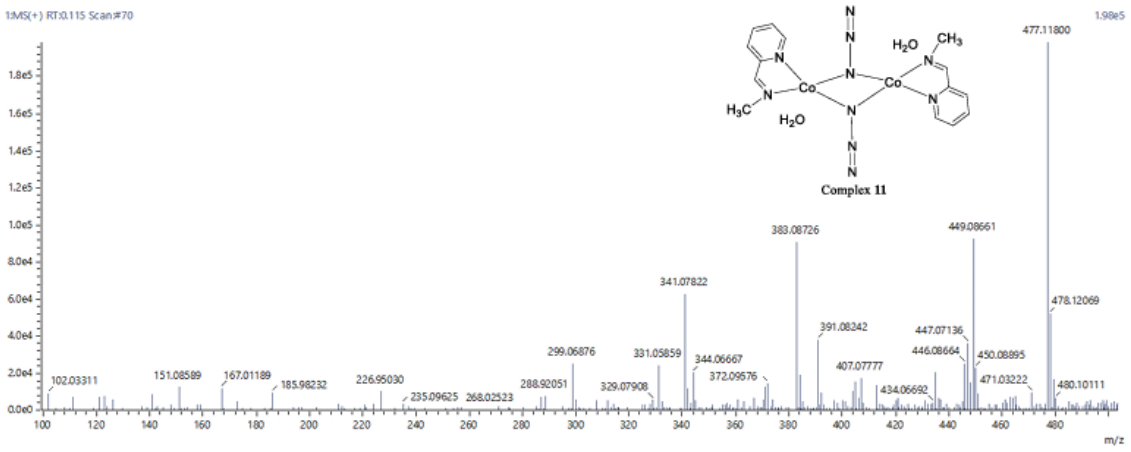

Figure S4. The mass spectrum of the complex **11**.

Table S1. Theoretical some geometric parameters for complexes **9–11**.

	Complex **9**			Complex **10**			Complex **11**	
Parameters	ωB97XD	CAM-B3LYP	Parameters	ωB97XD	CAM-B3LYP	Parameters	ωB97XD	CAM-B3LYP
Bond length (Å)			Bond length (Å)			Bond length (Å)		
Mn1–N2	1.967	1.969	Ni1–N2	1.933	2.151	Co1–N2	1.919	1.925
Mn1–N3	2.062	2.068	Ni1–N3	1.931	2.034	Co2–N3	1.919	1.914
Mn1–N6	1.948	1.942	Ni1–N6	1.903	2.069	Co1–N6	1.970	1.969
Mn1–N7	2.041	2.031	Ni1–N5	2.471	2.062	Co1–N7	1.970	1.966
Mn1–N5	1.953	1.958	Ni1–N4	1.937	1.989	Co2–N6	1.970	1.966
Mn1–N4	2.051	2.060	N6–N38	1.199	1.188	Co2–N7	1.970	1.966
N6–N38	1.206	1.204	N38–N39	1.145	1.154	Co1–N5	1.869	1.873
N7–N40	1.196	1.194	N2–C8	1.347	1.339	Co2–N4	1.869	1.878
N38–N39	1.140	1.138	N3–C9	1.351	1.366	N6–N38	1.200	1.201
N40–N41	1.149	1.147	N5–C10	1.263	1.268	N7–N40	1.200	1.201
N2–C8	1.372	1.372	N4–C18	1.274	1.323	N38–N39	1.142	1.140
N3–C9	1.346	1.345	N5–C26	1.445	1.449	N40–N41	1.142	1.140
N5–C10	1.320	1.320	N4–C30	1.454	1.449	N2–C8	1.359	1.358
N4–C18	1.274	1.272	C8–C10	1.479	1.471	N3–C9	1.359	1.358
N5–C26	1.446	1.447	C9–C18	1.460	1.415	N5–C10	1.296	1.291
N4–C30	1.448	1.450				N4–C18	1.296	1.292
C8–C10	1.411	1.408				N5–C26	1.454	1.455
C9–C18	1.462	1.460				N4–C30	1.454	1.454
						C8–C10	1.437	1.438
						C9–C18	1.437	1.439
Bond angles (°)			Bond angles (°)			Bond angles (°)		
N6–Mn1–N7	95.77	95.51	N6–Ni1–N2	91.16	88.12	N6–Co1–N7	79.56	79.75
N6–Mn1–N2	95.61	95.63	N6–Ni1–N3	92.87	92.16	N6–Co1–N2	99.09	99.16
N7– Mn1–N3	90.33	90.24	N2–Ni1–N5	76.10	78.04	N2– Co1–N5	82.52	82.52
N2– Mn1–N5	80.45	80.48	N3–Ni1–N4	82.89	80.79	N3– Co2–N4	82.52	82.54
N3– Mn1–N4	77.74	77.68	N5–Ni1–N4	115.9	115.0	N6– Co2–N7	79.56	79.62
N5– Mn1–N4	88.44	88.97	N6–Ni1–N4	155.0	155.7	Co1– N6–Co2	93.19	93.51
N6–Mn1–N4	166.7	166.0				Co1– N7–Co2	93.18	93.85
						N6– Co1–N5	178.4	178.3
Dihedral angles (°)			Dihedral angles (°)			Dihedral angles (°)		
Mn1–N2–C12–C16	179.4	179.0	Ni1–N2–C12–C16	-179.4	-171.5	Co1–N2–C12–C16	179.7	179.9
Mn1–N3–C24–C34	177.6	177.4	Ni1–N3–C24–C34	177.8	177.1	Co1–N3–C24–C34	179.7	179.4

Table S2. Second–order perturbation theory analysis of Fock matrix on NBO basis for complexes **9–11**.

Donor (*i*)	Acceptor (j)	$E^{(2)}$ (kcal/mol)		Donor (*i*)	Acceptor (j)	$E^{(2)}$ (kcal/mol)		Donor (*i*)	Acceptor (j)	$E^{(2)}$ (kcal/mol)	
		ωB97XD	CAM-B3LYP			ωB97XD	CAM-B3LYP			ωB97XD	CAM-B3LYP
		6–311+G(d,p)//LanL2DZ				6–311+G(d,p)//LanL2DZ				6–311+G(d,p)//LanL2DZ	
Complex **9**				Complex **10**				Complex **11**			
LP(1)N6	LP*(4)Mn1	9.56	9.85	LP(1)N6	LP*(6)Ni1	1.19	16.73	LP(1)N6	LP*(5)Co1	14.23	14.09
LP(1)N7	LP*(4)Mn1	15.56	16.08	LP(1)N5	LP*(6)Ni1	50.28	44.75	LP(1)N7	LP*(6)Co1	16.12	14.09
LP(1)N5	LP*(5)Mn1	65.72	63.21	LP(1)N3	LP*(7)Ni1	21.30	18.87	LP(1)N5	LP*(5)Co1	67.51	64.31
LP(1)N3	LP*(4)Mn1	37.06	35.53	LP(1)N4	LP*(8)Ni1	20.80	29.60	LP(1)N3	LP*(5)Co2	62.96	59.32
LP(1)N4	LP*(6)Mn1	23.61	21.62	LP(1)N2	LP*(7)Ni1	21.38	39.33	LP(1)N4	LP*(5)Co2	82.41	76.28
LP(1)N2	LP*(4)Mn1	66.59	62.78	LP(1)N6	σ*(N6-Ni1)	43.46		LP(1)N2	LP*(6)Co1	66.57	63.85
π*(N2-C8)	π*(N5-C10)	34.30	36.38	π*(N2-C8)	π*(N5-C10)	31.41	52.29	LP(1)N6	LP*(6)Co2	39.30	38.21
π*(N2-C8)	π*(C12-C16)	30.98	30.61	π*(N2-C8)	π*(C12-C16)	43.94	14.68	LP(1)N7	LP*(5)Co2	39.47	38.30
π*(N2-C8)	π*(C14-C20)	43.33	43.26	π*(N2-C8)	π*(C14-C20)	58.67	16.42	π*(N2-C12)	π*(C8-C14)	81.74	23.66
π*(N3-C9)	π*(N4-C18)	32.70	35.50	π*(N3-C9)	π*(N4-C18)	31.19	33.70	π*(N2-C12)	π*(C16-C20)	182.43	23.29
π*(N3-C9)	π*(C22-C36)	54.78	55.33	π*(N3-C9)	π*(C22-C36)	62.53	65.54	π*(N3-C24)	π*(C9-C22)	81.73	34.07
π*(N3-C9)	π*(C24-C34)	36.91	37.00	π*(N3-C9)	π*(C24-C34)	52.18	56.03	π*(N3-C24)	π*(C34-C36)	182.37	23.29

$E^{(2)}$ Hyperconjugative interaction energy (stabilization energy)

Table S3. Experimental and theoretical some characteristic vibration frequencies of synthesized complexes **9–11** and L_1 ligand.

FT-IR (cm^{-1})	FT-IR (cm^{-1})	ωB97XD	CAM-B3LYP	FT-IR (cm^{-1})	ωB97XD	CAM-B3LYP	FT-IR (cm^{-1})	ωB97XD	CAM-B3LYP	Vibrational mode assignments
		6-311+G(d,p)//LanL2DZ			LanL2DZ			LanL2DZ		
L_1 ligand		Complex **9**			Complex **10**			Complex **11**		
3070	3098	3082	3083	3056	3060	3061	3123	3118	3127	$\nu_{CH\ (ring)}$
3053	3032	3045	3046	3029	3015	3018	3163	3052	3054	$\nu_{CH\ (imine)}$
2994	2975	2962	2963	2972	2967	2956	3000	3002	3004	$\nu_{as\ (methyl)}$
2967	2926	2920	2928	2925	2913	2921	2977	2921	2928	$\nu_{s\ (methyl)}$
	2852	2897	2907	2892	2891	2900	2927	2921	2928	$\nu_{s\ (methyl)}$
	2059	2127	2136	2111	2079	2087	2015	2157	2160	$\nu_{NN\ (azide)}$
		2093	2103				2002	2140	2142	$\nu_{NN\ (azide)}$
1592	1656	1664	1666	1653	1680	1683	1681	1607	1608	$\nu_{C=N\ (imine)}$
1567	1627	1615	1616	1631	1614	1614	1637	1581	1584	$\nu_{C=C\ (ring)}$
	1596	1592	1591	1598	1582	1583	1597	1561	1551	$\nu_{C=C\ (ring)}$
	1569	1575	1576	1568	1581	1581	1562	1530	1533	$\nu_{C=N\ (imine)} + \nu_{C=C\ (ring)} + \beta_{HCC\ (ring)}$
	1527	1540	1538	1536	1538	1538	1481	1465	1459	$\nu_{C=C\ (ring)} + \nu_{C=N\ (imine)} + \beta_{CCC\ (ring)} + \beta_{CCN\ (ring)}$
1473	1479	1477	1479	1478	1493	1491	1466	1450	1457	$\nu_{C=N\ (imine)}$
1456	1442	1457	1460	1446	1454	1454	1440	1447	1452	$\nu_{C=C\ (ring)} + \beta_{HCC\ (ring)} + \beta_{HCH\ (methyl)}$
1425	1408	1421	1415	1400	1408	1411	1407	1424	1431	$\beta_{HCC\ (ring)}$
1373	1370	1380	1385	1371	1385	1389	1366	1365	1361	$\nu_{NC\ (imine)} + \nu_{CC\ (imine\text{-}ring)} + \beta_{HCC\ (ring)}$
	1305	1345	1338	1338	1352	1349	1341	1341	1343	$\nu_{NN\ (azide)}$
1332	1286	1286	1285	1299	1318	1318	1284	1277	1281	$\beta_{HCC\ (ring)}$
1281	1223	1224	1246	1228	1223	1227	1233	1250	1246	$\nu_{CN\ (ring)} + \nu_{CC\ (ring)}$
1138	1155	1136	1137	1157	1138	1136	1156	1137	1137	$\nu_{CC\ (ring)} + \beta_{HCC(ring)}$
1087	1102	1101	1101	1103	1116	1115	1097	1097	1098	$\nu_{CC\ (ring)} + \nu_{CN\ (ring)} + \beta_{HCC\ (ring)}$
1073	1051	1043	1042	1047	1041	1042	1051	1040	1046	$\beta_{HCC\ (ring)}$
1017	1017	1022	1019	1024	1024	1021	1021	1020	1017	$\nu_{NC\ (imine\text{-}methyl)}$
997	962	992	992	941	921	930	927	953	960	$\beta_{CCN\ (ring)} + \beta_{CNC\ (ring)}$
897	877	869	870	882	868	873	877	892	877	$\nu_{CC\ (ring)} + \nu_{CN\ (ring)}$
783	775	760	763	771	787	762	767	751	755	$\tau_{HCCC\ (ring)}$
751	746	736	738	747	758	731	733	733	739	$\tau_{HCCN\ (ring)} + \tau_{HCCC\ (ring)}$
	667	658	661	670	664	663	691	711	700	$\beta_{NCC\ (imine)} + \beta_{CCC\ (ring)}$
579	636	652	654	640	651	653	639	630	638	$\beta_{NCC\ (ring)} + \beta_{CCC\ (ring)} + \beta_{CNC\ (imine)} + \beta_{CCN\ (ring)}$
	511	501	504	513	507	510	514	511	507	$\nu_{MnN/NiN/CoN\ (imine)}$

υ: Stretching; β: In-plane bending; τ: Torsion.

Table S4. Experimental and theoretical wavelength, oscillator strength, and major contributions for complexes **9–11**.

Experimental λ (nm) (Methanol)	Methanol			
	λ (nm)	Osc. Strength	Molecular orbital contributions H: HOMO, L: LUMO	
Complex **9**				
	TD-ωB97XD/6-311+G(d,p)//LanL2DZ			
	671.9	0.0329	H→L β (84%)	H-1→L+1 β (10%)
263.7	261.2	0.0064	H-5→L+1 β (6%)	H-8→L β (5%)
	247.1	0.3148	H-6→L+1 β (18%)	H-2→L+3 α (17%)
202.7	208.73	0.0056	H-4→L+2 β (15%)	H-5→L+3 β (15%)
	TD-CAM-B3LYP/LanL2DZ			
	640.9	0.0326	H→L β (83%)	H-1→L+1 β (10%)
263.7	260.6	0.0163	H-5→L β (12%)	H-6→L+1 α (6%)
	248.9	0.2105	H-1→L+4 β (22%)	H-6→L+1 α (13%)
202.7	213.4	0.1758	H-2→L+5 β (20%)	H-3→L+3 β (15%)
Complex **10**				
	TD-ωB97XD/LanL2DZ			
	827.2	0.0011	H→L α (7%9)	H→L+4 α (8%)
	436.6	0.1732	H→L+10 α (25%)	H→L+6 α (24%)
280.9	282.4	0.0040	H-4→L β (9%)	H-2→L+5 β (8%)
226.1	229.2	0.0119	H→L+5 β (59%)	H-1→L+5 β (16%)
	TD-CAM-B3LYP/6-311+G(d,p)//LanL2DZ			
	726.3	0.0027	H→L β (82%)	H-2→L β (7%)
280.9	281.1	0.0074	H-2→L+3 α (28%)	H-3→L+3 β (13%)
	243.2	0.1358	H→L+8 α (24%)	H-7→L β (7%)
226.1	230.8	0.0290	H→L+17 α (10%)	H→L α (7%)
Complex **11**				
	TD-ωB97XD/LanL2DZ			
	601.9	0.2951	H→L α (23%)	H-1→L+1 α (28%)
337.7	325.9	0.1234	H-5→L+2 α (38%)	H-3→L+3 α (34%)
268.7	269.4	0.0391	H-4→L+7 α (27%)	H-5→L+6 α (13%)
	250.5	0.4110	H-10→L α (36%)	H-9→L+1 α (23%)
207.3	212.5	0.2802	H-15→L α (16%)	H-9→L+2 α (15%)
	TD-CAM-B3LYP/6-311+G(d,p)//LanL2DZ			
	608.7	0.2914	H→L α (23%)	H-1→L+1 α (28%)
337.7	328.7	0.1294	H-5→L+2 α (36%)	H-3→L+3 α (31%)
268.7	263.3	0.0206	H-8→L α (27%)	H-1→L+2 α (8%)
	250.4	0.4697	H-10→L α (45%)	H-9→L+1 α (31%)
207.3	213.8	0.0359	H-2→L+11 α (14%)	H-1→L+19 α (7%)

Table S5. Theoretical global chemical reactivity descriptors in the gas phase for complexes **9–11**.

Parameters (unit)	Complex **9**				Complex **10**				Complex **11**	
	ωB97XD		CAM-B3LYP		ωB97XD		CAM-B3LYP		ωB97XD	CAM-B3LYP
	α spin	β spin	α spin	β spin	α spin	β spin	α spin	β spin	α spin	α spin
E_{HOMO} (eV)	-7.565	-5.856	-7.075	-5.318	-7.147	-5.383	-6.625	-4.838	-5.941	-5.414
E_{LUMO} (eV)	-0.909	-1.020	-1.633	-1.665	-0.634	-0.634	-1.285	-1.281	-0.232	-0.837
ΔE (eV)	6.656	4.836	5.442	3.653	6.513	4.749	5.340	3.557	5.709	4.577
Electronegativity (χ, eV)	4.283	3.438	4.354	3.492	3.891	3.009	3.955	3.060	3.087	3.126
Chemical hardness (η, eV)	3.328	2.418	2.721	1.827	3.257	2.375	2.670	1.779	2.855	2.289
Chemical softness (S, 1/eV)	0.301	0.414	0.368	0.547	0.307	0.421	0.375	0.562	0.350	0.437
Electrophilic index (ω, eV)	2.756	2.444	3.484	3.337	2.324	1.906	2.929	2.632	1.669	2.135
Nucleophilic index (φ, 1/eV)	0.363	0.409	0.287	0.300	0.430	0.525	0.341	0.380	0.599	0.468

EK D. Avcı, D., Özge, Ö., Sönmez, F., Tamer, Ö., Başoğlu, A., Atalay, Y., & Zengin Kurt, B. (2024). In vitro α-glucosidase, docking and density functional theory studies on novel azide metal complexes. Future Medicinal Chemistry, 16(11), 1109–1125. https://doi.org/10.1080/17568919.2024.2342650

Future Medicinal Chemistry

ISSN: (Print) (Online) Journal homepage: www.tandfonline.com/journals/ifmc20

In vitro α-glucosidase, docking and density functional theory studies on novel azide metal complexes

Davut Avcı, Özgen Özge, Fatih Sönmez, Ömer Tamer, Adil Başoğlu, Yusuf Atalay & Belma Zengin Kurt

To cite this article: Davut Avcı, Özgen Özge, Fatih Sönmez, Ömer Tamer, Adil Başoğlu, Yusuf Atalay & Belma Zengin Kurt (2024) *In vitro* α-glucosidase, docking and density functional theory studies on novel azide metal complexes, Future Medicinal Chemistry, 16:11, 1109-1125, DOI: 10.1080/17568919.2024.2342650

To link to this article: https://doi.org/10.1080/17568919.2024.2342650

FUTURE MEDICINAL CHEMISTRY
2024, VOL. 16, NO. 11, 1109–1125
https://doi.org/10.1080/17568919.2024.2342650

Taylor & Francis
Taylor & Francis Group

RESEARCH ARTICLE

In vitro α-glucosidase, docking and density functional theory studies on novel azide metal complexes

Davut Avcı[*,a], Özgen Özge[a,b], Fatih Sönmez[c], Ömer Tamer[a], Adil Başoğlu[a], Yusuf Atalay[a] and Belma Zengin Kurt[d]

[a]Sakarya University, Faculty of Science, Department of Physics, 54187, Sakarya, Turkey; [b]Cappadocia University, Health Vocational School, Ürgüp, 50400, Nevşehir, Turkey; [c]Sakarya University of Applied Sciences, Pamukova Vocational High School, 54055, Sakarya, Turkey; [d]Bezmialem Vakif University, Faculty of Pharmacy, Department of Pharmaceutical Chemistry, 34093 Istanbul, Turkey

ABSTRACT

Aim: The goal of this study is to synthesize new metal complexes containing *N*-methyl-1-(pyridin-2-yl)methanimine and azide ligands as α-glucosidase inhibitors for Type 2 diabetes. **Materials & methods:** The target complexes (**12–16**) were synthesized by reacting *N*-methyl-1-(pyridin-2-yl)methanimine (L_1) with sodium azide in the presence of corresponding metal salts. The investigation of target protein interactions, vibrational, electronic and nonlinear optical properties for these complexes was performed by molecular docking and density functional theory studies. **Results:** Among these complexes, complex **13** ($IC_{50} = 0.2802 \pm 0.62\ \mu M$) containing Hg ion showed the highest α-glucosidase inhibitory property. On the other hand, significant results were detected for complexes containing Cu and Ag ions. **Conclusion:** Complex **13** may be an alternate anti-diabetic inhibitor according to *in vitro*/docking results.

GRAPHICAL ABSTRACT

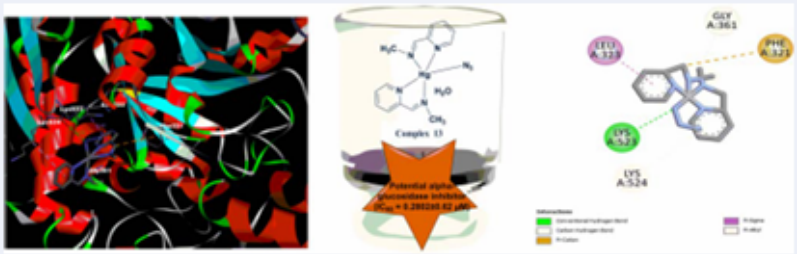

ARTICLE HISTORY
Received 26 January 2024
Accepted 4 April 2024

KEYWORDS
α-glucosidase/docking; azide; Cu/Hg/Cd/Ag/Zn ions; Schiff base; spectral elucidation; TD/DFT methods

1. Background

Many studies of azide metal complexes, in which azide ions (N_3^-) coordinate with various metal ions, such as Cu(II) [1–4], Zn(II) [5], Co(II) [5], Mn(II) [5], etc. to form stable complexes, are notable in coordination chemistry. The structural, spectral, optical, magnetic [6–8] and pharmaceutical [9,10] properties of these metal complexes have attracted great attention due to their different reactivity and potential applications in various fields. The azide ion serves as a versatile ligand with its linear trigonal planar geometry that can bind to metal centers via nitrogen atoms. Furthermore, this ligand has a high degree of coordination flexibility, which can also participate in the formation of monodentate, bidentate or polydentate complexes. Depending on the metal ion and coordination environment, azide complexes exist a wide variety of geometries, including distorted trigonal bipyramidal [3], distorted square pyramidal [5] and distorted octahedral [5,7] and bridge structures [1,2,4,11]. It was reported that synthesis of metal complexes including azide and/or heterocyclic ligands with various transition metals, such as cobalt [4,6–8], copper [1–4], zinc [5], iron [8], erbium [12] and platinum [13]. The utilization of these complexes underscores their role in advancing our understanding and utilization of these intriguing materials. Additionally, azide/azide derivative metal complexes, as well as compounds with heterocyclic rings including nitrogen, have been investigated for many biologi-

CONTACT Davut Avcı Tel.: +90 264 295 6097; davci@sakarya.edu.tr

Supplemental data for this article can be accessed at https://doi.org/10.1080/17568919.2024.2342650

cal activities. These include antimicrobial and antifungal properties [3], as well as anticancer potential [14,15]. Their capacity to interact with biological targets and demonstrate selective cytotoxicity underscores their significance in biomedical research [16–19]. In this context, studying azide metal complexes having various application potentials in the fields of physics, chemistry, material science and biology is valuable in terms of the synthesis of new azide metal complexes, revealing new results by investigating their different properties, as well as contributing to the development of new technologies.

α-Glucosidase enzyme (EC 3.2.1.20), having a significant impact on the digestion and absorption of carbohydrates, is found in the small intestines of the digestive system and is known to provide the digestive process by breaking down complex carbohydrates into simple sugars [20–24]. With the help of this enzyme, the 1,4-glycosidic bond in polysaccharides is hydrolyzed, resulting in the creation of α-D-glucose. As a result, during absorption, α-D-glucose is formed and enters the circulation, which raises postprandial hyperglycemia [23,25]. The activity of the α-glucosidase enzyme is a process regulated by using α-glucosidase inhibitors, which bind to the α-glucosidase enzyme and reduce or stop its activity, as well as slowing down the digestive process and allowing carbohydrates to be absorbed more slowly. It is noteworthy that α-glucosidase inhibitors are widely used in the treatment of Type 2 diabetes and that Type 2 diabetes is a common metabolic disease worldwide. Acarbose, miglitol and voglibose, which function as α-glucosidase inhibitors, are currently used as clinically prescribed drugs in the treatment of Type 2 diabetes [22]. Although some side effects of these inhibitors cause digestive system problems such as abdominal pain, diarrhea and bloating, there are already many studies using α-glucosidase inhibitor [26–40]. Therefore, scientists are studying new enzyme inhibitors [41–45] associated with various diseases. They aim to develop options and clinical treatments [46] that are both safer and more effective against specific targets. The synthesis of more effective new inhibitors taking these effects into consideration continues to be an important research topic today.

In the development of science and technology, it is extremely important to correlate quantum chemical results with experimental results and calculate quantities that can be obtained directly from experimental measurements. Many studies conducted in recent years show that theoretical and experimental research are handled together and density functional theory (DFT) methods are used extensively. The electronic structure and characteristics of molecular systems (organic, inorganic, etc.) are extensively studied. This is achieved using the DFT levels [47–50], providing valuable insights into their properties and behavior. Additionally, further advancements in understanding are facilitated through the application of more sophisticated computational methods [51–53]. The ligands used in these systems allow examining the electronic structure, geometry, spectral and optical properties of coordination compounds consisting of metal ions/atoms and obtaining detailed information about the structure. In addition to comparing the values calculated using DFT methods with experimental data, it is important to shed light on the stability, electronic transitions, optical properties and magnetic behavior of metal complexes and to enable the design of new materials for various applications. The development of improved exchange-correlation functionals and the inclusion of solvent effects have further enhanced the predictive power of DFT in studying metal complex behavior. It seems that the selection of functionals suitable for the complex structure from the developed exchange-correlation functionals and the inclusion of solvent effects further increase the predictive power of DFT in examining metal complex behavior. CAM-B3LYP (a long-range corrected version of B3LYP using the Coulomb attenuation method from Handy and co-workers) [54] and ωB97XD (the last functional including empirical dispersion and long-range corrections suggested by Head-Gordon and co-workers) [55,56] functionals are known to reliably predict the geometries of metal complexes, energies and spectroscopic properties, making them a popular choice for a wide range of applications.

Azomethine and azide groups are regarded as highly potent ligands in medicinal applications of coordination chemistry [5,17,20,22]. Because these ligands have a high degree of coordination flexibility, which can also participate in the formation of monodentate, bidentate or multidentate complexes. Moreover, it is well-known that they play important roles in potential biological activities. Therefore, these ligands were chosen in the synthesis of target complexes. So as to design and create more powerful α-glucosidase inhibitors, novel five metal complexes (**12–16**) including *N*-methyl-1-(pyridin-2-yl)methanimine (L_1) and azide (N_3^-) ligands were synthesized as a result of our ongoing studies. The structures of these complexes (**12–16**) were determined by ^{1}H and ^{13}C NMR (except for complex **12** including Cu ion), mass (LC-HRMS) and FTIR spectra. The IC_{50} values against α-glucosidase were obtained. *In vitro* α-glucosidase study on synthesized complexes and examination of their electronic properties by experimental and DFT methods play an important role in determining the structure–activity relationship. In addition, molecular docking study was conducted to determine the interactions of the target protein with the ligands and to interpret the activity results. Furthermore, the unique properties and capabil-

ities of the DFT/ωB97XD and DFT/CAM-B3LYP functionalities allow these methods to obtain deeper insights into the behavior of metal complexes in structure–property relationships.

2. Experimental & computational details

2.1. Spectroscopic implements

The NMR spectrometer (Varian Infinity Plus, Oxford, UK) was utilized to define the structure of the synthesized the *N*-methyl-1-(pyridin-2-yl)methanimine (L_1) ligand and complexes **13–16**. The synthesized compounds were dissolved in 500 μl of DMSO-d_6 containing tetramethylsilane (0.03 vol. %) as an internal standard. Temperature of the samples during the data acquisition was at 29°C. The ^{1}H and ^{13}C NMR measurements were fulfilled at 300 and 75 MHz, respectively. The ^{1}H and ^{13}C NMR spectra for each sample were obtained with 32 and 5000 accumulations, and pulse angles were 45 and 20 degrees, respectively. The structures of novel five metal complexes (**12–16**) were determined by using the SHIMADZU LCMS-9030 (OR, USA) model triple quadrupole liquid chromatograph mass spectrometer. The concentrations of samples were prepared at 50 ppm in methanol. LC-MS spectra were recorded at the following conditions: Mobile phase A: acetonitrile; Mobile phase B: water; pump system A:B concentration: 50:50%; flow: 0.5000 ml/min; pump A and B pressures: 30 bar; oven temperature: 28.7°C; interface type: electrospray ionisation; interface voltage (+)/(-): +4.50/-3.50 kV. The FT-IR spectra in the range of 4000–400 cm^{-1} for complexes **12–16** in powder form were recorded at the Perkin Elmer UATR-TWO (Perkin Elmer Spectrum-two equipped with ATR) spectrophotometer (CT, USA). The methanolic solutions of samples were prepared at 10^{-5} M and electronic absorption wavelengths (UV-Vis spectra) in the 900-200 nm range were obtained with the SHIMADZU UV-2600 UV-Vis spectrophotometer. Using the CHNS-932 (Leco, MI, USA) elemental analyzer, elemental studies of the synthesized complexes **12–16** in powder form were carried out.

2.2. The synthesis of the N-methyl-1-(pyridin-2-yl) methanimine (L_1) & complexes 12–16 {[$Cu_2(L_1)_2(N_3)_3$], (12), [$Hg(L_1)_2(N_3)\cdot H_2O$], (13), [$Cd(L_1)_2(N_3)$], (14), [$Ag(L_1)(N_3)_2\cdot 2H_2O$], (15), [$Zn_2(L_1)_2(N_3)_2Cl_2\cdot 4H_2O$], (16)}

2-Pyridinecarboxaldehyde (99%), methylamine solution (33 wt.% in absolute ethanol), sodium azide (≥99.5%), copper(II) acetate monohydrate (≥99.0%, $Cu(OAc)_2\cdot H_2O$), mercury(II) acetate (≥98.0%, $Hg(OAc)_2$), cadmium(II) acetate (99.995%, $Cd(OAc)_2$), silver nitrate (≥99.0%, $AgNO_3$), zinc chloride (≥98%, $ZnCl_2$) reagents, magnesium sulfate (anhydrous, ≥99.5%), triethylamine (for synthesis), ethanol (absolute for analysis), dimethyl sulfoxide-D6 (DMSO-d_6, ≥99.8%) purchased from Sigma-Aldrich (Sternheim, Germany) and Merck (Darmstadt, Germany) were utilized without any special reprocessing. Figure 1 depicts the synthesis methods of complexes **12–16**.

The synthesis and NMR spectra of the *N*-methyl-1-(pyridin-2-yl)methanimine is presented in Supplementary Material (Supplementary Figure S1).

Synthesis of complexes **12–16** (Figure 1): 1 mmol of corresponding metal salts ($(Cu(OAc)_2\cdot H_2O$/$Hg(OAc)_2$/$Cd(OAc)_2$/$AgNO_3$/$ZnCl_2$) were added to *N*-methyl-1-(pyridin-2-yl)methanimine (L_1) (2 mmol) dissolved in 15 ml of absolute ethanol. After 20 min, 2 mmol NaN_3 dissolved in 5 ml water was added to this solution. The mixture was stirred at ambient temperature for overnight (complexes **12–14**) or for 3 h (complexes **15**,**16**), then allowed to evaporate at ambient temperature. It took around 7 to 10 days to acquire complex compounds in powder form. The structures of these products (**12–16**) were confirmed by ^{1}H and ^{13}C NMR (except for complex **12** including Cu ion), and mass spectroscopy. Complex **12**: Anal. Calc. for $C_{14}H_{16}Cu_2N_{13}$: C, 34.08; H, 3.27; N, 36.90; found: C, 34.42; H, 3.45; N, 36.63. Calculated exact mass (m/z): 492.0244 ($C_{14}H_{16}Cu_2N_{13}$); found: LC-HRMS (m/z): 492.9582 ([M]$^+$). Complex **13**: ^{1}H NMR (DMSO-d_6, 300 MHz) δ/ppm: 8.66 (1H, d, J = 4.6 Hz), 8.62 (1H, s), 7.99–8.05 (1H, m), 7.91–7.94 (1H, m), 7.60–7.66 (1H, m), 3.51 (3H, s). ^{13}C NMR (DMSO-d_6, 75 MHz) δ/ppm: 162.65, 162.60, 150.70, 150.65, 147.55, 140.98, 140.90, 129.24, 129.22, 129.20, 129.16, 128.30, 46.93, 46.84. Anal. Calc. for $C_{14}H_{18}HgN_7O$: C, 33.57; H, 3.62; N, 19.57; found: C, 33.86; H, 3.84; N, 19.02. Calculated exact mass (m/z): 502.1279 ($C_{14}H_{18}HgN_7O$); found: LC-HRMS (m/z): 502.7797 ([M]$^+$). Complex **14**: ^{1}H NMR (DMSO-d_6, 300 MHz) δ/ppm: 8.72 (1H, d, J = 4.7 Hz), 8.51 (1H, d, J = 1.5 Hz), 8.05–8.12 (1H, m), 7.90–7.93 (1H, m), 7.63–7.68 (1H, m), 3.41 (3H, s). ^{13}C NMR (DMSO-d_6, 75 MHz) δ/ppm: 161.89, 150.06, 150.02, 140.70, 128.49, 127.45, 46.36. Anal. Calc. for $C_{14}H_{16}CdN_7$: C, 42.60; H, 4.09; N, 24.84; found: C, 42.12; H, 3.86; N, 25.27. Calculated exact mass (m/z): 396.0501 ($C_{14}H_{16}CdN_7$); found: LC-HRMS (m/z): 399.0392 ([M+2H]$^+$). Complex **15**: ^{1}H NMR (DMSO-d_6, 300 MHz) δ/ppm: 8.64 (1H, d, J = 4.2 Hz), 8.52 (1H, d, J = 1.5 Hz), 7.99–8.05 (1H, m), 7.86–7.88 (1H, m), 7.58–7.62 (1H, m), 3.56 (3H, s). ^{13}C NMR (DMSO-d_6, 75 MHz) δ/ppm: 163.83, 151.61, 150.98, 139.06, 127.43, 125.50, 48.66. Anal. Calc. for $C_7H_{12}AgN_8O_2$: C, 24.15; H, 3.47; N, 32.19; found: C, 24.84; H, 3.75; N, 31.82. Calculated exact mass (m/z): 347.0134 ($C_7H_{12}AgN_8O_2$); found: LC-HRMS (m/z): 348.7087 ([M]$^+$). Complex **16**: ^{1}H NMR (DMSO-d_6, 300 MHz) δ/ppm: 8.65 (1H, s, br), 8.58 (1H, s), 8.16 (1H, s,

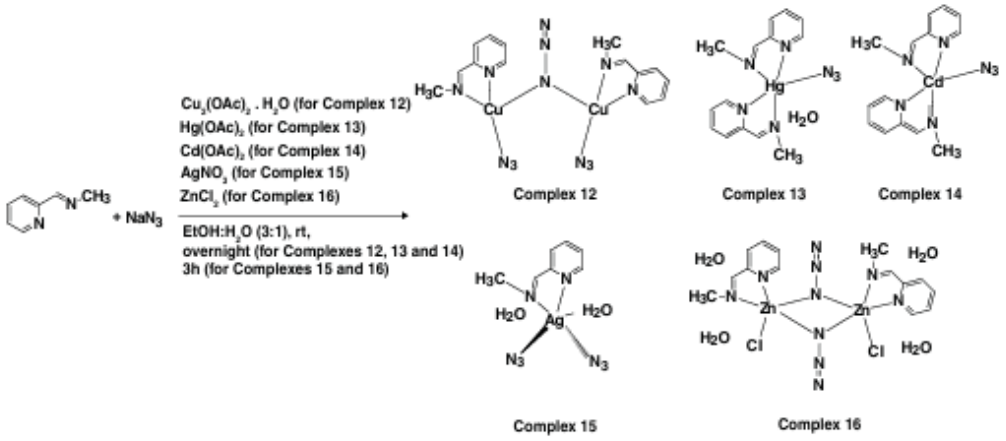

Figure 1. Synthesis of complexes **12–16.**
rt: Room temperature.

br), 8.00 (1H, s, br), 7.73 (1H, s, br), 3.37 (3H, s). ^{13}C NMR (DMSO-d_6, 75 MHz) δ/ppm: 162.43, 162.39, 149.76, 149.66, 140.64, 140.61, 128.22, 128.14, 128.08, 126.09, 126.02, 45.62, 45.54. Anal. Calc. for $C_{14}H_{24}Cl_2N_{10}O_4Zn_2$: C, 28.12; H, 4.04; N, 23.42; found: C, 28.65; H, 4.48; N, 22.94. Calculated exact mass (m/z): 593.9942 ($C_{14}H_{24}Cl_2N_{10}O_4Zn_2$); found: LC-HRMS (m/z): 597.1465 ([M+2H]$^+$). The ^{1}H and ^{13}C NMR (except for complex **12** including Cu ion), and mass (LC-HRMS) spectra were presented in Supplementary Material (Supplementary Figures S2–S10).

2.3. α-Glucosidase inhibitor activity

The IC_{50} values against α-glucosidase of complexes **12–16** were defined taking into considering reported previously [30–32,36]. The detailed technique of α-glucosidase assay was provided in Supplementary Material. Taking into account A_c (the absorbance of the control) and A_s (the absorbance of the samples) in the equation below, the IC_{50} values against α-glucosidase for complexes **12–16** were obtained.

$$\text{Glucosidase inhibition\%} = \left[\frac{(A_c - A_s)}{A_c}\right] \times 100$$

The calculations of IC_{50} for complexes **12–16** were used the Graphpad Software.

2.4. Computational details

To investigate the features of structural, vibrational, electronic and nonlinear optics (NLO), the Gaussian 16, Revision C.01 [57] and GaussView 6 [58] programs were utilized. The CAM-B3LYP [54] and ωB97XD methods [55,56] with 6–311+G(d,p)//LanL2DZ [59,60] basis set in the ground state were applied to obtain the optimum geometrical structures, vibrational frequencies and natural bond orbital (NBO) results for complexes **12** and **16**. For complexes **13–15**, the same properties were examined by considering DFT/CAM-B3LYP and ωB97XD/LanL2DZ levels. Time-dependent DFT (TD–DFT) levels [61] with the conductor-like polarizable continuum model (CPCM) [62] were used to investigate electronic absorption wavelengths (λ) and oscillator strength of complexes **12–16** in MeOH. The SWizard [63] and Chemissian [64] programs were applied to define major contributions in electronic transitions. By using the CAM-B3LYP and ωB97XD levels in gas phase, the NLO properties (the parameters of microscopic polarizabilities (α and $\Delta\alpha$), first- and second-order hyperpolarizabilities (β and γ) via equations presented in Supplementary Material were examined. Finally, the DFT/CAM-B3LYP level was utilized to survey the molecular electrostatic potential (MEP) surfaces.

2.5. Docking procedure

AutoDock4 program [65] and AutoDockTools (ADT1.5.7) [66] was utilized to examine the interactions between the *Saccharomyces cerevisiae* isomaltase (Protein Data Bank [PDB] ID: 3A4A) template structure provided from the Protein Data Bank and synthesized complexes **12–16**. By considering the optimized structures of complexes **12–16** and genistein obtained at the DFT/CAM-B3LYP method, the inhibition constants (K_i) and binding energies of these complexes were calculated from docking findings. The Discovery Studio 4.0 program [67] provides 2D and 3D views of interactions between amino acid residues in enzyme structure and

complexes **12**, **13** and **15**. The docking details are also given in Supplementary Material.

3. Results & discussion

3.1. The chemical descriptions of the produced complexes

The *N*-methyl-1-(pyridin-2-yl)methanimine (L_1) was characterized by ^{1}H and ^{13}C NMR spectra. The structures of synthesized complexes **12–16** were verified by using ^{1}H and ^{13}C NMR (except for complex **12** including Cu ion), mass spectra (Supplementary Figures S2–S10), as well as FTIR spectra. The aromatic proton signals for L_1 appeared at the range of 7.44 and 7.93 ppm, aromatic CH neighbor pyridine-N and CH protons belonging to imine were observed at 8.61 and 8.33 ppm, respectively (in ^{1}H NMR spectra given in Supplementary Figure S1). In ^{1}H NMR spectra of complexes **13–16**, the aromatic protons, aromatic CH neighbor pyridine-N and CH protons belonging to imine shifting the peak downfield were obtained at the range from 7.58 to 8.16 ppm, from 8.64 to 8.72 ppm, and from 8.51 to 8.62 ppm, respectively (Supplementary Figures S3, S5, S7 & S9). The aromatic carbon signals for the L_1 ligand emerged at the range of 120.89 and 163.84 ppm, while these carbon signals for complexes **13–16** were detected at the range from 125.50 to 163.83 ppm (in ^{13}C NMR spectra given in Supplementary Figures S1, S3, S5, S7 & S9). The carbon signal belonging to imine in L_1 ligand was observed at 154.81 ppm, whereas this signal shifting the peak upfield was obtained at the range of 149.76 and 151.61 ppm in complexes **13–16** (Supplementary Figures S3, S5, S7 & S9). Considering these chemical shifts in upfield or downfield in NMR spectra of L_1 ligand and complexes **13–16**, the forming of complexes was supported. Besides, the structures of complexes **12–16** verified by mass spectra (Supplementary Figures S2, S4, S6, S8 & S10).

Supplementary Figure S11 displays the optimized structures (obtained at DFT/CAM-B3LYP) of complexes **12–16** confirmed by ^{1}H and ^{13}C NMR (except for complex **12** including Cu ion), and mass spectra (Supplementary Figures S2–S10). DFT/ωB97XD and DFT/CAM-B3LYP levels were applied to obtain the geometrical parameters (bond lengths and angles and dihedral angles) given in Supplementary Table S1. The azide ions (N_3^-), can both enable the assembly of binuclear complexes and bind to transition metal atoms with different coordination modes [68].

Complex **12** $[(Cu)_2(L_1)_2(N_3)_3]$ consists of the coordination of two L_1 ligands and one azide ligand with Cu(II) ion by forming a bridge with two Cu(II) ions over the N atom of the azide ligand. It was understood that a complex structure with distorted tetrahedral geometry was formed by the coordination of the L_1 ligand and azide ligands to Cu(II) ions via N atoms.

Complex **13** $[Hg(L_1)_2(N_3)\text{-}H_2O]$ and complex **14** $[Cd(L_1)_2(N_3)]$ consist of the coordination of two L_1 ligands and an azide ligand with the Hg(II) and Cd(II) ions, respectively. It was understood that both complex structures with distorted trigonal bipyrimidal geometry was formed when two L_1 ligands and an azide ligand coordinated to the Hg(II) and Cd(II) ions via N atoms. Besides, complex **13** includes the uncoordinated water molecule.

Complex **15** $[Ag(L_1)(N_3)_2\cdot 2H_2O]$ is comprised of an L_1 ligand and the coordination of two azide ligands with an Ag(I) ion. It was understood that a complex structure with distorted tetrahedral geometry was formed when an L_1 ligands and two azide ligands coordinated to the Ag(I) ion via N atoms. Complex **15** contains also the uncoordinated two water molecules.

Complex **16** $[(Zn)_2(L_1)_2(N_3)_2Cl_2\cdot 4H_2O]$ consists of the coordination of two L_1 and azide ligands and a Cl atom with Zn(II) ion by forming a tetrahedral bridge with two Zn(II) ions over the N atoms of two azide ligands. It was understood that a complex structure with distorted trigonal bipyramidal geometry was formed by the coordination of an L_1 and two azide ligands and a Cl atom to Zn(II) ion via N atoms.

These results are consistent with the coordination geometries of Cu(II), Zn(II) and Ag(I) coordinated with different ligands [1,2,5,6,69,70].

Supplementary Table S1 contains theoretical some geometrical parameters for complexes **12–16**. These complexes are comprised of five-membered chelate rings occurred by L_1 ligand with metal ions. For complexes **12–16**, the M(metal)–N2 bond lengths between the metal ion and pyridine N atom of the complexes were obtained at 2.143, 2.350, 2.418, 2.253, 2.280 Å by using DFT/CAM-B3LYP level. The similar bond lengths between the metal ion and imine N atom of the complexes were calculated at 2.086, 2.509, 2.263, 2.355, 2.135 Å by using the same DFT level, respectively. In addition, in all complexes, the theoretical bond lengths obtained by the DFT/ωB97XD level are similar trends. For complexes **12–16**, the N2–M–N5 bond angles among imine N, metal ion and azide N in the coordination environment were found to be 78.09, 71.93, 68.82, 73.12, 74.87° with DFT/CAM-B3LYP level, respectively. On the other hand, the N–M–N bond angles among imine/pyridine N, metal ion and azide N in the coordination environment were observed the values greater or less than 90°, regardless of coordination geometry. These results indicate the presence of a distorted coordination geometry in the synthesized complexes **12–16**. Despite the coordination environment/geometry differences, the theoretical results of the complexes are compatible with the previously reported ones [1,2,4,5,69–71].

Studying conjugative interactions, charge transfer in molecular systems and intra- and inter-molecular bonding are accomplished successfully with NBO analysis [72–74]. By considering the second-order perturbation approach [75,76], the hyperconjugative interactions were obtained. In NBO analysis, the large $E^{(2)}$ energy value is an indication that the interactions between electron acceptors and electron donors are more intense and intramolecular and intermolecular charge transitions are high. The natural bond orbital calculation outcomes of the synthesized complexes **12–16** are given in Supplementary Table S2. The interactions between LP(n) nitrogen orbital pairs and LP*(n) metal(II)/(I) (Cu(II), Hg(II), Cd(II), Ag(I), Zn(II)) displayed the n→n* interactions indicate the coordination environment around the metal ions in the complex structures. The $E^{(2)}$ values belonging to these interactions were obtained at the range of 6.01 and 47.25 kcal/mol at the DFT/CAM-B3LYP level (Supplementary Table S2). Additional significant interactions in the complexes indicate stabilization within the L_1 ligand. It is concluded that the bonding and antibonding orbitals exhibit charge transfer (CT) interactions, which cause the system to stabilize.

The FTIR spectra for the synthesized complexes **12–16** demonstrate the wavenumbers in the range of 4000–400 cm^{-1}. The corresponding theoretical vibrational frequencies computed at the DFT/ωB97XD and DFT/CAM-B3LYP levels to get closer to the experimental IR spectra were multiplied by 0.96. The experimental and theoretical characteristic vibrational wavenumbers were presented in Supplementary Figure S12, Supplementary Tables S1 & S4. The $\nu_{CH(ring)}$, $\nu_{CH(imine)}$ and $\nu_{CH(methyl)}$ stretching modes appeared at the range from 3095 to 2926 cm^{-1} for complex **12**, from 3137 to 2931 cm^{-1} for complex **13**, from 3089 to 2919 cm^{-1} for complex **14**, from 3070 to 2917 cm^{-1} for complex **15**, from 3070 to 2910 cm^{-1} for complex **16**. These results are coherent with previously reported for the Schiff base metal complexes [3,18,21,28,29,31,68]. The corresponding ones for complexes **12–16** obtained at DFT/ωB97XD were found at 3093–2904 cm^{-1} range, 3150–2895 cm^{-1} range, 3089–2897 cm^{-1} range, 3117–2927 cm^{-1} range and 3073–2910 cm^{-1} range, respectively (Supplementary Tables S3 & S4). The vibrational bands emerging at the range of 2032 and 2060 cm^{-1} were assigned as ν_{NN} asymmetric stretching modes belonging to the azide ligand. These findings are compatible with the modes reported in different complexes [2,4,5]. Theoretical these bands were calculated at 1885 and 2178 cm^{-1}, and 1844 and 2185 cm^{-1} ranges, in order of the DFT/ωB97XD and DFT/CAM-B3LYP levels. Moreover, the $\nu_{C=N(imine)}$ stretching modes of the C=N bond (imine) of the L_1 for complexes **12–16** observed at 1654, 1653, 1658, 1648 and 1655 cm^{-1} were obtained theoretically at 1662, 1671, 1687, 1692 and 1701 cm^{-1} (with DFT/ωB97XD level), respectively (Supplementary Tables S3 & S4). Besides, the $\nu_{NC(imine)}$ stretching modes of the N–CH_3 bond of the L_1 for complexes **12–16** emerged at the range of 1015 and 1028 cm^{-1} range, and the corresponding values computed at DFT/ωB97XD and DFT/CAM-B3LYP levels were obtained at the range of 1011 and 1025 cm^{-1}, 1006 and 1023 cm^{-1}, respectively. The $\nu_{CC(ring)}$ stretching modes attributed to ring C=C bond emerged within the ranges 1588–1623 cm^{-1} in FTIR spectra, 1589–1614 cm^{-1} in DFT/ωB97XD level, and 1588–1615 cm^{-1} in DFT/CAM-B3LYP level, as can be seen in Supplementary Tables S3 & S4. These results are consistent with similar group frequency values in different structures in previous reports [5,20,22,26–28,71]. The vibration bands appearing at 1341, 1304, 1330, 1333 and 1340 cm^{-1}, which are assigned as the $\nu_{NN(azide)}$ symmetric stretching vibration, are attributed to the coordination of the metal ion with the N atom of the azide. The corresponding vibrational modes obtained at DFT/ωB97XD and DFT/CAM-B3LYP levels were found at the range from 1291 to 1362, and from 1283 to 1359 cm^{-1}, respectively. The $\beta_{HCC(ring)}$ in-plane bending modes appeared at the range of 1039 and 1573 cm^{-1} in FTIR spectra were found at the range 1039 and 1591 cm^{-1} in DFT/ωB97XD level, and range 1036 and 1590 cm^{-1} DFT/CAM-B3LYP level. Furthermore, the detailed stretching, in-plane and out-of-plane bending, torsion vibrational modes belonging to ring, azide, imine and methyl groups for complexes **12–16** are tabulated in Supplementary Table S4.

3.2. Analysis of the electronic absorption spectra & electronic transitions

The electronic absorption spectra and the plot of experimental E_g (optical band gap energy) in methanol for synthesized complexes **12–16** are given in Figure 2. The corresponding theoretical wavelengths, oscillator strengths as well as major contributions to the electronic transitions were computed at TD-DFT/ωB97XD and TD-DFT/CAM-B3LYP levels. Additionally, the molecular orbitals and atoms/functional groups that make important contributions to electronic transitions were determined with the SWizard [63] and Chemissian [64] programs. According to Figure 2A, three absorption peaks appeared in bridge-structured complexes **12** and **16**, while two maximum absorption peaks emerged in other complexes **13–15**. In complex **12**, the absorption peaks appeared at 371.1, 264.5 and 203.5 nm, while in complex **16**, the absorption peaks emerged at 280.6, 231.5 and 213.8 nm. The absorption peaks of 251.1 and 207.3 nm for complex **13**, 264.5 and 244.5 nm for complex **14**, and 258.4 and 204.6 nm for complex **15** were detected (Supplementary

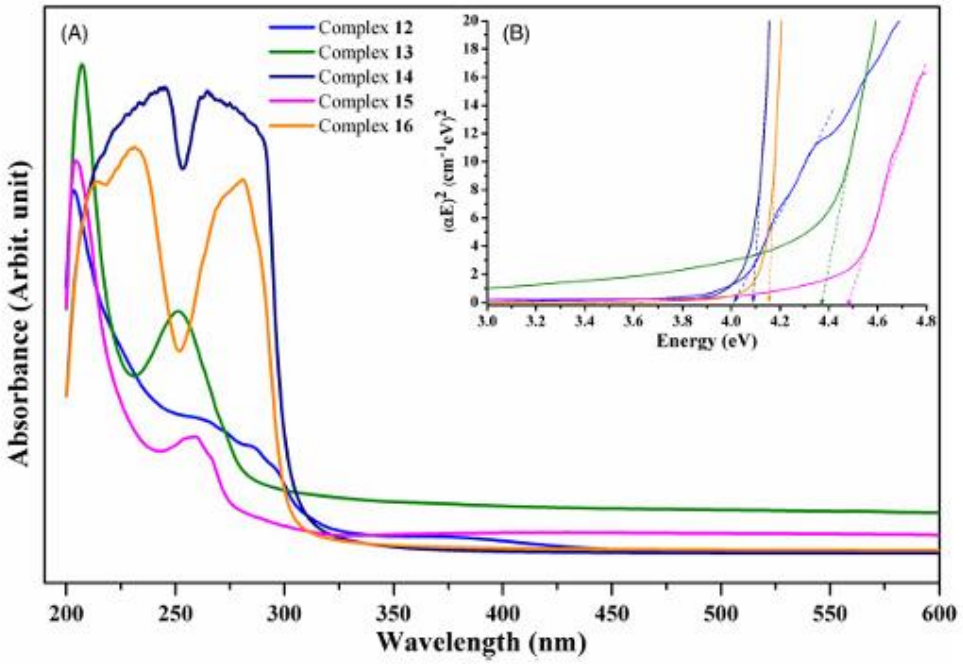

Figure 2. Optical spectra. **(A)** The UV-Vis spectra and **(B)** the plot of experimental E_g (optical band gap energy) in methanol for complexes **12–16.**

Table S5). These peaks were attributed to intra-ligand $\pi \rightarrow \pi^*$, ligand-to-metal/metal-to-ligand and $n \rightarrow \pi^*$ transitions. Figure 3 displays ligand-ligand charge transfer in the high energy region as charge transitions within the ligand.

It has been reported that large contributions from metal orbitals to the lowest occupied molecular orbital (LUMO) in complex structures can increase the π-acceptor property of the ligand [77]. The metal orbital contributions to the highest occupied molecular orbital (HOMO)/HOMOs and LUMO/LUMOs of complexes **12–16** were obtained at the range from 2 to 37% (HOMO/HOMOs) and from 3 to 37% (LUMO/LUMOs), by using TD-CAM-B3LYP level. The LUMO/LUMOs contributions of the L_1 including 2-pyridyl and imine groups, and azide (N_3) ligands for complexes **12–16** vary between 20 and 100% (in L_1), 0 and 45% (in N_3), respectively (Supplementary Table S5). Due to the obtained larger LUMO/LUMOs contributions for L_1, the L_1 ligand has the more electron acceptor property. It is clear from Figure 3 that the electron density for complex **12** is localized in the Cu ion, L_1, and azide on one side for the HOMO α-level, localized in the L_1 and azide on the other side for LUMO α-level. In complexes **13** and **14**, HOMO and LUMO α-levels are localized on the L_1 ligand including pyridyl and imine group in opposite parts. For the HOMO α-levels of complexes **15** and **16**, the electron density is mostly localized on the metal ions and azide ligand, while in the LUMO α-levels, it is predominantly located on the L_1 ligand. (Figure 3). Supplementary Table S5 shows the remarkable metal-to-ligand charge transfer (MLCT), ligand-to-ligand charge transfer (LLCT) and ligand-to-metal charge transfer (LMCT) transitions. The 54% contribution for HOMO→LUMO α spin for complex **12** depicts the MLCT transition obtained at the contributions of Cu (20%), L_1 (30%) containing pyridyl (22%) and imine (8%) groups and N_3 (50%) ligand in HOMO, and L_1 (61%) and N_3 (36%) in LUMO. In complex **13**, the absorption wavelength obtained at 536.2 nm (f = 0.0007) displays the contribution of 99% HOMO→LUMO changing from pyridyl (45%), imine (51%), H_2O (2%) to pyridyl (60%), imine (38%), N_3 (2%) and attributed to the LLCT transition. The LMCT transition for complex **15** was calculated at the contribution of 43% H-1→L β spin coming from pyridyl (7%), imine (2%), N_3 (90%) to Ag (37%), pyridyl (11%), imine (9%), N_3 (43%). The detailed percentage contributions in HOMOs→LUMOs transitions and assignments for HOMOs and LUMOs were presented in Supplementary

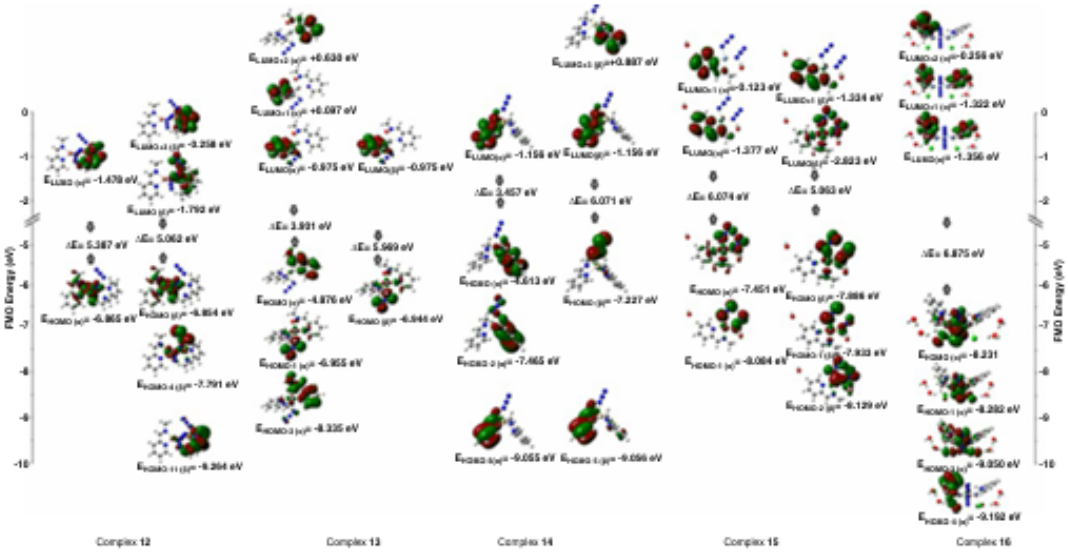

Figure 3. Frontier molecular orbitals and their energies that contribute the most to the electronic transition obtained by the DFT/CAM-B3LYP method in methanol for complexes **12–16.**
DFT/CAM-B3LYP: Density functional theory/Coulomb attenuation method- Becke, 3–parameter, Lee–Yang–Parr; FMO: Frontier molecular orbital: HOMO: Highest occupied molecular orbital; LUMO: Lowest occupied molecular orbital.

Table S5, considering the metal ion and its environments. The frontier molecular orbital contributions in electronic transitions obtained DFT/ωB97XD level are presented in Supplementary Table S6.

MEP surfaces are used to understand the structure–activity relationship (SAR) for many molecular systems. These surfaces are related to electron density. The red and yellow areas on the MEP surface illustrate the negatively charged region with high electron density while the blue areas are spaces with positive charges. Green areas depict spaces where there is no potential and it is neutral [78]. MEP surfaces of complexes **12–16** were described by DFT/CAM-B3LYP level. The regions of complexes **12–16** with the highest electron density are shown in Supplementary Figure S13, where lone pairs of electronegative atoms are linked to the strong red electron clouds around the azide ligand. Areas showing nucleophilic reactivity were observed around the -CH groups in the L_1 ligand, which has the highest positive potential. In this way, the possible hydrogen bond interactions and reactive parts can be revealed in these complexes.

It is concluded from Figure 2B that the experimental optical band gap energy (Eg) values of complexes **12–16** were obtained at 4.01, 4.37, 4.09, 4.48 and 4.16 eV, in order. The HOMO-LUMO band gap results obtained from DFT/CAM-B3LYP calculations in α-spin level were obtained at 5.172, 3.797, 2.952, 5.672 and 6.422 eV, respectively. It seems that there are consistent results between experimental and theoretical approach errors.

Molecular parameters χ (electronegativity), η (chemical hardness), S (chemical softness), ω (electrophilicity), φ (nucleophilicity) were calculated using HOMO and LUMO energy values [79] and their results are given in Supplementary Table S7. Chemical hardness (η) is known as the resistance of chemical systems to changing their electronic distribution. The η, χ, S parameters are indicators of chemical reactivity and stability of systems. The χ, η, S, ω and φ parameters of complexes **12–16** in α spin obtained at the DFT/CAM-B3LYP level were found at the range from 2.957 to 4.645 eV, from 1.476 to 3.211 eV, from 0.311 to 0.678 1/eV, from 2.302 to 3.360 eV, from 0.298 to 0.434 1/eV, respectively, seen in Supplementary Table S7. The low η parameters obtained in these synthesized complexes indicate that intra-ligand charge transfer (ILCT) occurs. These results are coherent with previously reported ones in different structures [77,80].

3.3. The analysis of nonlinear optics parameters

The synthesis and related computational research of NLO materials have been intensively studied due to their potential applications in optoelectronics and telecommunications technology, such as data storage and processing [81–87]. Theoretical NLO studies are taken into consideration in order to calculate the response of molecules to these properties if doing an experimental investigation is not feasible on the NLO properties of newly synthesized molecules. The findings obtained from these stud-

ies have the potential to shed light on electronic devices that are considered to be developed or designed. In this context, the $\overline{\alpha}$ and $\Delta\alpha$ indicating the linear optical (LO), β/γ demonstrating the second-/third-order NLO parameters of complexes **12–16** were obtained at DFT/ωB97XD and DFT/CAM-B3LYP levels in gas phase by using equations (7)-(10) [81,83] given in Supplementary Material, as can be seen in Supplementary Table S8.

To compare/evaluate the obtained theoretical results, p-nitroaniline (pNA) [88] and urea [89,90] were referenced as prototype compounds. According to the DFT/CAM-B3LYP level, the mean polarizability ($\overline{\alpha}$) values of complexes **12–16** in the gas phase obtained at 29.78×10^{-24} and 49.75×10^{-24} esu ranges exhibited higher than that of pNA (17×10^{-24} esu) [88]. It has been observed that the polarization tendency increases in the large molecules. On the other hand, the β parameters of complexes **12–16** in the gas phase were obtained at the range of 2.28×10^{-30} and 18.21×10^{-30} esu, 2.33×10^{-30} and 17.05×10^{-30} esu in order of the DFT/ωB97XD and /CAM-B3LYP levels (Supplementary Table S8). While these results were observed to be greater than the β results of urea (0.32×10^{-30} esu [89] and 0.130×10^{-30} esu [90]), lower values than those of pNA (9.2×10^{-30} esu [88]) were obtained, except for complexes **13,16**. Based on the γ values for complexes **12–16** in the gas phase in the same levels, the highest values of 85.71×10^{-36} and 96.93×10^{-36} esu for complex **12** were calculated while the smallest values of 1.66×10^{-36} and 15.32×10^{-36} esu for complex **15**. It is observed that the γ values of complex **12** are about 5.7/12.2 and 6.5/13.8-times higher than those of pNA (15×10^{-36} esu) [88]/urea (7×10^{-36} esu) [89]. It is concluded from the β and γ results that complexes **15** and **12** are high efficiency regarding the microscopic second- and third-NLO features, respectively. Depending on the electronic structure of the complexes, the effects of the metal ion and its coordination environment in the structure were also observed in the differences in the calculated NLO parameters.

3.4. α-Glucosidase inhibitory activity

The IC_{50} values for complexes **12–16** were obtained at the range from 0.2802 ± 0.62 and 420.88 ± 1.42 μM, seen in Table 1. Among these complexes against α-glucosidase, the complex **13** ($IC_{50} = 0.2802 \pm 0.62$ μM) exhibits the strongest inhibitory activity, whereas the complex **14** ($IC_{50} = 420.88 \pm 1.42$ μM) displays the lowest inhibition effect. Complex **13** ($IC_{50} = 0.2802 \pm 0.62$ μM) was observed at 48.39-times more effective compared with genistein ($IC_{50} = 13.56 \pm 1.21$ μM), utilized as a standard in this study.

For the SAR evaluation based on Table 1, the following results are deduced:

- The coordination of complex **13** $[Hg(L_1)_2(N_3)\cdot H_2O]$ and complex **14** $[Cd(L_1)_2(N_3)]$ were defined as a distorted trigonal bipyrimidal geometry. Complex **13** ($IC_{50} = 0.2802 \pm 0.62$ μM), having the larger atomic diameter of Hg, has better inhibitory activity than complex **14** ($IC_{50} = 420.88 \pm 1.42$ μM).
- The coordination of complex **12** $[(Cu)_2(L_1)_2(N_3)_3]$ and **16** $[(Zn)_2(L_1)_2(N_3)_2Cl_2\cdot 4H_2O]$ have a bridge structure with azide ligand. However, complex **12** was defined as a distorted tetrahedral geometry formed by the coordination of the L_1 ligand and azide ligands to Cu(II) ions via N atoms while complex **16** was described as a distorted trigonal bipyramidal geometry formed by the coordination of an L_1 and two azide ligands, and a Cl atom to Zn(II) ion via N atoms. Besides the differences in coordination geometry and environment between complexes **12** and **16**, complex **12** ($IC_{50} = 1.562 \pm 0.83$ μM) with a larger atomic diameter showed a higher inhibition effect than complex **16** ($IC_{50} = 171.5 \pm 1.72$ μM).
- Moreover, the α-glucosidase inhibition values of complexes **12** and **15** obtained at 1.562 ± 0.83 μM and 1.274 ± 0.32 μM, respectively. It can be stated that the small inhibition difference between complexes **15** and **12** is due to the difference in coordination in the structures as well as the fact that the atomic diameter of Cu metal is smaller than that of Ag.
- As a result, it is clear that there are differences in IC_{50} values depending on the role of metal ions and the coordination environment.

The different organic compounds were reported as α-glucosidase inhibitors with the IC_{50} values ranging from 4.51 ± 0.09 μM to 45.7 ± 0.23 μM [37–39]. The IC_{50} value of the Zn complex including N_2O_2 was observed at 0.23 mM [20]. In addition, the IC_{50} values of Cr, Mn, Co and Ni complexes including pyridine derivatives could not be observed but were obtained between 0.22 and 0.92 mM in other complexes [30,91,92]. Moreover, IC_{50} values for transition metal complexes between 6-methylpicolinic acid/Schiff-base and isothiocyanate were obtained at the range of 0.2376 ± 0.82 and >600 μM [30,71].

Additionally, it can be stated that complex **13** ($IC_{50} = 0.2802 \pm 0.62$) may be a good candidate for α-glucosidase inhibitor when the inhibition result is compared with previous studies involving similar metal ions [31,32,40,71,93,94]. The IC_{50} values of complexes **12** (1.562 ± 0.83) and **15** (1.274 ± 0.32) were also found to be significant. It is concluded that some metal complexes containing Schiff base and azide ligands tend to increase α-glucosidase inhibition.

Table 1. *In vitro* inhibition IC_{50} values (μM) for α-glucosidase of complexes **12–16** and ligands.

Ligand/complex	IC_{50} (μM)[†]
N-methyl-1-(pyridin-2-yl)methanimine ($\mathbf{L_1}$)	Not active
Sodium azide (NaN_3)	Not active
Complex **12** $[Cu_2(L_1)_2(N_3)_3]$	1.562 ± 0.83
Complex **13** $[Hg(L_1)_2(N_3)\cdot H_2O]$	0.2802 ± 0.62
Complex **14** $[Cd(L_1)_2(N_3)]$	420.88 ± 1.42
Complex **15** $[Ag(L_1)(N_3)_2\ 2H_2O]$	1.274 ± 0.32
Complex **16** $[Zn_2(L_1)_2(N_3)_2Cl_2\cdot 4H_2O]$	171.5 ± 1.72
Genistein	13.56 ± 1.21

[†]IC_{50} values represent the means ± S.E.M. of three parallel measurements ($p < 0.05$).

Since the structures in the synthesized complexes are not of similar geometry and coordination, a direct correlation is not expected between density functional theory calculations and the reactivity and α-glucosidase inhibitor activity of the compounds. In addition, the reactivities of the compounds depend on many different parameters (steric effect, reaction medium, structures of other components and nucleophilic and electrophilic behaviors, etc.). For these reasons, a direct relationship between the chemical reactivity parameter results calculated using DFT methods for these complexes and their inhibitor activities could not be obtained. However, an inverse correlation was observed between electric dipole moment and inhibitor activity of synthesized complexes. Complex **13**, the strongest inhibitor (IC_{50} = 0.280 μM) in this study, has the lowest dipole moment (μ = 5.87 Debye), while complex **14** and **16**, the weakest inhibitors (IC_{50} = 420.88 and 171.50 μM, respectively), have the highest dipole moment (μ = 12.25 and 11.77 Debye, respectively). On the other hand, a linear increase was seen between LUMO energies with rising inhibitory activity. Complex **13** has the highest E_{LUMO} energy, -1.058 eV, whereas E_{LUMO} energy of complex **14** is -1.538 eV.

3.5. Molecular docking & inhibition mechanism

Using the AutoDockTools (ADT1.5.7) [66] graphical user interface with the AutoDock4 software, the ligand–protein interactions of the complexes **12–16** were determined, and *S. cerevisiae* isomaltase (PDB ID: 3A4A) as target protein was considered as rigid. The binding energies and estimated inhibition constants (K_i) were defined by docking results. Discovery Studio 4.0 program [67] was utilized to display the 2D and 3D structures of the interactions between ligands and amino acid residues (Figures 4–6 & Supplementary Figures S14 & S15).

The binding energy values of the genistein taken as a standard inhibitor [71] and complexes **12–16** were found to be -6.35, -4.77, -4.97, -4.43, -4.93 and -4.70 kcal/mol, respectively. The K_i values related to these energies were calculated at 22.06 μM, 316.95 μM, 226.71 μM, 567.97 μM, 241.40 μM and 358.10 μM, respectively, seen in Table 2. The best inhibition values against α-glucosidase among complexes were obtained for complex **13** ($IC_{50} = 0.2802 \pm 0.62$ μM), at same time the lowest K_i value (26.71 μM) and binding energy (-4.97 kcal/mol) were calculated by considering docking results. The *in vitro* results were supported by docking study in order of complex from lowest to highest inhibitory activity.

Furthermore, the direct/indirect interactions with the enzyme active site change attaching to the coordination environment of complexes **12–16**. The interactions of some parts of complexes with amino acid residues are given in Table 2, Figures 4–6 & Supplementary Figures S14 & S15. These interactions can be listed as the conventional hydrogen bond, pi–cation, pi–sigma, pi–alkyl and charge–charge. By virtue of the docking results of complexes **12**, **13** and **15** exhibiting the best inhibition values against α-glucosidase among complexes, the interaction distance ranges from 2.53 to 4.92 Å emerged at the conventional hydrogen bond/pi-cation interactions between azide (N)/imine(C)/L_1(C) and amino acid residues Phe321(O)/Phe321, Lys523(O)/Phe321 and Pro312(O)/His280 for complexes **12**, **13** and **15**, respectively (Table 2). Besides, the other remarkable interactions demonstrate the pi–sigma for complexes **12**, **13**, the pi–alkyl for complexes **13**, **15**, as well as the pi–pi stacked for complex **15**. These interactions, having distance ranging from 3.34 to 5.37 Å, were observed between L_1 with amino acid residues Leu323(CD1)/Leu323(C) for pi–sigma, Lys524/Lys156 for pi–alkyl, and Tyr158 for pi–pi stacked. In comparison these results of the genistein, the conventional hydrogen bond and pi–alkyl interactions obtained at 2.73/2.45/3.29/2.88/3.14 and 4.19/5.25 Å distances are remarkable for Ile272/Ser298/Leu297/Ser291/Ala292 and Arg263/Ile272 residues with the C=O (benzopyran-4-one)/CO (5-hydroxy-benzopyran-4-one)/CO (7-hydroxy-benzopyran-4-one) and phenyl ring, seen in Table 2. Other than these interactions, having amide pi–pi stacked and pi–anion for complex **16** appeared at the distances of 5.57 and 4.06 Å, were depicted between Val404(C)/Glu405(N) and Glu405(OE2) residues and the *N*-methyl-1-(pyridin-2-yl)methanimine (L_1).

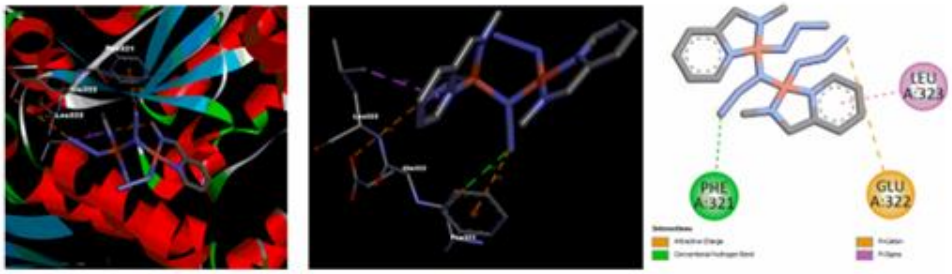

Figure 4. 3D- and 2D-structures displaying interactions between amino acid residues and ligands of the most active complex **12.**

Figure 5. 3D- and 2D-structures displaying interactions between amino acid residues and ligands of the most active complex **13.**

Figure 6. 3D- and 2D-structures displaying interactions between amino acid residues and ligands of the most active complex **15.**

The 1,4-glycosidic bond in polysaccharides is hydrolyzed via catalyzed by α-glucosidase, resulting in the creation of α-D-glucose. As a result, during absorption, α-D-glucose is formed and enters the circulation, which raises postprandial hyperglycemia [23,25]. α-glucosidase contains Asp, Glu, Gly, His, Phe, Thr, Tyr, Leu, Lys, etc. residues in the structure. Additionally, especially Arg, Asp, Glu, Trp and Tyr residues are located at the entrance of the active site of α-glucosidase and they have been played critical for the enzyme's catalytic activity [95–97]. As can be seen in Table 2, Figures 4–6 & Supplementary Figures S14 & S15, the synthesized complexes interacted with some of these residues by conventional hydrogen bond, pi–cation, pi–sigma, pi–alkyl and charge–charge interactions. It is considered that these interactions with the active pocket of glucosidase can hinder the substrate from entering, decrease the catalytic activity, and finally cause the inhibition of glucosidase activity. Moreover, hydrogen bond interactions can decrease the hydrophilicity of α-glucosidase and rise its hydrophobicity that supports to increase the stability of the inhibitor–enzyme complex.

A similar trend was obtained between docking K_i values and *in vitro* inhibition results. It is concluded that

Table 2. Protein–ligand interactions and distance values for complexes **12–16** and genistein.

Substrate	Receptor	Interaction	Distance (Å)	K_i (μM)	Binding energy (kcal/mol)	Ref.
Complex **12**				316.95	-4.77	
Azide (N)	Glu322 (OE1)	Charge–Charge	5.14			
Azide (N)	Phe321(O)	Conventional H-Bond	3.03			
Azide (N)	Phe321	Pi–Cation	4.92			
L_1	Leu323 (CD1)	Pi–Sigma	3.34			
Complex **13**				226.71	-4.97	
Azide (N)	Lys523 (O)	Conventional H-Bond	2.53			
Imine-CH_3 (C)	Gly361 (O)	Carbon H-Bond	3.36			
Imine (C)	Phe321	Pi–Cation	4.35			
L_1	Leu323 (C)	Pi–Sigma	3.43			
L_1	Lys524	Pi–Alkyl	5.37			
Complex **14**				567.97	-4.43	
L_1 (N)	Phe321	Pi–Cation	4.60			
L_1	Leu323	Pi–Alkyl	4.98			
L_1	Lys524	Pi–Alkyl	5.38			
Complex **15**				241.40	-4.93	
Azide (N)	Glu411 (OE2)	Charge–Charge	4.91			
Azide (N)	Asp242 (OD2)	Charge–Charge	4.03			
Azide (N)	Asp307 (OD1)	Charge–Charge	5.09			
Azide (N)	Asp307 (OD1)	Charge–Charge	4.08			
Azide (N)	Pro312 (O)	Conventional H-Bond	2.82			
L_1 (C)	His280	Pi–Cation	4.88			
L_1	Tyr158	Pi–Pi Stacked	4.65			
L_1	Lys156	Pi–Alkyl	5.34			
Complex **16**				358.10	-4.70	
Azide (N)	Val404 (O)	Conventional H-Bond	3.13			
Azide (N)	Tyr407 (O)	Conventional H-Bond	3.03			
Imine (N)	Tyr416	Pi–Cation	3.75			
Imine (C)	Tyr416	Pi–Cation	3.33			
Imine-CH_3 (C)	Tyr416	Pi–Cation	3.50			
L_1	Glu405 (OE2)	Pi–Anion	4.06			
L_1	Val404 (C)/Glu405 (N)	Amide–Pi Stacked	5.57			
L_1	Val404	Pi–Alkyl	5.50			
Genistein				22.06	-6.35	[71]
C=O (benzopyran-4-one)	Ile272	Conventional H-Bond	2.73			
CO (5-hydroxy-benzopyran-4-one)	Ser298	Conventional H-Bond	2.45			
CO (7-hydroxy-benzopyran-4-one)	Leu297	Conventional H-Bond	3.29			
CO (7-hydroxy-benzopyran-4-one)	Ser291	Conventional H-Bond	2.88			
CO (7-hydroxy-benzopyran-4-one)	Ala292	Conventional H-Bond	3.14			
Phenyl	Arg263	Pi–Alkyl	4.19			
Phenyl	Ile272	Pi–Alkyl	5.25			

the donor and acceptor properties in molecular systems may give rise to similarities and differences in localization, or delocalization of electron density in the molecule, as well as interactions with amino acid residues in the enzyme structure. Furthermore, by considering the enzyme kinetic studies [26,28,98], the majority of the metal complexes are non-competitive α-glucosidase inhibitors. Considering the literature, it is predicted that **12–16** complexes may be non-competitive inhibitors.

3.6. Molecular dynamic simulation

Molecular dynamic (MD) simulation calculations were performed for complexes **12–16** in ligands with the receptor using the GROMACS simulation package [99] via WebGro server [100]. Root mean square deviation (RMSD) profiles for protein–ligand complexes were assessed. The protein–ligand topology was generated by using Discovery Studio 4.0 program (Systèmes D. Dassault Systèmes Biovia; CA, USA) [67]. The MD simulation details are also given in Supplementary Material.

Considering that the stability of the system is inversely proportional to the amplitude of the fluctuations, the decrease in the stability of the systems is expressed by a higher RMSD value and higher fluctuations. It was determined that the α-glucosidase enzyme has an average RMSD of 0.24 nm. It appears to remain stable throughout the MD simulation, except for some large fluctuations between 20 and 30 ns (Supplementary Figure S16). The average RMSD of the α-glucosidase–compound-**13** system of 0.25 nm was obtained. While some fluctuations were observed during 15–25 ns, it was observed that the MD simulation remained stable until 50 ns.

The mean RMSD values of α-glucosidase–compound-**12/14/15** were calculated as 0.23, 0.26 and 0.31 nm, respectively. It was observed that α-glucosidase-**12/14/15** compounds were stable during the MD simu-

lation, except for a few minor/major deviations at 10–15, 15–20 and 10–20 ns, respectively. (Supplementary Figure S16). On the other hand, the average RMSD value of α-glucosidase–compound-**16** was obtained as 0.31 nm. It showed high stability throughout the entire 50 ns MD simulation, while some minor fluctuations were observed during 10–15 and 35–45 ns. Supplementary Figure S16 shows the RMSD plots for all complexes. It is thought that the amino acids in α-glucosidase cause fluctuations during the MD simulation because they have different structural regions (such as helices, β sheets and coil) [25].

4. Conclusion

In vitro α-glucosidase inhibitions and docking studies were performed on the *N*-methyl-1-(pyridin-2-yl)methanimine (L_1) and complexes **12–16** {$[Cu_2(L_1)_2(N_3)_3]$, (**12**), $[Hg(L_1)_2(N_3)\cdot H_2O]$ (**13**), $[Cd(L_1)_2(N_3)_2]$, (**14**), $[Ag(L_1)_2(N_3)_2\cdot 2H_2O]$, (**15**), $[Zn_2(L_1)_2(N_3)_2Cl_2\cdot 4H_2O]$, (**16**)} synthesized and characterized by ^{1}H and ^{13}C NMR (except for complex **12** including Cu ion), mass (LC-HRMS) and FT–IR spectra. The electronic spectral behaviors were investigated by UV–Vis spectra. The IC_{50} values of complexes **12–16** were obtained at the range from 0.2802 $\pm$ 0.62 to 420.88 $\pm$ 1.42 μM. The complex **13** demonstrates the best α-glucosidase inhibitory activity, while the complex **14** has the lowest inhibitory activity. Besides, the IC_{50} values of complexes **12** (1.562 $\pm$ 0.83) and **15** (1.274 $\pm$ 0.32) were also found to be significant. These results were backed up by the docking ones presenting receptor–ligand interactions. Additionally, by considering a total of 50 ns MD simulations, the molecular dynamics study revealed that the compounds were stable during MD simulation. Furthermore, the detailed theoretical characteristic analyses were fulfilled using ωB97XD and CAM-B3LYP levels of density functional theory. The coordination geometries of complexes **12–16** were confirmed by NBO results appearing among lone pair electrons (n) of nitrogen atoms and metal ions. The high contribution to LUMO/LUMOs results shows that the L_1 ligand has the strongest electron acceptor properties than the N_3 ligand. It is deduced that while IC_{50} values of the **15** and **12** against α-glucosidase are obtained remarkably, the β and γ results that complexes **15** and **12** are highly efficient in terms of microscopic second- and third-NLO properties, respectively. Among Schiff base–azide metal complexes, for Type-2 diabetes, complex **13** may be an alternate anti-diabetic inhibitor according to *in vitro*/docking results, as well as for NLO material, complexes **12** and **15** may be recommended as a candidate.

Summary points

- In this study, new effective α-glucosidase inhibitor series of Schiff base-azide metal complexes {$[Cu_2(L_1)_2(N_3)_3]$, (**12**), $[Hg(L_1)_2(N_3)\cdot H_2O]$ (**13**), $[Cd(L_1)_2(N_3)_2]$, (**14**), $[Ag(L_1)(N_3)_2\cdot 2H_2O]$, (**15**), $[Zn_2(L_1)_2(N_3)_2Cl_2\cdot 4H_2O]$, (**16**); L_1: *N*-methyl-1-(pyridin-2-yl)methanimine) were synthesized. The electronic spectral features for these complexes characterized by ^{1}H and ^{13}C NMR (except for complex **12** including Cu ion), mass (LC-HRMS) and FT–IR spectra were examined by UV–Vis spectra.
- In complexes **12–16**, being α-glucosidase inhibitory potential, the IC_{50} values of 0.2802 $\pm$ 0.62 and 420.88 $\pm$ 1.42 μM range were obtained.
- Considering the CAM-B3LYP and ωB97XD/6–311+G(d,p)//LanL2DZ levels of density functional theory (DFT), the optimal ground state geometries and vibrational wavenumbers of the complexes **12–16** were computed, and the obtained results were compared with the corresponding experimental wavenumbers.
- The corresponding theoretical wavelengths, oscillator strengths as well as major contributions to the electronic transitions were calculated at TD-DFT/ωB97XD and TD-DFT/CAM-B3LYP levels. Additionally, the molecular orbitals and atoms/functional groups that make important contributions to electronic transitions were determined with the SWizard and Chemissian programs.
- Moreover, to survey nonlinear optical parameters of the complexes **12–16**, the CAM-B3LYP and ωB97XD/6–311+G(d,p)//LanL2DZ levels of density functional theory were used.
- Demonstration of target protein interactions with complexes **12–16** has been fulfilled by molecular docking studies.
- It is deduced that while IC_{50} results of the **15** and **12** against α-glucosidase are obtained remarkably, the β and γ results that complexes **15** and **12** are highly efficient in terms of microscopic second- and third-nonlinear optics properties, respectively.
- The experimental vibrational wavenumbers and absorption wavelength results were compared with corresponding theoretical ones, it was observed that the results were quite compatible.

Author contributions

D Avcı: methodology, software, formal analysis, writing-original draft, writing review and editing. Ö Özgea: data curation, formal analysis, visualization. F Sönmezc: formal analysis, investigation, writing, review and editing. Ö Tamera: investigation, software. A Başoğlua: methodology, software. Y Atalaya: methodology, software. BZ Kurt: formal analysis.

Financial disclosure

The work was supported by the Scientific Research Projects Unit of Sakarya University (2021-7-25-103). The authors have no other relevant affiliations or financial involvement with any organization or entity with a financial interest in or financial conflict with the subject matter or materials discussed in the manuscript apart from those disclosed.

Competing interests disclosure

The authors have no competing interests or relevant affiliations with any organization or entity with the subject matter or materials discussed in the manuscript. This includes employment, consultancies, honoraria, stock ownership or options, expert testimony, grants or patents received or pending, or royalties.

Writing disclosure

No writing assistance was utilized in the production of this manuscript.

Data availability statement

The data that support the findings of this study are available from the corresponding author upon reasonable request.

ORCID

Davut Avcı https://orcid.org/0000-0002-9011-6191

References

Papers of special note have been highlighted as: • of interest; •• of considerable interest

1. Song Y, Massera C, Roubeau O, et al. An unusual open cubane structure in a $\mu_{1,1}$-azido- and alkoxo-bridged tetranuclear copper(II) complex, $[Cu_4L_2(\mu_{1,1}\text{-}N_3)_2]\cdot 5H_2O$ (H_3L = N,N′-(2-hydroxylpropane-1,3-diyl)bis-salicylideneimine). Inorg. Chem. 2004;43:6842–6847. doi:10.1021/ic049317g
2. Liu X, Yang Q, Su Z, et al. 3D high-energy-density and low sensitivity materials: synthesis, structure and physicochemical properties of an azide–Cu(II) complex with 3,5-dinitrobenzoic acid. RSC Adv. 2014;4:16087–16093. doi:10.1039/C4RA00635F
3. Charlot M-F, Kahn O, Chaillet M, et al. Interaction between copper(II) ions through the Azido bridge: concept of spin polarization and ab initio calculations on model systems. J. Am. Chem. Soc. 1986;108:2574–2581. doi:10.1021/ja00270a014
4. Lehleh A, Beghidja A, Beghidja C, et al. Synthesis, crystal structure and thermal decomposition of Cu(II), Co(II), Mn(II) complexes with hetero-ligands containing cysteic acid, 4,4′-dimethyl-2,2′-bipyridine and azide. C R Chimie. 2011;14:462–470. doi:10.1016/j.crci.2010.12.002
5. Montazerozohori M, Mojahedi Jahromi S, Masoudiasl A, et al. Nano structure zinc (II) Schiff base complexes of a N_3-tridentate ligand as new biological active agents: spectral, thermal behaviors and crystal structure of zinc azide complex. Spectrochim Acta A. 2015;138:517–528. doi:10.1016/j.saa.2014.11.055
6. Wang Li-Y, Zhao B, Zhang Chen-X, et al. The first azide($\mu_{1,1}$)-bridged binuclear cobalt(II)-imino nitroxide complex with ferromagnetic behavior. Inorg. Chem. 2003;42:5804–5806. doi:10.1021/ic034710s
7. Pastor-Ramírez C, Zamorano-Ulloa R, Vazquez-Lima H, et al. Synthesis and magneto-structural study of distorted octahedral Co^{II} complexes with picolinamide and azide ($\mu_{1,1}$)-bridge. ChemistrySelect. 2021;6:1394–1403. doi:10.1002/slct.202004323
8. Wang Y-Q, Yue Q, Qi Y, et al. Manganese (III), iron (II), and mixed-metal metal–organic frameworks based on chains with mixed carboxylate and azide bridges: magnetic coupling and slow relaxation. Inorg. Chem. 2013;52:4259–4268. doi:10.1021/ic302162c
9. Hou J, Liu X, Shen J, et al. The impact of click chemistry in medicinal chemistry. Expert Opin. Drug Discov. 2012;7(6):489–501. doi:10.1517/17460441.2012.682725
10. Gao P, Sun L, Zhou J, et al. Discovery of novel anti-HIV agents via Cu(I)-catalyzed azide-alkyne cycloaddition (CuAAC) click chemistry-based approach. Expert Opin. Drug Discov. 2016;11(9):857–871. doi:10.1080/17460441.2016.1210125
11. Villanueva M, Mesa JL, Urtiaga MK, et al. A new alternating ferro- and antiferromagnetic, one-dimensional manganese(II) azide complex, $[Mn(dpa)(N_3)_2]_2$ crystal structure and spectroscopic and magnetic properties. Eur. J. Inorg. Chem. 2001;1581–1586. doi:10.1002/1099-0682(200106)2001:6<1581::AID-EJIC1581>3.0.CO;2-2
12. Cui G, Li Y, Shi T, et al. Synthesis and characterization of Eu(III) complexes of modified cellulose and poly(*N*-isopropylacrylamide). Carbohydr. Polym. 2013;94:77–81. doi:10.1016/j.carbpol.2013.01.045
13. Zhang J, Wang L, Zhong A, et al. Deep red PhOLED from dimeric salophen Platinum(II) complexes. Dyes Pigm. 2019;162:590–598. doi:10.1016/j.dyepig.2018.10.053
14. Zhao Y, Chen S, Shen F, et al. *In vitro* neutralization of autocrine IL-10 affects Op18/stathmin signaling in non-small cell lung cancer cells. Oncol. Lett. 2019;41:501–511. doi:10.3892/or.2018.6795
15. Wei S, Sun T, Du J, et al. Xanthohumol, a prenylated flavonoid from Hops, exerts anticancer effects against gastric cancer *in vitro*. Oncol. Lett. 2018;40:3213–3222. doi:10.3892/or.2018.6723
16. Yim CB, Dijkgraaf I, Merkx R, et al. Synthesis of DOTA-conjugated multimeric [Tyr3]octreotide peptides via a combination of Cu(I)-catalyzed "click" cycloaddition and thio acid/sulfonyl azide "sulfo-click" amidation and their *in vivo* evaluation. J. Med. Chem. 2010;53:3944–3953. doi:10.1021/jm100246m
17. Thamilarasan V, Jayamani A, Sengottuvelan N. Synthesis, molecular structure, biological properties and molecular docking studies on Mn^{II}, Co^{II} and Zn^{II} complexes containing bipyridine–azide ligands. Eur. J. Med. Chem. 2015;89(7):266–278. doi:10.1016/j.ejmech.2014.09.073
18. Jiang X, Yan M. Comparing the impact on the prognosis of acute myocardial infarction critical patients of using midazolam, propofol, and dexmedetomidine for sedation. BMC Cardiovasc. Disord. 2021;21:584. doi:10.1186/s12872-021-02385-9
19. Cao J, Chen C, Wang Y, et al. Influence of autologous dendritic cells on cytokine-induced killer cell proliferation, cell phenotype and antitumor activity *in vitro*. Oncol. Lett. 2016;12:2033–2037. doi:10.3892/ol.2016.4839
20. Balan K, Ratha P, Prakash G, et al. Evaluation of *in vitro* α-amylase and α-glucosidase inhibitory potential of N_2O_2 schiff base Zn complex. Arab J. Chem. 2017;10:732–738. doi:10.1016/j.arabjc.2014.07.002
    • **In the study titled evaluation of the *in vitro* α-glucosidase inhibitory potential of Schiff base Zn complex containing N_2O_2, the IC_{50} value for α-glucosidase inhibition was found to be 0.23 mM.**
21. Tripath IP, Kumar MM, Ruchita T, et al. Synthesis, spectral, electrochemical analysis and screening for α-glucosidase inhibition of some complexes of cobalt (II) and ethylenediamine. Res. J. Chem. Sci. 2014;4(6):13–17.
    • **By performing synthesis, spectral, electrochemical analysis, and α-glucosidase inhibition study of some Co(II) complexes containing ethylenediamine, α-glucosidase inhibition values for $[Co(en)_3]\cdot SO_4$ and**

$[Co(en)_3]\cdot 2Cl$ complexes were reported as 927.89 μM and 784.12 μM in low level.

22. Miyazaki R, Yasui H, Yoshikawa Y. α-glucosidase inhibition by new Schiff base complexes of Zn(II). Open. J. Inorg. Chem. 2016;6(2):114–124. doi:10.4236/ojic.2016.62007
23. Raju BC, Ashok AK, Kumar JA, et al. α-Glucosidase inhibitory antihyperglycemic activity of substituted chromenone derivatives. Bioorg. Med. Chem. 2010;18(1):358–365. doi:10.1016/j.bmc.2009.10.047
24. Yao Y, Sang W, Zhou M, et al. Antioxidant and α-glucosidase inhibitory activity of colored grains in China. J. Agric. Food Chem. 2010;58(2):770–774. doi:10.1021/jf903234c
25. Khan M, Ahad G, Alam A, et al. Synthesis of new *bis*(dimethylamino)benzophenone hydrazone for diabetic management: *in-vitro* and *in-silico* approach. Heliyon. 2024;10:e23323. doi:10.1016/j.heliyon.2023.e23323
26. Zheng J, Ma L. Silver(I) complexes of 2,4-dihydroxybenzaldehyde–amino acid Schiff bases-Novel noncompetitive a-glucosidase inhibitors. Bioorg. Med. Chem. Lett. 2015;25:2156–2161. doi:10.1016/j.bmcl.2015.03.078

    •• A series of silver(I) complexes containing Schiff bases were designed and tested for a-glucosidase inhibition, and all the silver complexes showed strong inhibitory activity at the micromolar level.
27. Deswal Y, Asija S, Dubey A, et al. Cobalt(II), nickel(II), copper(II) and zinc(II) complexes of thiadiazole based Schiff base ligands: synthesis, structural characterization, DFT, antidiabetic and molecular docking studies. J. Mol. Struct. 2022;1253:132266. doi:10.1016/j.molstruc.2021.132266

    •• The findings of this study served as the foundation for our investigation, and it also aided in the target compounds' chemical synthesis.
28. Zheng JW, Ma L. Assessment of silver(I) complexes of salicylaldehyde derivatives-histidine Schiff base as novel α-glucosidase inhibitors. Chin. Chem. Lett. 2016;27(2):283–286. doi:10.1016/j.cclet.2015.11.015

    •• The findings of this study served as the foundation for our investigation, and it also aided in the target compounds' chemical synthesis.
29. Yoshikawa Y, Hirata R, Yasui H, et al. Alpha-glucosidase inhibitory effect of anti-diabetic metal ions and their complexes. Biochimie 2009;91:1339–1341. doi:10.1016/j.biochi.2009.06.005
30. Avcı D, Altürk S, Sönmez F, et al. Three novel Cu(II), Cd(II) and Cr(III) complexes of 6-Methylpyridine-2-carboxylic acid with thiocyanate: synthesis, crystal structures, DFT calculations, molecular docking and α-Glucosidase inhibition studies. Tetrahedron. 2018;74:7198–7208. doi:10.1016/j.tet.2018.10.054
31. Avcı D, Altürk S, Sönmez F, et al. A novel series of mixed-ligand M(II) complexes containing 2,2′-bipyridyl as potent α-glucosidase inhibitor: synthesis, crystal structure, DFT calculations, and molecular docking. JBIC J. Biol. Inorg. Chem. 2019;24:747–764. doi:10.1007/s00775-019-01688-9

    •• The rationale for our study was based on comparison with the results of this study; additionally, this study found that the target compounds were more effective against α-glucosidase.
32. Avcı D, Altürk S, Sönmez F, et al. Synthesis, spectral properties, *in vitro* α-glucosidase inhibitory activity and quantum chemical calculations of novel mixed-ligand M(II) complexes containing 1,10-phenanthroline. Appl. Organomet. Chem. 2020;34:e5412. doi:10.1002/aoc.5412
33. Gollapalli M, Taha M, Javid MT, et al. Synthesis of benzothiazole derivatives as a potent α-glucosidase inhibitor. Bioorg. Chem. 2019;85:33–48. doi:10.1016/j.bioorg.2018.12.021
34. Ghani U. Re-exploring promising a-glucosidase inhibitors for potential development into oral anti-diabetic drugs: finding needle in the haystack. Eur. J. Med. Chem. 2015;103:133–162. doi:10.1016/j.ejmech.2015.08.043
35. Santos CM, Freitas M, Fernandes E. A comprehensive review on xanthone derivatives as α-glucosidase inhibitors. Eur. J. Med. Chem. 2018;157:1460–1479. doi:10.1016/j.ejmech.2018.07.073
36. Sun H, Ding W, Song X, et al. Synthesis of 6-hydroxyaurone analogues and evaluation of their α-glucosidase inhibitory and glucose consumption-promoting activity: development of highly active 5,6-disubstituted derivatives. Bioorg. Med. Chem. Lett. 2017;27(15):3226–3230. doi:10.1016/j.bmcl.2017.06.040
37. Wang G, Peng Z, Wang J, et al. Synthesis, *in vitro* evaluation and molecular docking studies of novel triazine-triazole derivatives as potential α-glucosidase inhibitors. Eur. J. Med. Chem. 2017;125:423–429. doi:10.1016/j.ejmech.2016.09.067
38. Fan M, Yang W, Peng Z, et al. Chromone-based benzohydrazide derivatives as potential α-glucosidase inhibitor: synthesis, biological evaluation and molecular docking study. Bioorg. Chem. 2023;131:106276. doi:10.1016/j.bioorg.2022.106276
39. Wang G, Chen M, Wang J, et al. Synthesis, biological evaluation and molecular docking studies of chromone hydrazone derivatives as α-glucosidase inhibitors. Bioorg. Med. Chem. Lett. 2017;27:2957–2961. doi:10.1016/j.bmcl.2017.05.007
40. Avcı D, Altürk S, Sönmez F, et al. A new dinuclear copper (II) complex of 2,5–Furandicarboxyclic acid with 4(5)–Methylimidazole as a high potential α-glucosidase inhibitor: Synthesis, Crystal structure, Cytotoxicity study, and TD/DFT calculations. Appl. Organomet. Chem. 2019;33(3):e4725. doi:10.1002/aoc.4725
41. Cui G, Zhao K, You K, et al. Synthesis and characterization of phenylboronic acid-containing polymer for glucose-triggered drug delivery^{+}. Sci. Technol. Adv. Mater. 2020;21:1–10. doi:10.1080/14686996.2019.1700394
42. Cui G, Bai Y, Li W, et al. Synthesis and characterization of Eu(III) complexes of modified D-glucosamine and poly(N-isopropylacrylamide). Mater. Sci. Eng. C. 2017;78:603–608. doi:10.1016/j.msec.2017.03.059
43. Zhao J, Liu Y, Zhu L, et al. Tumor cell membrane-coated continuous electrochemical sensor for GLUT1 inhibitor screening. J. Pharm. Anal. 2023;13:673–682. doi:10.1016/j.jpha.2023.04.015
44. Jing Y, Li L, Zhu-jun Y, et al. Polypeptide from *Moschus* suppresses lipopolysaccharide-induced inflammation by inhibiting NF-κ B-ROS/NLRP3 pathway*. Chin. J. Integr. Med. 2023;29(10):895–904. doi:10.1007/s11655-023-3598-z

45. Sohrabi M, Binaeizadeh MR, Iraji A, et al. A review on a-glucosidase inhibitory activity of first row transition metal complexes: a futuristic strategy for treatment of Type 2 diabetes. RSC Adv. 2022;12:12011–12052. doi:10.1039/D2RA00067A
46. Wei Zeng MD, Lu Yu MD, Jiarui Wu MB, et al. Clinical characteristics and long-term follow-up outcomes of myelin oligodendrocyte glycoprotein antibody-associated disease in Han Chinese participants. Medicine 2023;102:40. doi:10.1097/MD.0000000000035391
47. Gul S, Jan F, Alam A, et al. Synthesis, molecular docking and DFT analysis of novel *bis*-Schiff base derivatives with thiobarbituric acid for α-glucosidase inhibition assessment. Sci Rep. 2024;14:3419. doi:10.1038/s41598-024-54021-z
48. Ahmad R, Alam A, Khan M, et al. Antioxidant activity, molecular docking and quantum studies of new *Bis*-Schiff bases based on benzyl phenyl ketone moiety. ChemistrySelect. 2023;8:e202302338. doi:10.1002/slct.202302338
49. Ahmad R, Khan M, Alam A, et al. Synthesis, molecular structure and urease inhibitory activity of novel *bis*-Schiff bases of benzyl phenyl ketone: a combined theoretical and experimental approach. Saudi. Pharm. J. 2023;31:101688. doi:10.1016/j.jsps.2023.06.021
50. Waheed M, Idris S, Jan F, et al. Exploring the synthesis, structure, spectroscopy and biological activities of novel 4-benzylidene-1-(2-(2,4-dichloro phenyl)acetyl) thiosemicarbazide derivatives: an integrated experimental and theoretical investigation. Saudi Pharm. J. 2023;31:101874. doi:10.1016/j.jsps.2023.101874
51. Li B, Wang W, Zhao L, et al. Aggregation-Induced Emission-Based Macrophage-Like Nanoparticles for Targeted Photothermal Therapy and Virus Transmission Blockage in Monkeypox. Adv. Mater. 2024;36:2305378. doi:10.1002/adma.202305378
52. Zhang J, Zhong A, Huang G, et al. Enhanced efficiency with CDCA co-adsorption for dye-sensitized solar cells based on metallosalophen complexes. Solar Energy. 2020;209:316–324. doi:10.1016/j.solener.2020.08.096
53. Idris S, Jan F, Waheed M, et al. Multifaceted bioactivity of thiosemicarbazide derivatives: synthesis, characterization, and DFT investigations on inhibition of α-amylase, hydroxyl radical scavenging, and iron chelating activities with molecular docking insights. J Mol Struct. 2024;1304:137669. doi:10.1016/j.molstruc.2024.137669
54. Yanai T, Tew DP, Handy NC. A new hybrid Exchange-correlation functional using the Coulomb-attenuating method (CAM-B3LYP). Chem Phys Lett. 2004;393:51–57. doi:10.1016/j.cplett.2004.06.011
55. Chai J-D, Head-Gordon M. Systematic optimization of long-range corrected hybrid density functionals. J Chem Phys. 2008;128:084106. doi:10.1063/1.2834918
56. Chai J-D, Head-Gordon M. Long-range corrected hybrid density functionals with damped atom-atom dispersion corrections. Phys Chem Chem Phys. 2008;10:6615–6620. doi:10.1039/B810189B
57. Frisch MJ, Trucks GW, Schlegel HB, et al. Gaussian 16. Revision C.01. Wallingford (CT): Gaussian, Inc.; 2016.
58. Dennington R, Keith TA, Millam JM. GaussView. Version 6.1. Shawnee Mission (KS); Semichem Inc.; 2016.
59. Frisch MJ, Pople JA, Binkley JS. Self-consistent molecular orbital methods 25. Supplementary functions for Gaussian basis set. J Chem Phys. 1984;80:3265–3269. doi:10.1063/1.447079
60. Hay PY, Wadt WR. Ab initio effective core potentials for molecular calculations. Potentials for the transition metal atoms Sc to Hg. J Chem Phys. 1985;82:270–283. doi:10.1063/1.448799
61. Runge E, Gross EKU. Density-functional theory for time-dependent systems. Phys Rev Lett. 1984;52:997–1000. doi:10.1103/PhysRevLett.52.997
62. Miertus S, Scrocco E, Tomasi J. Electrostatic interaction of a solute with a continuum. A direct utilizaion of Ab initiomolecular potentials for the prevision of solvent effects. J Chem Phys. 1981;55:117–129. doi:10.1016/0301-0104(81)85090-2
63. Gorelsky SI. SWizard Program. Revision 4.5. Canada; University of Ottawa; 2010. Available from: http://www.sg.chem.net/
64. Skripnikov L. Chemissian: software to analyze spectra, build density maps and molecular orbitals. Version 4.43. 2016. Available from: https://www.chemissian.com/
65. Morris GM, Huey R, Lindstrom W, et al. Autodock4 and AutoDockTools4: automated docking with selective receptor flexibility. J Comput Chem. 2009;30:2785–2791. doi:10.1002/jcc.21256
66. Sanner MF. Python: a programming language for software integration and development. J Mol Graphics Mod. 1999;17:57–61.
67. Systèmes D. Dassault Systèmes Biovia. San Diego (CA) USA; 2016.
68. Manca G, Cano J, Ruiz E. Exchange interactions in azido-bridged ligand Ni^{II} complexes: a theoretical analysis. Inorg Chem. 2009;48(7):3139–3144. doi:10.1021/ic802397k
69. Amirnasr M, Khalaji AD, Falvello LR, et al. Synthesis, characterization, and crystal structures of $[Ag(ca_2en)(PPh_3)(X)]$ (X = N_3, SCN) complexes. Polyhedron. 2006;25:1967–1970. doi:10.1016/j.poly.2005.12.021
70. Wu H, Wang F, Shi F, et al. Three- and four-coordinate Ag(I) complexes of crotonate and bis(benzimidazole)-2-oxapropane ligands: syntheses, crystal structures, DNA-binding studies and antioxidant activities. Transit Met Chem. 2015;40:555–564. doi:10.1007/s11243-015-9948-8
71. Özge Ö, Avcı D, Sönmez F, et al. Synthesis, DFT calculations, α-glucosidase inhibitor activity, and docking studies on Schiff base metal complexes containing isothiocyanate. Appl Organomet Chem. 2023;37:e7084. doi:10.1002/aoc.7084
•• The rationale for our study was based on comparison with the results of this study; additionally, this study found that the target compounds were more effective against α-glucosidase.
72. Weinhold F, Landis C. Valency and bonding: A natural bond orbital donor– acceptor perspective. Cambridge, UK: Cambridge University Press; 2005.
73. Altürk S, Avcı D, Tamer Ö, et al. A cobalt(II) complex with 6-methylpicolinate: synthesis, characterization, second- and third-order nonlinear optical properties, and DFT calculations. J Phys Chem Solids. 2016;98:71–80. doi:10.1016/j.jpcs.2016.06.008
74. Reed AE, Weinhold F. Natural bond orbital analysis of near-Hartree–Fock water dimer. J Chem Phys. 1983;78:4066–4073. doi:10.1063/1.445134

75. Glendening ED, Reed AE, Carpenter JE, et al. NBO Version 3.1. TCI. Madison: University of Wisconsin; 1998.
76. Foster JP, Weinhold F. Natural hybrid orbitals. J Am Chem Soc. 1980;102:7211–7218. doi:10.1021/ja00544a007
77. Gorelsky SI, Lever ABP. The electronic structure and spectra of $[Ru(NH_3)_4(LL)]^{2+}$ (LL = bpy, bpz, bqdi) studied by density functional theory and INDO/S. Charge transfer character of electronic transitions and their solvatochromism. Can J Anal Sci Spectr. 2003;48(1):93–105.
78. Luque FJ, Orozco M, Bhadane PK, et al. SCRF calculation of the effect of water on the topology of the molecular electrostatic potential. J Phys Chem. 1993;97:9380–9384. doi:10.1021/j100139a021
79. Pearson RG. Absolute electronegativity and hardness correlated with molecular orbital theory. Proc Nati Acad Sci USA. 1986;83:8440–8441. doi:10.1073/pnas.83.22.8440
80. Avcı D, Özge Ö, Başoğlu A, et al. Synthesis, crystal structures, and DFT calculations: novel Mn(II), Co(II) and Ni(II) complexes of *N*-(pyridin-2-ylmethylene)methanamine with isothiocyanate as promising optical materials. Opt Quantum Electron. 2023;55:408. doi:10.1007/s11082-023-04668-1
81. Oudar JL, Zyss J. Relations between microscopic and macroscopic lowest-order optical nonlinearities of molecular crystals with one-or two-dimensional units. Phys Rev A. 1982;26:2028–2048. doi:10.1103/PhysRevA.26.2028
82. Pierce BM. A theoretical analysis of third-order nonlinear optical properties of linear polyenes and benzene. J Chem Phys. 1989;91(2):791–811. doi:10.1063/1.457132
83. Avcı D. Second and third-order nonlinear optical properties and molecular parameters of azo chromophores: semiempirical analysis. Spectrochim Acta A. 2011;82:37–43. doi:10.1016/j.saa.2011.06.037
84. Chemla DS, Zysss J. Nonlinear Optical Properties of Organic Molecules and Crystals. London: Academic Press; 1987.
85. Faizan M, Mehkoom M, Afroz Z, et al. Experimental and computational investigation of novel dihydrated organic single crystal of 2,4,6-triaminopyrimidine and 3,5-dintrobenzoic acid: linear and nonlinear optical response with limiting performance. J Solid State Chem. 2021;300:122255. doi:10.1016/j.jssc.2021.122255
86. Kamaal S, Mehkoom M, Ali A, et al. Potential third-order nonlinear optical response facilitated by intramolecular charge transfer in a simple Schiff base molecule: experimental and theoretical exploration. ACS Omega. 2021;6:6185–6194. doi:10.1021/acsomega.0c05557
87. Mehkoom M, Afzal SM, Ahmad S, et al. The new pyrazoline derivative 5-(3,4-Dimethoxyphenyl)-3-(2,5-dimethylthiophene-3-yl),-4,5-dihydro-pyrazole-1-carbothioic acid amide (DDPA) as an advisable candidate for optical linearity, nonlinearity, and limiting performance. J Mol Liq. 2022;345:117018. doi:10.1016/j.molliq.2021.117018
88. Cheng LT, Tam W, Stevenson SH, et al. Experimental investigations of organic molecular nonlinear optical polarizabilities. 1. Methods and results on benzene and stilbene derivatives. J Phys Chem. 1991;95:10631–10643. doi:10.1021/j100179a026
89. Ledoux I, Zyss J. Influence of the molecular environment in solution measurements of the second-order optical susceptibility for urea and derivatives. Chem Phys. 1982;73:203–213. doi:10.1016/0301-0104(82)85161-6
90. Adant C, Dupuis M, Bredas J. *Ab initio* study of the nonlinear optical properties of urea: electron correlation and dispersion effects. Int J Quant Chem. 1995;56:497–507. doi:10.1002/qua.560560853
91. Yoshikawa Y, Ueda E, Kawabe K, et al. Development of new insulinomimetic zinc(II) picolinate complexes with a $Zn(N_2O_2)$ coordination mode: structure characterization, *in vitro*, and *in vivo* studies. JBIC J Biol Inorg Chem. 2002;7:68–73. doi:10.1007/s007750100266
92. Yasumatsu N, Yoshikawa Y, Adachi Y, et al. Antidiabetic copper (II)-picolinate: impact of the first transition metal in the metallopicolinate complexes. Bioorg Med Chem. 2007;15:4917–4922. doi:10.1016/j.bmc.2007.04.062
93. Avcı D, Altürk S, Sönmez F, et al. Synthesis, DFT calculations and molecular docking study of mixed ligand metal complexes containing 4,4′-dimethyl-2,2′-bipyridyl as α-glucosidase inhibitors. J Mol Struct. 2020;1205:127665. doi:10.1016/j.molstruc.2019.127655
94. Avcı D, Altürk S, Sönmez F, et al. Novel metal complexes containing 6-methylpyridine-2-carboxylic acid as potent α-glucosidase inhibitor: synthesis, crystal structures, DFT calculations, and molecular docking. Mol Divers. 2021;25:171–189. doi:10.1007/s11030-020-10037-x
95. Hermans MM, Kroos MA, van Beeumen J, et al. Human lysosomal a-glucosidase characterization of the catalytic site. J Biol Chem. 1991;266(21):13507–13512. doi:10.1016/S0021-9258(18)92727-4
96. Rye CS, Withers SG. Glycosidase mechanisms. Curr Opin Chem Biol. 2000;4:573–580. doi:10.1016/S1367-5931(00)00135-6
97. Dong Q, Hu N, Yue H, et al. Inhibitory activity and mechanism investigation of hypericin as a novel α-glucosidase inhibitor. Molecules. 2021;26:4566. doi:10.3390/molecules26154566
98. Wang Y, Ma L, Li Z, et al. Synergetic inhibition of metal ions and genistein on α-glucosidase. FEBS Lett. 2004;576:46–50. doi:10.1016/j.febslet.2004.08.059
99. Abraham MJ, Murtola T, Schulz R, et al. GROMACS: high performance molecular simulations through multi-level parallelism from laptops to supercomputers. SoftwareX. 2015;1:19–25. doi:10.1016/j.softx.2015.06.001
100. WebGRO for Macromolecular Simulations. Available from: https://simlab.uams.edu/

***In vitro* α-glucosidase, docking and DFT studies on novel azide metal complexes**

Supplementary Material

The synthesis of the *N*-methyl-1-(pyridin-2-yl)methanimine (L_1)

0.1 mol of 2-pyridine carboxaldehyde was dissolved in 10 mL of ethanol and 2 drops of triethylamine were dropped on it. The solution was cooled by taking it into an ice bath, and 0.1 mol of methylamine (33% ethanol solution) was added to it and stirred in an ice bath for 30 minutes, and at room temperature for 3.5 hours. The alcohol in the mixture was evaporated in the evaporator and 100 mL of chloroform was added to this mixture. This solution was washed three times with 25 mL of water. The organic phase was dried with anhydrous $MgSO_4$, filtered and evaporated in the evaporator. The *N*-methyl-1-(pyridin-2-yl)methanimine (L_1) was obtained as dark yellow oil and its structure was confirmed by ^1H and ^{13}C NMR spectra. ^1H NMR (DMSO-d_6, 300 MHz) δ/ppm: 8.61 (1H, dd, J_1 = 1.2 Hz, J_2 = 4.7 Hz), 8.33 (1H, s), 7.82-7.93 (2H, m), 7.44 (1H, td, J_1 = 1.2 Hz, J_2 = 5.0 Hz), 3.47 (3H, s). ^{13}C NMR (DMSO-d_6, 75 MHz) δ/ppm: 163.84, 154.81, 150.00, 137.57, 125.73, 120.89, 48.14.

α-Glucosidase inhibition assay

By using p−nitrophenyl−α−D−glucopyranoside (pNGP, Sigma, N1377, ≥99%) as the substrate, the α−glucosidase from Saccharomyces cerevisiae (Sigma, G5003) was determined as the target protein. The compounds and genistein were dissolved in DMSO (anhydrous, ≥99.9%). The enzyme and the substrate were dissolved in potassium phosphate buffer (0.05 M, pH 6.8). The enzymatic reaction mixture composed of α-glucosidase (0.02 U, 20 µL), substrate (1.25 mM, 30 µL), test compounds (10 µL) and potassium phosphate buffer (140 µL) was incubated at 37 °C for 30 min. After 30 min of incubation, the absorbance of yellow colour produced due to the formation of p-nitrophenol was measured using Synergy H1 (BioTek, USA) 96-well microplate reader at 405 nm. All experiments were performed in triplicates. The surveying of α−glucosidase inhibition activity for the complexes **12–16** was fulfilled by basing on our previously reported study [1-4],

Glucosidase inhibition = $[(A_c-A_s)/A_c]x100$

where A_c is the absorbance of control and A_s is the absorbance of samples, respectively. The calculation of IC_{50} values was performed by using Graphpad Software.

Theoretical details

The stability energy $E^{(2)}$ in NBO calculations was obtained by using eq. (1)

$$E^{(2)} = \Delta E_{ij} = q_i \frac{F(i,j)^2}{\varepsilon_i - \varepsilon_j} \quad (1)$$

In eq. (1), $F(i,j)^2$ is the off-diagonal NBO Fock matrix elements, ε_i and ε_j are diagonal elements, and q_i is the donor orbital occupancy for each donor (i) and acceptor (j) [5,6].

The molecular parameters computed from the HOMO and LUMO energies are the chemical hardness (η), electronegativity (χ), chemical softness (*S*), electrophilicity (ω) and nucleophilicity (φ) index. These parameters were calculated as follows eq. (2)-(6) [7,8].

$$\eta = \frac{(E_{LUMO} - E_{HOMO})}{2} \quad (2)$$

$$\chi = -\frac{(E_{HOMO} + E_{LUMO})}{2} \quad (3)$$

$$S = \frac{1}{\eta} \quad (4)$$

$$\omega = \frac{\chi^2}{2\eta} \quad (5)$$

$$\varphi = \frac{1}{\omega} \quad (6)$$

The theoretical microscopic electric dipole moment (μ), linear optical parameters ($\bar{\alpha}$ and Δα) described as the mean and anisotropy of polarizability, first- and second-order hyperpolarizability parameters (β and γ) for complexes **12–16** in gas phase were computed by using eq. (7)-(10) [9,10].

$$\bar{\alpha} = \frac{(a_{xx} + a_{yy} + a_{zz})}{3} \quad (7)$$

$$\Delta a = \left\{\frac{1}{2}\left[\left(a_{xx} - a_{yy}\right)^2 + \left(a_{yy} - a_{zz}\right)^2 + (a_{zz} - a_{xx})^2\right]\right\}^{1/2} \quad (8)$$

In eq. (7) and (8), the Cartesian components of $\bar{\alpha}$ and Δα are a_{xx}, a_{yy}, a_{zz}. 1 atomic unit (a.u.) of $\bar{\alpha}$ is converted to 0.1482×10^{-24} electrostatic unit (esu).

The theoretical β and γ parameters, known as first- and second-order hyperpolarizability parameters, were computed with eq. (9) and (10) [9,10],

$$\beta = (\beta_x^2 + \beta_y^2 + \beta_z^2)^{1/2} \quad (9)$$

$$< \gamma >= \frac{1}{5}\left[\gamma_{xxxx} + \gamma_{yyyy} + \gamma_{zzzz} + 2\left(\gamma_{xxyy} + \gamma_{xxzz} + \gamma_{yyzz}\right)\right] \quad (10)$$

In eq. (9), the Cartesian components of β are $\beta_x = \beta_{xxx} + \beta_{xyy} + \beta_{xzz}$, $\beta_y = \beta_{yyy} + \beta_{yxx} + \beta_{yzz}$, $\beta_z = \beta_{zzz} + \beta_{zyy} + \beta_{zxx}$. To obtain β in esu unit, 1 a.u. = 8.6393×10^{-33} esu conversion is used.

4

The Tauc and Menth equation is used to obtain the E_g (optical band gap energy) value, as shown in equation (11) [8].

$$(\alpha h\nu) = C(h\nu - E_g)^{1/2} \tag{11}$$

In this equation, the α (absorption coefficient) is obtained by using $\alpha = 2.303\,A/d$ by accounting for d and A, which represent the cuvette's width (1 cm) and absorbance in the UV–Vis range, respectively. Photon energy is abbreviated $h\nu$, while direct band gap energy is abbreviated E_g. Regarding the dependent effective masses of the bands, C is a proportionality constant.

5

Docking details

In order to investigate the protein-ligand interactions of the synthesized complexes **12–16**, the target protein (S. *cerevisiae* isomaltase (PDBID: 3A4A)) provided from the Protein Data Bank was selected as rigid and molecular docking study was carried out by the AutoDock4 [11] program implemented via the graphical user interface AutoDockTools (ADT1.5.7) [12]. The pdb files were generated for complexes **12–16** and genistein optimized at CAM-B3LYP level (in Gaussian 16W program) to use in docking. ADT1.5.7 was used to add Kollman charges, identify rotatable bonds, and join non-polar hydrogen atoms to carbon atoms. All calculations for complex-target flexible docking were performed using the Lamarckian genetic algorithm (LGA) method [13]. Grid and docking parameter file, PDBQT format for target and ligand (target.pdbqt, ligand.pdbqt) using AutoDock 4.2 were prepared. AutoGrid 4 was provided the determination of docking area. The grid box dimensions were determined as different points to cover the target binding site and accommodate complexes **12–16** and genistein to move freely. 3D affinity grid centered around the complexes **12–16** and and genistein binding site with a 1.0 Å grid point spacing was calculated for each of the following atom types: (a) receptor (protein): A (aromatic C), C, Ca, HD, N, OA, SA and (b) ligand: A, C, NA, N, SA, as well as Cu for complex **12**, Hg for complex **13**, Cd for complex **14**, Ag for complex **15**, Cl and Zn for complex **16**, only A and OA for genistein, e (electrostatic), and d (desolvation). Further docking parameters were used as: Population size: 150, mutation rate: 0.02, elitism: 1, crossover rate: 0.8, local search rate: 0.06, and energy evaluations: 2,500,000. Final docked conformations were achieved within a 2 Å root mean square deviation (RMSD) tolerance.

Complex **12**: grid points in xyz: 80, 80, 80 and grid box center in xyz: 20.689, -3.098, 18.634
Complex **13**: grid points in xyz: 80, 80, 80 and grid box center in xyz: 21.276, -2.782, 18.634
Complex **14**: grid points in xyz: 80, 80, 80 and grid box center in xyz: 21.276, -2.537, 18.634
Complex **15**: grid points in xyz: 80, 80, 80 and grid box center in xyz: 21.276, -2.597, 18.634
Complex **16**: grid points in xyz: 80, 80, 80 and grid box center in xyz: 21.276, -2.897, 18.634
Genistein: grid points in xyz: 60, 60, 60 and grid box center in xyz: 21.831, -0.612, 18.719

The docking results obtained here were used to explain the relative performance of the stabilization and binding energy of the complexes. 2-D and 3-D structures demonstrating interactions between amino acid residues and ligands of complexes **12–16** were visualized Discovery Studio 4.0 program [14]. In the study conducted to determine that the selected docking parameters were acceptable, the conformation Root Mean Square Deviation (RMSD) value of the native alpha-D-glucose ligand and re-docked co-crystallized ligand were compared in terms of structural alignment. The RMSD value obtained at 0.446 Å indicates that the selected docking parameters are acceptable [15]. Optimized parameters were used to dock for complexes **12–16** and genistein into the active site of the α-glucosidase homology model.

Molecular Dynamic (MD) simulation details

MD simulation calculations were performed for complexes **12-16** in ligands with the receptor using the GROMACS simulation package [16] via WebGro server [17]. Root mean square deviation (RMSD) profiles for protein–ligand complexes were assessed. The protein-ligand topology was generated by using Discovery Studio 4.0 program [14]. In a reasonable starting structure in terms of geometry and solvent orientation, it is important to stabilize the solvent and ions around the protein to initiate the actual dynamics. Additionally, bringing it to the temperature we want to simulate and ensuring the correct orientation of the solute (protein), after reaching the correct temperature (according to kinetic energies), pressure is applied to the system until it reaches the appropriate density. Initial parameters: GROMOS9643A1 force field parameters [18], water model as SPC (single point charge) [19], triclinic box type was selected, and this system was neutralized by taking salt type (NaCl) to achieve a molarity of 0.15 M. The steepest descent algorithm (5000 steps) for minimization was applied before the MD calculation. Equilibration and MD simulations were performed under an ensemble of NVT/NPT [20] (constant particle number, volume/pressure and temperature) called canonical/isothermal-isobaric. For such a process, 300 K temperature, 1.0 bar pressure, simulation time 50 ns (maximum time allowed), 5000 (approximate number of frame per simulation), and MD integrator (the leap-frog integrator) for all production simulations.

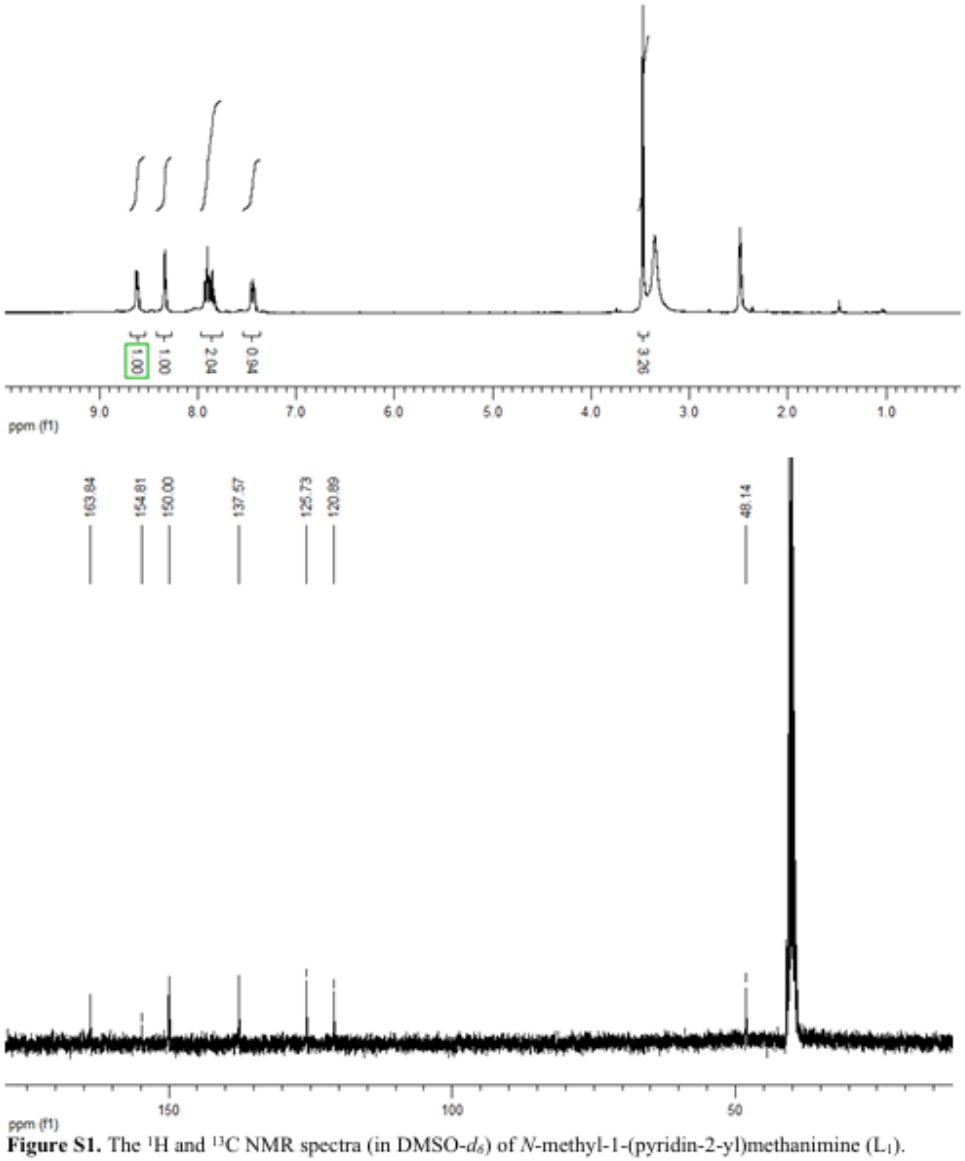

Figure S1. The ^{1}H and ^{13}C NMR spectra (in DMSO-d_6) of *N*-methyl-1-(pyridin-2-yl)methanimine (L_1).

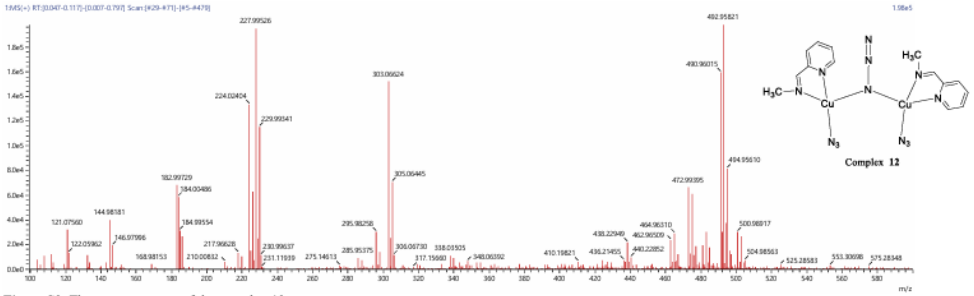

Figure S2. The mass spectrum of the complex **12**.

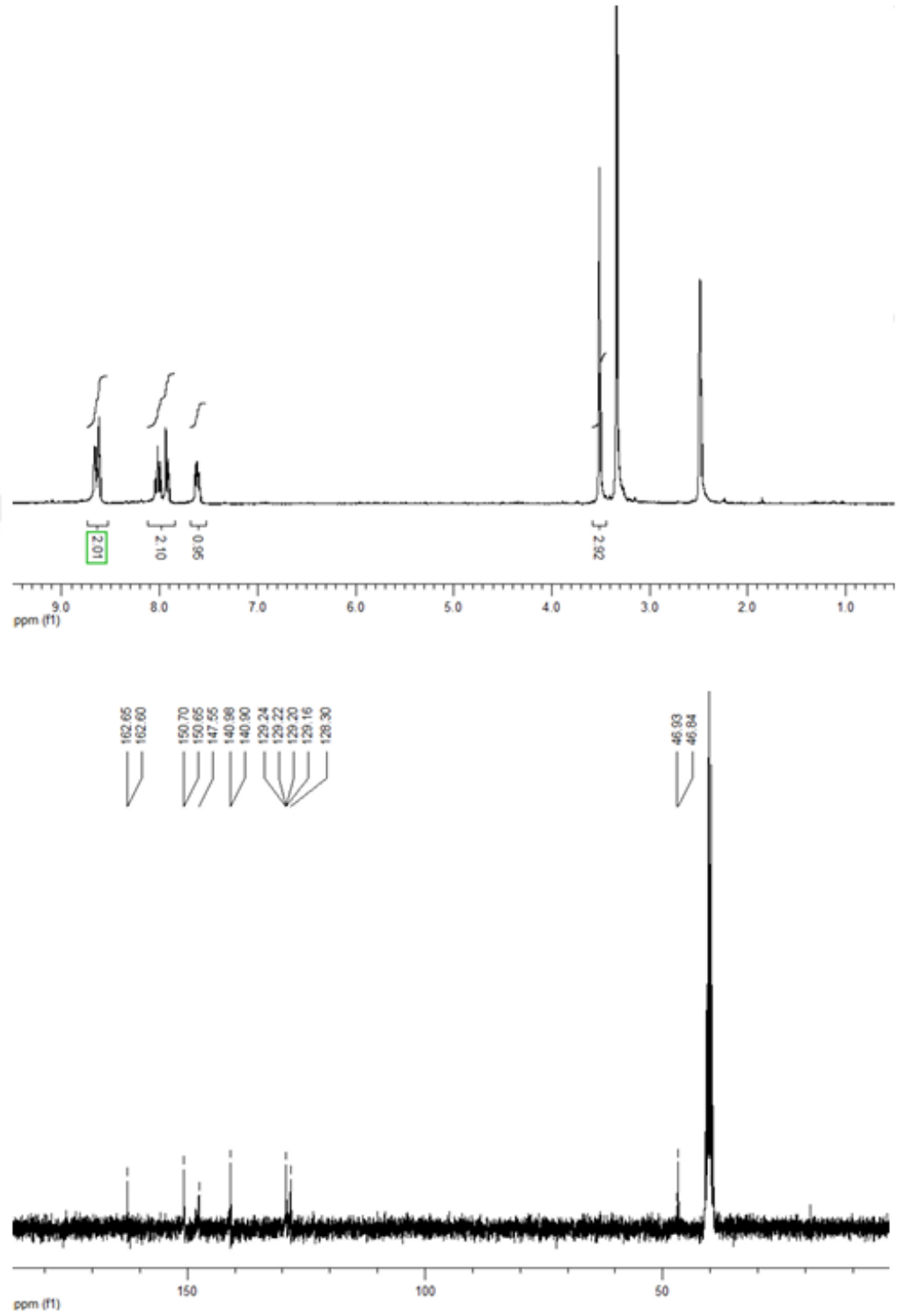

Figure S3. The ^{1}H and ^{13}C NMR spectra (in DMSO-d_6) of the complex **13**.

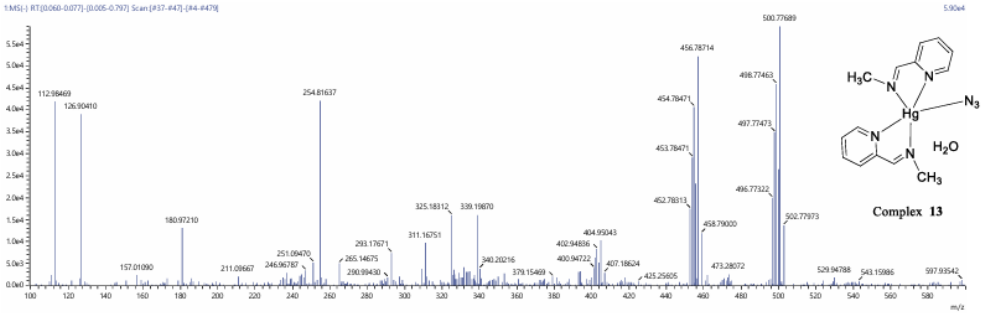

Figure S4. The mass spectrum of the complex **13**.

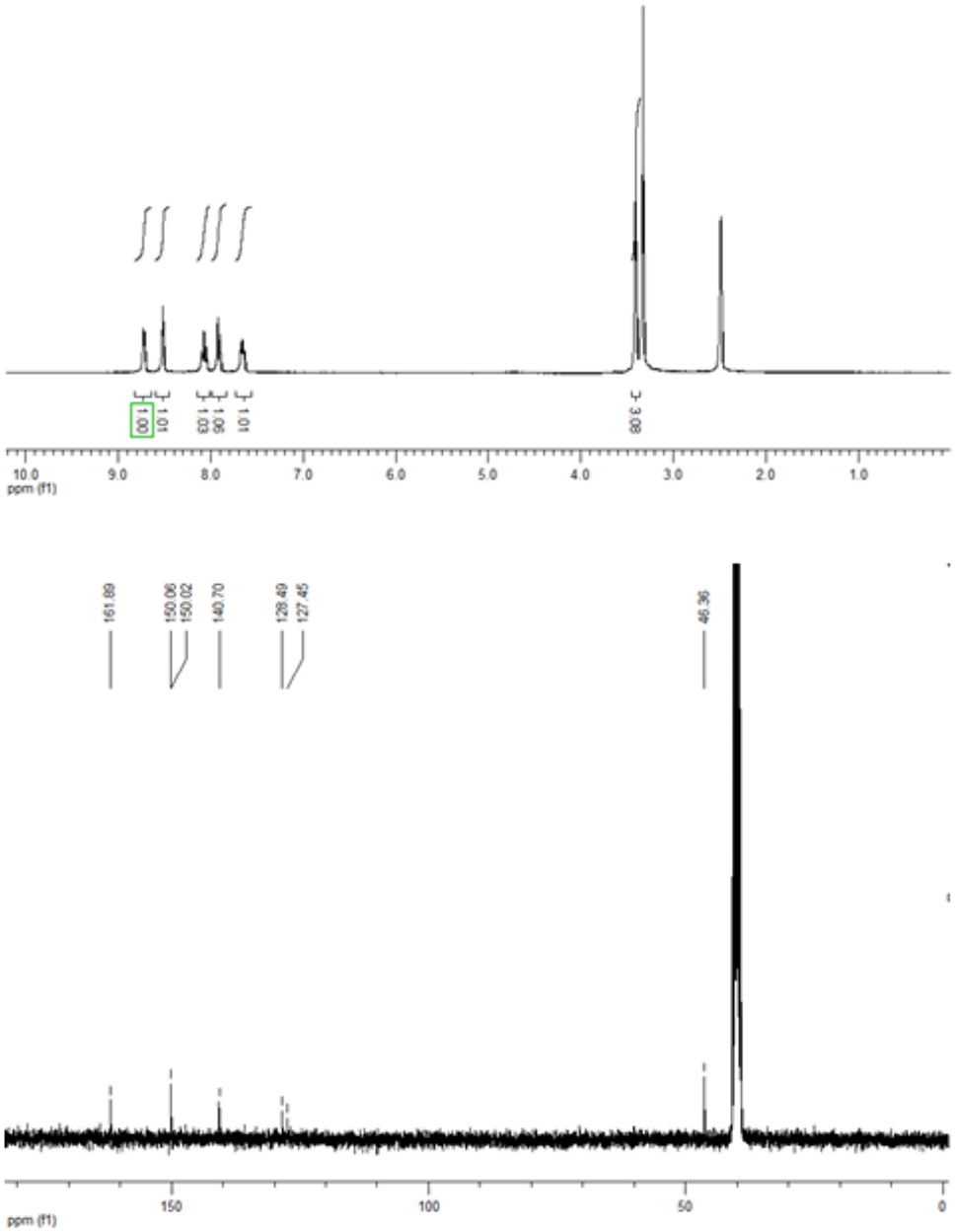

Figure S5. The ^{1}H and ^{13}C NMR spectra (in DMSO-d_6) of the complex **14**.

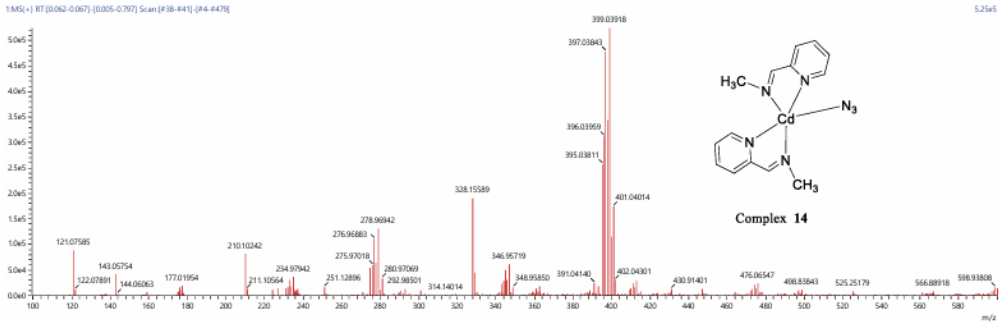

Figure S6. The mass spectrum of the complex **14**.

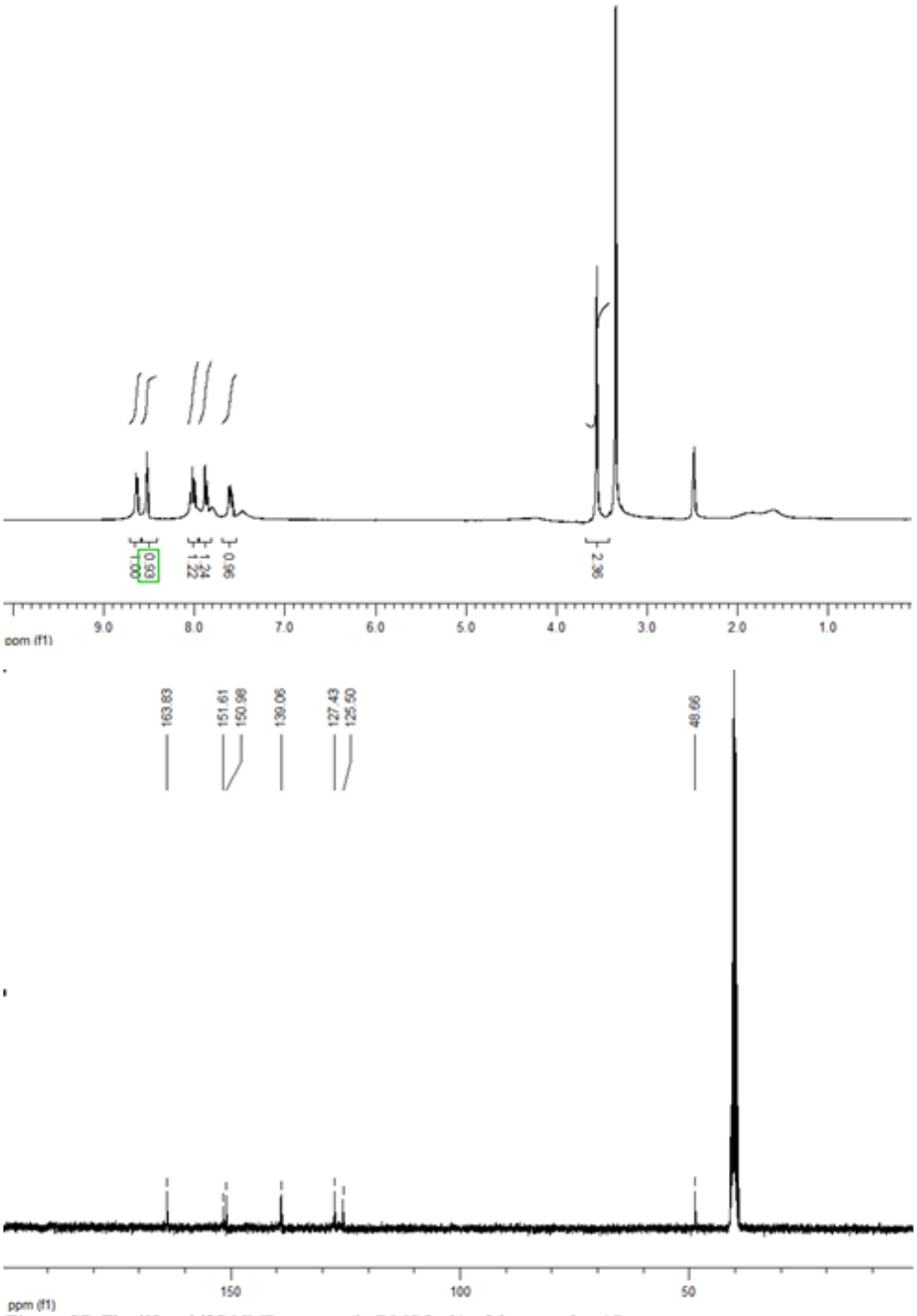

Figure S7. The ^{1}H and ^{13}C NMR spectra (in DMSO-d_6) of the complex **15**.

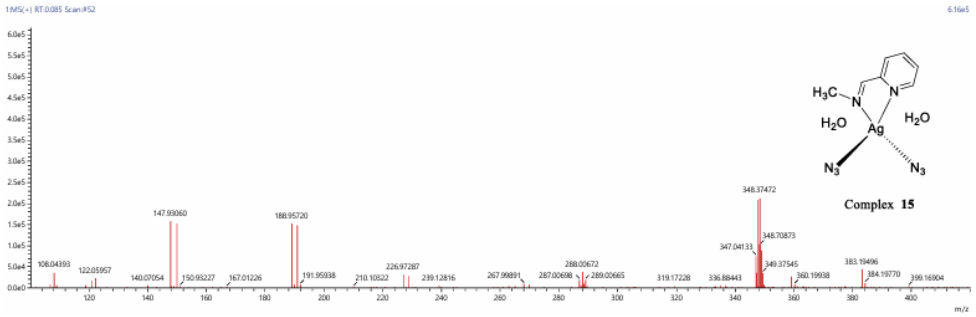

Figure S8. The mass spectrum of the complex **15**.

15

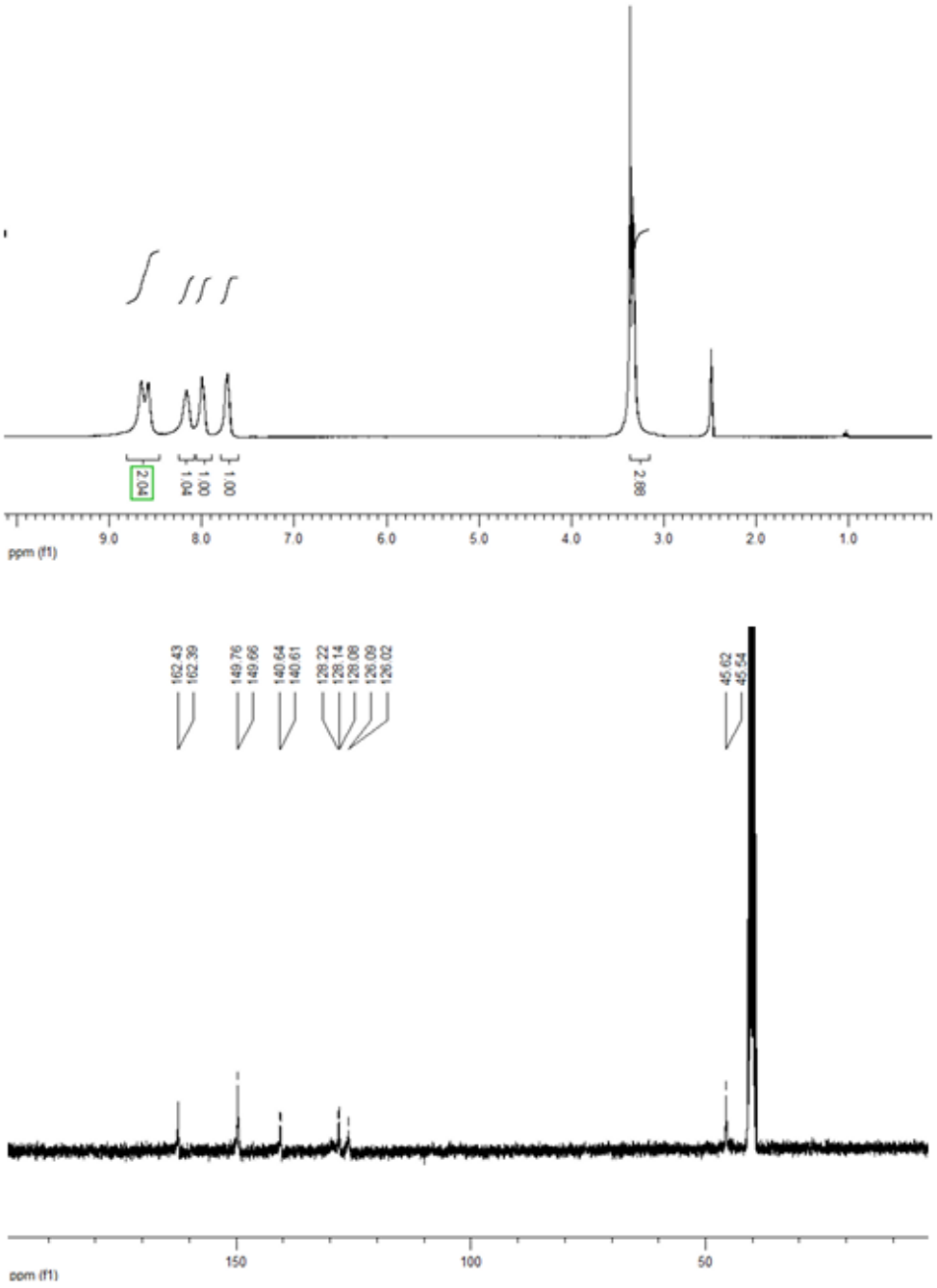

Figure S9. The ^{1}H and ^{13}C NMR spectra (in DMSO-d_6) of the complex **16**.

16

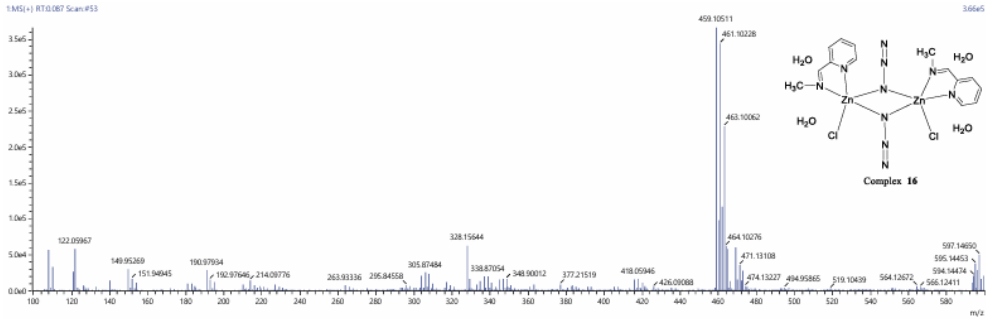

Figure S10. The mass spectrum of the complex **16**.

17

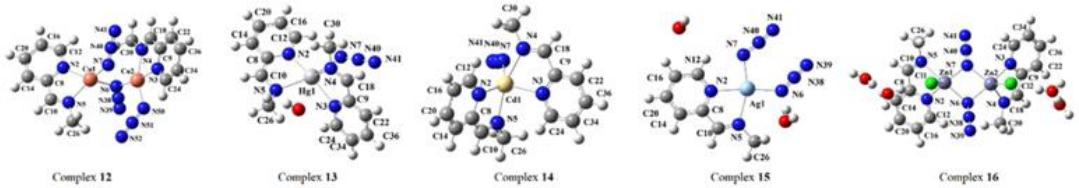

Complex **12** Complex **13** Complex **14** Complex **15** Complex **16**

Figure S11. Theoretical optimized structures of complexes **12–16** obtained at DFT/CAM-B3LYP level.
DFT/CAM-B3LYP: Density functional theory/Coulomb attenuation method- Becke, 3–parameter, Lee–Yang–Parr

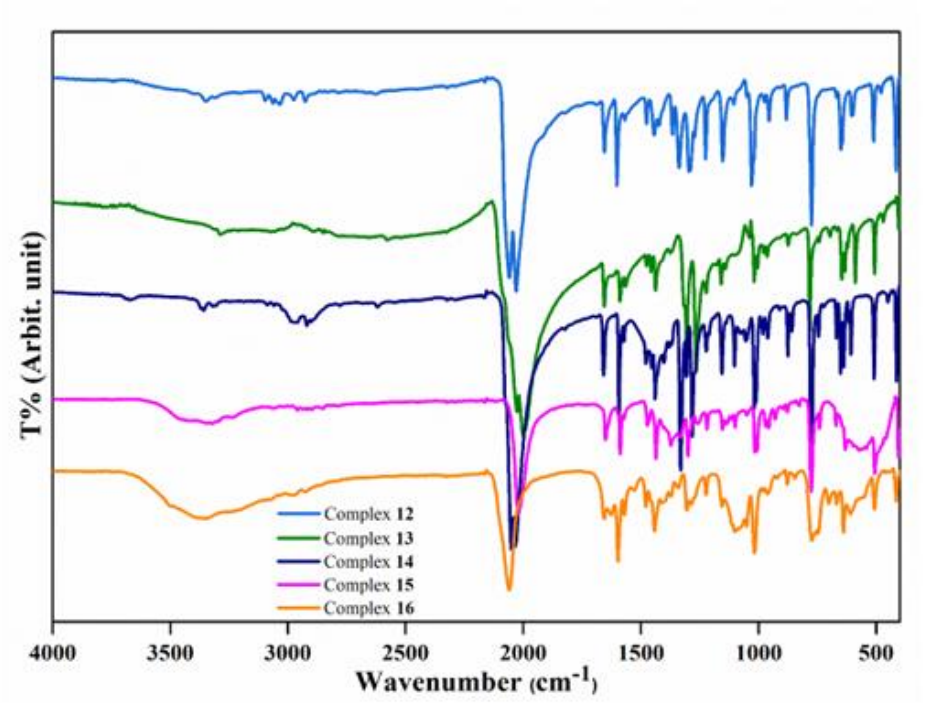

Figure S12. FTIR spectra of complexes **12–16.**

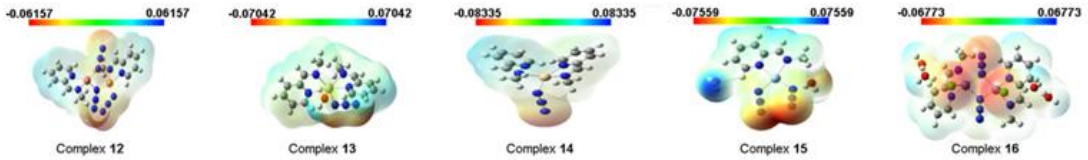

Figure S13. Molecular electrostatic potential (MEP) surfaces for the complexes **12–16**.

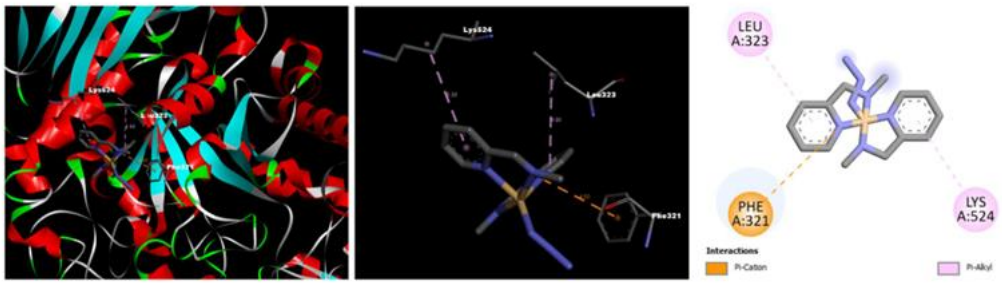

Figure S14. 3D- and 2D-structures displaying interactions between amino acid residues and ligands of the most active complex **14**.

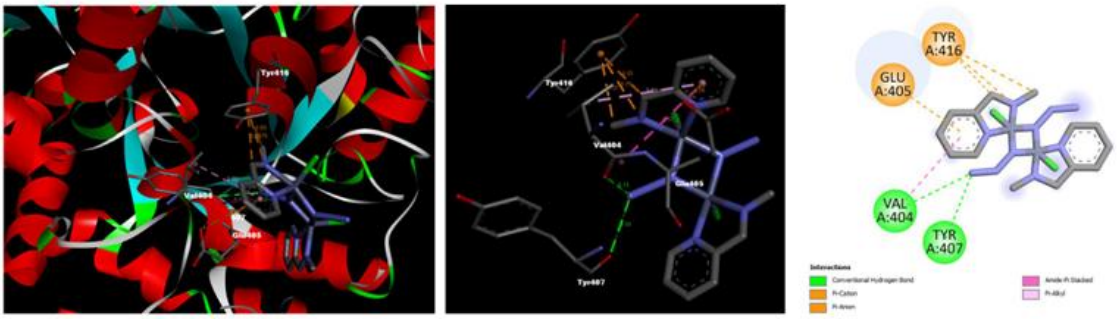

Figure S15. 3D- and 2D-structures displaying interactions between amino acid residues and ligands of the most active complex **16**.

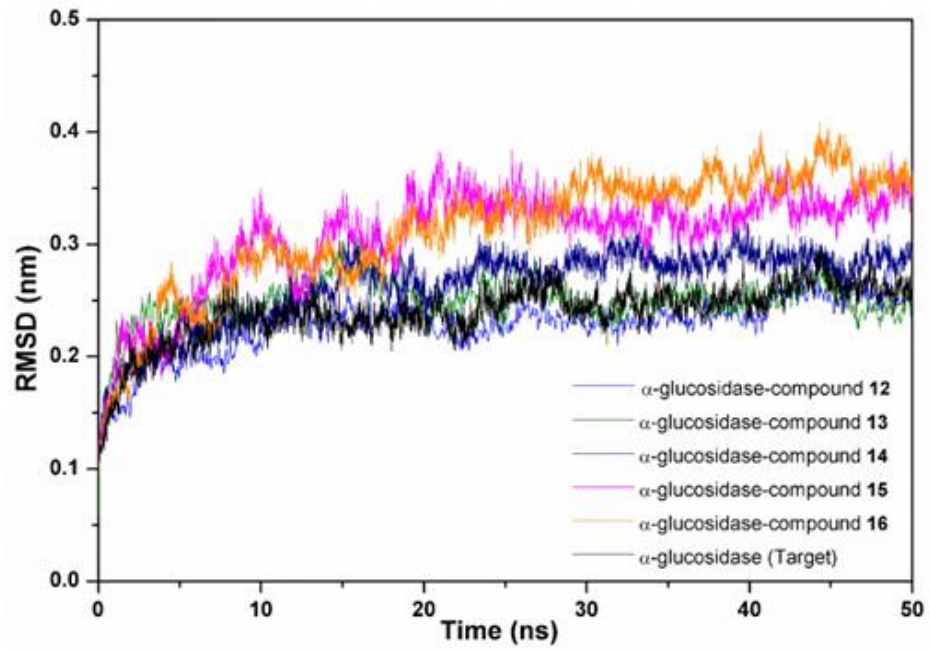

Figure S16. RMSD plots of all the complexes α-glucosidase/compounds **12–16** throughout the MD simulations. (The X-axis shows time in ns while the Y-axis shows the value of RMSD.)

Table S1. Theoretical some geometric parameters for complexes **12–16**.

Complex **12**			Complex **13**			Complex **14**		
Parameters	ωB97XD	CAM-B3LYP	Parameters	ωB97XD	CAM-B3LYP	Parameters	ωB97XD	CAM-B3LYP
Bond length (Å)			Bond length (Å)			Bond length (Å)		
Cu1–N2	2.211	2.143	Hg1–N2	2.361	2.350	Cd1–N2	2.424	2.418
Cu2–N3	2.069	2.068	Hg1–N3	2.467	2.455	Cd1–N3	2.282	2.277
Cu1–N6	2.127	2.081	Hg1–N7	2.368	2.368	Cd1–N6	2.176	2.177
Cu2–N6	1.985	1.977	Hg1–N5	2.402	2.431	Cd1–N5	2.452	2.450
Cu1–N5	2.031	2.086	Hg1–N4	2.511	2.509	Cd1–N4	2.263	2.263
Cu2–N4	2.084	2.093	N7–N40	1.224	1.223	N6–N38	1.229	1.228
Cu1–N7	2.003	2.014	N40–N41	1.191	1.190	N38–N39	1.180	1.180
Cu2–N50	1.942	1.941	N2–C8	1.385	1.383	N2–C8	1.355	1.354
N50–N51	1.202	1.199	N3–C9	1.355	1.354	N3–C9	1.397	1.396
N51–N52	1.143	1.143	N5–C10	1.362	1.363	N5–C10	1.283	1.281
N6–N38	1.208	1.208	N4–C18	1.288	1.286	N4–C18	1.348	1.348
N7–N40	1.188	1.186	N5–C26	1.469	1.470	N5–C26	1.462	1.462
N38–N39	1.138	1.136	N4–C30	1.466	1.466	N4–C30	1.465	1.465
N40–N41	1.156	1.153	C8–C10	1.423	1.421	C8–C10	1.484	1.482
N2–C8	1.341	1.341	C9–C18	1.483	1.481	C9–C18	1.421	1.419
N3–C9	1.340	1.339						
N5–C10	1.271	1.266	Bond angles (°)			Bond angles (°)		
N4–C18	1.269	1.268	N7– Hg1–N3	91.34	91.82	N7–Cd1–N2	124.4	120.91
N5–C26	1.451	1.449	N2– Hg1–N5	72.03	71.93	N2– Cd1–N5	68.65	68.82
N4–C30	1.447	1.447	N3– Hg1–N4	68.25	68.43	N3–Cd1–N4	76.42	76.70
C8–C10	1.474	1.472	N5– Hg1–N4	112.8	114.7	N5– Cd1–N4	158.7	159.82
C9–C18	1.473	1.471						
Bond angles (°)			Dihedral angles (°)			Dihedral angles (°)		
N6–Cu1–N2	121.9	118.9	Hg1–N2–C12–C16	-174.2	-174.5	Cd1–N2–C12–C16	-172.8	-177.4
N7–Cu1–N5	146.9	124.7	Hg1–N3–C24–C34	168.4	169.5	Cd1–N3–C24–C34	-176.2	-179.3
N6– Cu2–N3	169.4	170.4						
N4– Cu2–N50	166.7	160.4						
N2– Cu1–N5	78.89	78.90						
N4– Cu2–N3	78.30	78.09						
N5– Cu1–N6	108.8	119.9						
N50– Cu2–N6	98.60	98.63						
Dihedral angles (°)								
Cu1–N2–C8–C14	171.6	-179.1						
Cu2–N3–C9–C22	171.4	173.5						

Table S1. *(Continued)*

Complex **15**			Complex **16**		
Parameters	ωB97XD	CAM-B3LYP	Parameters	ωB97XD	CAM-B3LYP
Bond length (Å)			Bond length (Å)		
Ag1–N2	2.340	2.253	Zn1–N2	2.271	2.280
Ag1–N6	2.172	2.138	Zn2–N3	2.161	2.151
Ag1–N7	2.218	2.181	Zn1–N6	2.080	2.075
Ag1–N5	2.266	2.355	Zn1-N7	2.116	2.113
N6–N38	1.237	1.238	Zn2–N6	2.073	2.072
N7–N40	1.240	1.235	Zn2–N7	2.118	2.111
N38–N39	1.177	1.176	Zn1–N5	2.145	2.135
N40–N41	1.176	1.182	Zn2–N4	2.252	2.254
N2–C8	1.360	1.355	Zn1-Cl1	2.256	2.266
N5–C10	1.283	1.283	Zn2-Cl2	2.264	2.273
N5–C26	1.461	1.463	N6–N38	1.204	1.204
C8–C10	1.482	1.480	N7–N40	1.210	1.211
			N38–N39	1.137	1.135
			N40–N41	1.134	1.133
			N2–C8	1.336	1.337
Bond angles (°)			N3–C9	1.339	1.339
N6–Ag1–N7	89.35	99.84	N5–C10	1.267	1.265
N7– Ag1–N2	106.2	87.70	N4–C18	1.264	1.263
N2– Ag1–N5	73.50	73.12	N5–C26	1.448	1.450
			N4–C30	1.448	1.449
Dihedral angles (°)			C8–C10	1.477	1.475
Ag1–N2–C12–C16	179.4	-179.4	C9–C18	1.479	1.477
			Bond angles (°)		
			N6–Zn1–N7	79.72	79.45
			N6–Zn1–N2	90.23	91.56
			N2– Zn1–N5	74.56	74.87
			N3– Zn2–N4	74.81	75.07
			N6– Zn2–N7	79.83	79.58
			Zn1– N6–Zn2	101.4	101.2
			Zn1– N7–Zn2	98.74	98.69
			Dihedral angles (°)		
			Zn1–N2–C12–C16	171.9	170.1
			Zn2–N3–C24–C34	172.5	171.9

Table S2. Second–order perturbation theory analysis of Fock matrix on NBO basis for complexes **12–16**.

Donor (*i*)	Acceptor (j)	$E^{(2)}$ (kcal/mol)		Donor (*i*)	Acceptor (j)	$E^{(2)}$ (kcal/mol)		Donor (*i*)	Acceptor (j)	$E^{(2)}$ (kcal/mol)	
Complex **12**				Complex **13**				Complex **14**			
		ωB97XD	CAM-B3LYP			ωB97XD	CAM-B3LYP			ωB97XD	CAM-B3LYP
		6–311+G(d,p)//LanL2DZ				LanL2DZ				LanL2DZ	
LP(1)N6	LP*(6)Cu1	7.41	12.93	LP(1)N7	LP*(4)Hg1	12.88	13.50	LP(1)N7	LP*(6)Cd1	15.07	14.71
LP(1)N50	LP*(7)Cu2	30.30	18.34	LP(1)N5	LP*(5)Hg1	11.50	11.43	LP(1)N5	LP*(6)Cd1	6.33	6.01
LP(1)N5	LP*(6)Cu1	16.29	11.98	LP(1)N3	LP*(4)Hg1	9.71	9.71	LP(1)N3	LP*(6)Cd1	13.37	13.00
LP(1)N3	LP*(8)Cu2	19.18	23.67	LP(1)N4	LP*(6)Hg1	8.27	8.64	LP(1)N4	LP*(6)Cd1	17.81	16.94
LP(1)N4	LP*(7)Cu2	16.69	32.28	LP(1)N2	LP*(4)Hg1	15.57	14.16	LP(1)N2	LP*(6)Cd1	6.33	6.72
LP(1)N2	LP*(6)Cu1	10.14	11.46	π*(N2-C8)	π*(N5-C10)	34.88	24.41	π*(N2-C8)	π*(N5-C10)	24.32	25.60
LP(1)N6	LP*(6)Cu2	19.59	20.74	π*(N2-C8)	π*(C14-C20)	42.64	12.87	π*(N2-C8)	π*(C12-C16)	42.04	42.94
LP(1)N7	LP*(6)Cu1	19.66	20.14	π*(N3-C9)	π*(N4-C18)	34.62	34.68	π*(N2-C8)	π*(C14-C20)	60.81	60.27
LP(1)N7	LP*(9)Cu2	10.71	10.19	π*(N3-C9)	π*(C22-C36)	55.67	55.65	π*(N3-C9)	π*(N4-C18)	31.63	33.47
π*(N2-C8)	π*(N5-C10)	30.17	28.18					π*(N3-C9)	π*(C22-C36)	42.73	42.57
π*(N2-C8)	π*(C12-C16)	57.82	60.71					π*(N3-C9)	π*(C24-C34)	39.84	39.59
π*(N2-C8)	π*(C14-C20)	80.82	79.44								
π*(N3-C9)	π*(N4-C18)	29.83	32.82								
π*(N3-C9)	π*(C22-C36)	64.48	67.43								
π*(N3-C9)	π*(C24-C34)	42.50	45.74								
Complex **15**				Complex **16**				Complex **16**			
Donor (*i*)	Acceptor (j)	ωB97XD	CAM-B3LYP	Donor (*i*)	Acceptor (j)	ωB97XD	CAM-B3LYP	Donor (*i*)	Acceptor (j)	ωB97XD	CAM-B3LYP
		LanL2DZ				6–311+G(d,p)/LanK2DZ				6–311+G(d,p)//LanK2DZ	
LP(1)N6	LP*(4)Ag1	11.56	15.55	LP(1)N6	LP*(7)Zn1	30.32	30.60	π(C9-C22)	π*(N4-C18)	18.61	17.71
LP(1)N7	LP*(4)Ag1	11.04	15.42	LP(1)N7	LP*(7)Zn1	34.14	33.34	π(C9-C22)	π*(C34-C36)	36.16	31.14
LP(1)N5	LP*(5)Ag1	13.98	10.21	LP(1)N5	LP*(8)Zn1	36.22	34.69	π(C8-C14)	π*(N5-C10)	16.41	15.50
LP(1)N2	LP*(4)Ag1	10.54	13.46	LP(1)N3	LP*(6)Zn2	15.43	15.77	π(C8-C14)	π*(N2-C12)	32.10	27.37
π*(N2-12)	π*(C8-C14)	64.34	30.09	LP(1)N4	LP*(7)Zn2	47.25	45.28	π(C8-C14)	π*(C16-C20)	38.06	32.88
π*(N2-C8)	π*(C16-C20)	59.74		LP(1)N2	LP*(6)Zn1	33.23	33.19				
				LP(1)N6	LP*(6)Zn2	16.69	15.52				
				LP(1)N7	LP*(6)Zn2	12.99	13.47				
				LP(4)Cl1	LP*(6)Zn1	120.64	113.39				
				LP(4)Cl2	LP*(6)Zn2	110.77	104.14				
				π(C9-C22)	π*(N3-C24)	31.55	27.00				

$E^{(2)}$ Hyperconjugative interaction energy (stabilization energy)

Table S3. Experimental and theoretical selected characteristic vibration frequencies of synthesized complexes **12–16**.

FT-IR (cm^{-1})	ωB97XD	CAM-B3LYP	FT-IR (cm^{-1})	ωB97XD	CAM-B3LYP	FT-IR (cm^{-1})	ωB97XD	CAM-B3LYP	FT-IR (cm^{-1})	ωB97XD	CAM-B3LYP	FT-IR (cm^{-1})	ωB97XD	CAM-B3LYP	Vibrational mode assignments
	6-311+G(d,p)//LanL2DZ			LanL2DZ			6-311+G(d,p)//LanL2DZ			LanL2DZ			6-311+G(d,p)//LanL2DZ		
	Complex **12**			Complex **13**			Complex **14**			Complex **15**			Complex **16**		
3095	3093	3093	3137	3150	3143	3089	3089	3086	3070	3117	3110	3071	3073	3077	$\nu_{CH\ (ring)}$
3065	3017	3019	3073	3075	3033	3060	3018	3022	3054	3006	3003	3050	3024	3030	$\nu_{CH\ (imine)}$
3034	3014	3016	3019	3049	3028	3025	3001	2999	3017	3030	3034	3030	3010	3012	$\nu_{as\ (methyl)}$
2926	2904	2905	2931	2895	2902	2919	2897	2903	2917	2927	2904	2924	2910	2919	$\nu_{s\ (methyl)}$
2059	2105	2113	2032	1948	1951	2050	2019	2023	2020	1946	1940	2060	2178	2185	$\nu_{NN\ (azide)}$
1654	1662	1680	1653	1671	1673	1658	1687	1690	1648	1692	1682	1655	1701	1704	$\nu_{C=N\ (imine)}$
1602	1614	1615	1621	1606	1607	1618	1605	1606	1600	1609	1605	1623	1614	1615	$\nu_{C=C\ (ring)}$
1477	1460	1464	1458	1459	1461	1456	1457	1458	1466	1453	1449	1456	1448	1450	$\nu_{C=N\ (imine)}$
1420	1430	1423	1403	1429	1422	1402	1397	1395	1402	1424	1423	1406	1391	1395	$\beta_{HCC\ (ring)}$
1341	1362	1333	1304	1291	1283	1330	1333	1328	1333	1338	1286	1340	1356	1359	$\nu_{NN\ (azide)}$
1292	1289	1287	1267	1269	1275	1282	1279	1276	1300	1278	1256	1303	1354	1358	$\beta_{HCC\ (ring)}$
1028	1025	1023	1020	1023	1022	1020	1020	1019	1015	1011	1006	1015	1023	1017	$\nu_{NC\ (imine)}$

ν: Stretching; β: In-plane bending; γ: Out-of-plane bending; τ: Torsion.

Table S4. Experimental and theoretical some characteristic vibration frequencies of synthesized complexes **12–16**.

FT-IR (cm^{-1})	ωB97XD	CAM-B3LYP	FT-IR (cm^{-1})	ωB97XD	CAM-B3LYP	FT-IR (cm^{-1})	ωB97XD	CAM-B3LYP	Vibrational mode assignments
	6-311+G(d,p)//LanL2DZ			LanL2DZ			LanL2DZ		
	Complex **12**			Complex **13**			Complex **14**		
3095	3093	3093	3137	3150	3143	3089	3089	3086	$\nu_{CH\ (ring)}$
3065	3017	3019	3073	3075	3033	3060	3018	3022	$\nu_{CH\ (imine)}$
3034	3014	3016	3019	3049	3028	3025	3001	2999	$\nu_{as\ (methyl)}$
2975	2915	2923	2978	2928	2934	2988	2918	2925	$\nu_{s\ (methyl)}$
2926	2904	2905	2931	2895	2902	2919	2897	2903	$\nu_{s\ (methyl)}$
2059	2105	2113	2032	1948	1951	2050	2019	2023	$\nu_{NN\ (azide)}$
2032	2091	2105							$\nu_{NN\ (azide)}$
1654	1662	1680	1653	1671	1673	1658	1687	1690	$\nu_{C=N\ (imine)}$
1602	1614	1615	1621	1606	1607	1618	1605	1606	$\nu_{C=C\ (ring)}$
1597	1603	1608	1589	1599	1597	1593	1596	1596	$\nu_{C=C\ (ring)}$
1568	1575	1579	1565	1579	1559	1569	1553	1554	$\nu_{C=N\ (imine)} + \nu_{C=C\ (ring)} + \beta_{HCC\ (ring)}$
1507	1467	1471	1474	1478	1475	1480	1481	1475	$\nu_{C=C\ (ring)} + \nu_{C=N\ (imine)} + \beta_{CCC\ (ring)} + \beta_{CCN\ (ring)}$
1477	1460	1464	1458	1459	1461	1456	1457	1458	$\nu_{C=N\ (imine)}$
1444	1444	1445	1437	1455	1450	1439	1430	1428	$\nu_{C=C\ (ring)} + \beta_{HCC\ (ring)} + \beta_{HCH\ (methyl)}$
1420	1430	1423	1403	1429	1422	1402	1397	1395	$\beta_{HCC\ (ring)}$
1364	1390	1375	1374	1398	1394	1380	1368	1364	$\nu_{NC\ (imine)} + \nu_{CC\ (imine\text{-}ring)} + \beta_{HCC\ (ring)}$
1341	1362	1333	1304	1291	1283	1330	1333	1328	$\nu_{NN\ (azide)}$
1292	1289	1287	1267	1269	1275	1282	1279	1276	$\beta_{HCC\ (ring)}$
1220	1211	1214	1220	1241	1239	1220	1232	1233	$\nu_{CN\ (ring)} + \nu_{CC\ (ring)}$
1153	1138	1136	1159	1163	1155	1155	1163	1155	$\nu_{CC\ (ring)} + \beta_{HCC(ring)}$
1104	1098	1102	1141	1133	1130	1100	1092	1087	$\nu_{CC\ (ring)} + \nu_{CN\ (ring)} + \beta_{HCC\ (ring)}$
1051	1040	1042	1039	1039	1040	1052	1040	1040	$\beta_{HCC\ (ring)}$
1028	1025	1023	1020	1023	1022	1020	1020	1019	$\nu_{NC\ (imine)}$
953	920	930	1001	1006	1005	962	975	961	$\beta_{CCN\ (ring)} + \beta_{CNC\ (ring)}$
882	881	883	875	898	872	877	916	914	$\nu_{CC\ (ring)} + \nu_{CN\ (ring)}$
776	761	765	782	790	797	773	760	765	$\tau_{HCCC\ (ring)}$
745	735	739	745	742	746	747	740	743	$\tau_{HCCN\ (ring)} + \tau_{HCCC\ (ring)}$
668	660	662	695	715	721	670	661	661	$\beta_{NCC\ (imine)} + \beta_{CCC\ (ring)}$
649	654	645	646	631	633	653	632	631	$\beta_{NCC\ (ring)} + \beta_{CCC\ (ring)} + \beta_{CNC\ (imine)} + \beta_{CCN\ (ring)}$
511	511	514	507	510	507	508	518	522	$\beta_{CCC\ (ring)} + \beta_{CNC\ (imine)}$

υ: Stretching; β: In-plane bending; γ: Out-of-plane bending; τ: Torsion.

Table S4. (*Continued*)

FT-IR (cm^{-1})	ωB97XD	CAM-B3LYP	FT-IR (cm^{-1})	ωB97XD	CAM-B3LYP	Vibrational mode assignments
	LanL2DZ			6-311+G(d,p)//LanL2DZ		
	Complex **15**			Complex **16**		
3070	3117	3110	3071	3073	3077	$\nu_{CH\ (ring)}$
3054	3006	3003	3050	3024	3030	$\nu_{CH\ (imine)}$
3017	3030	3034	3030	3010	3012	$\nu_{as\ (methyl)}$
2961			2974	2918	2927	$\nu_{s\ (methyl)}$
2917	2927	2904	2924	2910	2919	$\nu_{s\ (methyl)}$
2020	1946	1940	2060	2178	2185	$\nu_{NN\ (azide)}$
	1885	1844		2162	2167	$\nu_{NN\ (azide)}$
1648	1692	1682	1655	1701	1704	$\nu_{C=N\ (imine)}$
1600	1609	1605	1623	1614	1615	$\nu_{C=C\ (ring)}$
1588	1589	1588	1596	1598	1592	$\nu_{C=C\ (ring)}$
1570	1563	1567	1573	1591	1590	$\nu_{C=N\ (imine)} + \nu_{C=C\ (ring)} + \beta_{HCC\ (ring)}$
1472	1482	1469	1475	1472	1475	$\nu_{C=C\ (ring)} + \nu_{C=N\ (imine)} + \beta_{CCC\ (ring)} + \beta_{CCN\ (ring)}$
1466	1453	1449	1456	1448	1450	$\nu_{C=N\ (imine)}$
1438	1435	1436	1438	1430	1434	$\nu_{C=C\ (ring)} + \beta_{HCC\ (ring)} + \beta_{HCH\ (methyl)}$
1402	1424	1423	1406	1391	1395	$\beta_{HCC\ (ring)}$
1372	1372	1361	1370	1358	1363	$\nu_{NC\ (imine)} + \nu_{CC\ (imine\text{-}ring)} + \beta_{HCC\ (ring)}$
1333	1338	1286	1340	1356	1359	$\nu_{NN\ (azide)}$
1300	1278	1256	1303	1354	1358	$\beta_{HCC\ (ring)}$
1220	1231	1233	1222	1267	1256	$\nu_{CN\ (ring)} + \nu_{CC\ (ring)}$
1151	1143	1148	1152	1211	1214	$\nu_{CC\ (ring)} + \beta_{HCC(ring)}$
1100	1104	1096	1102	1096	1094	$\nu_{CC\ (ring)} + \nu_{CN\ (ring)} + \beta_{HCC\ (ring)}$
1049	1050	1036	1050	1043	1045	$\beta_{HCC\ (ring)}$
1015	1011	1006	1015	1023	1017	$\nu_{NC\ (imine)}$
970	962	966	960	972	980	$\beta_{CCN\ (ring)} + \beta_{CNC\ (ring)}$
878	923	863	875	867	870	$\nu_{CC\ (ring)} + \nu_{CN\ (ring)}$
777	795	767	777	762	768	$\tau_{HCCC\ (ring)}$
740	758	765	740	735	740	$\tau_{HCCN\ (ring)} + \tau_{HCCC\ (ring)}$
670	660	661	669	661	664	$\beta_{NCC\ (imine)} + \beta_{CCC\ (ring)}$
630	635	640	642	633	636	$\beta_{NCC\ (ring)} + \beta_{CCC\ (ring)} + \beta_{CNC\ (imine)} + \beta_{CCN\ (ring)}$
506	518	521	505	500	507	$\beta_{CCC\ (ring)} + \beta_{CNC\ (imine)}$

υ: Stretching; β: In-plane bending; γ: Out-of-plane bending; τ: Torsion.

Table S5. Experimental and theoretical wavelengths, oscillator strengths, and major contributions for complexes **12–16**.

Experimental	Methanol/TD-CAM-B3LYP/6-311+G(d,p)//LanL2DZ		
λ (nm) (Methanol)	λ (nm)	Osc. Strength	Molecular contributions (SWizard and Chemissian programs) H: HOMO, L: LUMO, 2-pyridyl: C_5H_4N, imine group: CH=N−CH_3
Complex **12**			
371.1	373.4	0.0074	(54%) H [Cu(20%)+Pyridyl(22%)+Imine(8%)+N_3(50%)]→L α [Pyridyl(51%)+Imine(10%)+N_3(36%)]
			(8%) H−1[Cu(14%)+Pyridyl(32%)+Imine(5%)+N_3(49%)]→L+1 β [Pyridyl(49%)+Imine(12%)+N_3(36%)]
264.5	260.8	0.0685	(18%) H-11 [Cu(2%)+Pyridyl(50%)+Imine(16%)+N_3(32%)]→L β [Cu(17%)+Pyridyl(45%)+Imine(6%)+N_3(32%)]
			(7%) H-5 [Cu(37%)+Pyridyl(24%)+Imine(8%)+N_3(31%)]→L+1 β [Pyridyl(49%)+Imine(12%)+N_3(36%)]
203.5	223.1	0.0269	(23%) H-4 [Cu(8%)+Pyridyl(29%)+Imine(9%)+N_3(54%)]→L+3 β [Cu(10%)+Pyridyl(36%)+Imine(9%)+N_3(45%)]
			(7%) H-5 [Cu(8%)+Pyridyl(25%)+Imine(7%)+N_3(59%)]→L+2 α [Cu(10%)+Pyridyl(36%)+Imine(9%)+N_3(45%)]
Complex **13**			
	536.2	0.0007	(99%) H [Pyridyl(45%)+Imine(51%)+H_2O(2%)]→L α [Pyridyl(60%)+Imine(38%)+ N_3(2%)]
251.1	253.3	0.0496	(28%) H [Hg(4%)+Pyridyl(10%)+Imine(4%)+N_3(82%)]→L+2 β [Pyridyl(97%)+Imine(3%)]
			(25%) H-1 [Hg(3%)+Pyridyl(9%)+Imine(4%)+N_3(84%)]→L+1 α [Pyridyl(97%)+Imine(3%)]
207.3	202.8	0.1723	(37%) H-3 [Hg(4%)+Pyridyl(47%)+Imine(46%)+N_3(2%)]→L+2 α [Pyridyl(94%)+Imine(5%)]
			(18%) H-1 [Hg(3%)+Pyridyl(9%)+Imine(4%)+N_3(84%)]→L+2 α [Pyridyl(94%)+Imine(5%)]
Complex **14**			
	747.7	0.0006	(99%) H [Pyridyl(56%)+Imine(43%)]→L α [Pyridyl(59%)+Imine(40%)]
264.5	258.5	0.1002	(23%) H-2 [Pyridyl(56%)+Imine(37%)+N_3(6%)]→L+3 β [Pyridyl(97%)+Imine(3%)]
			(15%) H-4 [Pyridyl(98%)+Imine(1%)]→L+3 β [Pyridyl(97%)+Imine(3%)]
244.5	247.2	0.2775	(37%) H-5 [Pyridyl(72%)+Imine(28%)]→L α [Pyridyl(59%)+Imine(40%)]
			(36%) H-5 [Pyridyl(73%)+Imine(27%)]→L β [Pyridyl(59%)+Imine(40%)]
Complex **15**			
	748.9	0.0094	(59%) H [Ag(7%)+Imine(5%)+N_3(86%)]→L β [Ag(37%)+ Pyridyl(11%)+Imine(9%)+N_3(43%)]
			(20%) H-1 [Pyridyl(7%)+Imine(2%)+N_3(90%)]→L β [Ag(37%)+ Pyridyl(11%)+Imine(9%)+N_3(43%)]
258.4	257.8	0.0386	(43%) H-1 [Pyridyl(7%)+Imine(2%)+N_3(90%)]→L β [Ag(37%)+ Pyridyl(11%)+Imine(9%)+N_3(43%)]
			(16%) H-2 [Ag(10%)+N_3(87%)]→L+1 β [Ag(2%)+ Pyridyl(56%)+Imine(41%)]
204.6	204.0	0.0124	(61%) H-1 [Ag(6%)+N_3(94%)]→L+1 α [Pyridyl(96%)+Imine(4%)]
			(27%) H-2 [Ag(5%)+N_3(92%)]→L+1 α [Pyridyl(96%)+Imine(4%)]
Complex **16**			
280.6	275.6	0.0044	(34%) H [Zn(5%)+Pyridyl(52%)+Imine(10%)+N_3(31%)+Cl(2%)]→L α [Pyridyl(69%)+Imine(17%)+N_3(10%)]
			(16%) H-1 [Zn(18%)+Pyridyl(40%)+Imine(7%)+N_3(32%)+Cl(3%)]→L α [Pyridyl(69%)+Imine(17%)+N_3(10%)]
231.5	230.9	0.0056	(30%) H-3 [Zn(12%)+Pyridyl(39%)+Imine(9%)+N_3(28%)+Cl(11%)]→L+1 α [Zn(5%)+Pyridyl(61%)+Imine(30%)+N_3(3%)]
			(12%) H-2 [Zn(5%)+Pyridyl(38%)+Imine(9%)+N_3(45%)+Cl(3%)]→L+1 α [Zn(5%)+Pyridyl(61%)+Imine(30%)+N_3(3%)]
213.8	216.3	0.0757	(32%) H-4 [Pyridyl(45%)+Imine(47%)+N_3(3%)+Cl(4%)]→L+2 α [Pyridyl(55%)+Imine(30%)+N_3(9%)]
			(9%) H-15 [Zn(6%)+Pyridyl(65%)+Imine(10%)+N_3(4%)%)+Cl(3%)+H_2O(12%)]→L α [Pyridyl(69%)+Imine(17%)+N_3(10%)]

30

Table S6. Experimental and theoretical wavelength, oscillator strength, and major contributions for complexes **12–16**.

Experimental λ (nm) (Methanol)	Methanol			
	λ (nm)	Osc. Strength	Molecular orbital contributions H: HOMO, L: LUMO	
Complex **12**				
	TD-ωB97XD/6-311+G(d,p)//LanL2DZ			
371.1	381.5	0.0010	H→L α (47%)	H→L+1 β (18%)
264.5	260.2	0.0500	H-5→L+1 β (12%)	H-6→L+1 β (9%)
	247.6	0.1412	H-10→L+1 α (20%)	H-10→L+2 β (17%)
203.5	217.5	0.0068	H-4→L+3 α (28%)	H-4→L+3 β (12%)
	TD-CAM-B3LYP/LanL2DZ			
371.1	373.4	0.0074	H→L α (54%)	H-1→L+1 β (8%)
264.5	260.8	0.0685	H-11→L β (18%)	H-5→L+1 β (7%)
203.5	223.1	0.0269	H-4→L+3 β (23%)	H-3→L+2 α (7%)
Complex **13**				
	TD-ωB97XD/LanL2DZ			
	480.5	0.0006	H→L α (98%)	
251.1	250.1	0.0615	H-2→L β (33%)	H-5→L+1 β (11%)
207.3	200.2	0.4095	H-3→L+2 α (32%)	H-2→L β (18%)
	TD-CAM-B3LYP/6-311+G(d,p)//LanL2DZ			
	536.2	0.0007	H→L α (99%)	
251.1	253.3	0.0496	H→L+2 β (28%)	H-1→L+1 α (25%)
207.3	202.8	0.1723	H-3→L+2 α (37%)	H-1→L+2 α (18%)
Complex **14**				
	TD-ωB97XD/LanL2DZ			
	733.5	0.0031	H→L α (92%)	H→L+2 α (7%)
264.5	253.2	0.0776	H-2→L+3 β (24%)	H-4→L+3 β (16%)
244.5	246.7	0.2077	H-5→L α (27%)	H-5→L β (24%)
	TD-CAM-B3LYP/6-311+G(d,p)//LanL2DZ			
	747.7	0.0006	H→L α (99%)	
264.5	258.5	0.1002	H-2→L+3 β (23%)	H-4→L+3 β (15%)
244.5	247.2	0.2775	H-5→L α (37%)	H-5→L β (36%)
Complex **15**				
	TD-ωB97XD/LanL2DZ			
	384.7	0.0003	H→L α (70%)	H-5→L α (16%)
258.4	257.4	0.1740	H-4→L+1 β (24%)	H-4→L α (22%)
204.6	209.3	0.0345	H→L+2 α (16%)	H→L+7 α (15%)
	TD-CAM-B3LYP/LanL2DZ			
	748.9	0.0094	H→L β (59%)	H-1→L β (20%)
258.4	257.8	0.0386	H-1→L β (43%)	H-2→L+1 β (16%)
204.6	204.0	0.0124	H-1→L+1 α (61%)	H-2→ L+1 α (27%)
Complex **16**				
	TD-ωB97XD/6-311+G(d,p)//LanL2DZ			
280.6	271.6	0.0040	H→L α (26%)	H-1→L α (18%)
231.5	230.5	0.0098	H-3→L α (38%)	H-2→L+1 α (15%)
213.8	216.1	0.0723	H-5→L+2 α (23%)	H-4→L+2 α (7%)
	TD-CAM-B3LYP/LanL2DZ			
280.6	275.6	0.0044	H→L α (34%)	H-1→L α (16%)
231.5	230.9	0.0056	H-3→L+1 α (30%)	H-2→L+1 α (12%)
213.8	216.3	0.0757	H-4→L+2 α (32%)	H-15→L α (9%)

Table S7. Theoretical global chemical reactivity descriptors in the gas phase for complexes **12–16**.

Parameters (unit)	Complex **12**				Complex **13**				Complex **14**			
	ωB97XD		CAM-B3LYP		ωB97XD		CAM-B3LYP		ωB97XD		CAM-B3LYP	
	α spin	β spin	α spin	β spin	α spin	β spin	α spin	β spin	α spin	β spin	α spin	β spin
E_{HOMO} (eV)	-6.814	-6.793	-6.528	-6.509	-5.355	-7.171	-4.855	-6.604	-5.016	-7.025	-4.490	-6.461
E_{LUMO} (eV)	-0.815	-0.814	-1.356	-1.412	-0.446	-0.445	-1.058	-1.057	-0.888	-0.887	-1.538	-1.538
ΔE (eV)	5.999	5.979	5.172	5.097	4.909	6.726	3.797	5.547	4.128	6.138	2.952	4.923
Electronegativity (χ, eV)	3.815	3.804	3.942	3.961	2.901	3.808	2.957	3.831	2.952	3.956	3.014	3.999
Chemical hardness (η, eV)	2.999	2.990	2.586	2.549	2.455	3.363	1.899	2.774	2.064	3.069	1.476	2.462
Chemical softness (S, 1/eV)	0.333	0.334	0.387	0.392	0.407	0.297	0.527	0.360	0.484	0.326	0.678	0.406
Electrophilic index (ω, eV)	2.427	2.420	3.005	3.078	1.714	2.156	2.302	2.645	2.111	2.550	3.205	3.248
Nucleophilic index (φ, 1/eV)	0.412	0.413	0.333	0.325	0.583	0.464	0.434	0.378	0.474	0.392	0.312	0.308

Parameters (unit)	Complex **15**				Complex **16**	
	ωB97XD		CAM-B3LYP		ωB97XD	CAM-B3LYP
	α spin	β spin	α spin	β spin	α spin	α spin
E_{HOMO} (eV)	-8.009	-8.177	-7.140	-7.456	-8.367	-7.856
E_{LUMO} (eV)	-1.007	-2.419	-1.468	-2.543	-0.963	-1.434
ΔE (eV)	7.002	5.758	5.672	4.913	7.404	6.422
Electronegativity (χ, eV)	4.508	5.298	4.304	4.999	4.665	4.645
Chemical hardness (η, eV)	3.501	2.879	2.836	2.457	3.702	3.211
Chemical softness (S, 1/eV)	0.286	0.347	0.353	0.407	0.270	0.311
Electrophilic index (ω, eV)	2.902	4.875	3.266	5.085	2.939	3.360
Nucleophilic index (φ, 1/eV)	0.345	0.205	0.306	0.197	0.340	0.298

Table S8. Theoretical electric dipole moment (μ, Debye), static isotropic and anisotropic polarizability ($\bar{\alpha}$ and Δα, x10^{-24} esu), static first− and second−order hyperpolarizability (β, x10^{-30} esu and γ, x10^{-36} esu) for complexes **12–16**.

Parameter	Complex **12**		Complex **13**		Complex **14**		Complex **15**		Complex **16**	
	ωB97XD	CAM-B3LYP	ωB97XD	CAM-B3LYP	ωB97XD	CAM-B3LYP	ωB97XD	CAM-B3LYP	ωB97XD	CAM-B3LYP
	6-311+G(d,p)		LanL2DZ		LanL2DZ		LanL2DZ		6-311+G(d,p)	
μ	8.47	7.29	5.87	5.97	12.25	12.15	10.68	10.71	11.77	10.28
μ	6.20 (pNA) [21] and 4.56 (Urea) [22]									
<α>	47.56	48.30	35.70	35.59	33.79	33.88	31.09	29.78	49.53	49.75
<α>	17 (pNA) [21]									
Δα	23.45	21.07	19.92	20.08	5.70	4.35	19.43	25.59	10.13	12.44
<β>	13.66	11.31	2.28	2.33	11.26	10.68	18.21	17.05	3.85	4.32
<β>	9.2 (pNA) [21], 0.32 (Urea) [22] and 0.13 (Urea) [23]									
<γ>	85.71	96.93	22.17	23.59	48.46	47.55	1.66	15.32	37.76	39.35
<γ>	15.0 (pNA) [21] and 7 (Urea) [22]									

References

1. Avcı D, Altürk S, Sönmez F, et al. Three novel Cu(II), Cd(II) and Cr(III) complexes of 6−Methylpyridine−2−carboxylic acid with thiocyanate: Synthesis, crystal structures, DFT calculations, molecular docking and α-Glucosidase inhibition studies. Tetrahedron 2018;74:7198–7208. doi: 10.1016/j.tet.2018.10.054
2. Avcı D, Altürk S, Sönmez F, et al. A novel series of mixed-ligand M(II) complexes containing 2,2′-bipyridyl as potent α-glucosidase inhibitor: synthesis, crystal structure, DFT calculations, and molecular docking. JBIC J. Biol. Inorg. Chem. 2019;24:747–764. doi: 10.1007/s00775-019-01688-9
3. Avcı D, Altürk S, Sönmez F, et al. Synthesis, spectral properties, in vitro α-glucosidase inhibitory activity and quantum chemical calculations of novel mixed-ligand M(II) complexes containing 1,10-phenanthroline. Appl. Organomet. Chem. 2020;34:e5412. doi: 10.1002/aoc.5412
4. Sun H, Ding W, Song X, et al. Synthesis of 6-hydroxyaurone analogues and evaluation of their α-glucosidase inhibitory and glucose consumption-promoting activity: Development of highly active 5,6-disubstituted derivatives. Bioorg. Med. Chem. Lett. 2017;27(15):3226–3230. doi: 10.1016/j.bmcl.2017.06.040
5. Altürk S, Avcı D, Tamer Ö, et al. A cobalt(II) complex with 6-methylpicolinate: synthesis, characterization, second- and third-order nonlinear optical properties, and DFT calculations. J. Phys. Chem. Solids 2016;98:71–80. doi: 10.1016/j.jpcs.2016.06.008
6. Foster JP, Weinhold F. Natural hybrid orbitals. J. Am. Chem. Soc. 1980;102:7211–7218. doi: 10.1021/ja00544a007
7. Pearson RG. Absolute electronegativity and hardness correlated with molecular orbital theory. Proc. Nati. Acad. Sci. USA 1986;83:8440–8441. doi: 10.1073/pnas.83.22.8440
8. Avcı D, Özge Ö, Başoğlu A et al. Synthesis, crystal structures, and DFT calculations: novel Mn(II), Co(II) and Ni(II) complexes of *N*-(pyridin-2-ylmethylene)methanamine with isothiocyanate as promising optical materials. Opt. Quantum Electron. 2023;55: 408. doi: 10.1007/s11082-023-04668-1
9. J Oudar JL, Zyss J. Relations between microscopic and macroscopic lowest-order optical nonlinearities of molecular crystals with one-or two-dimensional units. Phys. Rev. A 1982;26:2028–2048. doi: 10.1103/PhysRevA.26.2028
10. Avcı D. Second and third-order nonlinear optical properties and molecular parameters of azo chromophores: Semiempirical analysis. Spectrochim. Acta A 2011;82:37−43. doi: 10.1016/j.saa.2011.06.037
11. Morris GM, Huey R, Lindstrom W, et al. Autodock4 and AutoDockTools4: automated docking with selective receptor flexibility. J. Comput. Chem. 2009;30:2785–2791. doi: 10.1002/jcc.21256
12. Sanner MF. Python: A Programming Language for Software Integration and Development. J. Mol. Graphics Mod. 1999;17:57–61.
13. Morris GM, Goodsell DS, Halliday RS, et al. Automated Docking Using a Lamarckian Genetic Algorithm and and Empirical Binding Free Energy Function, J. Comput. Chem. 1998;19(14):1639–1662. doi: 10.1002/(SICI)1096-987X(19981115)19:14<1639::AID-JCC10>3.0.CO;2-B
14. Systèmes D, Dassault Systèmes Biovia: San Diego, CA, USA 2016.
15. Özge Ö, Avcı D, Sönmez F, et al. Synthesis, DFT calculations, α-glucosidase inhibitor activity, and docking studies on Schiff base metal complexes containing isothiocyanate. Appl. Organomet. Chem. 2023;37:e7084. doi: 10.1002/aoc.7084

16. Abraham MJ, Murtola T, Schulz R, et al. GROMACS: High performance molecular simulations through multi-level parallelism from laptops to supercomputers. SoftwareX 2015;1:19–25. doi: 10.1016/j.softx.2015.06.001
17. WebGRO for Macromolecular Simulations. Available from: https://simlab.uams.edu/.
18. Schuler LD, Daura X, van Gunsteren WF. An improved GROMOS96 force field for aliphatic hydrocarbons in the condensed phase. J. Comput. Chem. 2001;22(11):1205–1218. doi: 10.1002/jcc.1078
19. Berendsen HJC, Grigera JR, Straatsma TP. The missing term in effective pair potentials. J. Phys. Chem. 1987;91:6269–6271. doi: 10.1021/j100308a038
20. Lemkul JA, From Proteins to Perturbed Hamiltonians: A Suite of Tutorials for the GROMACS-2018 Molecular Simulation Package. Living J. Comput. Mol. Sci. 2019;1:5068. doi: 10.33011/livecoms.1.1.5068
21. Cheng LT, Tam W, Stevenson SH, et al. Experimental investigations of organic molecular nonlinear optical polarizabilities. 1. Methods and results on benzene and stilbene derivatives. J. Phys. Chem. 1991;95:10631–10643. doi: 10.1021/j100179a026
22. Ledoux I, Zyss J. Influence of the Molecular Environment in Solution Measurements of the Second-Order Optical Susceptibility for Urea and Derivatives. Chem. Phys. 1982;73:203–213. doi: 10.1016/0301-0104(82)85161-6
23. Adant C, Dupuis M, Bredas J. Ab initio study of the nonlinear optical properties of urea: electron correlation and dispersion effects. Int. J. Quant. Chem. 1995;56:497–507. doi: 10.1002/qua.560560853

ÖZGEÇMİŞ

Ad-Soyad : Özgen ÖZGE

ÖĞRENİM DURUMU:

- **Lisans** **:** 2009, Sakarya Üniversitesi, Fen-Edebiyat Fakültesi, Fizik
- **Yükseklisans** **:** 2019, Sakarya Üniversitesi, Fizik Anabilim Dalı

MESLEKİ DENEYİM VE ÖDÜLLER:

- 2012-2019 yılları arasında Sakarya Üniversitesi'nde Kısmi zamanlı öğrenci asistanlık görevini yürütmüştür.
- 2011-2012, 2014-15 ve 2015-2016 eğitim-öğretim dönemlerinde MEB'de ücretli öğretmenlik yapmıştır.
- 2022-Halen Kapadokya Üniversitesi'nde Öğretim Görevlisi olarak çalışmaktadır.

TEZDEN TÜRETİLEN ESERLER:

- Avcı, D., Özge, Ö., Başoğlu, A., Sönmez, F., Tamer, Ö., Dege, N., & Atalay, Y. (2023). Synthesis, crystal structures, and DFT calculations: novel Mn(II), Co(II) and Ni(II) complexes of N-(pyridin-2-ylmethylene)methanamine with isothiocyanate as promising optical materials. Optical and Quantum Electronics, 55, 408. https://doi.org/10.1007/s11082-023-04668-1
- Özge, Ö., Avcı, D., Sönmez, F., Tamer, Ö., Dege, N., Başoğlu, A., Atalay, Y., & Zengin Kurt, B. (2023). Synthesis, DFT calculations, α-glucosidase inhibitor activity, and docking studies on Schiff base metal complexes containing isothiocyanate. Applied Organometallic Chemistry, 37(5), e7084. https://doi.org/10.1002/aoc.7084
- Avcı, D., Özge, Ö., Sönmez, F., Başoğlu, A., Tamer, Ö., & Atalay, Y. (2024). Novel schiff base-azide metal complexes: Synthesis, spectral, nonlinear optics, and DFT studies. Materials Science in Semiconductor Processing, 179, 108523. https://doi.org/10.1016/j.mssp.2024.108523
- Avcı, D., Özge, Ö., Sönmez, F., Tamer, Ö., Başoğlu, A., Atalay, Y., & Zengin Kurt, B. (2024). In vitro α-glucosidase, docking and density functional theory

- studies on novel azide metal complexes. Future Medicinal Chemistry, 16(11), 1109–1125. https://doi.org/10.1080/17568919.2024.2342650

DİĞER ESERLER:

- Dege, N., Özge, Ö., Avcı, D., Başoğlu, A., Sönmez, F., Yaman, M., Tamer, Ö., Atalay, Y., & Zengin Kurt, B. (2021). Concentration effects on optical properties, DFT, crystal characterization and α-glucosidase activity studies: Novel Zn(II) complex. Spectrochimica Acta Part A: Molecular and Biomolecular Spectroscopy, 262, 120072. https://doi.org/10.1016/j.saa.2021.120072
- Özge, Ö., Avcı, D., Tamer, Ö., Başoğlu, A., Atalay, Y., (2023). Spectroscopic and non-linear optical investigations for a polycyclic organic compound by using DFT methods. Turkish Physical Society 39th International Physics Congress. Bodrum, Muğla, Türkiye.
- Özge, Ö., Avcı, D., Başoğlu, A., Tamer, Ö., Atalay, Y., (2022). DFT calculations on structural, spectroscopic and non-linear optical parameters of Diiodobis(2-aminopyridine)Cadmium(II). Book of Full Text Proceedings Turkish Physical Society 38th International Physics Congress (TPS38), 4, 2, 69-75. https://www.tfd38.org/HizmetSayfalari/31/TPS-38-Book-of-Full-Text-Proceedings.html
- Özge, Ö., Avcı, D., Başoğlu, A., Tamer, Ö., Atalay, Y., (2020). DFT Investigations on The Potential NLO Chromophores Containing The 2-Phenyl-6-Nitrobenzimidazole Group. Book of Full Text Proceedings Turkish Physical Society 36th International Physics Congress (TPS36), 2, 02, 32-38.
- Özge, Ö., Avcı, D., Başoğlu, A., Tamer, Ö., Atalay, Y., (2020). Theoretical Calculations on Structural, Spectroscopic and Non-Linear Optical Parameters of Molecules Containing 2-Aryl Group. Book of Full Text Proceedings Turkish Physical Society 36th International Physics Congress (TPS36), 2, 07, 169-175.